Fuel Gasification

Published on June 1, 1967 on http://pubs.acs.org | doi: 10.1021/ba-1967-0069.fw001

Fuel Gasification

A symposium sponsored
by the Division of
Fuel Chemistry at the
152nd Meeting of the
American Chemical
Society, New York, N. Y.
Sept. 12-13, 1966.

Frank C. Schora, Jr.

Symposium Chairman

ADVANCES IN CHEMISTRY SERIES 69

AMERICAN CHEMICAL SOCIETY
WASHINGTON, D.C. 1967

Library of Congress Catalog Card 87–31495

PRINTED IN THE UNITED STATES OF AMERICA

Advances in Chemistry Series

Robert F. Gould, *Editor*

AMERICAN CHEMICAL SOCIETY PUBLICATIONS

FOREWORD

ADVANCES IN CHEMISTRY SERIES was founded in 1949 by the American Chemical Society as an outlet for symposia and collections of data in special areas of topical interest that could not be accommodated in the Society's journals. It provides a medium for symposia that would otherwise be fragmented, their papers distributed among several journals or not published at all. Papers are refereed critically according to ACS editorial standards and receive the careful attention and processing characteristic of ACS publications. Papers published in ADVANCES IN CHEMISTRY SERIES are original contributions not published elsewhere in whole or major part and include reports of research as well as reviews since symposia may embrace both types of presentation.

PREFACE

In the continually changing picture of fuel and energy technology, there is an ever-present need for improving the utility of fuels. Processes for converting solid fuels to a more desirable form—specifically high B.t.u. gas—are now receiving renewed interest in the United States.

The United States abandoned its interest in conversion processes with the advent of natural-gas pipelining. This same disinterest is now occurring in other parts of the world owing to the promise of large natural gas reserves in Europe and Australia. In fact, at this writing, research on conversion processes outside the United States is nearing a complete halt.

In the United States, however, the renewed interest in conversion processes is stimulated by several factors. The major one is the need to ensure an abundant and inexpensive supply of pipeline gas to serve our economy. U.S. natural gas reserves are presently estimated to be sufficient to the year 2000. However, to ensure an adequate supply of pipeline gas at reasonable costs up to and through the year 2000, supplemental pipeline gas processes will be needed.

Another impetus to develop such processes is the desire of the U.S. Department of the Interior to ensure the continued utilization of coal. As our most abundant fossil fuel, it represents about 85% of the fuel reserves of this country. With the advent of nuclear technology and the pollution problems associated with burning sulfur-bearing coal in conventional power plants, much of this market will be lost to the atom. The continued use of this vast energy source will depend upon the ability to convert it into more versatile and desirable fuels.

This symposium is a compilation of a major portion of the research and development work now being done in the United States and elsewhere. Much of the technology being developed here is an outgrowth of technology initiated in Europe but now abandoned. With the support of this work by the U.S. Department of the Interior through the Bureau of Mines and the Office of Coal Research along with support from the American Gas Association and the gas and coal industries it now appears that the technology may reach a stage of commercialization within a few

years. This volume will acquaint the reader with the present status of the various programs now underway and will provide a background for the development work which lies ahead.

Chicago, Ill.
June 28, 1967

FRANK C. SCHORA

Decaking of Coal in Free Fall

STANLEY J. GASIOR, ALBERT J. FORNEY, and JOSEPH H. FIELD

U. S. Department of the Interior, Bureau of Mines, Pittsburgh Coal Research Center, 4800 Forbes Ave., Pittsburgh, Pa.

A strongly caking coal from the Pittsburgh seam of small lump size (1/8–3/8 in.) was converted to a noncaking char (decaked) in about 2 seconds by dropping it through a countercurrent flow of steam containing 5.5–12.7 mole % oxygen at 250–330 p.s.i.g. and 560°–680°C. The steam:coal weight ratio ranged from 2.0 to 0.57, and the oxygen:coal weight ratio ranged from 0.26 to 0.12. As the coal decaked, its volatile matter decreased from 35.6 to 24.9% while its free-swelling index decreased from 8.0 to 1.0. The treated coal was considered decaked because it did not cake when exposed to hydrogen for 5 minutes at 600°C.

Most bituminous coals mined near Eastern populous areas are caking, yet these are the areas which require large quantities of high B.t.u. pipeline gas. Our object has been to find a practical way to convert these strongly caking coals to noncaking fuel, suitable for fixed bed gasification —a preliminary step in making pipeline gas. A fixed bed gasifier applicable to production of synthesis gas containing methane has been used commercially in several parts of the world.

In previously reported experiments we have converted caking coals to noncaking coal char by treating coal of 1/8–1-1/2 in. for 3 hours in static bed (*3*), coal of 18–100 Tyler mesh size for 5 min. in a fluidized bed (*1*), and coal of 4–8 Tyler mesh in size for 2 sec. in free fall (*2*). Nitrogen and carbon dioxide, steam, or a mixture of all three with small amounts of oxygen were used as the heating and treating gas.

In further experimental work in free fall we have converted strongly caking bituminous coal from the Pittsburgh seam of 1/4–3/8 in., in addition to coal of 4–8 Tyler mesh, to a noncaking form in about 2 sec. by dropping it through a countercurrent flow of steam containing oxygen. In all cases the treated or decaked coals had a free-swelling index (FSI) of 2.0 or less, which is indicative of a weakly-to-noncaking coal. Further-

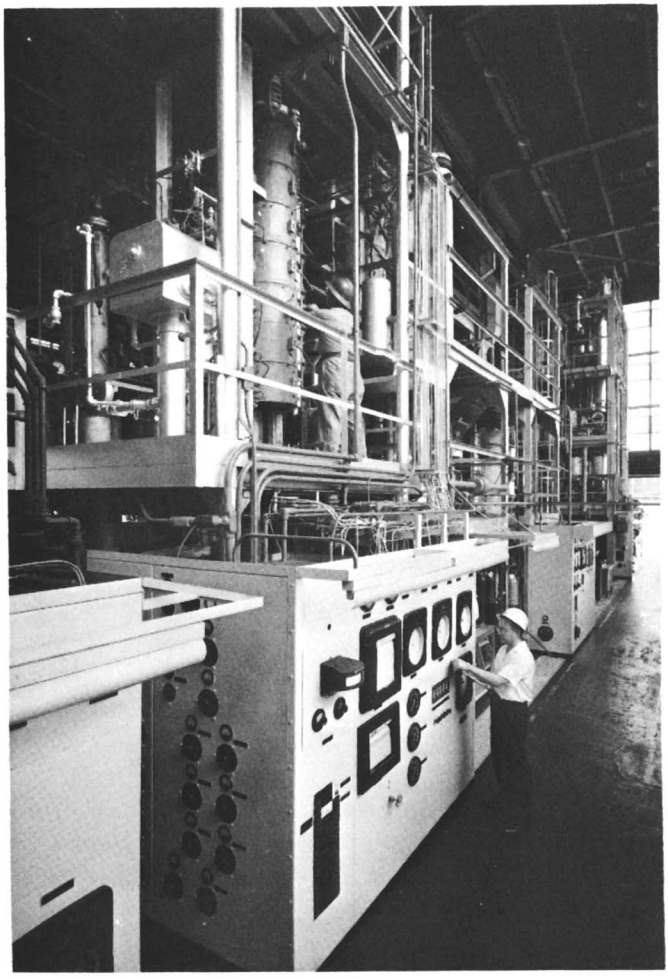

Figure 1. Pilot plant for decaking coal

more, when the treated coals were exposed to hydrogen at 600°C. and atmospheric pressure for 5 min., they showed little or no tendency to cake.

Experimental

Apparatus. The experimental work was done in the same pilot plant used in earlier studies (2) (Figure 1). A flow diagram of the system is shown in Figure 2. The system contains a steam generator, feed and receiver hoppers, a screw feeder, and a treatment vessel. This vessel, called a treater, is a 2-in. diameter, schedule 80 pipe, 20 ft. long, made of 304 stainless steel. It is surrounded by 16 individually controlled electric heaters that compensate for radiation loss and supply additional

heat when needed. No elaborate temperature control system is required because steam supplies most of the heat for the treatment, only little coming from the partial oxidation of the coal. Temperature is measured by thermocouples located at 6-, 12-, and 16-ft. levels of the treater. In some early tests a spiral rod, shown in Figure 2, was inserted into the treater to increase the coal-to-gas contact time, but coal particles tended to stick to the spiral rod, and it was removed.

Coal. Pittsburgh seam coal was selected for the tests because of its commercial importance, its reputation as a typically strong caking coal, and easy access at our experimental mine at Bruceton, Pa. The maximum size of the coal treated (3/8 in.) was limited by the inside diameter of the treater (1.939 in.). During treatment the coal tends to become sticky while swelling to about 1-1/2 times its original size.

Procedure. A quantity of 2 lbs. of coal of 4–8 Tyler mesh or 1/4–3/8-in. size was charged to the feed hopper and heated rapidly with steam to just below the softening temperature of the coal (350°C. for Pittsburgh-seam coal). This temperature was previously (3) determined as the value at which a fixed bed of coal offered an increase in resistance to gas flow. The heated coal was fed from the hopper at a controlled rate by a screw feeder into the 20-ft. long treater where it fell freely through a countercurrent flow of steam containing oxygen to a receiver,

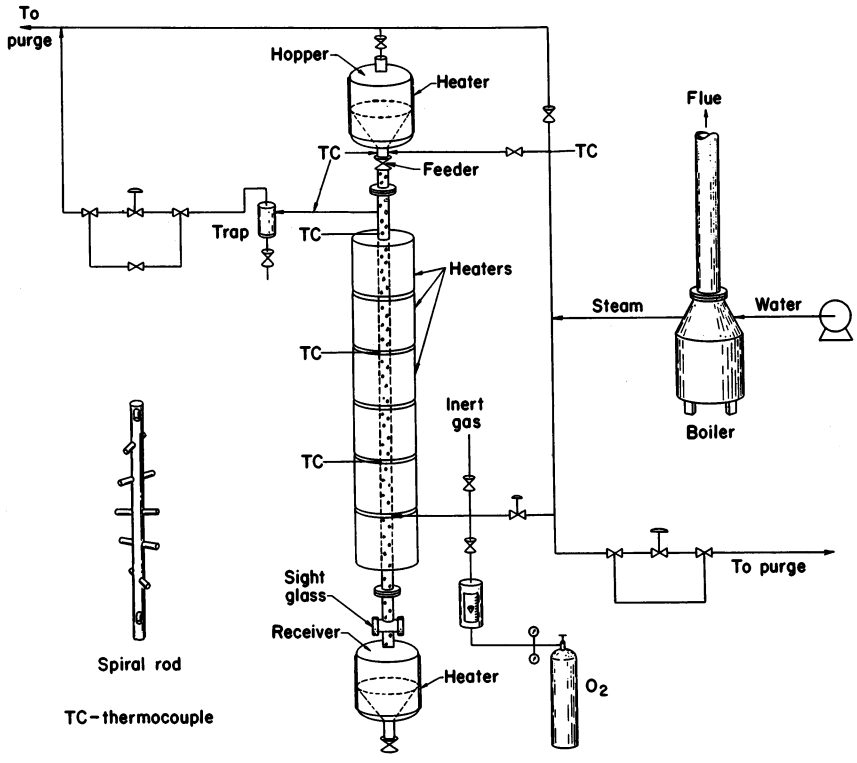

Figure 2. Schematic of the pilot plant for treating coal in free fall

Table I. Conditions for Treating a

Test No.	Pressure, p.s.i.g.	Size of Coal, in.	Size of Coal, Tyler mesh	Coal Feed, lb./hr.	Treating Gas Rate, lb./hr. Steam	Treating Gas Rate, lb./hr. O_2
77	250	¼–⅜	–	60	120	12.4
115	300	–	4–8	50	40	10.4
917	300	–	4–8	40	56	10.4
1028	330	–	4–8	70	40	6.0

where it was quenched with inert gas. The inert gas contained about 88% nitrogen and 12% carbon dioxide. The falling coal was in contact with the steam-oxygen mixture for about 2 sec.; each test lasted 2–3 min. The coal passed through a temperature range of 310°–430°C. as it fell through the reactor. The relation of this temperature rise with time of fall is referred to as coal heat cycle (Table I). To determine the degree of decaking, the treated coal was exposed to hydrogen for 5 min. at 600°C. If it did not cake during hydrogen exposure, decaking was considered successful. Correlation of hydrogen-exposure results with free-swelling indices (ASTM Test D-720-57) indicated that decaked coal produced from coal of initial high FSI values was noncaking during the hydrogen exposure, when its FSI had been reduced to 1.5 or less, and only weakly caking when its FSI was 2.0.

Results

Tests 77, 115, 917, and 1028 (Table I) are typical of experiments performed to date. In test 77, 2 lbs. of 1/4–3/8-in. coal was heated to 330°C. in 10 min. with steam. Before the coal could be treated effectively, it had to be heated to just below its softening temperature. During this preheating the coal showed only a loss of moisture. Then it dropped through the 20-ft. long treater at a rate of 60 lbs. of coal/hr. (3000 lb./hr.-sq. ft.). It fell through a countercurrent flow of steam containing 5.5 mole % of oxygen at an average temperature of 680°C. and 250 p.s.i.g. The steam:coal weight ratio was 2.0, and the oxygen:coal weight ratio was 0.21. Each coal particle expanded about 50% and fissured as shown in Figure 3. The treated coal did not cake when exposed to hydrogen for 5 min. It had a FSI of 1.0 and was considered decaked. Its volatile matter content was 24.9%.

In test 115, a 4–8 Tyler mesh coal was heated to 310°C. in 10 min. with steam and then dropped through the treater at a rate of 50 lbs. of coal/hr. through a countercurrent flow of steam containing 12.7 mole % oxygen at 560°C. and 300 p.s.i.g. The steam:- and oxygen:coal weight

Pittsburgh Seam Coal in Free Fall

Gas:Coal Ratio		*Average Reactor Temp., °C.*	*Coal Heat Cycle*		*Weight Loss of Coal, %*
Steam	O_2		*Temp., °C.*	*Time, sec.*	
2.0	0.21	680	330–430	2	15.3
0.8	0.21	560	310–430	2	4.0
1.4	0.26	605	310–430	2	10.2
0.57	0.12	605	310–430	2	6.9

ratios were 0.8 and 0.21, respectively. The treated coal caked only slightly when exposed to hydrogen at 600°C. It had a FSI of 2.0, and its volatile matter content was 30.8%.

In test 917 the same size coal was similarly heated and then dropped through the treater at a rate of 40 lbs. of coal/hr. Steam containing 9.4 mole % oxygen flowed countercurrent to the coal at 605°C. and 300 p.s.i.g. The steam:- and oxygen:coal weight ratios were 1.4 and 0.26, respectively. The treated coal did not cake when exposed to hydrogen at 600°C. It had a FSI of 1.5, and its volatile matter content was 26.7%.

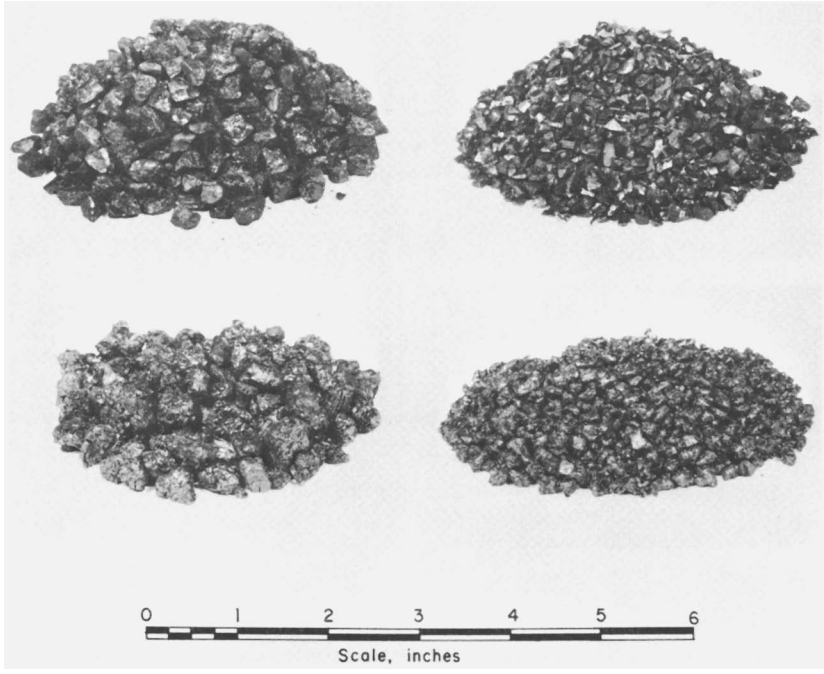

Figure 3. Raw and decaked coal

In test 1028, a 4–8 Tyler mesh coal was similarly preheated to 310°C. and then fed to and through the treater at a rate of 70 lbs. of coal/hr. Steam containing 7.8 mole % oxygen flowed countercurrent to the coal at 605°C. and 330 p.s.i.g. The steam:- and oxygen-coal weight ratios were 0.57 and 0.12, respectively. The treated coal caked only slightly when exposed to hydrogen at 600°C. It had a FSI of 2.0, and a volatile matter content was 31.9%. Analyses of the coal before and after treatment are shown in Table II.

The reactor was visually inspected after each test; no coal particles were found adhering to the reactor walls.

Table II. Analysis of Coal and Decaked Coal

	Proximate, %				*Ultimate, m.a.f., %*					
Test No.	*Moisture*	*Volatile Matter*	*Fixed Carbon*	*Ash*	*H*	*C*	*N*	*O*	*S*	*Free-Swelling Index*
Pittsburgh Seam Coal	2.0	35.6	54.4	8.0	5.6	84.3	1.7	7.0	1.4	8.0
77	0.3	24.9	67.2	7.6	4.5	85.4	1.7	7.1	1.3	1.0
115	.3	30.8	63.8	5.1	4.6	84.6	1.6	7.5	1.7	2.0
917	.5	26.7	63.8	9.0	4.9	83.9	1.8	8.2	1.2	1.5
1028	.6	31.9	62.3	5.2	4.8	84.2	1.8	7.7	1.5	2.0

Discussion

To alter or destroy the caking property of a strongly caking coal of small lump size in free fall effectively, both treatment temperature and gas composition must be kept within fairly narrow limits. The oxygen prevented agglomeration, but little of it reacted with the coal as evidenced by the appearance of the decaked coal. This agrees with previous experience in the fixed bed (3). We decaked coal, which had been preheated to 310°–330°C., in a 20-ft. treater in 2 sec. at 560°–680°C. with steam containing 5.5–12.7 mole % oxygen. When either the preheat or reaction temperature was too low, the coal never reached the temperature where it would decake during the 2 sec. that it took to fall 20 ft. Thus, the caking property of the coal remained unchanged. When the reaction temperature was too high or the oxygen was insufficient, the coal agglomerated and plugged the treater.

Results with 4–8 Tyler mesh and 1/4–3/8-in. coals indicate that larger size coal would require higher temperature and more oxygen.

This decaking technique offers promise as part of an integrated coal pretreatment and high pressure steam-oxygen coal gasification process

which requires nonagglomerating feed (*4*). Incorporating decaking with gasification should be simple. Both processes are at the same pressure and use the same gases. The process would be economical because the steam:coal weight ratio for decaking is equal to or less than that required by the commercial Lurgi (*5*) gasifier; also the oxygen:coal weight ratio is less than that required in the Lurgi gasifier. Furthermore, the gases and tars produced from volatile matter in the coal during decaking can be fed directly to the gasifier as fuel, thus conserving energy and also solving the problem of effluent or off-gas from the pretreatment. The treater might serve as feed lock hoppers for pressure gasifiers, thus minimizing additional capital investment.

Conclusions

A pilot-plant study has shown that the caking property of bituminous coal of small lump size can be altered or destroyed by rapidly heating the coal to or through its plastic temperature range while it falls freely through a countercurrent flow of high temperature steam-containing oxygen. Larger sized particles require more severe treating conditions as evidenced by comparing treatment of 4–8 mesh and 1/4–3/8-in. samples. Conditions required to decake coal could be met at commercial coal gasification plants with little additional expenditure of energy. However, gasification plants commonly use coal of particle size larger than used here. We were limited to a maximum size of 3/8 in. by the swelling of the coal and the diameter of the treater. A treater of larger diameter would be required to determine the optimum conditions for larger particles.

With larger sized particles of 3/8 in., the size of the expanded coal particle was an appreciable part of the free tube cross-section. Additional studies should be made in a larger pretreater to determine optimum conditions of operation.

Literature Cited

(1) Forney, A. J., Kenny, R. F., Gasior, S. J., Field, J. H., *Ind. Eng. Chem. Prod. Res. Develop.* 3, 48 (1964).
(2) Gasior, S. J., Forney, A. J., Field, J. H., *Mining Eng.* 74-78 (March 1965).
(3) Gasior, S. J., Forney, A. J., Field, J. H., *Ind. Eng. Chem. Prod. Res. Develop.* 3, 43 (1964).
(4) Oppelt, W. H., Perry, H., MacPherson, J. L., Vitt, E. J., *U.S. Bur. Mines Rept. Invest.* 6721 (1966).
(5) Von Fredersdorff, C. G., Elliott, M. A., "Chemistry of Coal Utilization," suppl. vol., H. H. Lowry, ed., p. 990, Wiley, New York, 1963.

RECEIVED November 21, 1966.

2

Coal Pretreatment in Fluidized Bed

V. J. KAVLICK and B. S. LEE

Institute of Gas Technology, Chicago, Ill.

A 10-in. diameter continuous fluidized-bed reactor system is being operated to produce nonagglomerating coal from high volatile bituminous coal by mild surface oxidation. Minimum pretreatment is defined by acceptability of the coal as a feed to the hydrogasifier. This corresponds to 24–26% volatile matter in the pretreated coal. The following operating variables, in the order of importance, contribute to satisfactory pretreatment—reaction temperature of 725°–750°F., oxygen reacted:coal feed ratio of 1.0:1.5 std. cu. ft./lb., and a coal residence time of 1–2 hours.

During development of the IGT coal hydrogasification process for making synthetic pipeline gas (*4, 7*), the most reactive part of coal for producing methane was found to correspond to its volatile matter. Therefore, research efforts were concentrated on high volatile bituminous coals. However, when such coals were exposed to an atmosphere of hydrogen at high temperature and pressure, rapid and severe fusion of the coal particles caused caking and agglomeration in the reactor bed. To prevent this agglomeration, the coal must be pretreated to destroy its agglomerating tendency before being used as hydrogasification feed. This program was initiated to establish operating conditions that would produce, with a minimum of pretreatment, a nonagglomerating material that retains maximum volatile matter, and to supply sufficient feed for the hydrogasification test program.

Background

Much work has been reported on the destruction of caking properties of coal. Low temperature carbonization, if carried far enough, drives off enough volatile matter so that the remaining char does not agglomerate. Examples of this are Consolidation Coal Co.'s Montour char used in much of the early hydrogasification work, and the more recent char

produced by FMC Corp. by multistage pyrolysis (*6*). However, the Montour char contains only about 17% volatile matter, while the original Montour bituminous coal contained 31%.

Several investigations (*2, 3, 5*) concluded that the agglomerating tendency is destroyed by oxidizing the surface of the coal particles. Treatment in small fluidized-bed reactors with nitrogen, steam, carbon dioxide, or helium (*2, 3*) all failed to destroy the caking properties. However, adding a small amount of oxygen to these inert gases produced nonagglomerating coal. Minimizing pretreatment, therefore, requires minimizing the extent of such oxidation.

Investigators agree that since oxidation is involved, a fluidized bed would be necessary to dissipate the heat released and to maintain a uniform bed temperature without hot spots. However, much of the reported work was conducted in small batch reactors (*2, 3*). In a large continuous unit, the uniformity of pretreatment and the residence time required would be quite different. In addition, batch reactors, after being charged, require a time to heat the charge up to the reaction temperature.

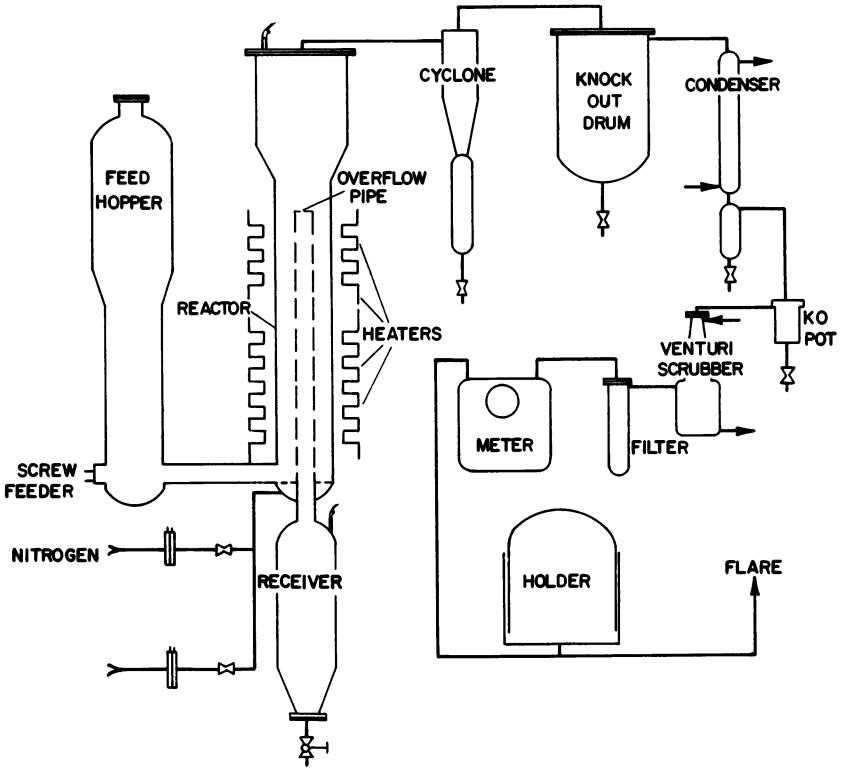

Figure 1. Continuous-feed coal pretreatment unit

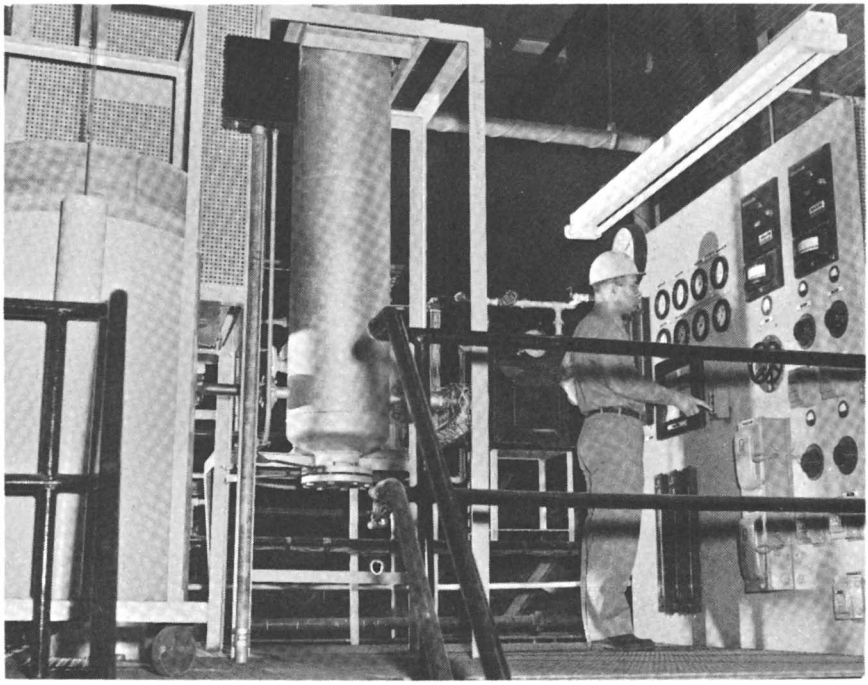

Figure 2. Fluid-bed pretreater, feed hopper, and panel board

This makes the residence time at reaction temperature uncertain. A continuous operation avoids this problem, but the backmixing in a fluidized bed leads to short-circuiting of some untreated coal. For this program, a continuous unit capable of fairly high throughput was designed and built.

Equipment and Procedure

The pretreater system is shown schematically in Figure 1. Figures 2 and 3 give actual views of some sections. The pretreater is a 10-in. Schedule 40 pipe, 15 ft. long, made of A-335 alloy. The upper portion is enlarged for solids disengagement. Heat is supplied to the reactor by external electrical heaters. The bottom 76 inches of the reactor are heated by a 12-kw. furnace. The next 56 inches are surrounded by four zones of heaters, each with four Hevi-Duty heating elements, providing 2.7 kw. per zone. The enlarged portion of the reactor is heated by six 1-kw. strip heaters. Variable voltage transformers control the power input to the heaters, which are needed primarily at start-up. Once the reaction is initiated, little external heat is required.

A 1/8-in. thick sintered stainless steel plate serves as the gas distributor. Preheated inlet gas enters a plenum chamber and then passes through the distributor. Offgases pass through a cyclone for fines removal and then to a knockout pot for heavy tar condensation. After the gas is

cooled in a water-jacketed condenser, the oils and water are collected. A final venturi water scrubber and cartridge filters remove the oil and tar mist from the gas. The gas is then metered, sampled, and vented.

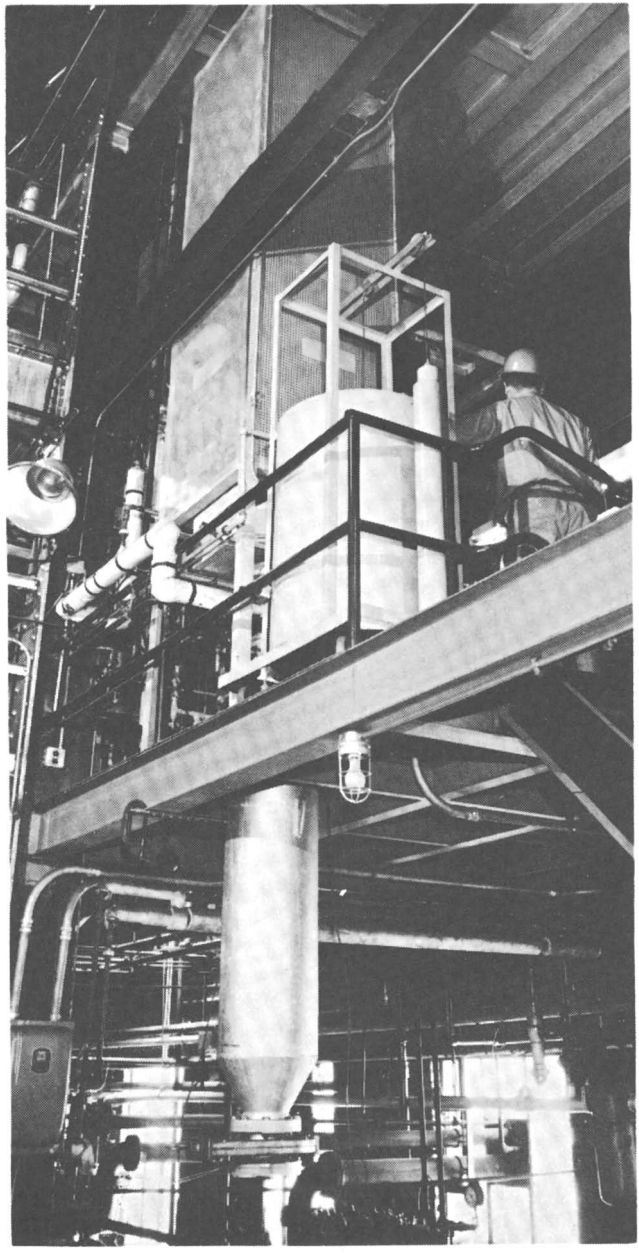

Figure 3. Fluid-bed pretreater and residue receiver

The coal is crushed in a hammer mill, dried, and then screened to −16 + 80 mesh. About 500 lb. of coal are charged to a hopper, which is connected at the bottom to the pretreater by a screw feeder. The feed enters the pretreater about 6 inches above the distributor plate. Feed rates of up to 100 lb./hr. can be attained. A 3-in. diameter overflow pipe controls the bed height. The overflow collects in a receiver and is periodically dumped into drums. Fines from the bed were originally returned to the bed by an internal cyclone with a dipleg sealed in the bed, but tar tended to build up in the cyclone and caused the reactor pressure to increase. At present, a heated external cyclone with a collector pot is installed and operates much more smoothly.

Temperature is measured and recorded by a group of thermocouples in the bed at several levels, and pressure taps at various points indicate the state of fluidization. Both gases and solids are sampled and analyzed.

In addition to chemical analyses, an agglomeration test was performed on each sample to give a quick indication of the degree of pretreatment. This test is a modified version of that reported by Forney *et al.* (3). A sample in a stainless steel wire mesh boat is placed in a quartz tube heated by an electric furnace. Nitrogen is purged through the system while the temperature is brought up to 1400°F. Hydrogen is then passed through the system for 1/2 hr.; nitrogen is again used during cooling. We found that the Bureau of Mines test (3) was too mild at 600°C. (1112°F.) and too strong at 900°C. (1652°F.) and did not correspond to the hydrogasifier conditions. With our conditions, materials that are free-flowing or slightly crusted would pass through the hydrogasifier without difficulty.

Discussion of Results

Of the coals to be studied in this project, attention was focused on high volatile bituminous coal. Most of the work was devoted to Pittsburgh No. 8 seam coal from Ireland mine, with some tests on Ohio No. 6 seam coal from Broken Arrow mine and a highly volatile West Virginia No. 5 block coal. Proximate and ultimate analyses of these are given in Table I. Typical run data and product analyses are shown in Table II.

Besides the visual evaluation from the agglomeration test, the volatile-matter content was chosen as the quantitative index of pretreatment severity. Operating experience with the hydrogasifier showed that minimum coal pretreatment must reduce the volatile matter to 24–26%. Various aspects of pretreatment are discussed in more detail below.

Pretreatment Temperature. Perhaps the most critical operating variable is temperature. The coals tested have a plastic point temperature around 700°F. Below this temperature, we could not produce a free-flowing coal with a 2-hr. residence time and a wide range of oxygen concentrations in the pretreatment gas. On the other hand, localized combustion begins at bed temperatures near 775°F. The heat released can not be dissipated by the bed, and runaway temperature results.

Table I. Analyses of High Volatile Content Bituminous Coals Tested in Pretreater

Coal Source	*Pittsburgh No. 8 Ireland Mine*	*Ohio No. 6 Broken Arrow Mine*	*West Virginia No. 5 Block*
Run No.	FP-44	FP-38	FP-48
Proximate Analysis, wt.%			
Moisture	1.1	2.4	1.1
Volatile Matter	34.7	40.2	34.6
Fixed Carbon	52.5	52.5	56.5
Ash	11.7	4.9	7.8
Total	100.0	100.0	100.0
Ultimate Analysis (dry), wt.%			
Carbon	71.1	75.3	77.1
Hydrogen	5.01	5.63	5.25
Sulfur	4.04	3.53	1.17
Ash	11.88	5.00	7.86
Screen Analysis, USS, wt.%			
+20	3.2	4.5	4.0
+30	21.7	23.8	21.0
+40	24.6	24.3	22.7
+60	26.4	25.4	24.4
+80	12.4	11.3	12.6
−80	11.7	10.7	15.3
Total	100.0	100.0	100.0

Similar observations were made by Agarwal *et al.* (*1*) in operating a fluidized coal dryer. They noted that combustion occurred on the air distributor deck when stagnant pockets of coal caused by poor gas distribution reached temperatures of about 800°F. Consequently the practical pretreatment temperature range is quite narrow—between 725° and 750°F. The necessary close temperature control can be maintained with a fluidized bed.

Extent of Coal Oxidation. Since pretreatment is an oxidation process, the extent of oxidation is clearly related to the extent of pretreatment. We found that minimum pretreatment required reaction of more than 1.0 std. cu. ft. of oxygen per pound of coal fed. Figure 4 shows the region of operation in terms of temperature and oxygen consumption required for successful pretreatment. Increasing the oxygen consumption would produce more and more devolatilized coal, which is contrary to our desire to peserve as much volatile matter as possible. Minimum pretreatment, therefore, requires oxygen consumption of 1.0–1.5 std. cu. ft./lb. of coal fed.

We investigated the effect of oxygen concentrations ranging from 2 to 21% (air) by volume in the pretreatment gas by blending the

Table II. Operating Data and Product

Coal Source	*Pittsburgh No. 8*			
Run No.	FP-11	FP-14	FP-25	FP-31
Temperature, °F.				
Average	765	666	749	750
Maximum	775	698	757	751
Coal feed rate, lb./hr.	49	76	37	18
Coal residence time, min.	53	51	111	228
Feed gas rate, std. cu. ft./hr.	603	590	760	584
Oxygen concentration, vol.%	21.0	9.8	9.8	9.9
Oxygen/Coal, std. cu. ft./lb.	2.6	0.76	2.0	3.2
Agglomeration test results[a]	C	C	F	F
Proximate Analysis, wt.%				
Moisture	0.4	0.3	1.0	0.8
Volatile Matter	27.4	30.3	24.7	21.3
Fixed Carbon	58.5	55.6	65.0	63.8
Ash	13.7	13.8	9.3	14.1
Total	100.0	100.0	100.0	100.0
Ultimate Analysis (dry), wt.%				
Carbon	69.8	69.7	72.0	69.2
Hydrogen	4.11	4.33	3.81	3.37
Sulfur	[b]	[b]	[b]	[b]
Ash	13.74	13.88	9.38	14.21

[a] C = caked, F = free flowing, PC = partially caked.

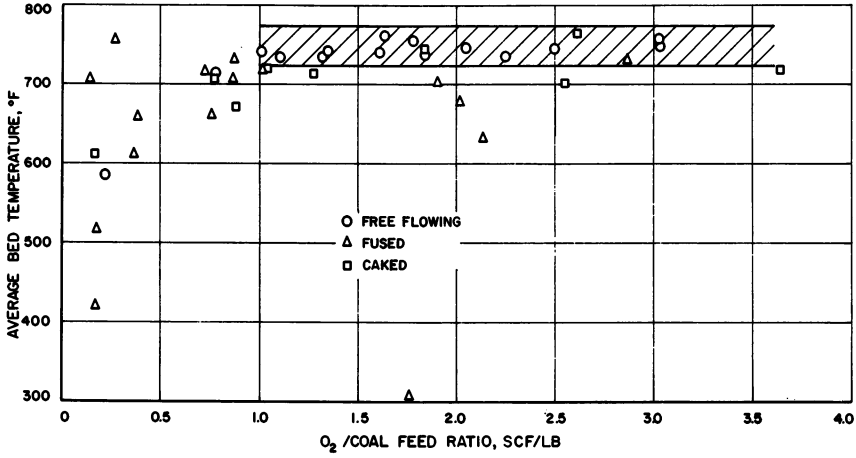

Figure 4. Pretreatment results as a function of bed temperature and unit oxygen consumption

Analyses of Selected Pretreatment Runs

Ohio No. 6			*W. Va. No. 5*
FP-33	FP-35C	FP-39	FP-48
749	634	739	738
752	648	746	744
28	56	47	51
120	116	98	81
630	574	663	619
10.5	21.0	9.3	5.9
2.4	2.1	1.3	0.72
F	C	F	PC
0.3	0.4	1.5	0.3
24.6	36.6	26.6	25.2
68.6	58.5	66.9	67.9
6.5	4.5	5.0	6.6
100.0	100.0	100.0	100.0
75.7	74.9	74.9	77.9
3.85	4.91	3.83	4.33
[b]	[b]	2.75	0.96
6.56	4.49	5.09	6.59

[b] Not analyzed.

correct amounts of air and nitrogen. The oxidation rate was rapid enough to consume all the oxygen fed so no oxygen breakthrough was noted in the effluent gas. Pretreatment is governed by the amount of oxygen which has reacted rather than by the oxygen concentration. However, at high oxygen concentration, faulty gas distribution leads to localized combustion. Moreover, with the fluidizing velocity essentially fixed by the coal particle-size distribution, the coal residence time must be shortened at the higher oxygen concentration to maintain the same oxygen consumption per pound. We found 10% oxygen to be satisfactory. In large scale operations, such a mixture can be obtained cheaply by adding air to the recycled pretreater effluent in the proper proportions. We are, however, studying the use of air (21% oxygen) in pretreatment.

Coal Residence Time. Because the oxidation rate is fast, there is essentially no residence time required for chemical reaction. In a plug flow reactor, coal feed rate would depend only on the oxygen input rate and the unit oxygen consumption. Moreover, if gas distribution is uniform, the oxidation would be uniform. In a continuous fluidized-bed reactor, however, residence time must be long enough to minimize the effect of the short-circuiting of untreated feed into the product. The

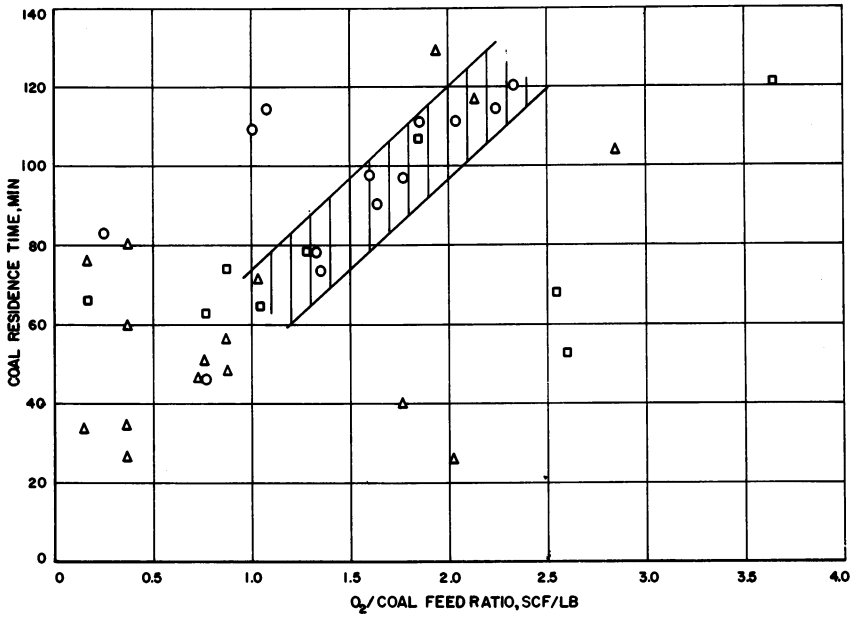

Figure 5. Pretreatment results as a function of coal residence time and unit oxygen consumption

solids' mixing in the fluid bed results in a coal particle-age distribution and hence a distribution in the extent of oxidation. Therefore, the average residence time and unit oxygen consumption are greater for a continuous fluidized bed than for a batch unit. Also, gas of higher oxygen concentration cannot be used with a correspondingly higher coal feed rate—and hence shorter residence time—to maintain the same unit oxygen consumption because shortened residence time leads to increased short-circuiting of untreated coal. If the residence time is not shortened, the volume of bed material required would exceed the capacity of our unit. So most of our work has been done at oxygen concentrations of 10% or less.

Figure 5 shows the region of operation for successful pretreatment in terms of coal residence time and unit oxygen consumption. The two are related in almost direct proportion. Residence times of 1/2–2-1/2 hr. were investigated. Minimum pretreatment at reasonable feed rates requires coal residence times of between 1 and 2 hours.

Petrographic Study. To understand better the mechanism of the pretreatment reaction, samples of coal before and after pretreatment were mounted and examined petrographically (*8*). A skin of high reflectance was formed on the coal particles by the surface oxidation. Variation in the skin thickness was not significant, indicating rapid sur-

face reaction and slow penetration below the skin. Short-circuited untreated coal particles can be identified as those without this skin. A free-flowing sample had fewer "skinless" particles than a sample that caked.

Acknowledgment

The work reported here was under co-sponsorship of the American Gas Association and the U.S. Department of Interior, Office of Coal Research. Permission of the sponsors to present this paper is greatly appreciated.

Literature Cited

(1) Agarwal, J. C., Davis, W. L., King, D. T., *Chem. Eng. Progr.* **58**, 85 (1962).
(2) Chanabasappa, K. C., Linden, H. R., *Ind. Eng. Chem.* **48**, 900 (1956).
(3) Forney, A. J., Kenny, R. F., Gasior, S. J., Field, J. H., *Ind. Eng. Chem. Prod. Res. Develop.* **3**, 48 (1964).
(4) Huebler, J., Schora, F. C., *Chem. Eng. Progr.* **62**, 87 (1966).
(5) Jenkins, G. I., "Chemical Engineering in the Coal Industry," pp. 25-31, Pergamon Press, London, 1956.
(6) Jones, J. F., Eddinger, R. T., Seglin, L., *Chem. Eng. Progr.* **62**, 73 (1966).
(7) Linden, H. R., *Chem. Eng. Progr. Symp. Ser.* **61** (54), 76 (1965).
(8) Mason, D. M., Schora, F. C., ADVAN. CHEM. SER. **69**, 18 (1967).

RECEIVED December 22, 1966.

3

Coal and Char Transformation in Hydrogasification

D. M. MASON and F. C. SCHORA, JR.

Institute of Gas Technology, Chicago, Ill.

Petrographic and related properties of high volatile bituminous coal at different stages in the hydrogasification process were investigated. Coal particles inflate to cenospheres when pretreated with diluted air in a fluid bed at elevated temperature to destroy agglomerating power. The loss of agglomerating power is attributed to formation of a skin of reacted coal that can be distinguished by its high reflectance. We believe this skin tends to remain rigid and limits further enlargement of particles during the later high temperature stages of the process. The pretreated particles and the residue particles after hydrogasification in a moving bed vary greatly in structure and reflectance.

In the present IGT hydrogasification program we have undertaken a study of the petrographic and physical properties of the coals used and the chars produced in the various stages of the gasification process. In the past, we have attempted to study the kinetics and operation of the system without knowing what was really happening to the coal. The usual chemical analyses were conducted, but the results fell far short of indicating what was occurring within the individual coal particles. Also we believed that the identification of what made coal desirable for gasification might hinge on more than the usual coal analysis. We therefore began a study of the petrographic and physical properties of coals and chars, which had two objectives:

(1) To find out as much as possible about what happens to the coal and how it behaves in the process.

(2) To develop a correlation between the petrographic properties of coals and their suitability for hydrogasification.

Changes in the process concept as it is developed add to the complexity of the second objective. For example, if pretreatment becomes

unnecessary as a result of process improvements, the assessment of a coal's suitability may be substantially modified, as will be shown. The work reported here applies mainly to the first objective although it provides a background for the second.

For the process study, nine coals ranging in rank from low volatile bituminous to lignite have been selected. Of these, high volatile strongly caking coal from the Pittsburgh No. 8 seam was selected for the initial and most extensive hydrogasification study because it was expected to be the most difficult to process. The work reported here is limited to this coal.

In the hydrogasification process the coal is treated in three successive stages:

(1) Pretreatment to destroy the agglomerating power of the coal.

(2) First-stage hydrogasification, at 1200° to 1300°F., with pretreated coal as the feed.

(3) Second-stage hydrogasification, at 1700° to 2000°F., with first-stage residue as the feed.

The chars resulting from each of these stages as well as the initial coal feed have been examined.

Experimental

We mounted samples of feed coal in epoxy resin under hydraulic pressure as described by Cole and Berry (*2*). An apparatus and procedure for vacuum-mounting the fragile chars was developed and is described elsewhere (*8*). Samples of pretreated coal and hydrogasification residue were sieved, and tests were made on the sieve fractions to avoid error from size segregation.

Petrographic observations were made with a Zeiss Universal microscope. A 40×, 0.65 N.A. Antiflex oil immersion objective and 12.5× Kpl eyepieces were used for maceral analysis. Reflectance in oil was determined at a wavelength of 548 mμ, essentially as described by Schapiro and Gray (*10*) and by Harrison (*5*), though our microscope is a different make. A Zeiss 40×, 0.85 N.A. achromat "Auff POL" oil immersion objective and the same kind of eyepiece as above were used. The aperture in the eyepiece restricted the field to about a 2.5-μ diameter. Zeiss immersion oil with a refractive index of 1.515 at 20°C. was used. To obtain a more easily adjustable signal for our fixed-range recorder, we modified the output circuit of the Photovolt 520M photometer. A switch and 2000-ohm potentiometer were added so that in one switch position the photometer output meter was operative and the recorder signal could be taken in the original mode of the instrument, while in the other position the signal could be taken from the potentiometer.

Glass standards obtained from Bituminous Coal Research, Inc., were used for reflectance calibrations below 2%. For reflectance calibrations above 2%, a brilliant-cut diamond mounted in Bakelite was used as a standard. The refractive index of diamond at 548 mμ was obtained from the equation of Schrauf (*9*); the reflectance (5.32%) was calculated

from the refractive index according to the Fresnel formula for normal incidence.

Porosities of char samples were calculated from the particle density and true density. The particle density was determined by Ergun's gas flow method (3), which we shortened by making measurements with only three rates of flow at each of two bed densities. The estimate of the standard deviation from 21 duplicate determinations was 7%. We determined true density by helium displacement in a Beckman air pycnometer.

Table I. Typical Analyses of Ireland Mine Coal Fed to Pretreater

Proximate Analysis, wt. %	
Moisture	0.9
Volatile Matter	32.7
Ash	14.1
Fixed carbon	52.3
Total	100.0

Ultimate Analysis (Dry Basis), wt. %	
Carbon	67.6
Hydrogen	4.62
Sulfur	4.33
Nitrogen	1.18
Ash	14.22
Oxygen (by difference)	8.05
Total	100.00

Petrographic Analysis, vol. % (mineral-matter-free)	
Vitrinite	88
Exinite	2
Resinite	Trace
Fusinite	1
Semifusinite	4
Micrinite	5
Total	100
Mean maximum reflectance of vitrinite: 0.68%	

Sieve Analysis, USS, wt. %	
20	3.7
−20+30	22.4
−30+40	24.8
−40+60	25.5
−60+80	11.7
−80+100	5.2
−100+200	4.3
−200+325	1.1
−325	1.3
Total	100.0

Results

Feed Coal and Pretreatment. Pittsburgh No. 8 coal was obtained from the Ireland mine of the Consolidation Coal Co. Proximate, chemical, sieve, and maceral analyses of the feed to a typical pretreatment run are given in Table I. As discussed later, the important petrographic characteristics of the coal are the mean maximum reflectance of the vitrinite and the content of (1) exinite, the group of macerals having the lowest reflectance and highest hydrogen content; (2) vitrinite, the component constituting the bulk of the coal and having an intermediate reflectance and hydrogen content; and (3) the inertinite group (fusinite, semifusinite, and micrinite) having a high reflectance and low hydrogen content.

Pilot plant pretreatment of the coal to destroy its agglomerating power consists of treating the crushed coal with nitrogen-diluted air in a continuous, single-stage fluid bed at 700°–800°F. The most striking feature of the pretreated coal particles (Figure 1) is their inflation to cenospheres. Because of the mixing in the fluid bed and the resulting variations in particle residence times, the extent of modification varies greatly from particle to particle. A few have a reflectance as low as that of the original coal and appear to be unchanged, with exinite still present in attrital areas. Appearance of vesicles (a term we have chosen in

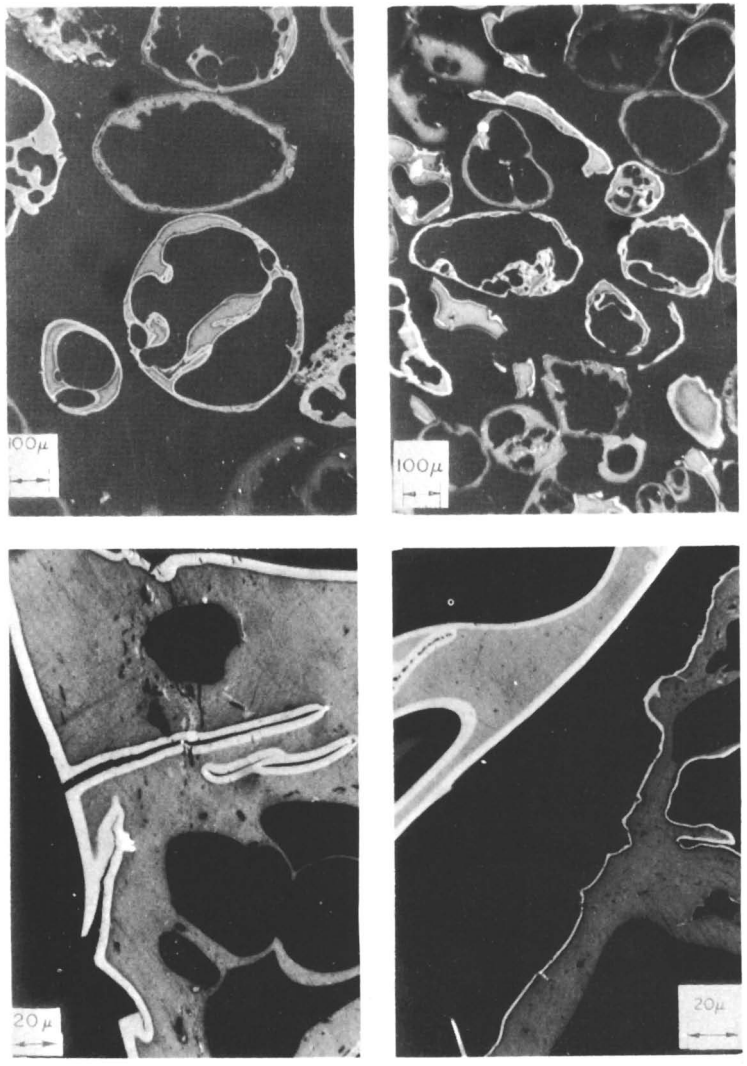

Figure 1. Pretreated coal

preference to "pore" because these cavities are generally unconnected) and increase in the reflectance occur as the pretreatment progresses. Micrinite becomes difficult to distinguish; fusinite and semifusinite remain intact. An outer zone of reflectance greater than that of the interior appears on most particles. The high reflectance of this skin is attributed to reaction with oxygen; there was no indication, such as uneven thickness or development of a similar skin on fusinite particles, that the skin was formed by condensation of tar on the particle surface. Increased reflectance in the mass of the particle is apparently caused by carbonization only. Reflectance of the skin ranges from 2 to 2.6%; reflectance of the interior ranges from about 0.8%, as observed on the vitrinite of the original coal, up to about 2%. The skin extends into cracks and is present in the interior of some vesicles, though usually with reduced thickness.

A quantitative measure of swelling from pretreatment is given by the porosities of two sieve fractions: 66% for the −30+40 mesh fraction, and 59% for the −60+80 mesh fraction (Table II).

Hydrogasification Residues. Residues from first- and second-stage hydrogasification runs that are believed to represent typical conditions for the integrated process were chosen for intensive study. In the first-stage run the pretreated coal reacted with a hydrogen-natural gas-steam mixture containing 30 mole % steam, 43 mole % hydrogen, and 27 mole % hydrocarbon. The bed temperature averaged 1205°F., and the pressure was 1030 p.s.i.g. About 21% of the pretreated coal (m.a.f.) was gasified. In the second-stage run, the residue from a first-stage run reacted with a hydrogen-steam mixture containing 39 mole % steam. The temperature averaged 1825°F., and the pressure was 1023 p.s.i.g. About 52% of the feed (m.a.f.) was gasified, equivalent to 41% of the pretreated coal. Residence time of the coal was 36 minutes in each run.

Table II. Particle and True Densities of Hydrogasification Feed and Residue

Sample	*Sieve Size, USS*	*Density, grams/cc.*		*Porosity, %*	*Ash Content (Moisture-Free), wt. %*
		Particle	*True*		
Pretreated coal	−30+40	0.51	1.52	66	13.7
	−60+80	0.63	1.53	59	15.6
Residue, 1st-stage hydrogasification	−30+40	0.48	1.80	73	17.3
	−60+80	0.54	1.77	70	19.1
Residue, 2nd-stage hydrogasification	−30+40	0.69	2.10	67	33.0
	−60+80	0.95	2.64	64	54.2
Residue, free-fall hydrogasification	−30+40	0.26	2.13	88	—

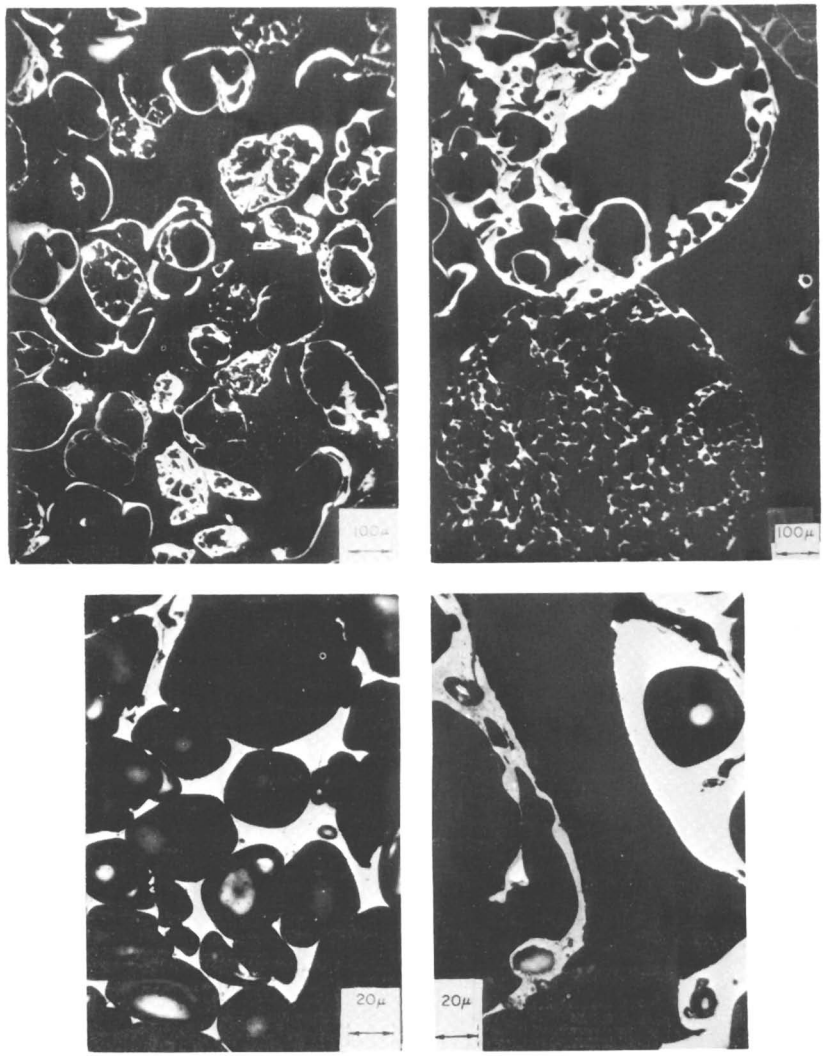

Figure 2. Residue from first-stage hydrogasification

In a petrographic examination of the first-stage residue, no trace of the high reflectance skin that is conspicuous in the pretreated coal was present in any particle (Figure 2). Occasional particles of the second-stage residue had a dark skin (Figure 3). Kinship of this dark skin with the pretreatment skin was evident from their similarity in form and in pattern of occurrence, particularly in cracks and around vesicles. While the contrast gives an appearance of darkness to this skin, measurements showed that the reflectance of this "dark" skin was actually greater than

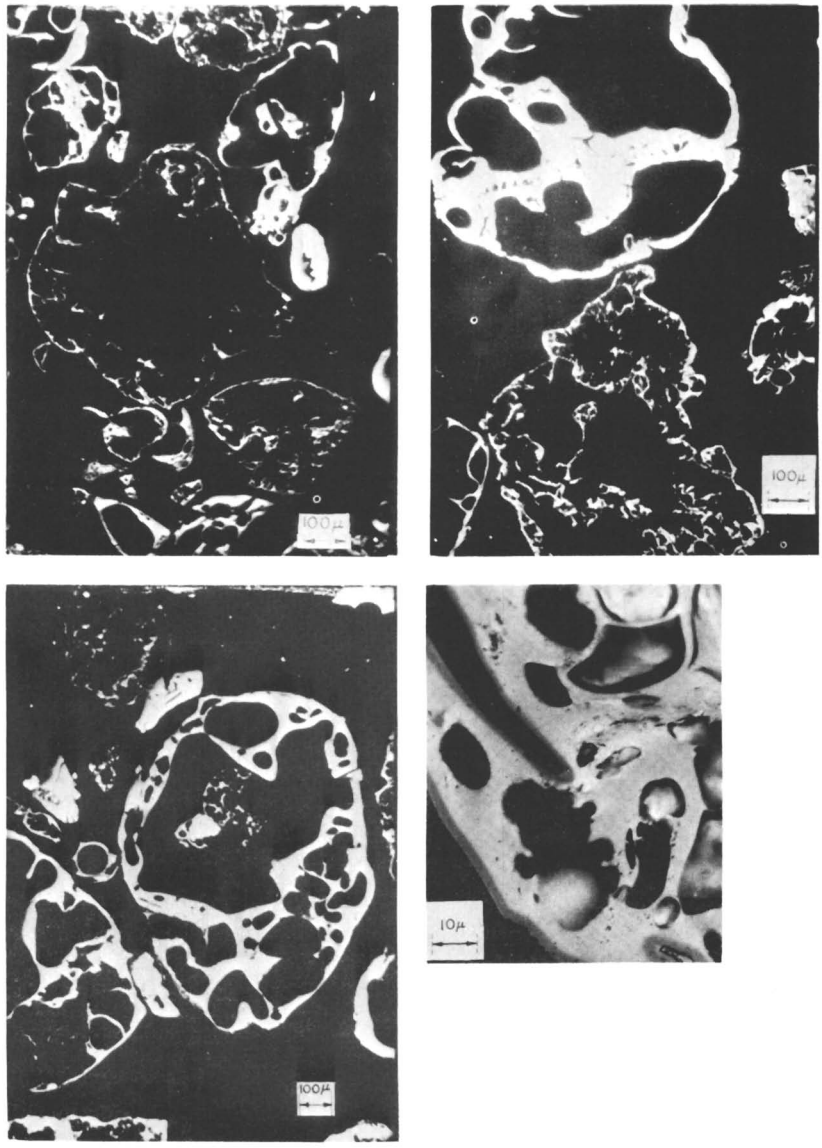

Figure 3. Residue from second-stage hydrogasification

that of the skin of the pretreated coal. Evidently the reflectance of the substrate had, during the second stage, increased more rapidly and become greater than that of the skin.

Particles from both first- and second-stage runs showed a great variation in both reflectance and structure. Some particles appear unchanged in structure from the pretreated coal. In others, additional

vesicles, particularly small ones, have formed in addition to those present in the pretreated coal. In some of the particles, the vesicle walls are extremely thin or have partly disappeared to leave a skeleton structure. In these highly inflated particles, the exterior wall frequently appears more substantial than the interior vesicle walls, which may be an effect of the pretreatment skin.

Particles from a run in which untreated coal was fed were also examined. This coal was from Pittsburgh No. 8 seam but from a different mine—Consolidation Coal Co.'s Montour 4 mine. The hydrogasification reaction was conducted entirely in 18 feet of free fall. The run could not be completed because of gradual caking of coal in the feed tube and in the reactor. However, the structure of the residue that was obtained is of interest (Figure 4). It is much more uniform in appearance and reflectance than residues from runs with pretreated coal. Almost all of the particles have a degenerate foam structure—*i.e.*, they are filled with

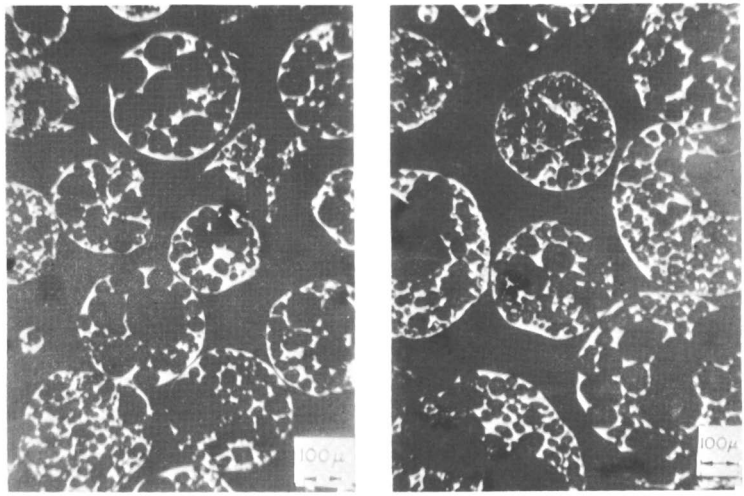

Figure 4. Residue from free-fall hydrogasification

small vesicles or cells, many of whose walls have broken, leaving a skeletal structure. The exterior walls sometimes appear thicker than interior walls, resembling to some extent the pretreated coal residue. However, the free-fall particles show numerous holes in their exterior walls that are absent in the pretreated coal residue. Also, the particle density and porosity (Table II) show that the particles have, on the average, swelled much more than residue from pretreated coal.

The free-fall residue also differs from the pretreated coal residue in that it has a grainy or mottled texture (Figure 5) in contrast to the smooth, unmottled appearance (except for small voids) of most particles

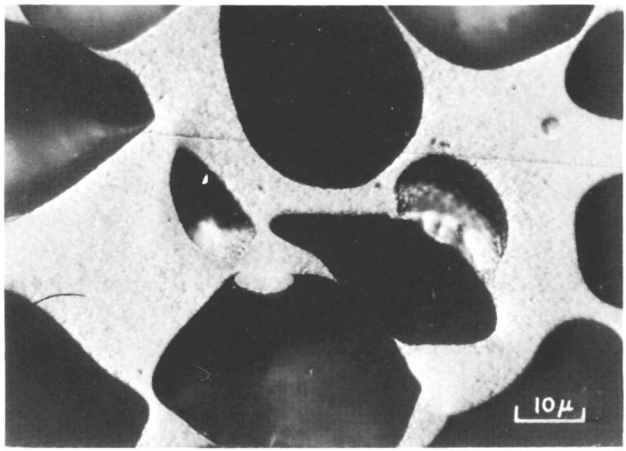

Figure 5. Texture of free-fall residue from untreated coal

of residue from pretreated coal (Figure 6). A few particles of the latter have a foam structure and a mottled texture and are probably derived from feed particles that escaped pretreatment. Also, this material occasionally appears as a cement in agglomerated particles of the residue from pretreated coal; this and its foam structure indicate that it has passed through a fusion stage. Fusion of these particles is also indicated by their anisotropy, according to theories of coking and graphitization (*6*). The anisotropy is attributed to the formation of microscopic regions where the molecules are ordered in a pregraphitic layer structure. With a quartz, length-fast, first-order red plate and crossed polars under high magnification, the mottling appears as red rods, roughly 0.2×1 μ in size, in an anisotropic (blue or yellow) matrix. Unmottled residue particles from pretreated coal show only occasional small areas of anisotropy around vesicles.

Discussion

From previous work it is known that a high hydrogen-to-carbon ratio, a low rank, and a high content of volatile matter are conducive to high reactivity in hydrogasification (*4*). Thus, the inertinite group (fusinite, semifusinite in part, and micrinite) is expected to be unreactive. It is also known that the reflectance of the vitrinite in a coal is a good indicator of its rank and volatile matter content. Thus, if pretreatment were not necessary, both high exinite content and low reflectance of the vitrinite would be desirable. However, with the present degree of pretreatment, in which exinite is largely destroyed, this component is of little value. Similarly, with caking coals full value cannot be obtained

from the increasing reactivity and potential yield indicated by the decreasing reflectance of the vitrinite. Thus our second objective—characterizing coal with respect to its suitability for hydrogasification—depends greatly on process development in this area. There is some likelihood that in a large commercial plant pretreatment can be avoided.

Pretreatment affects the process in other ways. Sieve analyses of residues from the first stage of hydrogasification show no increase (sometimes a small decrease) in average particle size; thus, essentially no additional swelling of the coal particles occurs in this stage, although the rate of heating is probably as high as and the loss of volatiles more than in pretreatment. We attribute the dimensional stability of the particles to rigidity of the pretreatment skin. The few particles that escaped substantial pretreatment no doubt swell, but this may be balanced by attrition and gas-solid reaction on the exterior surface of the particles. Later runs with less severely pretreated coal show that additional swelling can occur in this stage. Additional swelling may be advantageous because the larger particles present a greater amount of easily accessible surface for reaction. Also, they settle or fall more slowly in free fall, thus providing a longer reaction time for such a stage. On the other hand, swelling in which the pretreatment skin is disrupted and liquefied coal is exposed may lead to excessive agglomeration.

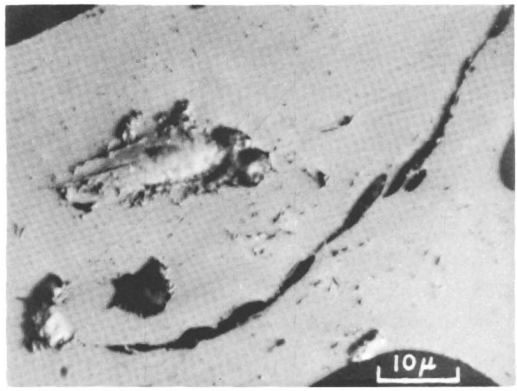

Figure 6. Texture of residue from pretreated coal

The first-stage residue shows an increase in average porosity (Table II), which we attribute to gasification (including pyrolysis) of the coal in the interior of the particle.

In the second stage of hydrogasification, the particle size of the char decreases several percent. We attribute this mainly to attrition, although there may be some decrease in the average diameter caused by gasification reactions on the exterior surface. Decreased porosity (Table II) is

attributed to attrition of char particles, which leaves a greater proportion of low porosity shale particles.

The particle-to-particle variation of the structure and reflectance of the residue is of interest because it probably indicates variation in reactivity. The possibility that the subclass of vitrinite in the original coal may have an effect has been considered. There is the well-known differentiation between telenite and collinite in the Stopes-Heerleen system (7). Others have preferred the subclassification—attrital and non-attrital vitrinite (1)—which preserves a feature of Thiessen's system (7). However, many of our coal particles are not composed of a single sub-

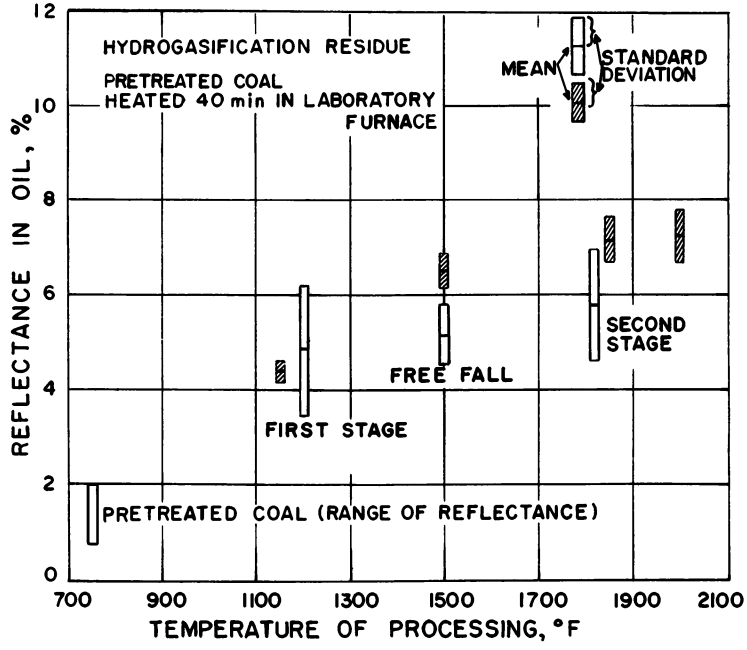

Figure 7. Reflectance of hydrogasification feed and residues

class, while individual residue particles are rather uniform in both structure and reflectance (except for the particles that contained fusinite or semifusinite). Thus it appears that the history of the particle in the process is a likelier source of the observed variation although the vitrinite subclass may have a minor role. Structural variation can easily be explained on the basis of particle-to-particle variation in the amount of pretreatment; extended pretreatment of a particle results in greater loss of both volatile matter and the potential for plasticity at higher temperature. Thus in the subsequent hydrogasification stage, such particles de-

velop less internal pressure and, in addition, are more resistant to the flow needed to develop additional vesicles.

The large variation in reflectance is more difficult to explain. The average reflectance of residue particles of the three hydrogasification runs that have been discussed are plotted against run temperature in Figure 7.

Table III. Reflectance of Pretreated Coal and Char Heated in Hydrogen at 1850°F.

		Reflectance in Oil, %	
Sample	*Time of Heating, min.*	*Mean*	*Standard Deviation*
Pretreated coal	10	6.90	0.38
	20	7.36	0.50
	40	7.17	0.47
	120	7.41	0.72
Residue, second-stage hydrogasification	0	5.78	1.19
	20	6.83	1.32
	40	6.74	1.53

The standard deviations of the reflectance readings (one per particle) are also shown to indicate the particle-to-particle variation. For comparison we also show the reflectance of pretreated coal heated for 40 minutes at temperatures in the same range. The residues from the two moving-bed hydrogasification runs show much greater variations than either the heated coal or the residue from the free-fall hydrogasification run. The bed temperature, as measured by an internal thermocouple, differed by less than 100°F. from the average reactor-wall temperature (the normal or reported one) throughout the bed of coal, which has a 36-minute residence time. However, the temperature of the more reactive individual particles may rise substantially above the bed temperature because of the heat evolved in the reaction, particularly in the first stage where the feed is highly reactive. We think this explains the origin of the high reflectance particles of the first-stage residue. The low reflectance of other particles, particularly in the second-stage residue, is not as easily explained. To obtain more information on this question, samples of pretreated coal and second-stage residue were heated in a laboratory tube furnace in hydrogen at atmospheric pressure. The data, reported in Table III, show that the length of the heating period at 2850°F., from 10 minutes to 40 minutes, had little effect on the reflectance of the laboratory-heated samples of pretreated coal and that the wide range of reflectance of the second-stage hydrogasification residue was retained when it was heated to the same temperature. Also it should be noted that the rise in reflectance with temperature is not very steep above 1300°F.

Conclusions

From this work we tentatively conclude that:

(a) The reflectance of the residue particles does not depend solely on the maximum temperature to which they have been subjected.

(b) Variation in the amount of pretreatment can explain only a part of the observed particle-to-particle variation of reflectance of the residue.

(c) Particle-to-particle variations in the temperature and length of hydrogasification processing, such as might be caused by channeling and bypassing, are not the main cause of the reflectance variation.

(d) The wide range of reflectance is probably an effect of the prolonged treatment with high pressure hydrogen or steam, or both. A possible mechanism is the enlargement of submicroscopic pores, which would reduce the refractive index and thus the reflectance. Greater reaction in one particle than in another could occur if the reaction is self-accelerating.

Acknowledgments

Richard Chang and Mouin Saadeh made some of the measurements. The advice of G. H. Cady, consultant on petrography, is gratefully acknowledged.

Literature Cited

(1) Brown, H. R., Cook, A. C., Taylor, G. H., *Fuel* **43**, 111 (1964).
(2) Cole, D. L., Berry, W. F., "Preparation and Polishing of Coal and Coke for Petrographic Analysis," Bituminous Coal Research, Inc., Monroeville, Pa., 1965.
(3) Ergun, S., *Anal. Chem.* **23**, 151 (1951).
(4) Feldkirchner, H. L., Linden, H. R., *Ind. Eng. Chem. Process Design Develop.* **2**, 153 (1963).
(5) Harrison, J. A., *Proc. Illinois Mining Inst.* **69**, 18 (1961).
(6) Kipling, J. J., Shooter, D. V., *Carbon* **4**, 1 (1966).
(7) Krevelen, D. W. van, "Coal," pp. 66-70, Elsevier, Amsterdam, 1961.
(8) Mason, D. M., *Microscope* **15**, 22 (1967).
(9) Mellor, J. W., "Comprehensive Treatise on Inorganic and Theoretical Chemistry," Vol. V, p. 767, Longmans, Green, London, 1940.
(10) Shapiro, N., Gray, R. J., *Proc. Illinois Mining Inst.* **68**, 83 (1960).

RECEIVED May 22, 1967. Work sponsored by the American Gas Association, Research and Development, and the U. S. Department of the Interior, Office of Coal Research.

Gasification of Coal in a Slagging Pressure Gasifier

J. A. LACEY

The Gas Council, Midlands Research Station, Solihull, England

The development of a pilot-scale slagging gasifier for producing more than 5 × 10^6 cu. ft./day of gas from weakly caking bituminous coal at 20 atm. is described. An intermittent slag discharge system was used which allowed the slag to be tapped at a rate of more than 10,000 lb./hr. Performance data are given for the operation of the gasifier on coke, a washed 902-rank coal, an untreated coal, and a coal with a high fusion point ash. The results confirmed that the slagging gasifier had a high output, low steam consumption, and that coals with a wide range of ash fusion temperatures could be gasified.

In 1955 The Gas Council, Midlands Research Station at Solihull, began to be actively concerned in developing a fixed bed slagging gasifier as a possible means for providing the gas industry with large gasification units to gasify a wide range of solid fuels at high efficiency and low cost. A lean gas with a low carbon monoxide content, to be enriched with hydrocarbons to a calorific value of 500 B.t.u./cu. ft., was required. At this time the Lurgi process was well-established in many parts of the world, but it used an excess of steam in the steam-oxygen mixture supplied to the gasifier to prevent clinker formation in the fuel bed. As a result it was desirable to use coal of a high ash fusion temperature, and the comparatively small steam decomposition in the short contact time in the hot gasification zone limited the throughput of the gasifier and produced large volumes of phenolic liquor with its attendant disposal problem. It appeared then that better performance could be achieved by increasing the hot zone temperature of the gasifier and operating under slagging conditions.

The essence of slagging gasification is that the steam supplied per unit volume of oxygen is only that required for gasification. Under these

conditions temperatures some hundreds of degrees centigrade above the fusion point of the ash are generated at the steam-oxygen inlet, and the ash fuses to a liquid slag. Certain advantages follow, including high thermal efficiency, high throughput, a choice of fuel unrestricted by low ash fusion temperature or reactivity, and the absence of a mechanical grate. Gasification under slagging conditions does, however, introduce high temperature hazards at elevated pressures. A review of the most important gasification processes including slagging gasifiers has been reported (*1*).

The first slagging gasifier erected at Solihull was operated on coke at 5 atm. and was used to assess the material requirements for gasification and to investigate methods of controlling slag flow and removing slag from a pressure system (*2, 3*). This gasifier had a flat-bottomed hearth with a side slag outlet consisting of a 3/4 in. silicon carbide tube 30 in. long. Slag outlet blockages were frequent owing to the high heat loss from the slag until an intermittent system of tapping was developed. Slag was allowed to accumulate in the hearth by directing up the tap tube hot combustion gases from a tunnel burner and was then run off at a high rate by deflecting the burner and applying a differential pressure across the hearth. It was considered that this system of operation justified further development, but the side offtake was not satisfactory. The gasifier was therefore redesigned to take a new hearth with a short water-cooled slag tap at the center and was rebuilt together with the necessary auxiliary plant to provide for operation on bituminous coal at 25 atm. pressure and a gas output of 5 million cu. ft./day (*2, 3*).

Description of Plant

Details of the gasifier are shown in Figure 1. The fuel bed, 3 ft. diameter by 10 ft. deep, was contained within a refractory lined pressure vessel, at the top of which was mounted a water-cooled stirrer to break up any agglomerations in the fuel bed. Coal, premixed with a suitable flux, entered the gasifier through the fuel lock hopper, flowed by gravity through the stirrer unit, and was distributed over the top of the fuel bed as the stirrer rotated. The fuel capacity within the stirrer unit was just sufficient, when operating at the designed load, to ensure that the feed was maintained to the fuel bed during the period that the lock hopper was being recharged. Coal moved down the gasifier as it was continuously gasified by the steam-oxygen mixture that was injected into the bottom of the bed through four water-cooled tuyeres. In front of the tuyeres the temperature generated by the combustion of fuel with oxygen melted the ash, which then drained into the hearth below. The hot zone was confined to the center of the gasifier away from the refractory walls by projecting the tuyeres 6 in. into the fuel bed, and using a blast velocity of about 200 ft./sec.

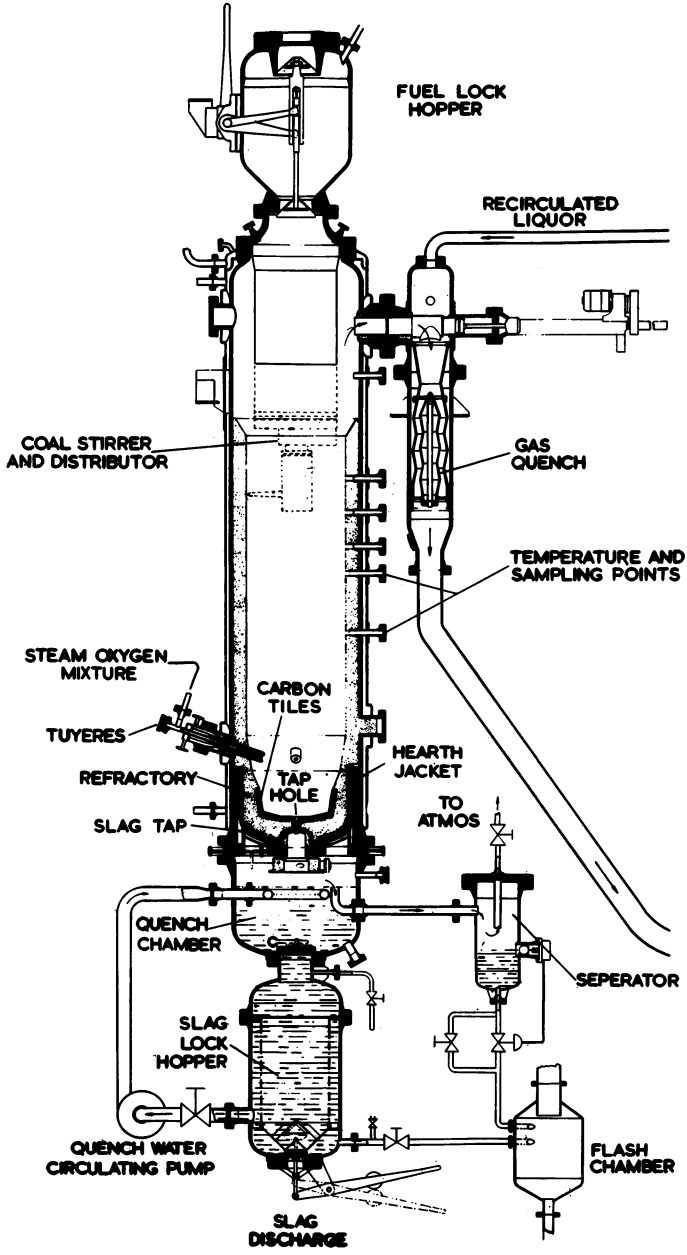

Figure 1. Slagging gasifier

The hearth of the gasifier was contained within a water jacket supported from a carrier ring fitted between the main flanges of the gasifier and the quench chamber. Slag was discharged vertically down into water in the quench chamber, where it formed a glassy black frit that

settled in the slag lock hopper. Water was circulated at a high rate, from the slag hopper through a cooler and back into the quench chamber *via* a perforated ring, to create highly turbulent conditions that avoided stratification and helped quench and break up the slag.

The product gases left the gasifier through an offtake, fitted with a scraper that kept it free of tar and dust deposits, and were quenched by liquor recirculated from the base of the waste heat boiler. After leaving the waste heat boiler, the gases passed through a final cooler to a reducing valve that controlled the plant pressure. Tar and liquor condensate from the gas was blown down through valves controlled by the level of liquid in the sumps of the waste heat boiler and final cooler and passed into a large storage tank where the two phases were separated.

The cooled gases from the plant were burned at ground level within an acoustically lined enclosure at the base of a 120-ft. high chimney stack.

Development of the Slag Tap

In small slagging gasifiers the heat capacity of the slag stream, even when the ash content of the fuel is increased artificially by fluxing, is low in proportion to the high rate of heat loss; problems with viscous slag, solidifying slag, and stalactite formation are common when continuous tapping is attempted. To avoid these difficulties, the tapping system for the experimental gasifier was based on intermittent tapping from a reservoir of slag contained in the hearth. This gave a homogeneous slag with consistent flow properties and enabled gasifying media to be introduced through the tap hole in an attempt to control the slag temperature independently of the main gasification reactions, but the increased slag residence time in the hearth encouraged separation of liquid iron.

The fuels used in the slagging gasifier had a high iron content. In fact it was the presence of the iron compounds that gave the ash the low melting point and good flow properties for which the fuels were originally chosen. The strongly reducing conditions in the hearth inevitably led to formation of iron, although the degree of reduction was greatly reduced by introducing oxygen through the tap hole. In the absence of a suitable refractory it was necessary to develop a water-cooled metal slag tap which was compatible with the slag under the conditions existing in the hearth and would also withstand liquid iron. To preserve the slag tap, it was necessary to have a high heat transfer rate to the cooling water to form a protective layer of solidified slag and freeze any iron before it damaged the tap. It was therefore desirable to construct the slag tap with metal having a high thermal conductivity, use high cooling water rates, and avoid iron accumulation in the hearth. Originally austenitic stainless steels were used because of the type of slag tap burner employed, but later carbon steel was found satisfactory.

As a consequence of iron attack the hearth, slag tap, and slag tap burners went through several stages of development; these have been

described in detail by Hebden *et al.* (*4*). The hearth depicted in Figure 1 was abandoned at an early stage. It was unsatisfactory because of the erosion of the carbon tiles near the tap hole by the slag tap gases, and its shape permitted iron to collect. The slag tap withstood small quantities of iron, but it was found that masses of 10–30 lb. iron accumulated and destroyed the slag tap as they flowed uncontrollably from the hearth. Experience indicated that the hearth should slope steeply towards the tap hole with the minimum opportunity for iron to collect at any point. Thus, the hearth and slag tap were shaped like funnels, and the slag tap was tapped as frequently as possible to limit iron accumulation.

The hearth and slag tap that proved reliable for more than 100 hrs. operation and which were used for the performance tests are shown in Figure 2. The floor of the refractory hearth sloped downward at 45° to a carbon steel slag tap assembly, at the center of which was the slag tap tube 1½ in. diameter by 2 in. long. Little erosion of the refractory hearth occurred since we found that the high temperature gases and slag were confined to a zone about 20 in. diameter in the center of the gasifier and the refractory walls at the side were protected by unburnt fuel. Below the slag tap two swinging burners were mounted. The tap burner controlled the slag tapping and was used to introduce air, oxygen, and town gas into the slag tap tube, where combustion occurred, giving a linear gas velocity high enough to hold back the slag in the hearth. The auxiliary burner, which had a refractory tunnel, was normally in the retracted position and was used to clear the tap hole in the event of blockage—a purpose for which the tap burner was unsuited. It was necessary to use this burner only on rare occasions.

The slag tap shown in Figure 2 was not completely immune from iron attack, which when it did occur was invariably confined to an area at the outer edge of the tap cone entrance that was difficult to cool effectively. To give this vulnerable area added protection, water-cooled coils of copper tubing were installed in the hearth. The high heat transfer rates possible with the copper tubing enabled it to withstand large amounts of iron without suffering any damage. Copper is a promising material for constructing the slag tap, which has been redesigned so it can be made from this material.

Slag Tapping

The intermittent slag-tapping system proved so easy to operate and trouble free that we could adopt an automatic tapping system. Initially, tapping was controlled on a time basis but later by the slag level in the hearth. With the slag-tap burner directing the hot gases up through the tap hole, the slag level in the hearth increased. On reaching the level of a collimated beam of gamma rays from the level detector, about

12 in. above the tap hole, a sequence of operations was started to tap the slag. The tap burner was swung away from the tap hole, and on reaching its fully retracted position, a control valve on a vent line from the quench chamber was opened to reduce the pressure in the quench chamber below that of the gasifier. A controlled differential pressure across the hearth was maintained for a preset time period to force the slag to flow from the hearth, and the control valve was then closed. As the pressure in the slag quench chamber built up, owing to the gases supplied to the burner, the slag flow stopped, and the tap burner was swung back to the tap hole. In a typical cycle the slag was tapped for 20 seconds every 4–6 minutes.

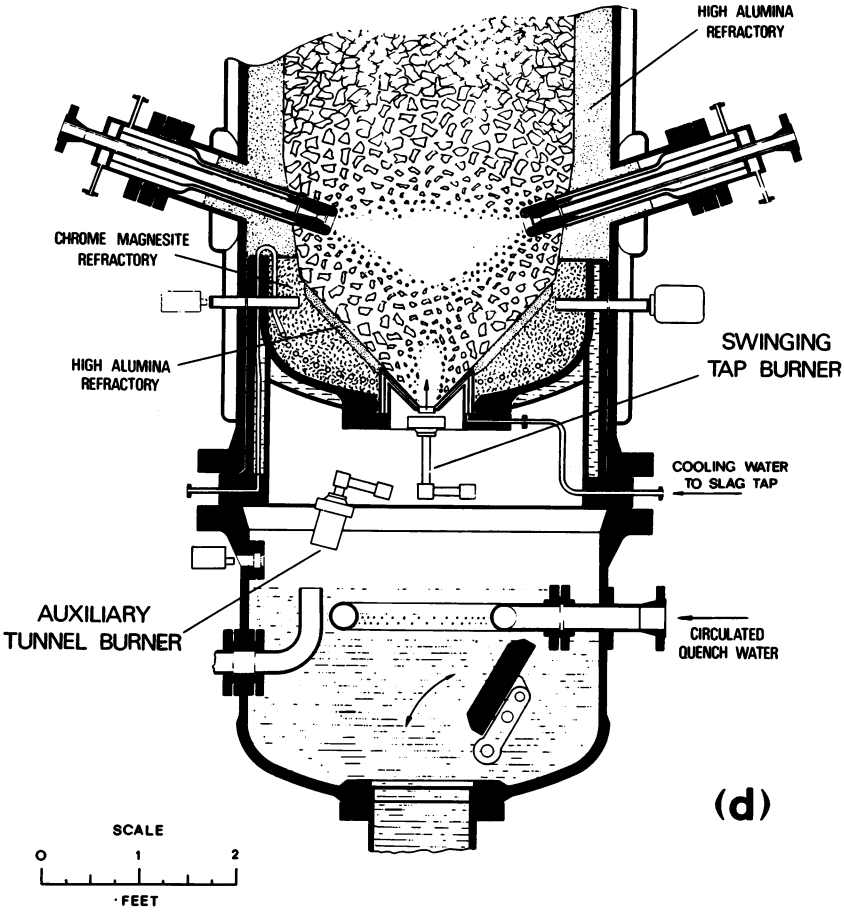

Figure 2. Cross-section of hearth and quench chamber

During the development work on coke the slag was tapped at differential pressures of 5–15 lb./sq. in. When coal was tested, at these differential pressures fuel was entrained in the slag stream. The differential

tapping pressures were gradually reduced, and it was possible to drain slag from the hearth at more than 10,000 lb./hr. with a pull of 1 lb./sq. in. At these low differentials carbon could not be detected in the slag, and the temperature of the slag stream was more uniform than at the higher differential pressures.

While the arrangement of swinging burners worked well in the pilot plant, mechanical devices of this type would not be practical on a large scale. They could be replaced by a fixed-burner arrangement mounted below the slag tap, which would allow iron to pass through the tap hole at any time, while the slag was retained and intermittently tapped to maintain a constant level, or reservoir, in the hearth.

Gasifier Performance

The first phase of the experimental program was to develop the hearth design and the slag-tapping system; for this purpose a free-flowing slag was required. Avenue coke was selected as a suitable fuel on the basis of its silica ratio, a parameter which gives a good correlation between the viscosity and temperature of slags (5). The coke was mixed with blast furnace slag in the proportion 2 parts slag to 1 part ash to increase the volume of slag to be tapped. This simplified plant operation and avoided any complications that might arise with coal so that attention could be concentrated on the hearth and slag tap. When the design of the hearth and slag tap had progressed sufficiently to enable the plant to be operated continuously for 4 days, the changeover was made from coke to coal.

The first experimental runs with coal were made with Donisthorpe washed doubles, a weakly caking coal that was known to behave well in slagging boilers. It was mixed with blast furnace slag to increase its ash content and was successfully gasified at 300 p.s.i.g. and an oxygen rate of 40,000 cu. ft./hr. Using the same fuel the gasifier was next operated at its designed gas output of 5 million cu. ft./day for a test period of 81 hrs. to obtain data from which the performance of the gasifier could be accurately assessed.

The next run was to attempt to gasify a smaller and dirtier coal with a high proportion of adventitious ash—*i.e.*, untreated singles with an ash content of 11%. With the higher ash content it was no longer necessary to ballast the fuel, but to preserve approximately the same silica ratio, a flux of dolomite was added in the ratio 0.3 lb./lb. ash. The gasifier worked well on the dirtier coal without any difficulty with the fuel bed or with tapping the slag.

We then established the limit of the gasifier output, and a run was made at 7½ million cu. ft./day—*i.e.*, 50% above the designed output. The gasifier operated smoothly, and slag tapping was consistent; however, as the run progressed, difficulties were experienced with the gas-cooling system, and the run was terminated after 10 hrs. The factor that limited the output was lock hoppering of the fuel. At this output the distributor

was empty before recharging and repressurising the lock hopper could be completed. This resulted in a widely fluctuating gas outlet temperature which was normally fairly steady at 350°–400°C.; it now fluctuated between 200° and 800°C. A greater capacity in the distributor and another lock hopper would be required before any material increase in output could be attempted.

The final run made with the slagging gasifier was to test its ability to handle a coal with a high fusion point; a coal in the highest range of silica ratios was selected from Newstead Colliery in the East Midlands coalfield. The ash content of 6% was fluxed by adding dolomite to reduce the silica ratio to 65, and in a run of 10 hours no difficulty was experienced in tapping the slag, which was remarkable for its free-flowing character. This indicated that a lower flux:ash ratio or higher steam:oxygen ratio could have been used.

Fuel. The details of the fuel and the chemical composition of the fuel ash and flux used in the performance tests are given in Tables I and II.

Table I. Fuel Analysis

	Test No.				
	54	*67*	*70*	*71*	*72*
Fuel	Avenue No. 2 Coke	Donisthorpe D.S. Nuts	Donisthorpe Untreated Singles	Donisthorpe D.S. Nuts	Newstead Doubles
Nominal size, in.	1½–1	1½–1	1–½	1½–1	2–1
Rank	—	902	902	902	802
Ultimate Analysis, wt.%					
Carbon	88.0	71.3	68.7	74.6	73.8
Hydrogen	0.75	5.0	4.75	5.0	4.7
Nitrogen	1.05	1.55	1.5	1.55	1.55
Sulfur	1.15	1.45	1.8	1.3	0.7
Chlorine	0.05	0.15	0.05	0.2	0.3
Oxygen, errors, etc.	1.45	13.2	11.75	11.7	11.15
Ash	7.55	7.35	11.45	5.65	7.6
	100.0	100.0	100.0	100.0	100.0
Moisture as charged	9.45	12.7	15.1	13.8	12.6

Performance Data. Performance data obtained during one test on coke and four tests on coal are summarized in Table III and cover changes in fuel, fuel size, gasifier output, and ash fusion properties. The fuel quantities are expressed as dry and ash free, and all product gas volumes are given on a nitrogen-free basis to simplify comparison. The greater part of the nitrogen content of the gas produced originated from the air

supplied to the slag tap burner and varied between 5 and 7% depending on the operation of the slag tap and the gasifier output. To obtain a product gas with a low nitrogen content suitable for synthesis, the slag tap burner could be run on a mixture of make gas, oxygen, and steam.

Table II. Ash and Flux Compositions

Composition wt. %	*Avenue No. 2 Coke*	*Donisthorpe D.S. Nuts*	*Donisthorpe Untreated Singles*	*Newstead Doubles*	*Blast Furnace Slag*	*Dolomite*
Al_2O_3	26.81	28.50	27.52	32.40	20.6	2.18
SiO_2	44.18	38.60	44.53	47.0	33.40	0.86
Fe_2O_3	15.24	15.60	15.49	4.52	1.63	1.07
TiO_2	1.03	1.22	1.17	0.95	0.73	0.04
Mn_3O_4	0.17	0.22	0.23	0.20	1.26	0.18
P_2O_5	0.45	0.49	0.32	1.25	0.12	0.17
Na_2O	2.36	1.09	0.55	2.14	0.53	0.08
K_2O	2.11	1.38	2.17	0.80	1.26	0.12
CaO	5.14	5.71	4.75	5.95	33.10	30.2
MgO	1.05	2.06	2.17	1.70	6.15	21.6
SO_3	1.46	6.21	2.59	3.49	1.0	0.01
Ash Properties						
Silica ratio[a]	67	62	69	80	46	—
Fusion Temp., °C.						
Initial deformation	1110	—	1165	1235	1230	—
Hemisphere point	1215	1250	1350	1355	1250	—
Flow point	1330	1345	1470	1545	1320	—

[a] Silica ratio $= \frac{SiO_2 \times 100}{SiO_2 + \text{Equiv. } Fe_2O_3 + CaO + MgO}$

The steam-oxygen ratio was maintained almost constant. A ratio of 1.1 vol./vol. gave satisfactory slagging conditions on coal, being slightly reduced when operating with the higher melting point ash (Test 72). Similarly, the rates of supply of gas, air, and oxygen were not varied significantly.

The gas compositions are characterized by low carbon dioxide and high carbon monoxide contents. In the high output run (Test 71) the calorific value of the gas was unaffected, and the organic sulfur content was higher than expected; Lurgi gas usually contains less than 10 grains/100 cu. ft.

During the coal tests the rate of slag flow through the tap hole, calculated from the slag-tapping times, was between 10,000 and 14,000 lb./hr. whereas the rates were as high as 30,000 lb./hr. with coke. This was not caused by any difference in the rheological properties of the

slags but by using lower differential pressures across the hearth when tapping coal slag.

The absence of volatile matter and the lower reactivity result in a coke with a higher oxygen consumption than coal. The variation in the oxygen consumption figures for coal are hardly significant, but they reflect the increase which can be expected with higher ash contents and use of a flux. The specific throughput figures are noteworthy in that for these conditions a gasification rate of 1,000–1,500 lb. d.a.f. coal/hr. sq. would appear to be readily attainable without any undue sacrifice in performance. Gas output from the fuel bed is extremely high and is equivalent to more than 30,000–42,000 cu. ft./hr. per sq. ft. of fuel bed.

Mass and Heat Balances. Owing to the scale of operations it was difficult to measure accurately the make gas, and a carbon balance was used to obtain this major item. A typical mass balance is given in Table IV. The hydrogen and oxygen items show differences which are rela-

Table III. Performance Data

	Operated at	
Test No.	*54*	*67*
Duration, hr.	*54*	*81*
Supplied		
Fuel	Avenue Coke	Donisthorpe D.S. Nuts
Size, in.	1½–1	1½–1
Feed rate, lb./hr.	3640	6930
Flux	Blast Furnace Slag	Blast Furnace Slag
Flux: ash ratio, lb./lb.	0.83	0.75
Steam: oxygen ratio, vol./vol.	1.17	1.10
Steam rate, lb./hr.	1,650	2,038
Oxygen rate, cu. ft./hr.	30,100	39,650
Slag tap burner		
Gas rate, cu. ft./hr.	3,000	3,000
Air rate, cu. ft./hr.	16,050	16,050
Oxygen rate, cu. ft./hr.	1,200	900
Produced		
Gas, N_2-free basis		
CO_2	1.85	2.55
C_nH_m	0.0	0.45
H_2	27.25	28.05
CO	70.45	61.3
$C_nH_{2n} + 2$	0.45	7.65
	100.0	100.0

tively small and can be attributed to the loss of flash steam during the blowing down of liquor from the waste heat boiler.

A heat balance for the same test is given in Table V. It shows that 1.5% of the total heat supplied is lost as high grade heat from the hearth, 0.8% being in the slag stream and 0.7% being in the cooling water from the tuyeres and slag tap. The heat lost from the jacket and stirrer amounts to a similar quantity, but in a commercial gasifier this would be recovered as gasification steam. Of the total heat supplied 80.3% appears as potential heat in gas and 90.8% as potential heat in gas plus by-products.

Ash and Slag Balances. By making a mass balance of constituents in the fuel ash, flux, and slag and assuming a quantitative recovery of such refractory oxides as alumina, lime, magnesia, and titania, other constituent losses were evaluated. As expected the losses increased as the temperature in the tuyere zone increased, and the percentage loss of each constituent could be correlated with the steam:oxygen ratio. Actual

Obtained on the Slagging Gasifier
300 lb./sq. in.

70	*71*	*72*
30	*12*	*14*
Donisthorpe Untreated Singles	Donisthorpe D.S. Nuts	Newstead Singles
1–½	1½–1	2–1
6520	10150	6560
Dolomite	—	Dolomite
0.3	0.0	0.32
1.10	1.10	1.06
2,040	2,965	2,045
39,640	57,615	41,240
2,735	3,000	3,000
12,590	16,050	16,050
1,120	1,200	1,200
3.5	2.7	2.35
0.7	0.55	1.05
29.25	28.1	28.65
60.05	60.85	60.55
6.5	7.7	7.25
100.0	100.0	100.0

Table III.

Test No.	*54*	*67*
Duration, hr.	*54*	*81*
Value of *n*	1.0	1.123
Calorific value, B.t.u./cu. ft.	315	374
H_2S, grains/100 cu. ft.	—	250
Organic sulfur, grains/100 cu. ft.	—	20
Rate, cu. ft./day	3.7×10^6	5.1×10^6
Slag, lb./hr.	542	938
Tapping time, min./hr.	1.1	4.0
Dust carryover, lb./hr.	19.7	77.5
Tar, lb./hr.	—	508
Liquor, lb./hr.	—	1,609
Permanganate value, p.p.m.	—	30,100
Specific Data		
Consumption		
Fuel, lb./hr. sq. ft.	516	981
Steam, lb./therm	3.40	2.56
Oxygen, cu. ft./therm	71.4	55.2
Production		
Gas, cu. ft./ton	94,800	68,800
therms/ton	299	258
therms/hr. sq. ft.	69	113
Dust, % fuel charged	0.45	0.9
Tar, gal./ton	—	15.4
Liquor, lb./therm	—	2.0

[a] Fuel figures are on a dry and ash-free basis.

temperatures measured by sighting an optical pyrometer through the tuyeres ranged from 1800°C. at a steam:oxygen ratio of 1.3 vol./vol. to more than 1950°C. at 1.10 vol./vol.

In addition to the loss of the more volatile constituents such as sulfur, phosphorus, chlorine, and oxides of sodium and potassium there was a loss of iron oxides owing to the formation of metallic iron, and also of silica. Silica loss was caused by its reduction to volatile silicon monoxide, which was subsequently reoxidized and removed in the gas stream as silica fume. With coke the silica loss was 5% at a steam:oxygen ratio of 1.3, but this increased rapidly at a ratio of about 1.10 vol./vol. to more than 15%. Typical losses of sodium oxide, potassium oxide, and sulfur were 5, 5, and 40% respectively at 1.3 vol./vol., increasing to 40, 40, and 80% at a ratio of 1.10 vol./vol. These materials were deposited in varying degrees in the gas offtake and in the sumps of the waste heat boiler and final cooler. The deposits in the gas offtake were enriched with alkali metal oxides and had a silica concentration of more than 50%. Most of the material was removed in the bottom of the waste heat

Continued

70	*71*	*72*
30	*12*	*14*
1.128	1.129	1.114
366	375	379
233	—	144
12	—	—
5.0×10^6	7.23×10^6	5.09×10^6
1,026	534	602
5.3	3.1	3.6
69	229	63
501	—	453
1,807	—	1,413
34,700	—	35,600
924	1,440	930
2.66	2.62	2.54
56.2	54.7	56.6
71,900	66,500	72,400
263	250	274
109	158	114
0.8	1.84	0.8
16.2	—	15.5
2.35	—	1.76

boiler, but finely divided solids with an ash content greater than 90%, of which 75% was silica, separated from the gas in the final cooler and were removed in the blow down.

The loss of ash constituents from the coals tested were significantly lower than for coke, except for chlorine and sulfur. Silica losses were negligible, apart from the test with untreated coal that contained a high proportion of shale.

The loss of iron oxides is important in operating a slagging gasifier owing to the hazard of liquid iron and the effect upon the flow properties of the slag. Iron oxide acts as a flux, and its loss raises the melting point, increases the silica ratio, and increases the slag viscosity. A controlled series of experiments with coke showed that there was little effect on the reduction of iron oxides by decreasing the steam:oxygen ratio from 1.40 to 1.20 vol./vol., but a further decrease to 1.10 vol./vol. almost doubled the iron formation. However, this trend could be reversed by supplying extra oxygen to the gases passing through the tap hole, and reduction of the iron oxides was decreased to 15%. Although reduc-

Table IV. Mass Balance for Test 67 (lb./hr.)

	Carbon	*Hydrogen*	*Oxygen*
In			
Coal	5323	373	993
Moisture	—	121	972
Steam and Oxygen	—	226	5106
Slag Tap Burner	41	15	378
	5364	737	7449
Out			
Gas	4896	509	5925
Dust	48	2	6
Tar	406	38	45
Liquor	14	176	1376
Difference	0	12	97
	5364	737	7449

tion occurred in the experiments with coal between 20 and 30%, this could have been improved greatly by supplying a larger proportion of the gasifying media through the tap hole.

Tar and Liquor. Although the tar and liquor condensates from the gas were separated in two stages, they were discharged into a common separating tank for ease of handling. This, together with the high liquor circulation rate from the sump of the waste heat boiler to provide the gas quench, produced a tar-water emulsion. However, the emulsion was not persistent, and three phases that could be separated without much difficulty were formed; a lower layer of solids, a middle layer of tar, and an upper layer of liquor.

Table V. Heat Balance for Test 67

	Therms/hr.	*%*
In		
Coal (potential)	958	95.8
Town gas (potential)	13.5	1.35
Steam and oxygen (latent and sensible)	28.5	2.85
	1000.0	100.0
Out		
Gas (potential)	803.0	80.3
Gas and vapours (latent and sensible)	55.5	5.55
Tar (potential)	84.4	8.44
Dust (potential)	8.6	0.86
H_2S ammonia, etc. (potential)	4.6	0.46
Slag (sensible)	8.0	0.8
Cooling water from tuyeres and hearth (sensible)	6.6	0.66
Cooling water from gasifier hacket and stirrer (sensible)	15.2	1.52
Unaccounted-for losses	14.1	1.41
	1000.0	100.0

The liquor originated almost entirely from the moisture in the coal and had a permanganate value of 30,000 p.p.m.—*i.e.*, more than twice that from a Lurgi gasifier. Its smaller volume, and hence its reduced capacity to take into solution oxygen-absorbing agents means, however, that its total oxygen-absorbing potential per therm of gas is only half that of Lurgi liquor.

The tar, even after prolonged standing, retained about 20–25% water and about 4% suspended solids. It has been analyzed by the Coal Tar Research Association (7) and found to have the general characteristics associated with a vertical retort tar—*i.e.*, similar yields of pitch, naphthalene, and tar acids. The high ratio of 2:1 methyl naphthalene and the high content of light oil, which was greater than that normally found in a carburetted water-gas tar, indicated a high temperature of formation.

Table VI. Size Distribution in Fuel Bed

	Test 67			*Test 70*		
Fuel Size, in.	*As Charged*	*Below Stirrer*	*At Tuyere Level*	*As Charged*	*Below Stirrer*	*At Tuyere Level*
1½–1	24.6	—	—	—	—	—
1–¾	40.0	—	—	21.0	—	—
¾–½	21.0	59.1	10.9	15.6	21.4	9.2
½–¼	9.7	29.9	49.3	53.0	57.0	29.2
¼–⅛	1.4	3.1	8.1	2.2	8.6	30.1
below ⅛	3.3	3.7	29.7	8.2	14.0	30.6

Behavior of the Fuel Bed. There was no evidence of channelling as a result of blockage of part of the fuel bed with fines or any other abnormal behavior while operating the slagging gasifier for a total of 500 hrs. with coke and 300 hrs. with coal. Screen analysis of the fuel bed at the end of the experimental tests with coal indicated that degradation increased as the fuel moved down the bed, but there were two main zones where this occurred—in the caking zone at the top of the bed owing to the action of the stirrer, and in the tuyere zone owing to the highly turbulent motion of the fuel. Table VI shows the size distribution in the fuel bed immediately below the stirrer and at the tuyere level when the fuel charged to the gasifier was 1½–1 in. and 1–½ in. The proportion of fuel below ⅛ in. at the tuyere level showed little variation in the tests on coal and averaged 30%.

The fuel below ⅛ in. entering the gasifier in Test 70 was more than double that in Test 67, but there was no significant change in the amount of dust carryover. In each of these tests the gas output was equivalent to four times that of a typical Lurgi gasifier, but the fuel carryover was less than 1% of the fuel charged. However, on raising the gas output by 50% (Test 71) the carryover was doubled. With coke the carryover was only half that associated with coal, owing to the absence of any mechanical breakage by the stirrer and the lower gas velocity above the fuel bed. There is little doubt that the carryover could be reduced by improved stirrer design and perhaps by recirculating tar dust mixtures as done in the commercial Lurgi gasifier.

Comparison with a Lurgi Gasifier. The Donisthorpe coal used in the slagging gasifier for Tests 67 and 71 is similar to the coal used at the Lurgi gasification plant at Westfield, so that it is possible to make a direct comparison between performances of the two. Table VII compares the performance data from Test 67 with data given by Ricketts (*6*).

Recent developments in the Lurgi process have resulted in lower steam consumptions and corresponding increases in gasifier output, but the output is still much lower than a slagging gasifier. At Westfield it has been possible to obtain nearly 20% more crude gas than the guaranteed maximum of 12 million cu. ft./day, although at the higher loads more exacting operating conditions are required to avoid clinker formation. This compares with an output from the slagging gasifier of 5.2 million cu. ft./day of gas having a higher calorific value, which can be increased by 50% to 7.3 million cu. ft./day without any significant loss of performance. The output of the experimental slagging gasifier when operating at a lower pressure is therefore more than half that of the commercial Lurgi gasifier. When expressed as the weight of fuel gasified or the volume of synthesis gas ($CO + H_2$) per unit cross-sectional area of shaft, the output of the slagging gasifier is at least four times greater than the Lurgi gasifier.

In Table VII the material requirements of the two gasifiers are compared for the production of a therm of crude gas and for 1000 cu. ft. of synthesis gas. Steam requirements show the greatest difference, that of the slagging gasifier being about one-fifth of the Lurgi gasifier. However, the composition of the crude gases should be considered when comparing steam consumption if the gas is to be detoxified or if synthesis gas is required. In the Lurgi crude gas there is sufficient undecomposed steam to carry out the required reduction in carbon monoxide content without added steam or liquor, but extra steam would be needed with the slagging gasifier because of its high carbon monoxide content, small volume of undecomposed steam, and lower outlet temperature. Under these conditions the slagging gasifier loses some of its advantage in steam consumption.

The oxygen consumption per therm of crude gas from the slagging gasifier is about 10–12% higher than that of the Lurgi gasifier. This is because of formation of a smaller proportion of the exothermic products (carbon dioxide and methane) and the loss of high grade heat to the hearth slag tap and tuyere cooling water. The oxygen consumption per unit volume of synthesis gas shows little difference between the two gasifiers.

Conclusions

A pilot-scale slagging gasifier has been developed that will gasify coke and weakly caking coals, and performance data have been obtained at 20 atm. The gasifier had a low steam consumption, high output, high thermal efficiency, and handled coal with a wide range of ash fusion temperatures provided that dolomite was used to flux the more refractory ashes. A crude gas output of 7½ million cu. ft./day, equivalent to 42,000 cu. ft./hr. per sq. ft. of fuel bed, was obtained without any limitation by the fuel bed.

Table VII. Comparison of the Slagging Gasifier and a Commercial Lurgi Plant

	Lurgi Gasifier	*Slagging Gasifier*
Operating Pressure, lb./sq. in.	355	300
Fuel		
Rank	902	902
Size range, in.	1¼–⅜	1½–¼
Ash, including flux, %	14.6	11.4
Moisture, %	15.6	14.7
Steam: oxygen ratio, vol./vol.	5.4	1.10
Crude Gas Composition, vol. %		
CO_2	24.6	2.5
C_nH_m	1.1	0.45
CO	24.6	60.5
H_2	39.8	27.75
$C_nH_{2n} + 2$	8.7	7.6
N_2	1.2	1.0
	100.0	100.0
Calorific value, B.t.u./cu. ft.	309	371
Steam consumption, lb./therm crude gas	11.6	2.56
Steam consumption, lb./1000 cu. ft. ($CO + H_2$)	56.1	10.7
Oxygen consumption, cu. ft./therm crude gas	49.5	55.2
Oxygen consumption, cu. ft./1000 cu. ft. ($CO + H_2$)	238	236
Synthesis gas ($CO + H_2$) output, cu. ft./hr. per sq. ft.	4930	26,700
Gasification rate, lb. d.a.f. coal/hr. per sq. ft.	210	981
Efficiency $\frac{\text{(potential heat gas)}}{\text{(potential heat coal)}}$	81	82.5

Comparing the results with those of a Lurgi installation showed that the steam consumption and liquor volume were one-fifth, and the gas output per unit area of the fuel bed was from four to seven times greater than the Lurgi gasifier. The slagging gasifier produced a gas with a high carbon monoxide content, and there was little undecomposed steam to convert it. However, with the added steam necessary to convert the carbon monoxide to the level required for synthesis gas, the over-all steam consumption would be lower than for the Lurgi gasifier. For detoxification to the level required in the United Kingdom it would be logical to convert part of the carbon monoxide and use methane synthesis to remove the remainder, at the same time increasing its calorific value.

The system of intermittent tapping, in which a reservoir of slag was maintained in the hearth to enable the slag to be run off at a high rate by applying a controlled differential pressure, proved quite satisfactory. Coal with a low ash fusion temperature, uncleaned coal with a high proportion of adventitious ash, and coal with a refractory ash when suitably fluxed, gave a homogeneous slag that was tapped without blocking the slag tap. This tapping system could be used for scale up to a commercial size by modifying the slag tap burner design to allow the free drainage of iron from the hearth.

Experience with the slagging gasifier indicated that water-cooled metal surfaces were essential for the slag tap and areas of the hearth exposed to hot slag but were prone to attack by liquid iron. Iron attack was greatly reduced by maximizing heat transfer through the metal surfaces, by preventing iron from accumulating in the hearth, and by introducing oxidizing gases through the tap hole to retain the bulk of the iron in solution in the slag. The water-cooled steel slag tap used in the gasifier withstood hot slag and iron for long periods but occasionally suffered some damage from iron attack. Complete resistance to iron attack is an obvious design requirement, and recent experiments suggest that this can be achieved by using copper.

The development of the slagging gasifier has now reached a stage that requires the proving of designs and materials for longer periods of time, possibly on a prototype gasifier. However, in the United Kingdom the gasification of solid fuels, even with the improvements offered by operating under slagging conditions, cannot presently compete economically with the new oil gasification processes. An alternate route for producing gas from coal, by hydrogenation and gasification in a fluidized bed, is therefore being investigated on the pilot-plant scale.

Acknowledgments

The work described was carried out under the direction of F. J. Dent and D. Hebden.

Literature Cited

(1) Bituminous Coal Research, *B.C.R. Rept.* **L-156** (March 1965).
(2) Hebden, D., Edge, R. F., *Gas Council Res. Commun.* **G.C. 50** (1958).
(3) Hebden, D., Edge, R. F., *Trans. Inst. Gas Engrs.* **108**, 492 (1958-59).
(4) Hebden, D., Lacey, J. A., Horsler, A. G., *Gas Council Res. Commun.* **G.C. 112** (1964).
(5) Hoy, H. R., Roberts, A. G., Wilkins, D. M., *Proc. Joint Conf. Gasification Processes, Hastings* (1962).
(6) Ricketts, T. S., *J. Inst. Gas Engrs.* **3** (10) 563 (1963).
(7) Vaughan, G. A., Coal Tar Res. Assoc., Rept. No. **0348 B** (1965).

RECEIVED January 17, 1967. Published by permission of The Gas Council.

5

High B.t.u. Gas by the Direct Conversion of Coal

PAUL S. LEWIS,[1] SAM FRIEDMAN, and RAYMOND W. HITESHUE

U. S. Department of the Interior, Bureau of Mines, Pittsburgh Coal Research Center, 4800 Forbes Ave., Pittsburgh, Pa.

The direct conversion of untreated coal into high B.t.u. gas offers means for augmenting natural gas supplies. The U. S. Bureau of Mines reports data for the dilute-phase hydrogenation of high volatile A bituminous coal and for the hydrogenation of partially devolatilized coal (char) in a moving bed. Conditions are 1500 and 3000 p.s.i.g. and 725°C. for coal and 700° and 900°C. for char. The concept of integrating these two operations into a continuous process is discussed. Stream flows and compositions are given for a conceptional plant producing 90 million std. cu. ft./day of 916 B.t.u. gas. Results indicate that development of a process is feasible, and the work is continuing.

Processes for generating high B.t.u. gas from coal are being developed for future use when there is an economic need for manufactured gas (*2, 5*). Several processes based on both coal and petroleum are available, and various estimates of production costs or selling price have been published (*1, 3, 4, 6*). Those processes based on coal can be divided into two general categories: indirect and direct. Indirect processes are those requiring the coal carbon to be converted into synthesis gas (hydrogen and carbon monoxide) which, after adjusting the gas composition and removing impurities, reacts catalytically at moderate pressure and temperature to produce methane. Direct processes are those in which the coal carbon combines with hydrogen to produce methane in a noncatalytic operation at high pressure and temperature. Each approach has both advantages and disadvantages, and thus far a clear-cut superiority has not been demonstrated for either one. This paper reports the

[1] Present address: U.S. Bureau of Mines, P.O. Box 880, Morgantown, W. Va.

progress made by the Pittsburgh Coal Research Center of the U. S. Bureau of Mines in developing a direct process for converting coal to high B.t.u. gas.

The Bureau's concept of hydrogenating coal to methane in dilute-phase concurrent flow originated from an earlier attempt to produce hydrocarbon gases by entraining feeds of strongly caking and noncaking coals in a stream of hydrogen which passed through a hot reactor in turbulent flow. Even though the gas velocity was high, coal carbonization in the reactor always stopped the flow. These experiments indicated the possibility of devolatilizing the coal to dry char providing the coal particles were small and dispersed throughout a stream of hot gas. Under these conditions the coal particles would be heated rapidly, and if the diameter of the reactor were large relative to the entering feed stream, the coal would pass through its plastic range without agglomerating into a large mass or sticking to the wall of the reactor. This was successfully demonstrated several years ago using strongly caking coal, hvab Pittsburgh seam, and hydrogen at 1000 p.s.i.g. The reactor had a diameter of 3 in. and was heated to a nominal temperature of 800°C. while the entering stream of coal had a diameter of 5/16 in. A dry, free-flowing, nonagglomerated char was produced during free-fall through a heated zone 4 ft. long.

Since then, a dependable system for hydrogasifying coal in dilute phase has been developed, and experimental data are being obtained. In addition, some data have been obtained for hydrogenating dilute-phase char. These experimental results are presented, and a theoretical process is discussed which integrates these two operations for producing high B.t.u. gas on a commercial scale.

Dilute-Phase Hydrogenation

The reaction of coal with hydrogen in dilute phase is intended as a means whereby strongly caking coals can react at high temperatures as-received without incurring agglomeration. The primary products are hydrocarbon gases and a solid residue of coal which is dry, free-flowing, nonagglomerated char that can be processed further by hydrogenation, gasification, or burned as fuel; in addition, a minimal amount of hydrocarbon liquids might be produced. One anticipated application of dilute-phase hydrogasification is the direct conversion of coal to high B.t.u. gas.

Until recently, a major portion of the work was concerned with developing ways to feed strongly caking coal into gas mixtures at high temperatures and pressures. When this problem was solved, experiments were made to determine the operability limits of the system with respect

to coal throughput and to explore the effects of hydrogen:coal ratio on the quality of the product gas and char.

All experiments in dilute-phase hydrogasification used a feed of Pittsburgh seam coal having a free-swelling index of 8 and a volatile content of 41% moisture- ash-free basis. Ultimate and proximate analyses

Table I. Analyses of High Volatile A Bituminous Coal

	As Received, %	*M.a.f., %*
Ultimate Analysis		
Carbon	78.5	84.0
Hydrogen	5.4	5.7
Nitrogen	1.6	1.7
Sulfur	1.4	1.5
Oxygen[a]	7.2	7.1
Ash	5.9	—
Moisture	0.7	—
Proximate Analysis		
Moisture	0.7	—
Volatile matter	38.2	40.9
Fixed carbon	55.2	59.1
Ash	5.9	—

[a] By difference.

are given in Table I. This choice of feed was based on the premise that procedures for overcoming agglomeration would apply to any other coal whereas the reverse might not be true. The feed was sized 50 × 100 mesh sieve fraction, U.S. Standard.

The feed gas was a mixture of methane and hydrogen having a composition simulating that which could be obtained by the partial conversion of char with hydrogen to produce methane; various gas compositions were used. The feed rate closely approximated 175 std. cu. ft./hr. The additional methane produced by hydrogenating coal in dilute phase using a methane-rich mixture could conceivably raise the heating value of the gas leaving the reaction zone to better than 900 B.t.u. per std. cu. ft. on a clean, dry basis. While the coal was being partially devolatilized, it was also being transformed into dry, free-flowing char which could be hydrogenated in a moving bed without agglomerating.

Equipment and Procedure. The basic elements of the dilute-phase system are shown schematically in Figure 1. Feed gas of a given composition was made by blending metered quantities of methane and hydrogen in a gasholder which supplied the gas mixture to a compressor. The compressed gas was heated during flow through coiled tubing immersed in a lead bath to 700°C. and entered the top of a reaction vessel heated by external furnaces, where it contacted the incoming stream of coal. The coal entered the reactor through a nozzle whose diameter was as large as 1/2 in. and in concurrent flow with the hot gas, passed through

the reaction space which was 8 ft. long and 3 in. in diameter. The reactor was heated to a nominal temperature of 725°C. which means that its temperature was brought to a maximum of 725°C., and constant temperatures were reached over the system before starting the coal feed. Some variations in temperatures occurred, especially after coal feed was started. Pressure was equalized throughout the coal-feeding system by providing a parallel flow path between the feeder, nozzle, and reaction space. Product gas passed through a water-cooled vessel, in which water and a small quantity of oil vapors were condensed and collected, and the gases were then reduced in pressure, metered, and collected in a gasholder. A small flow of gas was withdrawn and passed through an analyzer which continuously recorded the specific gravity of the gas, thereby showing when steady conditions had been attained; about 15 min. were required to reach steady conditions. Samples of the product gas were withdrawn at intervals and analyzed.

Results and Discussion. In dilute-phase hydrogasification, the composition of the effluent gas is determined by the feed gas rate and composition and the gas yield. The feed gas rate and composition can be selected somewhat freely, but the gas yield depends on many variables, some of which interact. The most prominent variables are coal rate, hydrogen:coal ratio, maximum temperature attained by the solids and the vapors, residence times of the solids and the vapors, total pressure, hydrogen partial pressure, particle size and density, gas viscosity, heat

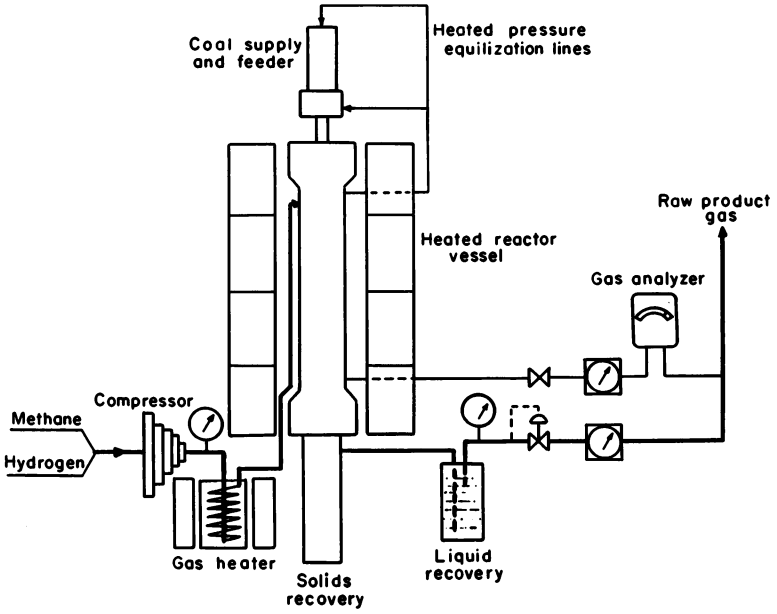

Figure 1. Schematic diagram of dilute-phase hydrogasification apparatus

capacity of the feed gas, and thermal conductivity of the gases. Obviously, in an investigation which is primarily concerned with developing a process, a study of all the variables is not the primary objective. However, some experimental data have been obtained showing the gross effect of several important variables. The results are given in Table II for experiments at 1500 p.s.i.g. and in Table III for 3000 p.s.i.g.

The effect of coal rate on converting coal to gaseous and liquid products was investigated at both pressures using hot feed gas at a rate of 175 std. cu. ft./hr. and an approximate composition of 50% hydrogen, 48% methane, and 2% nitrogen. Over the relatively narrow range of 5–7 lbs./hour, the quantity of coal coverted to gases plus a small amount of oil and water was approximately 35–33% based on m.a.f. coal. Coal conversion decreased with increasing coal rates, being approximately

Table II. Dilute-Phase Hydrogasification at 1500 p.s.i.g. and a Nominal 725°C. Reactor Temperature

Coal feed rate, lb./hr.	5.9	6.0	6.3	6.4	6.5	6.7	7.5	7.6	9.1
Gas feed rate, std. cu. ft./hr.	173	173	175	179	177	175	174	176	177
Composition, % methane[b]	42	3	44	47	61	43	43	44	42
Gross heating value, B.t.u./std. cu. ft.	617	346	627	648	747	621	623	632	617
Conversion, wt. %									
Coal, m.a.f.	35	37	[a]	32	32	34	[a]	32	28
Carbon	28	30	[a]	26	26	27	[a]	25	22
Product gas, nitrogen-oxygen free									
Hydrogen, vol. %	41.6	76.7	40.4	38.2	25.3	40.9	38.5	35.7	34.7
Methane, vol. %	56.4	20.3	57.2	58.5	73.2	56.7	58.5	61.2	62.2
Ethane, vol. %	1.4	2.1	1.7	2.5	1.5	1.7	2.0	2.4	2.1
Carbon monoxide, vol. %	0.6	0.9	0.7	0.8	0.5	0.7	1.0	0.7	1.0
Gross heating value, B.t.u./std. cu. ft.	734	495	744	764	853	741	757	780	784
Gain in heating value, B.t.u./std. cu. ft.	117	149	117	116	106	120	134	148	167
Percent based on feed gas	19	43	19	18	14	19	21	23	27
Yields, wt. %, m.a.f. coal									
Methane	18.4	22.0	15.9	14.6	13.3	16.4	15.3	17.2	17.1
Ethane	3.0	4.9	3.9	5.7	3.4	3.5	3.5	4.3	3.1
Carbon monoxide	1.4	2.0	1.5	1.8	0.9	1.4	1.8	1.3	1.5
Recoveries, wt. %									
Over-all	97	96	92	97	95	96	92	96	101
Carbon	96	97	94	97	95	95	90	98	99
Hydrogen	100	102	99	100	97	99	97	100	102
Ash	115	101	103	98	102	105	100	88	110

[a] Conversion values not meaningful.
[b] Balance is hydrogen and 2% nitrogen.

Table III. Dilute-Phase Hydrogasification at 3000 p.s.i.g. and a Nominal 725°C. Reactor Temperature

Coal feed rate, lb./hr.	5.3	6.0	6.2	6.3	6.5	6.6	6.8	7.2	7.8	8.3
Gas feed rate, std. cu. ft./hr.	174	182	174	174	174	177	176	176	175	174
Composition, % methane[a]	50	2	68	47	48	49	48	71	45	48
Gross heating value, B.t.u./std. cu. ft.	669	337	807	647	653	660	658	814	633	667
Conversion, wt. %										
Coal, m.a.f.	33	42	32	33	35	33	34	31	29	31
Carbon	26	35	24	26	28	26	27	23	23	23
Product gas, nitrogen-oxygen free										
Hydrogen, vol. %	34.0	70.1	17.1	34.9	31.3	32.9	30.9	16.9	31.8	28.6
Methane, vol. %	64.0	28.6	81.0	63.6	66.3	65.5	66.9	81.0	65.0	67.8
Ethane, vol. %	1.5	0.8	1.7	1.5	1.8	1.6	1.7	1.6	2.6	2.6
Carbon monoxide, vol. %	0.5	0.6	0.1	0.0	0.5	0.0	0.4	0.3	0.6	1.0
Gross heating value, B.t.u./std. cu. ft.	792	533	910	786	808	798	811	905	810	829
Percent based on feed gas	18	58	13	21	24	21	23	11	28	20
Yields, wt. %, m.a.f. coal										
Methane	21.0	35.8	13.7	20.3	21.5	19.3	20.8	11.1	19.0	16.5
Ethane	3.9	1.9	3.5	3.5	3.7	3.6	3.7	3.3	4.5	4.2
Carbon monoxide	1.5	1.3	0.2	trace	1.0	0.0	0.8	0.6	1.0	1.6
Recoveries, wt. %										
Overall	98	97	95	97	96	102	96	91	98	97
Carbon	99	100	96	98	97	97	98	95	99	98
Hydrogen	101	97	98	100	100	101	100	98	102	99
Ash	100	102	101	98	100	103	101	105	90	100

[a] Balance is hydrogen and 2% nitrogen.

27% at a rate of 9 lbs./hr. because of the greater heat load imposed by the increased coal rate while the heat input was held constant. Carbon conversions were about 28–27% of m.a.f. coal at 6–7 lbs./hr. and decreased to about 22–23% at 9 lbs./hr.

The effect of coal rate on the yield of hydrocarbon gases (methane and ethane) is shown in Figure 2. Approximately 24% of the m.a.f. coal was converted to methane plus a little ethane at 6–7 lbs./hr. coal rate and 3000 p.s.i.g. while the corresponding yield at 1500 p.s.i.g. was approximately 20%. The greater yields were obtained at 3000 p.s.i.g. because both the hydrogen partial pressure and the retention time of the coal volatiles were twice as great as that obtained at 1500 p.s.i.g., which

accelerated the thermal decomposition and hydrogenation of the high molecular weight vapors. Hydrocarbon gas yields showed the same decreasing trend with increased coal rate as observed for conversion, resulting from the increased heat load causing coal temperatures to decrease.

The effect of pressure upon coal conversion appeared to be less than the accuracy of the conversion data—about 3%. Of course, when the total pressure was changed, other dependent variables also changed and

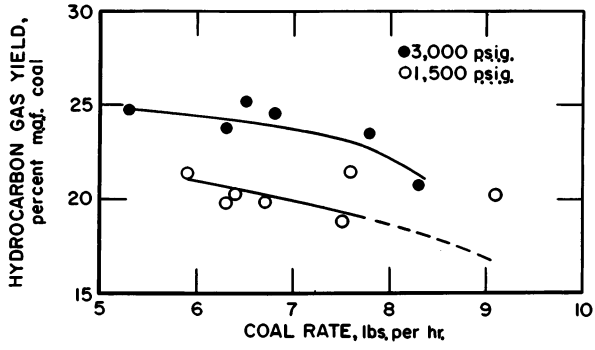

Figure 2. Effect of coal rate on hydrocarbon gas yield at approximately constant gas feed rate and composition

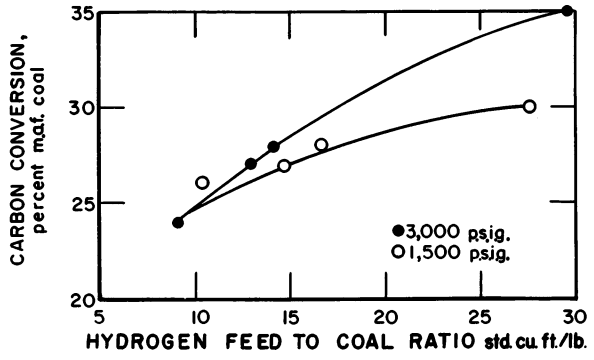

Figure 3. Effect of hydrogen concentration in feed gas on carbon conversion at approximately constant gas and coal rates

thereby effected conversion. A coal rate of 9 lbs./hr. seemed close to the limit of operability because coal temperatures were low and the coal was not being devolatilized sufficiently to produce dry char.

In another series of experiments, the coal and gas rates were approximately constant at 6–7 lbs./hr. and 175 std. cu. ft./hr. while the

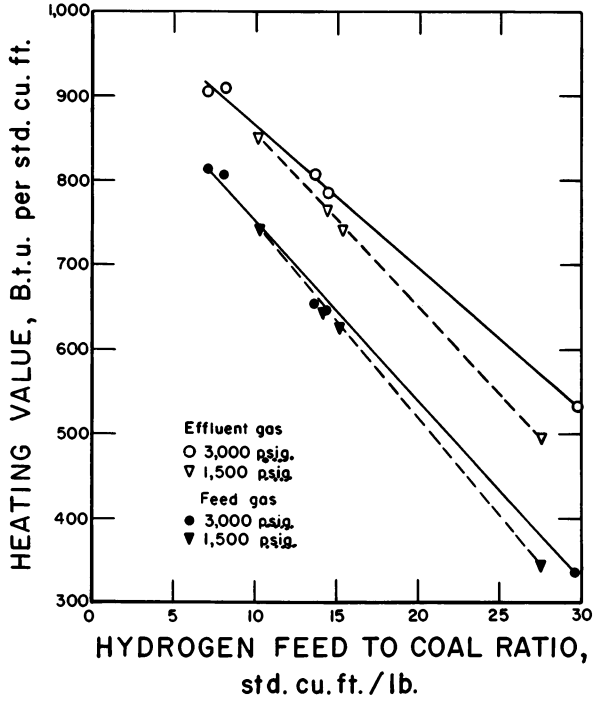

Figure 4. Effect of hydrogen feed to coal ratio on increasing the heating value of gas by dilute-phase hydrogenation

quantity of hydrogen supplied with the feed gas was varied over a fairly wide range between 50 and 175 std. cu. ft./hr. Coal and carbon conversions and yields of hydrocarbon gases decreased with decreasing hydrogen concentration in the feed gas; however, some of this change can be attributed to lower reaction temperatures which resulted from the change in feed gas composition. The change in carbon conversion over the range of hydrogen:coal ratios between 10 and 30 is shown in Figure 3. At 3000 p.s.i.g., carbon conversions were slightly greater and also decreased at a greater rate with respect to decreasing hydrogen:coal ratio than at 1500 p.s.i.g. Carbon conversions ranged from 24–35%, based on m.a.f. coal.

The hydrogen:coal ratio has an important bearing on the quality of the gas leaving the dilute-phase zone. If high B.t.u. gas is to be produced, the feed gas must have a composition that provides enough hydrogen to convert coal carbon to hydrocarbon gases in sufficient yield that the effluent gas exceeds 900 B.t.u./std. cu. ft. in gross heating value. This can be seen in Figure 4 which shows how the heating value of the effluent gas changed with the hydrogen:coal ratio at total pressures of

1500 and 3000 p.s.i.g. Conditions were the same as those relating to Figure 3. The increase in heating value was least at the lowest hydrogen:coal ratio, an increase of about 100 B.t.u./std. cu. ft. with feed gas containing 7.5 std. cu. ft./lb. of coal at a total pressure of 3000 p.s.i.g.; however, this was the feed ratio needed to produce an effluent gas having 910 B.t.u. heating value. An increase of 200 B.t.u. in the heating value was obtained at the opposite extreme where the hydrogen:coal ratio was 30 std. cu. ft./lb. The reduction in the differential heating value reflects both decreasing hydrogen partial pressure and the resulting loss of heat of reaction. Of course, these data represent one of many possible feed gas:coal ratios, a number of which certainly would give a high B.t.u. effluent gas. Many experiments would be required before an optimum feed ratio could be selected.

Hydrogenation of Char

Char from the hydrogenation of coal in dilute phase was hydrogenated continuously in a moving bed at 3000 and 1500 p.s.i.g. The objective was to determine the hydrogen:feed ratio that would produce an effluent gas of a certain selected composition for a particular conversion.

Equipment and Procedure. A schematic diagram of the system is shown in Figure 5. The reaction vessel, filled completely with dilute-phase char, consisted of a 5-ft. length of 1-in. pipe connected to a 6-ft. length of 1/2-in. pipe. The length of the heated zone was adjusted between limits of 6 and 24 in. according to the char conversion requirements of a particular experiment. A variable speed screw continuously discharged reacted char from the bottom of the vessel. A flow of compressed hydrogen was introduced into the screw housing, and heating occurred during upward flow in contact with the descending stream of hot char. The gases and vapors were withdrawn at the top of the heated zone and flowed through a cold vessel where the vapors condensed and were collected. The uncondensed gases were reduced in pressure, metered, and either collected in a holder from which samples were withdrawn or were discharged to the atmosphere. A small sidestream was passed continuously through a meter that measured its specific gravity. Gas composition could be controlled by varying the hydrogen:char ratio, and char conversion could be controlled by varying the retention time of the char in the reaction zone.

Results and Discussion. Table IV shows the results obtained when dilute-phase char was hydrogenated.

At 1500 p.s.i.g., 900°C., and a residence time of about 3-1/2 min., conversion of dilute-phase char was 34%, based on m.a.f. feed. At the hydrogen:char feed (m.a.f.) ratio of 11 std. cu. ft./lb., the effluent gas contained 67% methane, 31% hydrogen, and 1% each of ethane and carbon monoxide. When the residence time was increased to 7-1/2 min.,

char conversion increased to 52%. The composition of the effluent gas was 63% methane, 35% hydrogen, and 1% each of ethane and carbon monoxide. The hydrogen:char (m.a.f.) needed to produce gas of this composition was 32 std. cu. ft./lb. An experiment at 700°C. and 3000 p.s.i.g. produced a char conversion of 26% with a residence time of 3-1/2 min. Because hydrogen:char ratio of 25 std. cu. ft./lb. was used

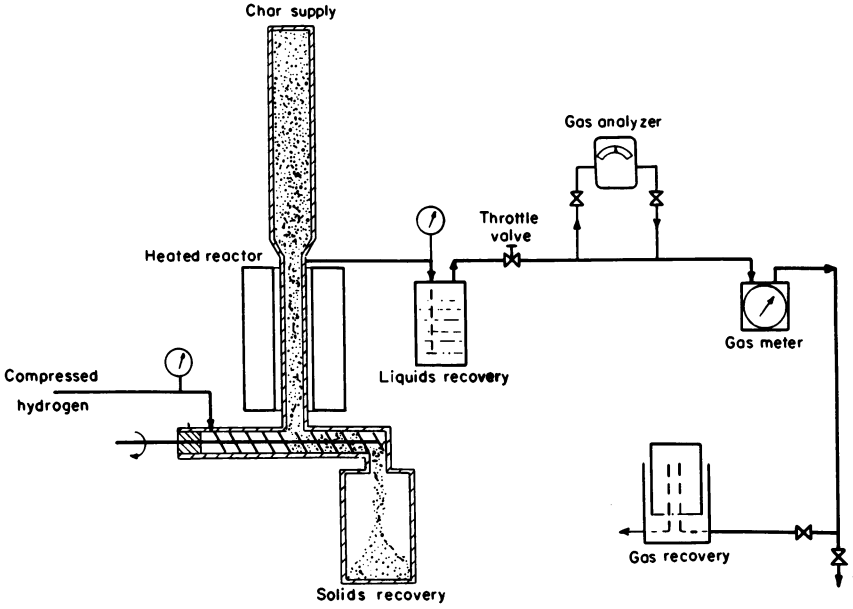

Figure 5. Schematic diagram of char hydrogasification apparatus

Table IV. Hydrogenation of Dilute-Phase Char

Pressure, p.s.i.g.	1500	1500	3000
Temperature, °C.	900	900	700
Residence time, min.	3.5	7.5	3.5
Hydrogen/char ratio, std. cu. ft./lb.	11	32	25
Conversion, wt. % of m.a.f. char	34	52	26
Effluent gas composition, %			
Hydrogen	31	35	62
Methane	67	63	36
Ethane	1	1	1
Carbon monoxide	1	1	1
Volatile content of residue, wt. % m.a.f. basis[a]	2.6	2.4	2.6

[a] Volatile content of feed char, 12.8%.

in this experiment, the concentration of methane was only 36%; the other concentrations were 62% hydrogen with 1% each of ethane and carbon monoxide.

These data emphasize the considerable range of char conversion and effluent gas compositions that could be obtained simultaneously by varying hydrogen:char ratios and retention times. Only a few minutes retention time was required to convert one-fourth to one-third of the char to methane under the conditions used. For equal retention times, more char was converted at 1500 p.s.i.g. and 900°C. than was converted at 3000 p.s.i.g. and 700°C.; hence, temperature had a greater influence than pressure on char conversion.

Conceptual Process

Two reaction stages are required in this conceptual process for converting coal directly to high B.t.u. gas: (1) a dilute-phase stage in which coal is partially devolatilized in a stream of hot gas containing a fairly high concentration of methane; decomposition and hydrogenation of the coal volatiles increases the methane concentration of the gas leaving this stage to the extent that removal of impurities will give a product exceeding 900 B.t.u./std. cu. ft. heating value; (2) a dense-phase stage in which the char from the first stage is hydrogenated in a moving bed, thus producing the hot methane-hydrogen mixture that is fed into the first stage. Over-all coal conversion can be varied widely by choice of residence time, pressure, and temperature; however, residence time of char in the reaction zone has the greatest influence on over-all conversion. Coal conversion is held at a level that will supply sufficient char for producing the required amount of hydrogen. Coal conversion would be approximately 54%, based on m.a.f. coal, and about 45% of the coal carbon would appear as hydrocarbon gases in the product.

Figure 6 is a simplified flow diagram of the conceptual process. Coal that has been crushed, dried, and sized to −100 mesh sieve size is fed through lock hoppers into the top of a reaction vessel, where it becomes dispersed into a dilute phase during free fall through hot gas entering in concurrent flow. The residence time of the coal in the dilute-phase stage is about 6–8 sec. and is assumed to result in converting approximately 25% of the coal while the coal volatiles, having a residence time of about 30 sec., are hydrocracked to gas. The partially devolatilized coal or char is held for 3–5 min. in the bottom section of the reactor where the hydrogen feed enters. Approximately 35% (ash-free basis) of the char is converted to methane. The gas leaving the top of the char bed mixes with a portion of the gas from the dilute-phase stage, and the combined stream is returned to the top of the dilute-phase stage. This hot gas

supplies the heat needed to bring the coal feed to reaction temperature. The hot, outgoing char residue exchanges heat with the cold, incoming hydrogen feed before being discharged into lock hoppers and conveyed to an entrained gasification plant where the hydrogen is produced. The raw product gas is withdrawn from the lower portion of the dilute-phase stage and contains mostly methane with some hydrogen and water vapor and small quantities of carbon oxides, ammonia, and hydrogen sulfide. This gas (200 atm. and about 800°C.) has considerable potential for useful work. We propose to recover electrical power by first removing the entrained solids (dust) and then expanding the gas through a turbine to an exit pressure of 40 atm. and temperature of 520°C. (970°F.). The gas, following cooling and cleaning at pressure to remove contaminants, could go directly into the transmission system, or it could be processed further to obtain additional methane from the small quantity of residual carbon monoxide and hydrogen.

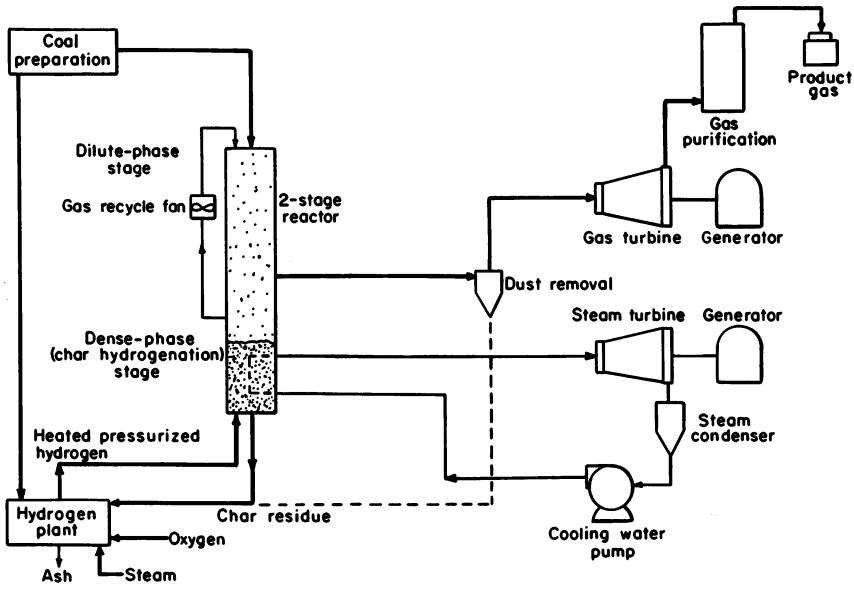

Figure 6. Simplified flow diagram of the conceptual process

The strongly exothermic hydrogenation reaction requires the removal of heat to control the temperature. This could be done by pumping water at 3000 p.s.i.g. through thin-walled tubing distributed throughout the char hydrogenation stage. The superheated steam generated in the tubing is collected and expanded through a turbine to generate additional power, and the condensate is returned to the pump.

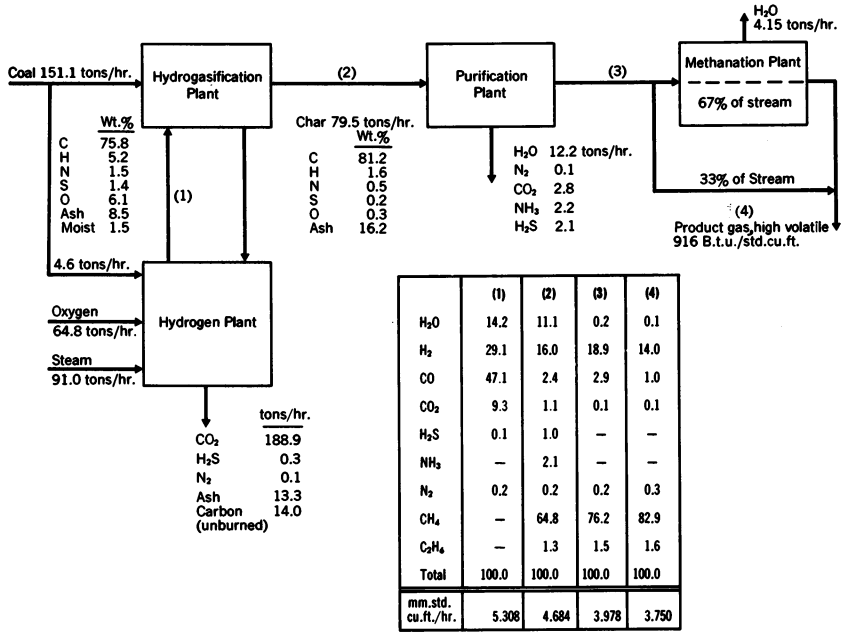

	(1)	(2)	(3)	(4)
H_2O	14.2	11.1	0.2	0.1
H_2	29.1	16.0	18.9	14.0
CO	47.1	2.4	2.9	1.0
CO_2	9.3	1.1	0.1	0.1
H_2S	0.1	1.0	–	–
NH_3	–	2.1	–	–
N_2	0.2	0.2	0.2	0.3
CH_4	–	64.8	76.2	82.9
C_2H_4	–	1.3	1.5	1.6
Total	100.0	100.0	100.0	100.0
mm.std. cu.ft./hr.	5.308	4.684	3.978	3.750

Figure 7. Stream flows and compositions as conceived for a hydrogasification plant producing 90 mm. std. cu. ft./day of high B.t.u. gas from coal

Figure 7 shows stream flows and compositions for a conceptual gasification plant producing 90 million std. cu. ft./day of 916 B.t.u./std. cu. ft. gas. The char leaving the plant is gasified to produce hydrogen feed. Obviously, the quantity of char depends on the amount of coal converted to gases and liquids in the hydrogasification plant. In the case illustrated, char fed to the hydrogen plant must be supplemented by a small amount of coal. The raw gas leaving the hydrogasification plant is cleaned to remove dust, moisture, carbon dioxide, nitrogen, and sulfur. About two-thirds of the clean gas is methanated to reduce the carbon monoxide and hydrogen content and to produce additional methane.

Conclusions

Exploratory experiments have shown that strongly caking coal can be partially devolatilized by dispersing it in dilute phase in a methane-hydrogen mixture which becomes enriched with hydrocarbon gases from the coal volatiles and thereby increased in gross heating value to 900 B.t.u./std. cu. ft. or more. The coal residue was a dry, free-flowing char which is quite reactive and easily hydrogenated to produce a methane-rich gas. The composition of this gas was determined by the hydrocarbon

gas yields and the hydrogen:char feed ratios, while the char conversion was fixed by the residence time and reaction temperature. The two operations were combined to form a conceptual process for producing high B.t.u. gas on a commercial scale.

Development of dilute-phase hydrogasification is continuing to determine the effect of higher coal temperatures on yields and gas composition. Coals other than Pittsburgh seam also will be tested.

Literature Cited

(1) Benson, H. E., Tsaros, C. L., "Abstracts of Papers," 149th Meeting, ACS, April 1965, p. 16J.
(2) Elliott, M. A., *Am. Gas Assoc. Operating Section Conf.*, **CEP-61-15** (1961).
(3) Hiteshue, R. W., Friedman, Sam, Madden, Robert, *U. S. Bur. Mines Rept. Invest.* **6376** (1964).
(4) Huebler, J., Schora, F. C., *Chem. Eng. Progr.* **62**(2), 87 (1966).
(5) Perry, H., *Petrol. Refiner* **41**, 89 (1962).
(6) Schultz, E. B., Jr., Linden, H. R., *Inst. Gas Technol. Res. Bull.* **29** (1960).

RECEIVED December 8, 1966.

6

Bench-Scale Studies of the Kellogg Coal Gasification Process

P. A. LEFRANCOIS, K. M. BARCLAY, and G. T. SKAPERDAS

The M. W. Kellogg Co., Research and Development Center, Piscataway, N. J.

The Kellogg coal gasification process uses molten sodium carbonate to catalyze and to supply endothermic heat for the carbon-steam gasification reaction. Combustion of coal with air supplies the heat to the circulating molten salt in a separate zone. The gasification product gas, after purification, can be used as synthesis gas to produce hydrogen or can be converted to synthetic natural gas for pipeline use. The program to develop this process was divided into three main areas—process research, corrosion research, and engineering design and economics. The bench-scale process research on gasification is reported here. Details are given of the experimental procedure and the effect of variables on the rate of gasification with steam of various carbonaceous solids in molten sodium carbonate.

The Kellogg coal gasification process is unique in applying molten sodium carbonate as a heat-transfer agent as well as a catalyst for the endothermic carbon-steam and exothermic carbon-oxygen reactions needed for coal gasification. The catalytic effects of sodium carbonate are well documented (*5*). Gasification occurs in the molten sodium carbonate by introducing steam containing finely-divided carbonaceous fuel at the bottom of the reactor. Heat for the gasification reaction comes from the molten salt. By continually circulating molten salt containing carbon from the gasifier to the combustor, combustion of the carbon by air injected at the bottom of the combustor produces heat which is transferred to the molten salt. The reheated melt is circulated back to the gasifier continuously. The product gas from the gasifier, after purification, can be used as a synthesis gas, to produce hydrogen, or it can be converted into synthetic natural gas for pipeline use. The preliminary engineering and economic aspects of the plant have been presented (*1, 3,*

4) and are continually being revised as experimental data are obtained. These engineering economic studies have helped to narrow the range of operating conditions and guided the process research reported here.

The bench-scale process research work was designed to define the area of operability as quickly as possible for the engineering studies. The rates of gasification and combustion of a broad range of carbonaceous fuels were required. The effects of the variables of the process were also desired—*i.e.*, temperature, pressure, superficial gas velocity, bed height, ash content in melt, particle size of fuel, carbon concentration in the melt and product gases. Also required were viscosity measurements of various melts, melt expansion from various gas flows, measurement of sodium salt carryover, and the development of a recovery procedure for sodium carbonate while separating the ash. Only the data on gasification will be presented here; the other studies will be given in future papers.

This paper presents the empirical approach we used to understand this complex system. The main question of operability and feasibility of gasification had to be answered. To accomplish this, a metal reactor was designed which would take an initial charge of fuel and allow us to determine the rate at which the carbon gasified in a large excess of steam. This was a batch-decay type of rate study. Continuous operation must be studied in larger equipment.

Some preliminary considerations helped us set limits for temperature, pressure, and velocity. Pure sodium carbonate melts at 1563°F. (2), but formation of some sodium hydroxide, as well as the presence of coal ash, tends to decrease the melting point. Consequently, the temperature range of interest is above 1500°F. Carbonaceous particles tend to float on the surface of unagitated liquid sodium carbonate. Mixing was accomplished with superficial gas velocities of 0.5 ft./sec. or higher. Although engineering studies indicated that commercial operating pressure would be about 400 p.s.i.a., the bench-scale unit had a maximum safe pressure of 150 p.s.i.a. Higher pressures must await tests in pilot plant equipment.

Experimental

Apparatus. The flow diagram of the experimental apparatus is shown in Figure 1. The reactor was made of 2-in. i.d. Inconel 600 pipe, Schedule 40, 26 in. long. A thermowell of 1/4-in., Inconel tubing entered at the bottom of the reactor. A 1/4-in. Inconel tube for steam and nitrogen entered from the top and extended to within 1/2 in. of the bottom of the reactor. Also affixed to the top of the reactor was a 1/2-in. pipe with two quick-opening ball-type valves, which served as a lock hopper for introducing the carbonaceous solid as 12/20-mesh material. Gases exited near the top of the reactor into 1/4-in. pipe which connected to a four-way tee, through which a horizontal and a vertical drill sealed by Conax fittings could be used to keep the exit line open. This was necessary because under certain conditions solid salt buildup in the exit line

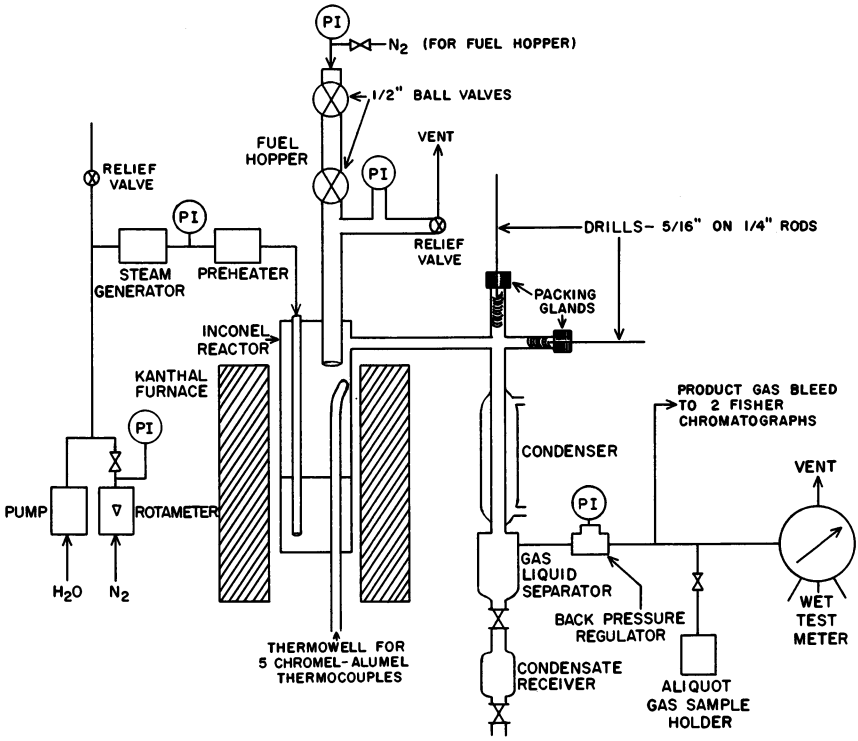

Figure 1. Flow diagram for bench-scale gasification unit

tended to plug the pipe. A water condenser was followed by a separator, a back-pressure regulator, sample taps for gas chromatographic equipment, and a wet-test meter.

Water was pumped using a Ruska positive displacement pump or Lapp diaphragm LS-10 and 20 pumps. This water, with a nitrogen bleed, went into a 40-in. long steam generator made of 1-in. pipe and appropriately wound with heating wire. A superheater, 20 ft. of 1/4-in. tubing in a coil 10 in. long, used a 12-in. long furnace. The outlet was connected to the 1/4-in. tubing that went internally to the bottom of the reactor. All exposed piping from the generator to the reactor and from the hopper to the reactor was wound with covered resistance wire. Nitrogen and other gases were delivered with conventional equipment through calibrated rotameters. The 90% steam–10% nitrogen stream was normally fed at 0.5 ft./sec. superficial gas velocity in the reactor.

A 24-in. long, 2.75-in. diameter Kanthal furnace heated the reactor. All thermocouples were Chromel-Alumel. Multiple-point recorders were used. Gases were analyzed using Fisher partitioners to obtain N_2, CO_2, CO, and hydrogen by difference. Mass spectrometric and other gas chromatographic equipment were utilized when necessary.

Procedure and Calculation. Operation consisted of introducing a total of 414 grams of pure, dense sodium carbonate and ash, if added,

which was melted and brought to the desired temperature with a flow of nitrogen through the steam inlet. This amount of molten salt was 4 in. deep under quiescent conditions. Steam rate was then set at pressure and held for 15 min., then stopped for a 5-min. period before the carbonaceous solid was introduced. Steam was then introduced 5 min. later for the start of the gasification run. Sufficient solid was charged, based upon its fixed carbon content, to give 4% by weight of carbon in the melt initially. Collection of aliquots of the gas in the nitrogen-devolatilization period and in the first 5 min. of gasification allowed complete determination of carbon disappearance. Product gas was analyzed at 5-min. intervals until all of the carbon added was consumed and the run was terminated. Total carbon gasified per 5-min. interval was calculated, and the percent carbon remaining at each time reading was plotted on semi-log paper. Three examples are given in Figure 2, and the data for these and other runs are summarized in Table I.

The data in Figure 2 show a reasonably linear relationship at least to 50–60% of the carbon consumed upon which the lines were drawn. Assuming pseudo-first-order kinetics, namely

$$k = \frac{2.3}{t} \log \frac{\mathrm{Co}}{\mathrm{C}}$$

at 50% carbon consumption—*i.e.*, C = 50% and Co = 100%, and t the time in minutes to get to 50% carbon consumption (making a correction for the initial lag at the start) allowed k, the specific reaction rate constant to be determined in reciprocal hours ($k = 2.3 \times 0.3 \times 60/t$ min.). For illustrative significance, this reaction rate constant was converted into pounds of carbon gasified per hour per cubic foot of molten salt with 4% carbon present in the melt. A density of 1.96 grams/ml. was used for molten sodium carbonate which set 82 grams carbon present per liter of sodium carbonate or 5.12 lbs. carbon per cu. ft. Thus $k \times 5.12$ gives the rate value used in the results.

In Figure 2 the points at greater than 60% carbon consumption (40% left) fall below the line. This indicates that gasification is increasing and is not simply first order in carbon concentration. However, for our objectives the above method of determining the rate has been adopted.

The apparent increase in rate may arise from the increase in surface as carbon was removed from the original particle. Although the conventional experimental rate equation for the carbon-steam reaction (*6*) states that steam is a part of the rate equation, it further states that steam also inhibits the rate. The test procedure used here maintains inlet steam at a fixed velocity and in large excess; thus any effect of the level of steam conversion should be negligible on the integral rates calculated here. In the runs shown in Figure 2, the maximum use of steam by carbon in a 5-min. period varied from 3.6 to 8.5% of the total steam available. Of

the runs shown in Table I, 10% steam utilization was the maximum value which occurred in run H-12. Analyses of the various feedstocks are given in Table II.

Results

Temperature. The gasification rate at atmospheric pressure and 0.5 ft./sec. superficial gas velocity was determined for bituminous coal at three temperature levels. The results are shown below.

Temperature, °F.	*Carbon, lb. gasified/hr./cu. ft.*
1740	6.5
1840	15.2
1940	33.0

The increases in gasification rate with increasing temperature were considerable and give an apparent activation energy of 50 kcal., which indicates that chemical reaction was controlling the rate.

Later it was established that 12/20-mesh particles of bituminous coal caked together and agglomerated while being charged into the melt in the reactor. These agglomerates naturally reacted more slowly than 12/20-mesh material and led to low gasification rates. Agglomeration was prevented by surface oxidation of bituminous coal with air at 300°F. Gasification of the oxidized material, as shown below, gave greatly improved rates. The activation energy was lowered to 27 kcal. which indicated that chemical reaction was still controlling. The effect of temperature on the rate of gasification of the other carbonaceous fuels is discussed below.

Pressure. The effect of steam pressure was determined with 30% steam in nitrogen at 1 atm., and with 90% steam in nitrogen at 1, 2, 3, 4, and 10 atm. The data have been obtained from runs using bituminous coal and coke derived from this coal by coking to 1740°F. in nitrogen. Initial runs were made at 1840°F., but rapid gasification decreased the accuracy of determining the rate constant, as shown by the scatter of points for the top curve in Figure 3. Dropping the melt temperature to 1740°F. gave an excellent series of points, as depicted in the middle curve of Figure 3. All these runs were made at 0.5 ft./sec. superficial gas velocity with a 4-in. bed of molten sodium carbonate and at an initial concentration of 4% carbon in the bed.

There appears to be a linear relationship between the logarithm of the rate and of the steam pressure. It must be mentioned that at the high steam pressures, water conversions were below 6%, while at the lowest steam pressure and 1740°F., a maximum of 49% of the water was consumed. Since commercial operation may use up to 75% of the water fed, extrapolating from the above data cannot be made to commercially

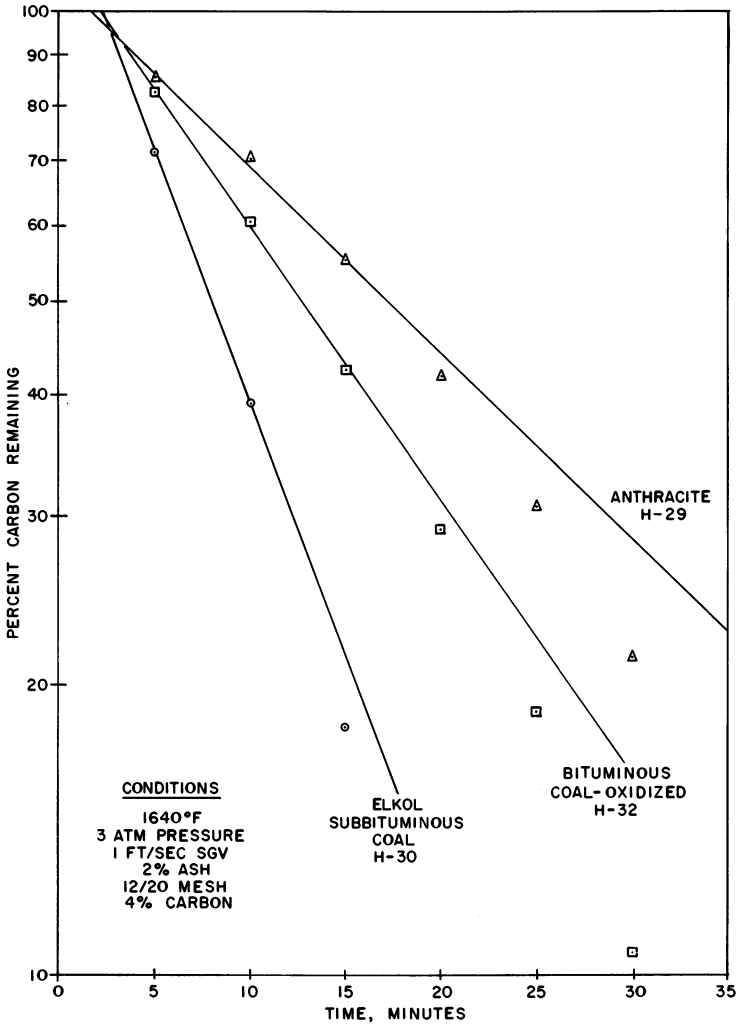

Figure 2. Examples of carbon disappearance with time

desired conditions. However, the rates at the higher pressures are encouraging. Runs at higher pressures must await construction of a pilot plant.

Bed Height. The effect of the height of the molten salt bed on the kinetics is important for commercial design, which at present calls for bed heights of 10–20 ft. Ideally for ease of design, one would prefer that bed height have no effect on the kinetics of gasification. Physical limitations of the test equipment have allowed only a small amount of evidence to be obtained in this area.

Table I. Experimental Data

	H-29	*H-30*
Feed	Anthracite	Elkol Subbitum.
Fixed carbon, %	82.5	48.5
Grams charged	20.5	35.6
Mesh size	12/20	12/20
Na_2CO_3, grams	405.7	405.7
Ash, grams	8.3	8.3
Bed height, in.	4	4
Ash in Na_2CO_3, %	2.0	2.0
Initial carbon in melt, %	3.9	4.0
Conditions		
Melt temp., °F.	1640	1640
Pressure, p.s.i.a.	45.1	45.4
Steam in N_2, %	90.6	91.7
Steam pressure, p.s.i.a.	40.9	41.6
Sup. gas velocity, ft./sec.	1.03	0.98
Run time, min.	45	25
H_2O/hr., cc.	1197	1197
N_2/min., cc.	2585	2232
Results		
Moles CO_2 + CO in prod. gas		
Devol. gas (+ CH_4)	0.110	0.262
0-5 min.	0.180	0.417
5-10 min.	0.199	0.474
10-15 min.	0.190	0.309
15-20 min.	0.168	0.158
last 5 min.	0.069	0.107
Carbon remaining (output), %		
5 min.	85.8	71.5
10 min.	70.2	39.2
15 min.	55.2	18.1
20 min.	42.0	7.3
Total C devolatilized, %	7.8	13.5
Total C to CO + CO_2, %	90.3	67.3
Total C to tar + loss, %	1.9	19.2
Gasif. rate constant		
k, input	2.30	7.38
k, output	2.65	7.27
Rate, lbs. C/hr./cu. ft. at 4% C	13.6	37.2

[a] Coke from bituminous coal at 1740°F. in N_2, 0.6% volatile matter and 6.2% ash
[b] Reused melt from previous run

The effect of bed heights from 2–8 in. was studied in the 2-in. diameter reactor. The results at 2, 3, 4, and 6 inches are shown in Figure 4. Conditions for these runs are also given. Adjusting the position of the

for Some Gasification Runs

Run					
H-32	*H-41*	*H-42*	*H-11*	*9986*	*H-12*
Bitum. Oxid.	Anthracite		Coke[a]		
58.3	82.5	82.5	93.2	93.2	93.2
29.6	21.3	21.3	9.5	19	38
12/20	12/20	12/20	12/20	12/20	12/20
405.7	405.7	[b]	405.7	405.7	[b]
8.3	8.3	—	8.3	8.3	—
4	4	4	4	4	4
2.0	2.0	2.6	2.0	2.0	2.1
4.0	4.1	4.1	2.1	4.1	7.9
1644	1645[c]	1642	1732	1740	1742
43.0	45.3	45.3	45.6	44.7	45.3
91.2	48.2[c]	53.6	90.7	88.6	91.0
39.2	21.8	24.3	41.4	39.6	41.2
0.98	1.03	0.93	1.03	1.05	1.02
40	40	40	25	35	45
1195	667	667	1192	1169	1190
2386	14870	11970	2546	3108	2444
0.188	0.180	0.024	0.035	0.189	0.083
0.247	0.137	0.181	0.192	0.264	0.511
0.310	0.205	0.210	0.191	0.322	0.557
0.257	0.197	0.204	0.143	0.241	0.497
0.187	0.185	0.188	0.102	0.160	0.415
0.067	0.105	0.123	0.080	0.067	0.071
82.6	89.1	86.9	72.7	78.9	81.6
60.6	72.8	71.6	45.5	53.1	61.6
42.5	57.1	56.8	25.2	33.8	43.7
29.2	42.4	43.2	10.7	21.0	28.7
9.4	12.5	1.7	4.7	12.8	2.8
70.6	87.9	95.9	95.9	84.7	94.1
20.0	—	2.4	—	2.5	3.1
3.84	2.58	2.35	5.68	4.60	4.51
3.93	2.58	2.46	5.68	4.92	4.81
20.1	13.2	12.6	29.1	25.2	24.6

[c] Hydrogen used in place of nitrogen

reactor in the furnace allowed identical temperature profiles to be obtained for 2- to 6-in. beds but not with an 8-in. high bed.

A significant effect of bed height on gasification rate was obtained in the 2-in. diameter reactor. It was concluded that this height effect must be caused by poorer contact of carbon and steam with increasing height.

Table II. Analyses

Source	*Anthracite* Greenwood Old Co. Lehigh Allentown, Pa.	*Bituminous* Island Creek #27 Logan Cy. W. Va.
Proximate Analysis (as rec'd), wt. %		
H_2O	4.68	1.31
Vol. Matter	5.68	37.30
Fixed Carbon	78.60	57.59
Ash	11.14	3.80
Sulfur	0.50	0.65
Ultimate Analysis (dry basis), wt. %		
C	82.46	83.60
H	2.62	5.14
N	0.76	1.48
S	0.52	0.66
O	1.95	5.27
Ash	11.69	3.85

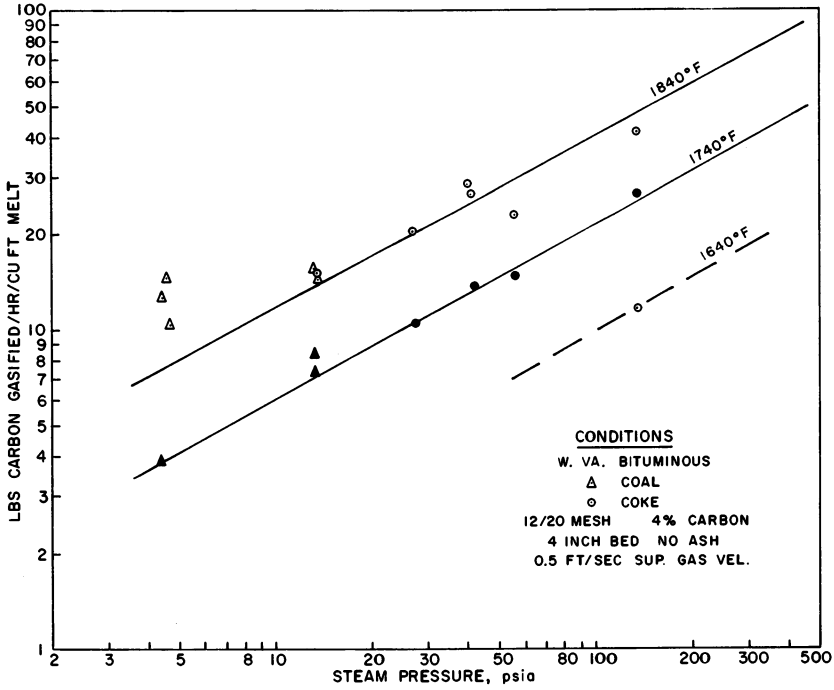

Figure 3. Effect of steam pressure on gasification rate

of Feedstocks

Subbituminous	*Lignite*		*Char*
Elkol Kemmerer Frontier, Wyo.	So. Beulah Knife River Beulah, N. D.	Renners Cove Consol. Coal Co., N. D.	FMC ex Ill. #6 Crown
18.79	31.20	32.90	—
39.21	30.30	32.35	3.5
39.40	29.50	28.54	76.4
2.60	9.00	6.21	20.1
0.63	1.17	0.69	3.1
73.50	66.35	66.35	76.8
4.52	3.33	4.11	1.4
1.50	1.96	1.10	1.2
0.78	1.70	1.03	3.1
16.50	13.58	18.16	0.1
3.20	13.08	9.25	17.4

Steam bubble size and carbon distribution are the principal variables. The latter appears most suspect at this time. A change in bubble size by a 3.25-fold decrease in diameter of the orifice inlet for steam did not have any effect on rate; thus bubble size does not appear to control the rate. It is believed that larger diameter reactors will allow better mixing to be achieved and thus lessen the effect observed here. Further evaluation must await construction of pilot plant equipment.

Superficial Steam Velocity. Original adoption of 0.5 ft./sec. superficial steam and nitrogen velocity was based upon simulated visual experiments with an aqueous zinc chloride system of 2 grams/cc. density and charcoal which showed excellent mixing at velocities of 0.25 ft./sec. and higher. The results of a separate study under gasification conditions are shown in Figure 5. The run at 2 ft./sec. taxed the steam generating and condensing system, as well as the heat supply from the Kanthal furnace. Temperature dropped from 1740° to 1710°F. in the initial part of the run, and the rate required a correction to adjust it to 1740°F. It does appear that the rate levels off at around 2 ft./sec. Gasification rate increases two-fold in going from 0.5 to 2 ft./sec. superficial velocity.

The velocity effect definitely indicates that this system is sensitive to mixing. An increase in velocity increases agitation and exposes more interfacial area for greater steam-carbon contact. It appears to substantiate the conclusion reached above in studying bed height.

Ash Content in Melt. In commercial operation, a steady-state content of ash will exist in the melt. The effect of bituminous coal ash of

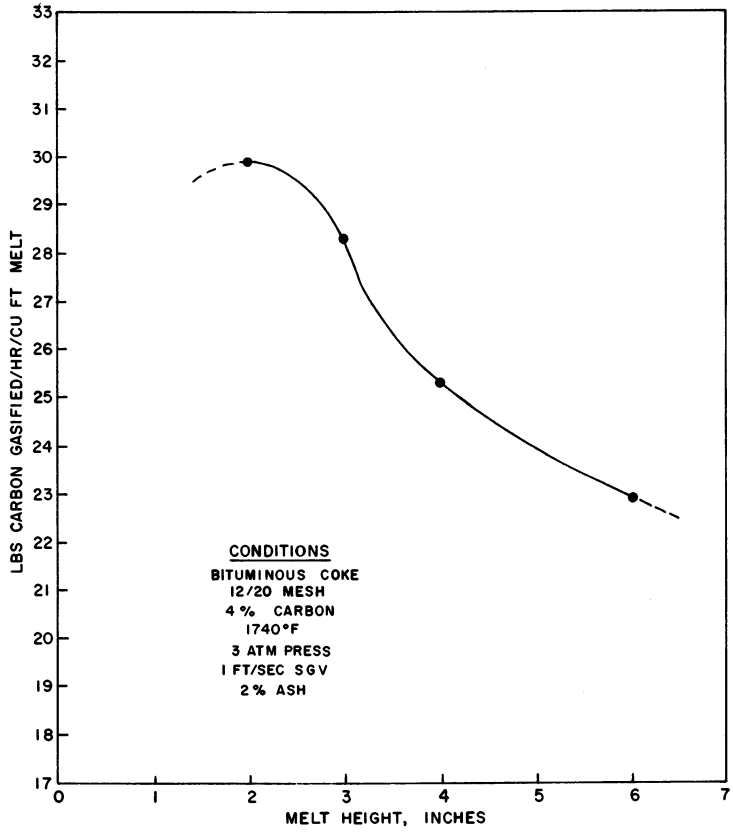

Figure 4. Effect of melt height on gasification rate

—100-mesh particles in the melt on the rate of gasification of bituminous coke was determined at two levels of superficial gas velocity. The conditions and results are shown in Figure 6. The major effect of enhanced rate occurs in the first few percent of added ash, with the effect greater at the lower velocity. Beyond 6–8% ash content, expansion of the melt into a lower temperature zone of the furnace interfered and caused a dropoff in rate. This is the main reason only 2% ash was used in most of the studies rather than a larger amount as contemplated for commercial operation.

The effect of ash appears to resemble the effect of velocity. Ash increases both the viscosity of the melt and the amount of froth; thus greater interfacial area is created, and better steam-carbon contact occurs.

Feedstock Evaluation. A broad spectrum of carbonaceous solids was acquired whose proximate and ultimate analyses are given in Table II. All of these feedstocks as well as oxidized bituminous coal and the coke

derived from bituminous coal used in the previous variable studies were evaluated under the usual gasification conditions given in Figure 7.

The position of the bituminous coal at the bottom, even below anthracite, was established to be a result of agglomeration of the 12/20-mesh particles to a larger size which reacted at a slower rate. Low temperature oxidation of the surface of the bituminous coal eliminated the caking tendency or reduced it to a low level, improving the gasification rate by a factor of almost 2. The behavior of the coke from bituminous coal was similar to that of anthracite. The two lignites from North Dakota were quite reactive, and the Wyoming subbituminous coal was slightly more reactive. The data for Renners Cove lignite appears to be out of line, but lack of material did not allow further evaluation. Top reactivity was achieved by a char made by FMC from an Illinois coal. This char had

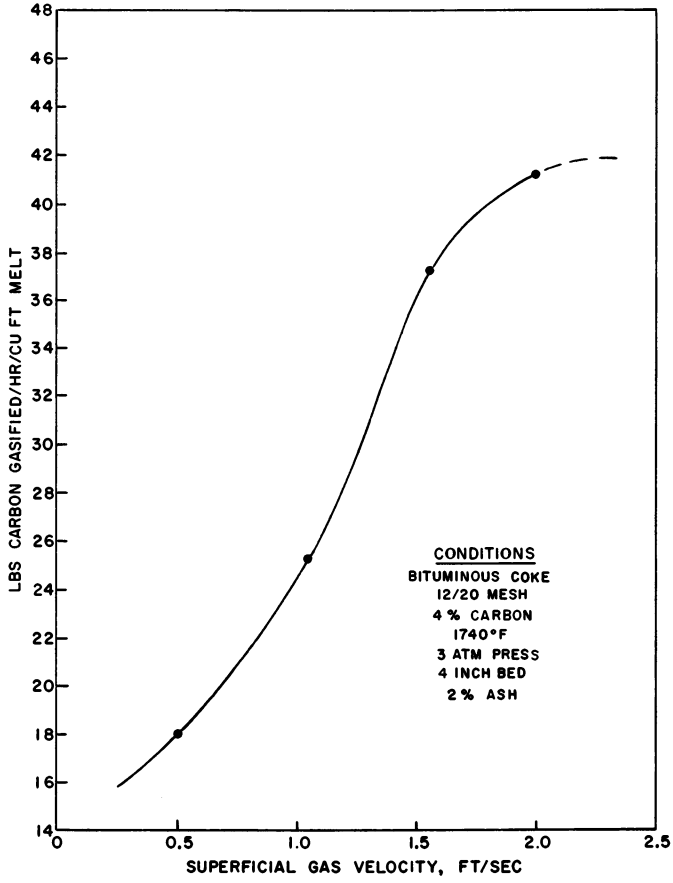

Figure 5. Effect of superficial gas velocity on gasification rate

high porosity and 80 sq. meters/gram surface area, which must have aided the reactivity.

From the above results, Table III shows the apparent activation energies as ranging from 5 to 34 kcal., in the diffusion to chemical con-

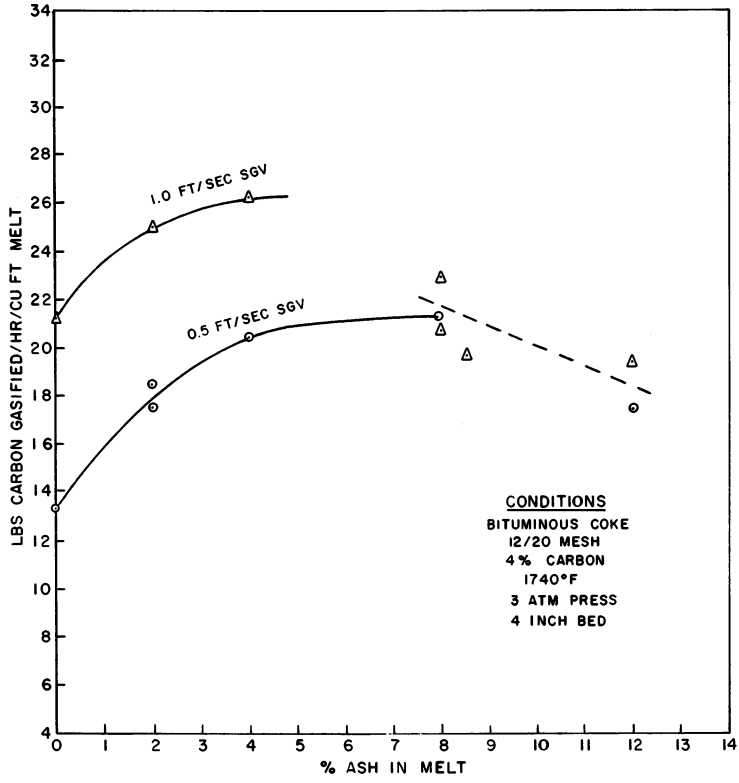

Figure 6. Effect of ash content in melt on gasification rate

Table III. Apparent Activation Energies and Relative Reactivities for Gasification of Feedstocks

Feedstock	*Rate, lbs. C /hr./cu. ft.* 1640°F.	1740°F.	*Relative Reactivity*	*Apparent Activation Energy, kcal.*
FMC Char	44	53	2.8	9
Elkol subbituminous coal	37	48	2.4	14
Renners lignite	37	41	2.3	5
Beulah lignite	28	40	1.9	19
Oxidized bituminous coal	20	34	1.5	27
Anthracite	14	24	1	28
Bituminous coke	13	25	1	34
Bituminous coal	—	19	—	—

trolling regimes, and shows also the relative reactivities, with anthracite as 1, indicating that FMC char is almost three times as reactive.

It must be noted that the above rates are conservative since they are based on only the fixed carbon content of the feedstock. In the test unit and under the procedure employed, about 7–14% of the carbon appeared in the devolatilized gas and 14–26% of the total carbon went to tar and loss. This occurred when the coal was added to the molten salt before the steam was cut in. In commercial operation with bottom feeding, the carbon in the volatile matter will be reformed in passing up the 10–20 ft.

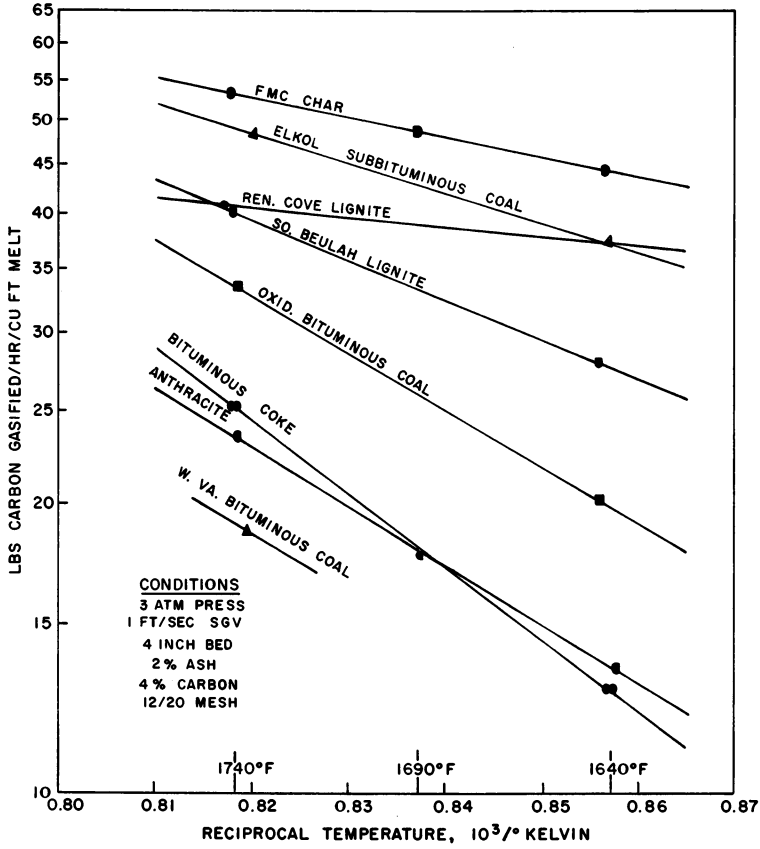

Figure 7. Feedstock evaluation. Effect of temperature on gasification rate

of molten salt. Thus, total pounds of carbon gasified per hour per cubic foot of melt will be greater than indicated by the above test unit results.

Methane at low concentrations was found in most devolatilized gas samples but rarely in any of the product gases during gasification. It is

believed that the large excess of steam, the high temperatures, and a potential catalytic effect of the Inconel reactor helped to reform any methane produced before exit from the reactor. Commercially, methane is expected to be in the product gas.

Particle Size. The effect of particle size of bituminous coke on the gasification rate was studied. Testing conditions were the same as for previous studies: 1740°F., 3 atm. absolute pressure, 1 ft./sec. superficial gas velocity, 2% bituminous coal ash in a melt of 4-in. height and 4% carbon charged initially. The results of the tests on three particles sizes are given in Table IV.

Table IV. Effect of Bituminous Coke Particle Size on Rate of Gasification

Mesh Size	*Sieve Opening, mm. arith. avg.*	*Gasification Rate, lbs./C/hr./cu. ft.*
4/8	3.6	19
12/20	1.3	25
80/100	0.16	31

A 2.8-factor increase in particle size over the normal 12/20-mesh material decreased the rate by 25%. An eight-fold decrease in size increased the rate by 24%. The explanation lies, reasonably, in surface area and distribution. Most of the runs gave first-order plots which showed increasing rate as the runs progressed. This indicates strongly that decreasing size of the carbon particles and the resultant increasing surface area may account for the increasing rate. The action of steam on various forms of carbon is known to increase the surface area; this is a widely used method of activating carbon. A commercial grind of about −10-mesh material cannot be evaluated reasonably in this unit because of the physical setup which leads to small particle loss from the reactor while charging and before reaction.

Miscellaneous. Some concern that gas temperature may have been below melt temperature was initiated when it was noted that the product gas composition indicated that equilibrium for the water-gas reaction, $CO + H_2O \rightarrow CO_2 + H_2$, was 200°–300°F. below the melt temperature. Several runs with superheated steam entering the reactor at 1500°–1600°F. instead of the usual 700°–900°F. had no effect on the gasification rate. It was concluded that equilibrium for the water-gas reaction was not dictated by melt temperature but by some metal wall temperature above the melt before the gas cooled and its composition became fixed.

In a study of the effect of individual product gases on rate, hydrogen definitely did not show any inhibitory effect on rate in this system. The use of 30% steam in hydrogen at atmospheric pressure was found to give about the same rate as 30% steam in nitrogen while gasifying bituminous

coal. At 3 atm. absolute pressure and with anthracite as feed, the gasification rate with 50% steam in hydrogen was identical to that from a duplicate run with 50% steam in nitrogen. Data for the anthracite tests are given in Table I, runs H-41 and 42. This absence of an inhibitory effect by hydrogen is contrary to the literature (*6*) and most probably arises from the system employed. One can only rationalize at this time that hydrogen, produced at the carbon-steam reaction site in the presence of the molten salt, is rapidly removed and thus cannot exert any inhibition. Despite the high concentration of hydrogen in the steam, it did not get to the reaction sites; otherwise inhibition would have occurred.

Although 30% steam in carbon dioxide, when compared with 30% steam in nitrogen, led to about a 25% decrease in rate, caution must be exercised since the difference between two large numbers—10.60 moles of carbon out and 9.53 moles of carbon as carbon dioxide in—represents the moles of carbon gasified. Hence, it is possible that carbon dioxide does show an inhibitory effect, but under normal conditions of less than 20% CO_2 in the product gas, the effect on rate is expected to be small. The effect of carbon monoxide on rate could not be determined. A run with 70% CO in steam showed that the CO reacted with the steam first, before the steam could react with the coal. This is possible in the Inconel inlet tube before exit was made into the molten salt.

Concentration of carbon from bituminous coke in the melt was varied in three runs at 1740°F., 3 atm. absolute pressure, 1 ft./sec. superficial gas velocity, and 2% bituminous coal ash in a 4-in. melt. Data for these tests are given in Table I in runs H-11, 9986 and H-12. Gasification rates for the initial carbon concentrations of 2.1, 4.1, and 7.9 were 15, 25, and 50 lbs. carbon/hr./cu. ft. of sodium carbonate at the carbon concentration stated, respectively. As expected, the pounds of carbon gasified follows the carbon concentration reasonably well, with perhaps a slightly higher efficiency for the lowest carbon concentration.

Conclusion

Process research generated on bench-scale equipment for the Kellogg molten salt gasification process has established the effect of variables in order to give a basis for designing larger units. The complicated nature of a solid-liquid-gas reacting system has been well demonstrated. The work has indicated the areas in which more information is needed, especially the effect of melt height in vessels of larger diameter.

Acknowledgment

Appreciation is expressed to the Office of Coal Research, U. S. Department of the Interior, for interest and financial support. Thanks are

expressed to the M. W. Kellogg Company for permission to publish, to J. P. Van Hook who initiated the early work, and to N. L. Manfredonia for capable assistance.

Literature Cited

(1) *Chem. Eng. News* **44**, 68 (1966).
(2) Janz, G. J., Ward, A. T., Reeves, R. D., *Rensselaer Polytech. Inst., Tech. Bull. Ser.* 103 (1964).
(3) Pieroni, L. J., Skaperdas, G. T., Heffner, W. H., *A. I. Ch. E. Symp. Processing Coal Its By-Products, Philadelphia, Pa., 1965.*
(4) Skaperdas, G. T., Heffner, W. H., *Am. Gas Assoc. Production Conf., Buffalo, N. Y., 1965.*
(5) Van der Hoeven, B. J. C., "Chemistry of Coal Utilization," Volume II, H. H. Lowry, ed., pp. 1603-1606, Wiley, New York, 1945.
(6) Von Fredersdorff, C. G., Elliott, M. A., in "Chemistry of Coal Utilization," Suppl. Vol., H. H. Lowry, ed., 931-939, Wiley, New York, 1963.

RECEIVED December 27, 1966.

Gasification of Coal under Conditions Simulating Stage 2 of the BCR Two-Stage Super-Pressure Gasifier

R. A. GLENN, E. E. DONATH, and R. J. GRACE

Bituminous Coal Research, Inc., Monroeville, Pa.

Weighed charges of coal slurry were injected into preheated rocking autoclaves under varying conditions, and gas-coal-superheated steam mixtures were fed into a continuous flow reactor. For the autoclave experiments, methane was the main reaction product, constituting 70–90% of the total B.t.u. in the gas at conversions of 10–60%. Sodium carbonate increased the methane yield. For lignite and bituminous coal in the continuous flow reactor, direct methanation was rapid and was influenced by the partial pressure of hydrogen. For conversions in the range of 45–60%, 25–45% of the B.t.u. in the coal was obtained directly as methane. These experiments confirm the basic concept of the two-stage super-pressure process, and more definitive data will be obtained from the 100 lb./hr. internally fired unit now planned.

To produce pipeline gas, coal gasification processes operating at elevated pressure and a low gas exit temperature produce a raw gas with a high methane content; this in turn leads to lower investment and operating costs than for processes that produce CO and H_2 as the principal products and do not form significant amounts of methane (*1, 2*). An entrained coal gasification process, using two reaction stages operating at 70 atm. pressure, offers promise for high yields of methane and the ability to process all types of coal, regardless of caking properties or size consist.

To achieve the required rapid reaction in an entrained system, both a reactive fuel and a means for rapid heating are necessary. The volatile

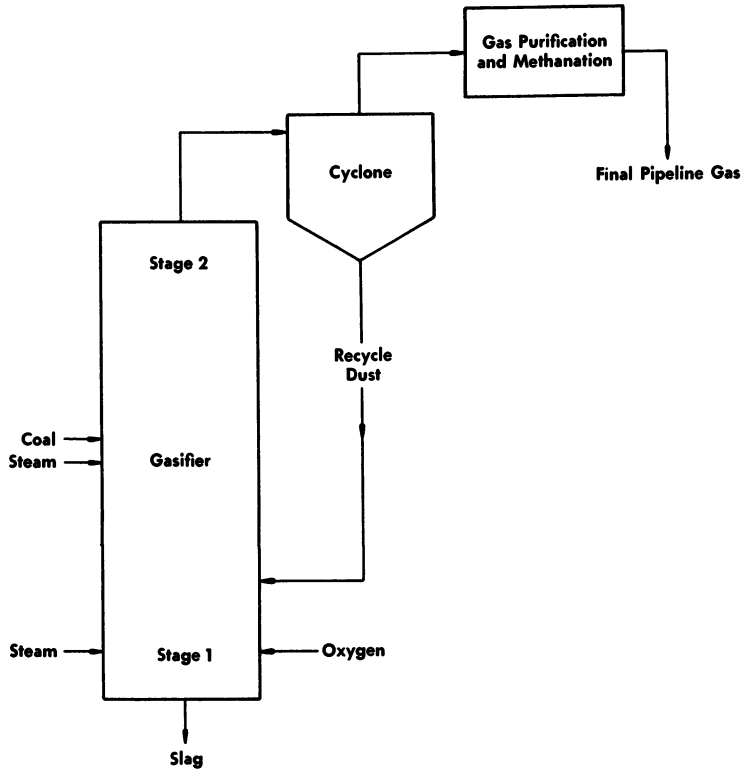

Figure 1. Simplified flow diagram for two-stage super-pressure gasifier

portion of bituminous coal or lignite is such a fuel, and to utilize it properly for generating gas of high methane content, a two-stage super-pressure process has been devised (Figure 1). In this process, heat and Stage 1 or synthesis gas are generated in Stage 1 by gasifying recycle char under slagging conditions with oxygen and steam. In Stage 2 fresh coal and steam are introduced into the hot synthesis gas issuing from Stage 1. The fresh coal is thereby rapidly heated to reaction temperature of about 1750°F. and partially converted into gas with a high methane content, mainly by pyrolysis of the volatile portion of the coal by reaction with steam and Stage 1 gas. For ultimate conversion into high B.t.u. pipeline gas, the combined gases laden with unreacted char leave Stage 2 and pass successively through steps of dust removal, shift reaction, acid gas removal, and methanation.

Since the process involves two stages, it has two types of problems that required further study. The first pertains to the slagging zone or Stage 1. Gas has been produced successfully on a commercial scale by slagging gasification of coal at atmospheric pressure (*3, 14*). For slagging gasification at elevated pressure, experimental processes have been

developed by various groups (*6, 7, 8, 9*). These investigations have shown that slagging coal gasification at elevated pressure is feasible and that development of a commercial process will be, except for the control of metallic iron formation, primarily a design problem. This previous work has also shown that meaningful results can only be obtained by experimentation on a scale that provides a minimum slag flow of 200 lb./hr., corresponding to a 1 ton/hr.-pilot plant using coal with 10% ash.

The second problem pertains to the direct-methanation zone, or Stage 2 of the process. Although various processes have been devised for utilizing the volatile portion of coal for gas production, little information is available on the primary formation of methane directly from it.

Higher yields of tar have been obtained at atmospheric pressure with increased heating rates (*10, 11, 12, 15*) and with the presence of certain fluidizing gases, such as air, steam, or helium (*4, 13*). Conditions for maximizing yields of tar in a transport reactor have been reported (*5*). Although methane yields in gasification processes have been reported at atmospheric and at elevated pressures (*2, 16*), data are not available for optimizing the conditions for Stage 2.

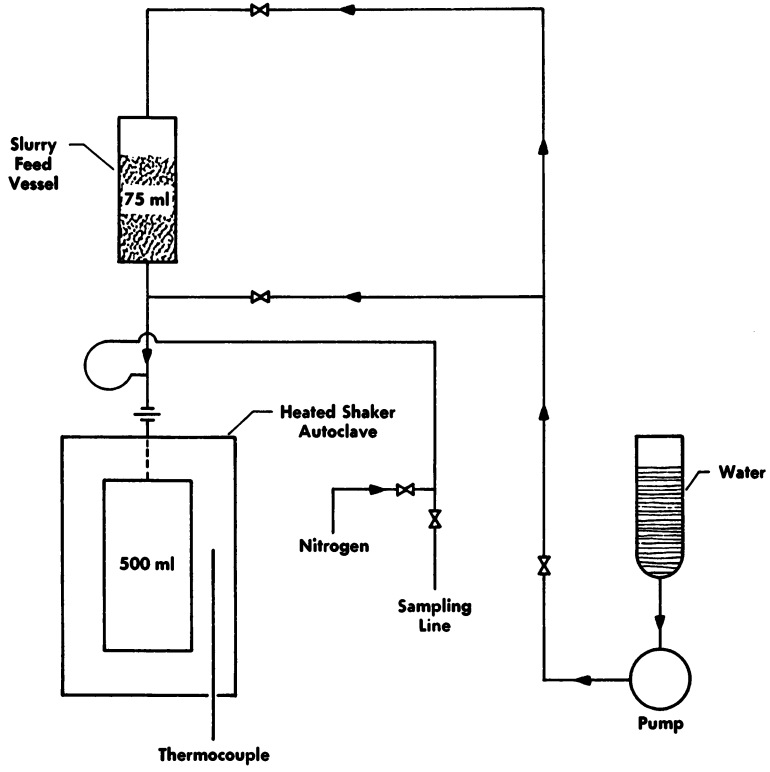

Figure 2. Flow diagram of batch autoclave reactor

This paper reports the results of laboratory research done to increase our knowledge concerning the rate of methane formation under conditions prevailing in Stage 2. These results were obtained using a different method of heating than that visualized for the actual process and equipment of a size that wall effects may have an influence even on the observed rapid reaction. Nevertheless, the data are considered adequate to design a larger, internally fired experimental unit with 20 times greater coal throughput.

Experimental

In the experimental studies, tests have been made on the direct steam methanation of coal in two types of equipment. Batch tests have been conducted in small rocking-type high pressure autoclaves. Continuous flow experiments have been made in a 1-in. reactor, 5 ft. long, under Stage 2 conditions using simulated Stage 1 gas.

Batch Autoclaves. In the batch studies of the direct steam methanation of coal, duplicate autoclave systems were used to obtain data as rapidly as possible without delay for cooling and reheating. One of the systems is shown diagrammatically in Figure 2. Both the feeder and reactor vessels are made of superstrength alloys, 19-9 stainless steel DL alloy, to permit operation at temperatures up to 1500°F. and pressures up to 10,000 p.s.i.g. The specially designed 75-ml. auxiliary feed vessel provides means for charging up to 30 grams coal as a 40 wt. % slurry. A view of the over-all reactor assembly is shown in Figure 3 together with an exploded view of the feed vessel fittings.

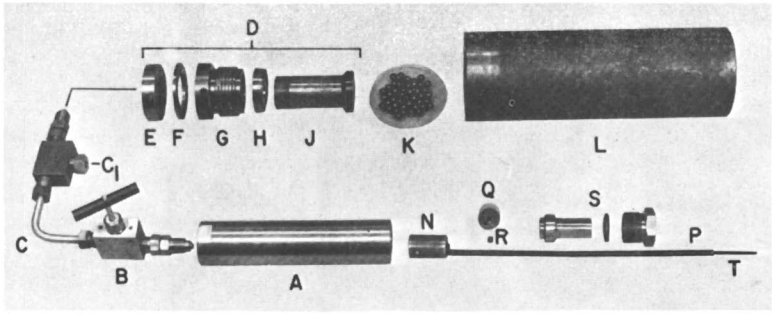

Slurry Feeder
- A — Slurry Feeding Cylinder Without Fittings
- B — Valve
- C — Connections, Feeder to Reactor T
- C_1 — Gas Outlet Connection

Reactor
- D — Cover
- E — Locknut
- F — Thrust Washer
- G — Main Nut
- H — Seal Ring
- J — Main Body
- K — 50 3/8" Diameter Stainless Steel Balls
- L — Reactor Body
- N — Piston Attached to Placement Rod (P)
- Q — Front View of Piston Showing Center Threaded Bleed Hole and Off-Center Threaded Hole for Rod
- R — Allen Set Screw to Plug Center Bleed Hole
- S — Cylinder Closure Fittings
- T — Allen Wrench to Fit Allen Set Screw

Figure 3. Exploded view of components of slurry feeder and reactor assembly

Table I. Batch Autoclave Experiments without Intermittent Sampling

	Test							
	12	*13*	*14*	*16*	*18*	*19*	*20*	*22*
Temperature, °C.	730	730	730	730	730	770	770	770
Time, min.	120	120	120	120	12	120	120	12
Coal used, grams (d.a.f.)	8.71	9.26	10.50	10.40	10.42	10.84	8.45	10.14
Catalyst, wt. % of coal	42.1	33.0	0	0	0	15.2	0	0
Residue, grams (d.a.f.)	4.43	4.47	6.37	6.71	7.23	4.63	4.97	6.75
Total pressure developed, atm.	354	326	308	181	263	243	168	188
Product partial pressures, atm.								
H_2O	306	283	273	145	247	165	130	161
CO_2	14.3	13.0	10.0	9.1	3.2	24.5	9.9	5.9
CO	0	0.1	0.4	0.6	0.4	0.6	0.6	0.5
H_2	15.3	13.6	9.3	9.3	2.9	26.4	11.4	6.3
CH_4	18.1	16.8	16.2	17.4	7.8	24.6	14.3	12.9
Gas volume, std. cu. ft./lb. d.a.f. coal	12.45	10.90	7.80	7.94	3.47	15.55	9.76	5.82
Coal converted, % d.a.f.	49.1	51.8	39.4	35.6	30.6	57.3	41.2	33.4
B.t.u. in gas, % B.t.u. in coal[a]	45.6	43.2	31.5	31.8	15.8	52.7	35.6	24.8
Carbon in gas, % C in coal	31.1	27.8	21.4	21.7	9.6	37.6	20.4	16.0
Carbon in CH_4, % C in coal	17.4	15.7	13.2	14.3	6.5	18.5	11.7	10.6
Preformed methane, %	83.0	83.2	87.0	87.7	90.9	78.5	82.8	88.5

[a] Based on total carbon in products

In typical operation, a weighed charge of coal slurry, consisting of a mixture of 40 wt. % of −325 mesh coal and 60 wt. % water with or without added sodium carbonate catalyst, was injected rapidly by hydraulic pressure into the preheated, rocking autoclave containing a measured volume of nitrogen tracer gas. The water in the slurry flashed into steam and reacted with the coal, forming methane and other gases.

The gaseous reaction products were sampled on a specified time schedule and analyzed by chromatography. After the system had cooled following the test, the residual gases were collected, and the residues, consisting mainly of carbon and ash, were removed, weighed, and analyzed.

Tests were made under controlled but widely varied conditions. The time of reaction was varied from 2 to 120 min.; the temperature from 730°C. to 770°C.; the pressure from 60 to 350 atm. The experimental data and results are summarized in Tables I and II.

Table I gives the data and results for those tests in which gas samples were taken only at the end of the tests. Table II gives the data and results for those tests in which gas samples were taken at stated intervals during the test as well as at the end. By this latter procedure, additional information was obtained on the effects of time on the reactions.

Continuous Flow Reactor. In the flow experiments under Stage 2 conditions using simulated Stage 1 gas, a continuous flow reactor with a design capacity of 5 lb./hr., a maximum operating temperature of 1800°F. (1000°C.), and a maximum working pressure of 1500 p.s.i.g. (100 atm.) was used. A schematic illustration of the total system using slurry feeding of coal is shown in Figure 4, and a general view of the safety stall and control area is shown in Figure 5.

The 5-ft. long reactor, made from Haynes 25 alloy, has a 3-in. o.d. and a 1-in. i.d. (Figure 6). Under operating conditions, the reactor volume of about 800 ml. provides a residence time of several seconds. The preheater furnace and each of the three sections of the reactor furnace are independently controlled by temperature-recorder controllers that regulate saturable core transformers. A metering piston-type pump is used to feed the slurry of coal in water. Pressurized Stage 1 gas—*i.e.*, simulated product gas from Stage 1—is fed into the slurry stream at the discharge port of the pump to facilitate trouble-free flow of the slurry up the vertical lines into the preheater.

The Stage 1 gas-coal–superheated steam mixture is discharged from the preheater into the reactor at a temperature of about 600°F. On

Table II. Batch Autoclave Experiments

	Test			
	35		*37*	
	35-2	*35-60*	*37-4*	*37-60*
Temperature, °C.	753	753	753	753
Time, min.	2	60	4	60
Coal used, grams (d.a.f.)	—	10.88	—	10.37
Catalyst, wt.% of coal	0	0	0	0
Residue, grams	—	7.20	—	6.84
Total pressure developed, atm.	191.4	188.7	211.8	183.2
Product partial pressures, atm.				
H_2O	177.9	152.6	190.3	141.0
CO_2	0.42	6.23	1.60	9.65
CO	0.56	0.45	1.04	0.73
H_2	0.97	7.65	2.73	10.52
CH_4	2.88	15.34	8.78	15.50
C_2H_4	0.15	—	—	0.11
C_2H_6	0.42	0.12	0.68	—
N_2	8.10	6.3	6.7	5.7
Gas volume, std. cu. ft./lb. d.a.f. coal	1.05	6.33	3.38	8.77
Coal converted, % d.a.f.	—	33.8	—	34.0
B.t.u. in gas, % B.t.u. in Coal[a]	10.3	28.5	17.1	33.4
Carbon in gas, %C in coal	3.7	18.1	11.0	23.4
Carbon in CH_4, %C in coal	2.1	12.4	7.6	14.3
Preformed methane, %	91.0	88.7	91.3	85.2

[a] Based on total carbon in products, assuming same correction applied for intermittent

entering the reactor, the mixture is raised to operating temperature in the upper section (Zone 1), reacts in the middle section (Zone 2), and is cooled to about 1000°F. in the lower section (Zone 3) before leaving the reactor. Temperature is controlled and measured by thermocouples in contact with the outside wall of the reactor. Temperatures inside the reactor with and without gas flowing did not differ significantly from temperatures of the outside reactor wall. For purposes of computing an effective reaction volume, that portion of the reactor heated within 40°F. of the maximum temperature is taken as the "reactor volume."

The product gases, containing the finely divided unreacted solids, are discharged from the reactor through a water-cooled condenser into a catchpot where the water condensate and solids are removed. From the catchpot the gases are fed through a pressure-reducing valve to a wet test meter for measurement and then on to storage in a gas holder or venting to the atmosphere.

In the condenser, cooling of the gas and flushing of the solids is facilitated by injecting water at the inlet to the condenser at a controlled rate from an auxiliary high pressure metering pump.

with Intermittent Sampling

Test								
39		*40*		*42*			*43*	
39-8	*39-60*	*40-2*	*40-60*	*42-8*	*42-13*	*42-60*	*43-4*	*43-60*
748	748	749	749	746	746	746	751	751
8	60	2	60	8	13	60	4	60
—	11.85	—	9.29	—	—	12.21	—	13.23
0	0	28	28	18.9	18.9	18.9	20.3	20.3
—	7.61	—	5.21	—	—	7.70	—	7.13
271.4	241.0	203.3	184.8	242.4	209	135.5	227.1	222.5
242.6	188.7	183.0	135.3	214.1	182.0	95.8	206.0	166.1
2.98	11.23	2.50	10.77	4.48	4.76	9.06	3.04	13.9
0.89	0.82	0.06	1.03	0.20	0.14	0.47	0.04	0.74
4.30	11.95	2.60	14.43	5.43	4.64	9.46	3.30	12.85
11.96	21.40	6.10	16.40	9.09	9.90	14.62	6.30	21.35
0.15	—	0.20	—	—	—	—	0.11	—
0.84	0.09	0.90	0.09	1.00	0.64	0.17	0.90	0.25
7.7	6.8	7.9	6.8	8.1	7.0	5.9	7.4	7.3
4.23	9.47	3.01	10.74	3.95	3.92	7.69	2.44	8.92
—	35.8	—	43.9	—	—	36.9	—	46.1
21.8	38.5	16.1	41.2	18.3	20.6	31.4	13.0	38.1
13.5	23.5	10.1	27.5	11.6	13.5	21.5	7.7	25.0
9.0	15.1	5.6	16.3	6.7	8.2	13.3	4.2	15.3
91.4	87.5	92.3	81.5	88.5	90.1	86.5	90.6	86.7

samples as for final sample

Sampling valves are located at the downstream exit of the condenser ahead of the catchpot. Gas leaves in a small stream that is withdrawn continuously from the system and monitored for changes in composition by a thermal conductivity meter; during predetermined intervals samples are taken from this stream for chromatographic analysis.

Argon, added to the Stage 1 gas as an internal reference, is used to determine any changes in gas quantity that occur during the test. The approximate composition of the Stage 1 gas was as follows: H, 18%; Ar, 10%; CO, 55%; CO_2, 17%.

Material balances are established using the usual data obtained from weight, flow, temperature, and pressure measurements; these are verified by comparison with the argon reference data.

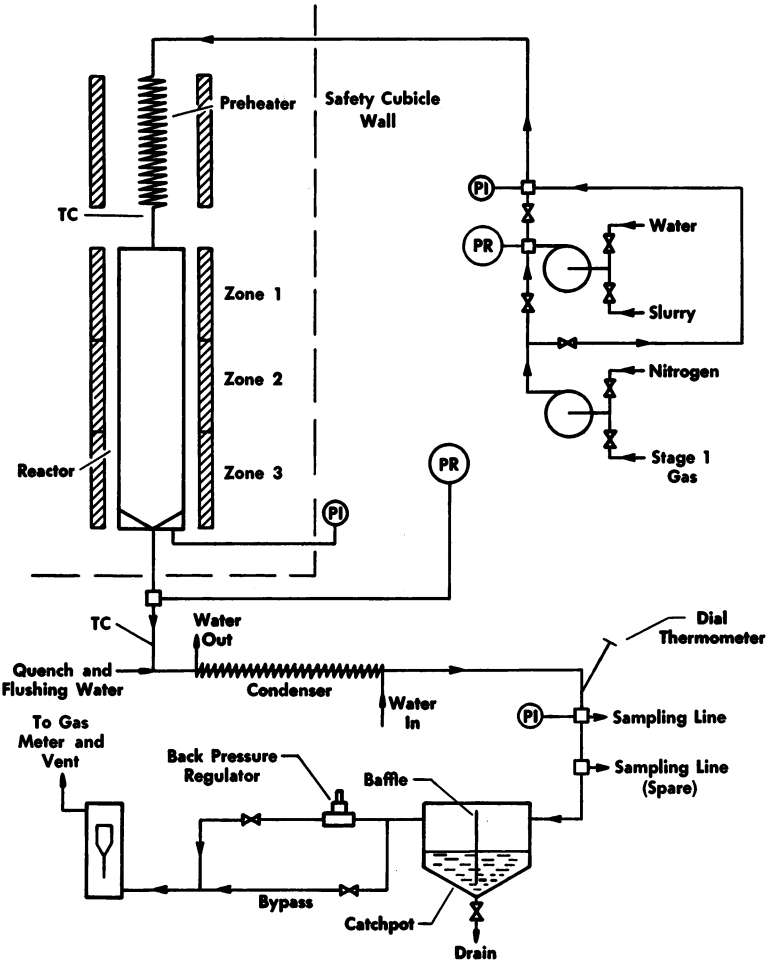

Figure 4. Flow diagram for continuous flow reactor assembly using slurry feeding

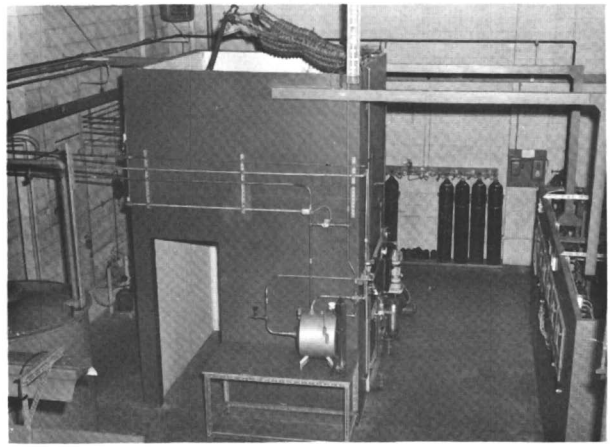

Figure 5. View of continuous flow reactor safety cubicle and control area

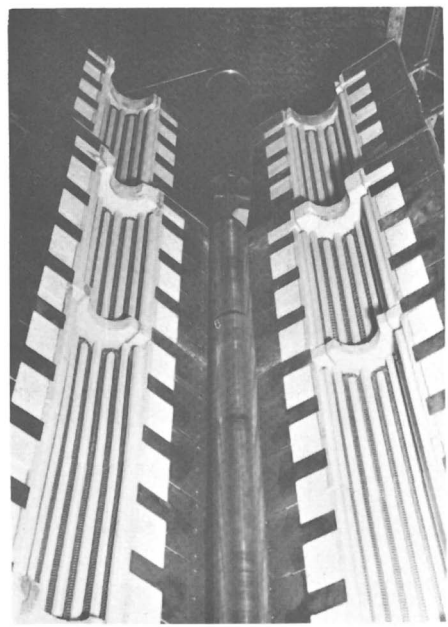

Figure 6. Top zones of continuous flow reactor with electric furnace open for inspection

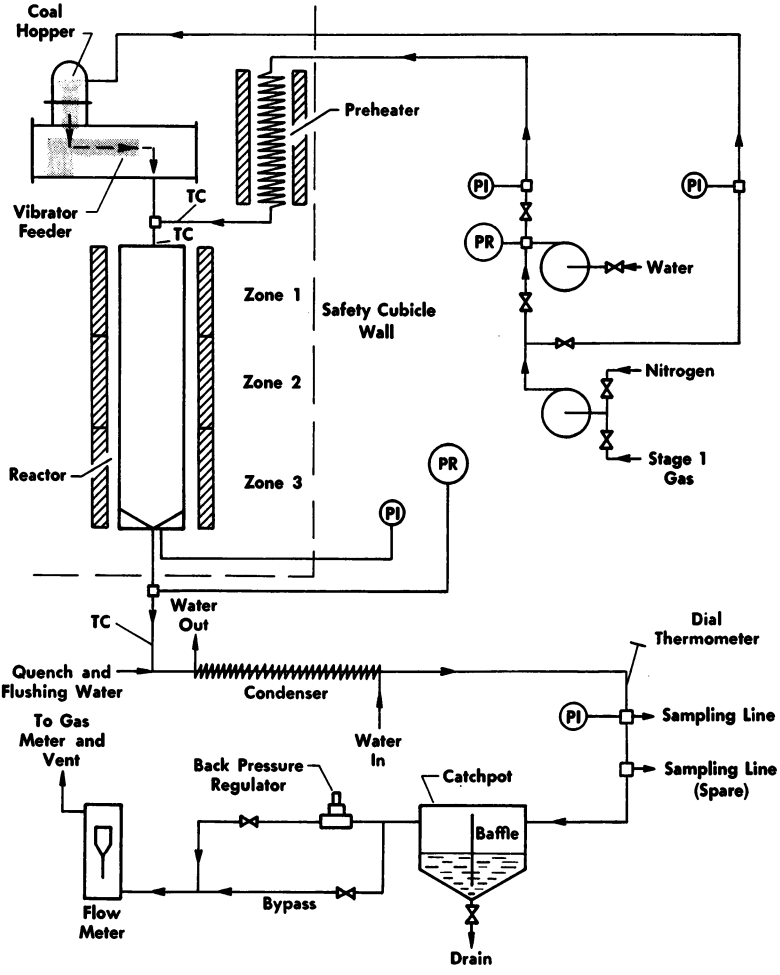

Figure 7. Flow diagram for continuous flow reactor assembly using dry feeding

The exact composition (dry basis) of the Stage 1 gas used in each test is determined by gas chromatography. The partial pressure of steam in the gases entering the reactor is based on the total input of water, including moisture present in the feed coal. The partial pressure of the Stage 1 gas is taken as the total operating pressure minus the partial pressure of the steam.

To calculate the amount of steam in the product gases, the total input water is adjusted for the amount consumed in the shift reaction and for the water produced from oxygen in the coal; to calculate the partial pressure of steam and other gases, the volume of the product gases is taken as the average of the input gas volume and the corrected output gas volume. The amount of CO_2 remaining in the catchpot liquids is

estimated from solubility data, and the observed CO_2 content of the product gas is adjusted accordingly. Ammonia and hydrogen sulfides are not considered.

To date, tests have been made in the flow reactor using both bituminous coal and lignite over a range of conditions approximating those which, at the moment, are considered optimum for Stage 2 operations.

Results

Experiments in the flow reactor with the Pittsburgh seam coal showed that it accumulated in the reactor. Even the results of short operations were falsified by the char present in the reactor and resulted in too high apparent coal conversion values. Mixing the coal with silica of small particle size (3 microns) remedied this problem, and the reactor remained free of deposits in tests of 12–18 min. duration. However, adding silica led to irregularly occurring and disappearing pressure buildups in the preheater coil and made it necessary to reduce the coal content in the slurry. This was especially true when temperatures necessary to assure complete vaporization of the water in the slurry and to superheat the steam were used in the preheater. Nevertheless, satisfactory tests could be made. Concentrations of 20% lignite in slurry were used. After heating the system and stabilizing the temperature, while feeding gas and water, tests approaching 1 hour of coal injection were made with lignite. Thus, in runs of short duration reliable results are obtained. The reactor in all cases was practically free of deposits. There were some occasional irregularities caused by transient pressure buildups in the preheater or the condenser.

Table III. Analytical Data on Test Coals

	High Volatile A Bituminous, Pittsburgh Seam (Allegheny County, Pa.)		*Lignite (Mercer County, N. D.)*	
Proximate analysis, %	*As Used*	*D.a.f.*	*As Used*	*D.a.f.*
Moisture	1.02	—	19.4	—
Ash	4.74	—	10.8	—
Volatile matter	37.60	39.80	27.8	40.0
Fixed carbon	56.64	60.20	42.0	60.0
Calorific value, B.t.u./lb.	14,100	14,970	8,540	12,270
Ultimate analysis, %				
C	79.19	83.90	51.80	74.27
H	5.48	5.71	5.54	4.85
N	1.52	1.62	0.64	0.91
S	1.35	1.43	1.08	1.55
O (by diff.)	7.73	7.34	30.14	18.42
Ash	4.73	—	10.80	—

Table IV. Tests in Continuous Flow Reactor Using High Volatile Bituminous Coal

	CFR Test		
	4	*7*	*8*
Operating Conditions			
Temperature, °F.	1730	1690	1720
Pressure, atm.	70	70	70
Reactor volume, cc.[a]	320	280	180
Residence time, sec.	6.5	5	3.0
Input			
Water, grams/min.	24	30	32
Partial pressures of materials in feed stream, atm.			
H_2O	35.7	38.0	41.5
H_2	6.2	5.5	5.4
CO	18.8	16.0	15.6
CO_2	5.6	5.0	4.8
C in coal, grams/min.	0.78[b]	2.68	2.37
Heat in coal, kcal./min.	7.75	26.6	23.5
Output			
Product gas, N liters/min.	33.0	33.0	32.5
Product water, N liters/min.	27.2	35.9	39.8
Partial pressures of materials in product gas, atm.			
H_2O	31.6	36.5	38.5
H_2	11.4	8.6	6.4
CO	15.2	16.0	16.0
CO_2	8.3	5.0	5.7
CH_4	0.2	0.7	0.86
Heat in CH_4, kcal./min.	1.7	6.7	8.5
Heat in ($CO + H_2$), kcal./min.	5.5	6.5	8.6
Heat in total gas, kcal./min.	7.2	13.2	17.1
C in coal gasified, grams/min.	0.1	0.71	1.9
Preformed methane, %	27	60	56
Yields, %			
C in CH_4	12	16	20
C in ($CO + CO_2$)	3	—	—
C in total gas	15	—	—
B.t.u. in CH_4	21	29	36
B.t.u. in ($CO + H_2$)	71	24	37
B.t.u. in total gas	92	53	73

[a] Within 40°F. of maximum temperature
[b] Coal without silica in this test

In the tests made using slurry feeding, the concentration of coal in relation to steam and Stage 1 gas was not as high as visualized for the commercial process. Thus, development of a dry coal feeder in which the coal feed rate is independent of the amount of water fed into the reactor represented a major improvement over the slurry feeding system.

The flow diagram for the continuous flow reactor assembly as modified to use the dry coal feeder is shown in Figure 7.

Source and analytical data on the coals used are given in Table III. The experimental data and results of tests in the continuous flow reactor over a wide range of conditions using both slurry feeding and dry coal feeding are summarized in Tables IV, V, VI, and VII. The data and

Table V. Tests Using Lignite in Continuous Flow Reactor with Slurry Feeding

	CFR Test				
	29A	*29B*	*30*	*31*	*32*
Operating Conditions					
Temperature, °F.	1740	1740	1740	1740	1740
Pressure, atm.	70.0	70.0	72.0	84.0	72.0
Reactor volume, cc.[a]	274	274	283	300	202
Residence time, sec.	3.0	3.9	3.2	3.9	3.4
Input					
Water, grams/min.	39.1	37.1	39.6	43.5	37.2
Partial pressures of materials in feed stream, atm.					
H_2O	39.1	49.3	40.5	51.0	52.6
H_2	6.1	4.1	6.2	7.2	3.5
CO	16.8	11.2	17.1	17.3	10.7
CO_2	5.1	3.4	5.2	5.4	3.1
C in lignite, grams/min.	4.70	4.60	4.48	5.05	7.60
Heat in lignite, kcal./min.	43.0	42.0	40.8	46.5	70.0
Output					
Product gas, N liters/min.	53.5	31.0	55.1	48.4	24.8
Product water, N liters/min.	40.2	41.1	40.6	44.9	42.5
Partial pressures of materials in product gas, atm.					
H_2O	30.0	39.8	30.6	40.4	45.5
H_2	15.4	11.8	15.3	17.6	12.0
CO	8.3	9.3	8.2	7.3	3.5
CO_2	12.1	10.0	13.9	13.8	7.6
CH_4	1.06	1.19	1.13	1.64	1.96
Heat in CH_4, kcal./min.	13.4	11.4	13.9	17.2	20.1
Heat in (CO + H_2), kcal./min.	10.0	6.9	9.1	2.7	13.3
Heat in total gas, kcal./min.	23.4	18.3	23.0	19.9	33.4
C in lignite gasified, grams/min.	1.11	1.30	2.40	1.46	1.27
Preformed methane, %	63.0	68.0	66.0	88.0	66.0
Yields, %					
C in CH_4	16.3	14.4	17.9	19.5	14.5
C in (CO + CO_2)	7.2	14.1	35.0	9.5	2.2
C in total gas	23.5	28.5	52.9	29.0	16.7
B.t.u. in CH_4	31.2	27.2	34.0	37.0	28.9
B.t.u. in (CO + H_2)	23.1	16.5	22.3	6.0	19.0
B.t.u. in total gas	54.3	43.7	56.3	43.0	47.9

[a] Within 40°F. maximum temperature

Table VI. Tests Using Lignite in Continuous Flow Reactor with Dry Feeding

	CFR Test				
	33	*34*	*35*	*36*	*38*
Operating Conditions					
Temperature, °F.	1720	1750	1725	1780	1770
Pressure, atm.	72.0	72.0	70.0	70.0	81.5
Reactor volume, cc.[a]	242	250	210	452	445
Residence time, sec.	3.4	2.4	4.2	10.4	8.5
Input					
Water, grams/min.	34.0	55.1	6.0	12.4	16.9
Partial pressures of materials in feed stream, atm.					
H_2O	43.3	51.1	11.7	24.8	34.0
H_2	5.2	3.8	10.7	8.3	8.6
CO	15.6	11.6	32.5	25.3	26.4
CO_2	4.6	3.4	9.5	7.4	8.0
C in lignite, grams/min.	9.70	14.80	17.20	5.90	18.80
Heat in lignite, kcal./min.	90.0	137.5	154.0	53.5	174.0
Output					
Product gas, N liters/min.	41.2	60.2	45.3	37.5	49.2
Product water, N liters/min.	36.9	63.4	5.8	7.4	11.6
Partial pressures of materials in product gas, atm.					
H_2O	34.1	33.0	6.9	11.5	15.5
H_2	13.4	14.8	13.1	16.9	18.0
CO	7.5	6.5	24.9	18.5	19.0
CO_2	12.6	12.2	14.3	16.0	18.0
CH_4	2.3	2.66	5.6	2.98	7.24
Heat in CH_4, kcal./min.	28.3	43.9	39.4	18.1	51.1
Heat in (CO + H_2), kcal./min.	6.3	33.7	4.6	5.6	17.6
Heat in total gas, kcal./min.	34.6	77.6	44.0	23.7	68.7
C in lignite gasified, grams/min.	3.0	5.90	3.94	2.83	6.76
Preformed methane, %	85.0	60.5	92.0	81.0	79.0
Yields, %					
C in CH_4	15.4	16.8	12.4	17.5	15.5
C in (CO + CO_2)	13.9	35.8	10.0	30.5	20.9
C in total gas	29.3	52.6	22.4	48.0	36.4
B.t.u. in CH_4	29.7	31.9	24.6	33.9	29.4
B.t.u. in (CO + H_2)	6.6	26.9	2.9	10.5	10.1
B.t.u. in total gas	36.3	58.8	27.5	44.4	39.5

[a] Within 40°F. maximum temperature

results from tests with high volatile A bituminous coal are shown in Table IV. Table V presents data and results from tests with lignite fed as a slurry and Table VI, with lignite fed as a dry powder. Gas analyses of the feed and product gases from all tests in the continuous flow reactor are presented in Table VII.

Discussion

In producing high B.t.u. pipeline gas from coal, the objective is to convert the carbon in the coal into as much methane as possible in the initial gasification step, and if not into methane, then into carbon monoxide which in another step can be converted to methane by catalytic hydrogenation.

Thus, in this study on the direct steam methanation of coal, either in batch autoclave tests or in continuous flow tests, the product gases of principal concern are methane, hydrogen, and carbon monoxide, and the greater the amount of methane in proportion to the amount of carbon monoxide and hydrogen, the smaller will be the final cost of the pipeline gas. As an index of this ratio of methane to carbon monoxide and hydrogen, the term "preformed methane" has been introduced and, by definition, is the amount of methane in the initial product of gasification expressed as a percent of the total methane potentially available including that from conversion of the carbon monoxide and hydrogen to methane

Table VII. Gas Analyses for Tests in Continuous Flow Reactor

CFR Test		*Composition, % by Volume (Dry Basis)*					
		A	H_2	*CO*	CO_2	CH_4	C_2H_6
7	Feed	9.8	18.8	54.5	16.9	—	—
	Product	8.4	25.4	43.4	20.7	2.1	—
8	Feed	9.8	18.8	54.5	16.9	—	—
	Product	8.3	20.0	50.5	18.5	2.7	—
29A	Feed	9.8	19.7	54.1	16.4	—	—
	Product	7.0	38.4	20.8	31.2	2.5	0.1
29B	Feed	9.8	19.7	54.1	16.4	—	—
	Product	6.4	40.1	14.6	35.1	3.6	0.2
30	Feed	9.9	19.6	54.1	16.4	—	—
	Product	6.8	36.7	19.8	34.1	2.5	0.1
31[a]	Feed	9.9	25.0	50.4	14.7	—	—
	Product	7.2	40.0	16.8	32.4	3.5	0.1
32	Feed	10.3	18.3	55.2	16.2	—	—
	Product	6.0	44.5	12.9	29.6	6.7	0.3
33	Feed	9.4	18.3	55.8	16.5	—	—
	Product	6.3	34.2	19.2	34.3	6.0	—
34	Feed	9.4	18.6	55.7	16.3	—	—
	Product	4.6	38.8	15.8	33.4	7.4	—
35	Feed	9.4	18.4	55.9	16.3	—	—
	Product	7.3	21.0	39.9	22.9	8.9	—
36	Feed	9.2	18.5	55.8	16.5	—	—
	Product	6.8	28.6	28.3	31.3	5.0	—
38	Feed	9.2	18.2	55.9	16.7	—	—
	Product	5.5	27.4	28.8	27.4	10.9	—

[a] Feed gas analysis calculated from product gas analysis before feeding of coal

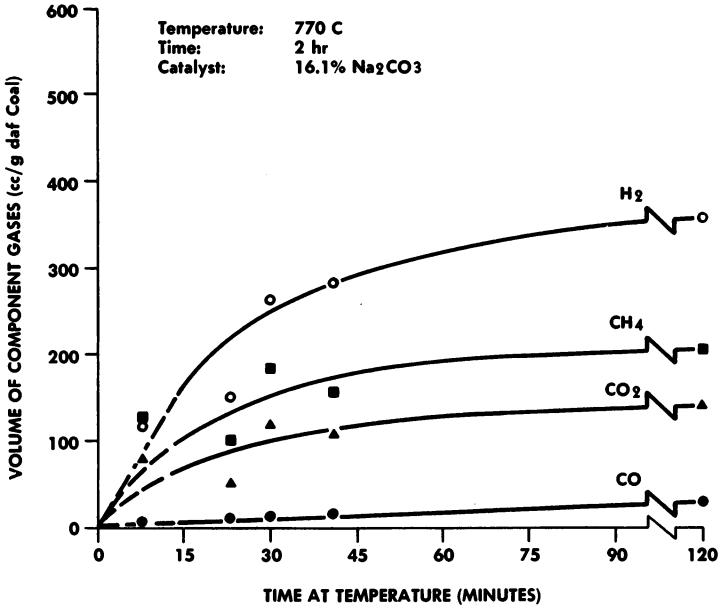

Figure 8. Effect of time at temperature on gas composition in batch autoclave test at 770°C.

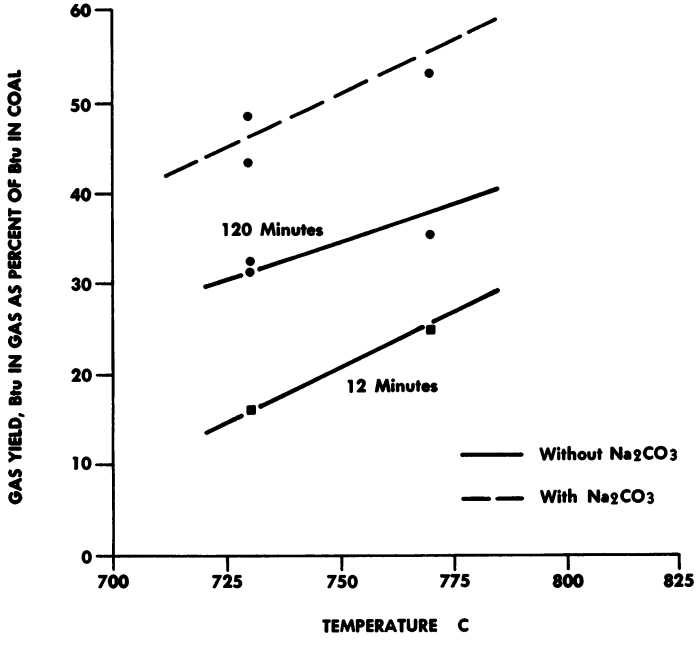

Figure 9. Effect of temperature on gas yield without catalyst in batch autoclave test

by catalysis. The amount of "preformed methane" is approximated according to the following equation.

$$\%CH_4^* = \frac{\%CH_4 \times 100}{\%CH_4 + 0.25\,(\%CO + \%H_2)}$$

where

$\%CH_4$, $\%CO$, $\%H_2$ = percent CH_4, CO, H_2 in product gas on a dry basis by analysis

$\%CH_4^*$ = percent preformed methane

On a volume basis, hydrogen is the main component of the product gas from the direct reaction of steam with coal in the autoclave tests. This is illustrated in Figure 8 which presents data from an experiment at 770°C. with a total reaction time of 2 hrs.

Over the range of temperature studied, an increase in conversion with an increase in temperature is observed in experiments at both 12 and 120 min.; an increase in conversion is observed with an increase in time at the same temperature. This is shown in Figure 9 in which the gas yield, expressed as a function of the B.t.u. content of the coal charged, is plotted *vs.* temperature at the different reaction times. Increasing the residence time from 12 to 120 min. increases the gas yield of about 15% of the coal heating value. A similar increase is caused by adding sodium carbonate to the coal; however, additional data are needed to establish the full significance of using catalysts, especially in such large amounts.

Over the entire range of experimental conditions covered by these experiments—*i.e.*, pressure, 60–350 atm.; temperature, 730–770°C.; reaction time, 2–120 min.—methane is the main product on a heating value basis. It constitutes more than 90% of the total B.t.u. in the gas at the 10% conversion level, and it still is more than 70% of the total B.t.u. in the gas formed even at 60% conversion level. All the data from batch autoclave tests are compared in Figure 10 on the basis of conversion of coal to gas and formation of preformed methane.

Methane is formed in good yield as well as in high concentration under the conditions of the autoclave tests. However, to attain the same high yields at short residence time as required in a commercial gasifier, the temperatures must be much higher than those explored in the autoclaves. Therefore, the continuous flow reactor was used next to determine the rate of methane formation and to establish the feasibility of using coal entrainment in Stage 2 of the two-stage process.

Data on the quality of the product gas obtained in the continuous flow reactor using both Pittsburgh seam coal and lignite are summarized

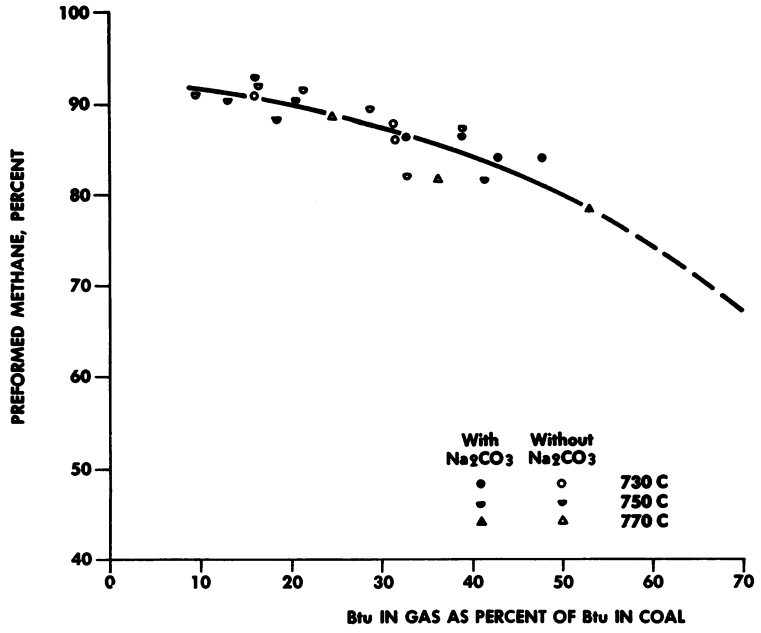

Figure 10. Yields of gas and preformed methane in batch autoclave tests

in Figure 11 where yield of preformed methane is plotted against conversion expressed on a B.t.u. basis. In addition, the curve for correlating the batch autoclave data and the yields used for cost estimating are shown for comparison. On the lower right, a correlation of the results obtained with Pittsburgh seam coal in the presence of silica is given. Lower methane concentrations are indicated than in the autoclave tests.

Methane concentrations are especially low in those tests in which the preheating of the coal slurry did not lead to complete vaporization of the water. In tests with thermocouples inside the reactor, the temperature inside the reactor drops considerably below that of the reactor walls under such conditions and thus could easily cause these low conversions. In later tests with lignite, methane concentrations and conversions were obtained equivalent to those observed in the autoclave tests with bituminous coal.

Experimental results on only the yield of methane in tests in the continuous flow unit are shown in Figure 12, a plot of the methane yield, expressed as percent of the calorific value of the coal converted into methane, *vs.* the precent of B.t.u. in coal converted to gas. The methane concentrations obtained in the flow unit are, as stated above, lower than those in the autoclave tests; consequently, the points for the continuous flow experiments also lie below the autoclave correlation curve at all

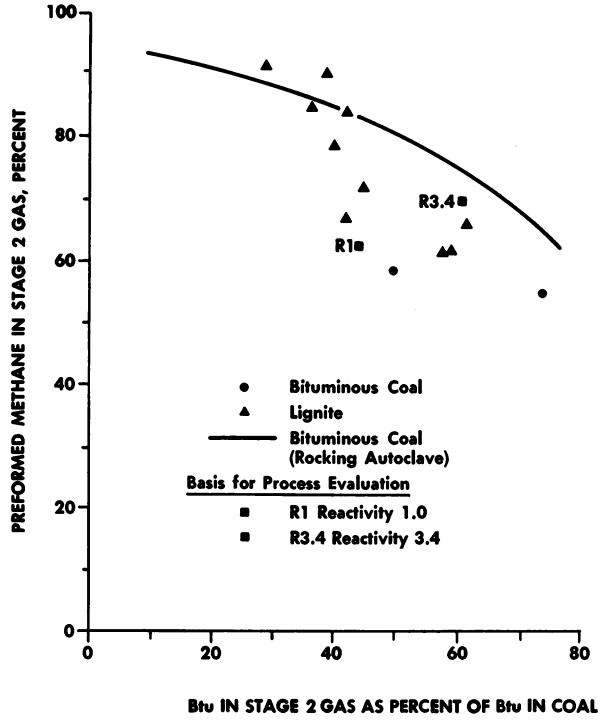

Figure 11. Correlation of total gas yield and preformed methane in continuous flow reactor tests

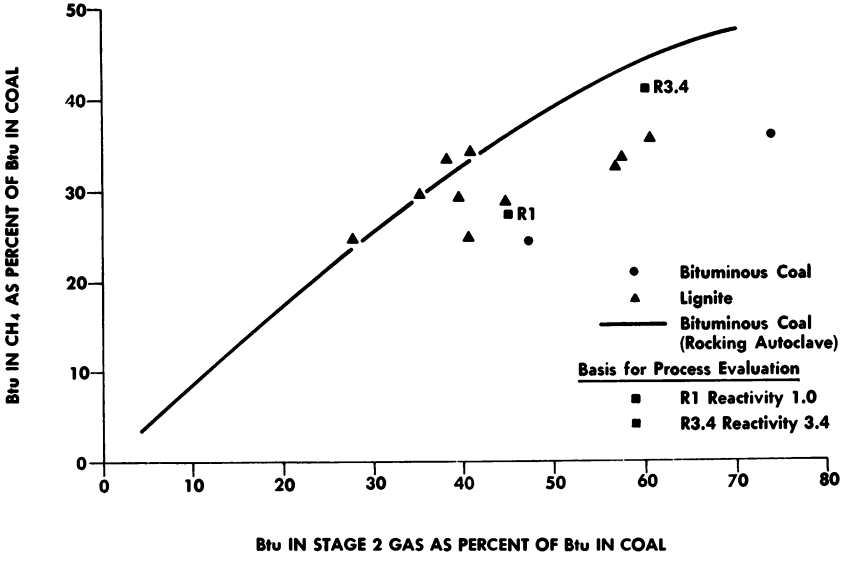

Figure 12. Correlation of total gas yield and methane formation in continuous flow reactor tests

levels of conversion. However, the points for the methane yield on a B.t.u. basis are close to those assumed for the cost calculations in the over-all engineering evaluation of the process projected to commercial-scale operation (2).

The wide scatter of points in Figures 11 and 12 reflect the wide variation in conditions used, and examination of them reveals certain correlations that merit further study. For this, the experiments using lignite may be categorized as follows according to the conditions used:

(a) Less than 3.5 sec. residence at 70 atm. and either below or above a peak reaction temperature of 1760°F.

(b) Same as (a), but more than 3.5 sec. residence time.

(c) Same as (a), but at 81 atm.

(d) Same as (a), but more than 3.5 sec. residence time and at 81 atm.

Figure 13 shows the rate of formation of methane as a straight-line function of the rate of lignite feeding, and thus as a first approximation independent of other reaction conditions. However, closer examination of the operating conditions for each point shows that high hydrogen partial pressure (above 15 atm.) at the reactor outlet, high total pressure (81 *vs.* 70 atm.), and high peak reactor temperature (above 1760°F. *vs.*

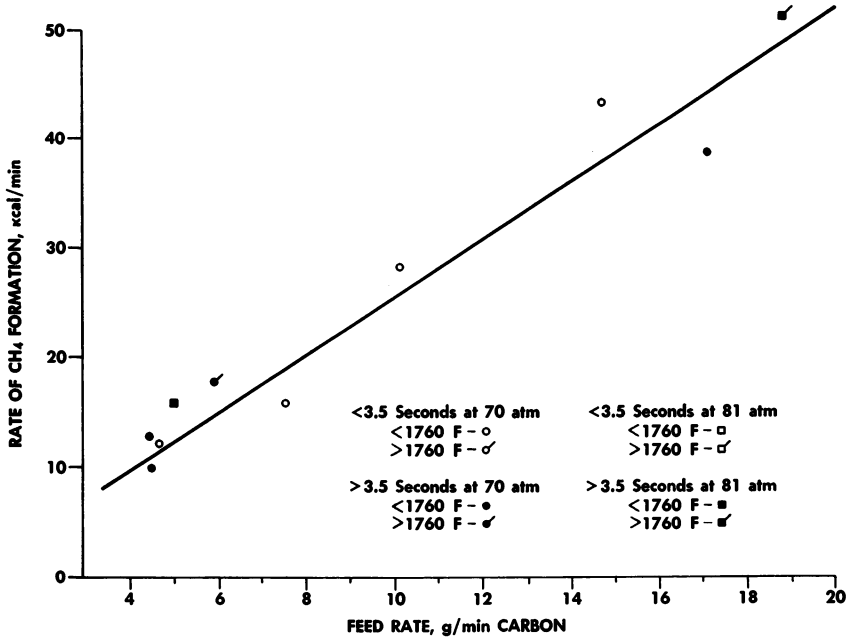

Figure 13. Effect of feed rate on methane formation in continuous flow reactor tests using lignite

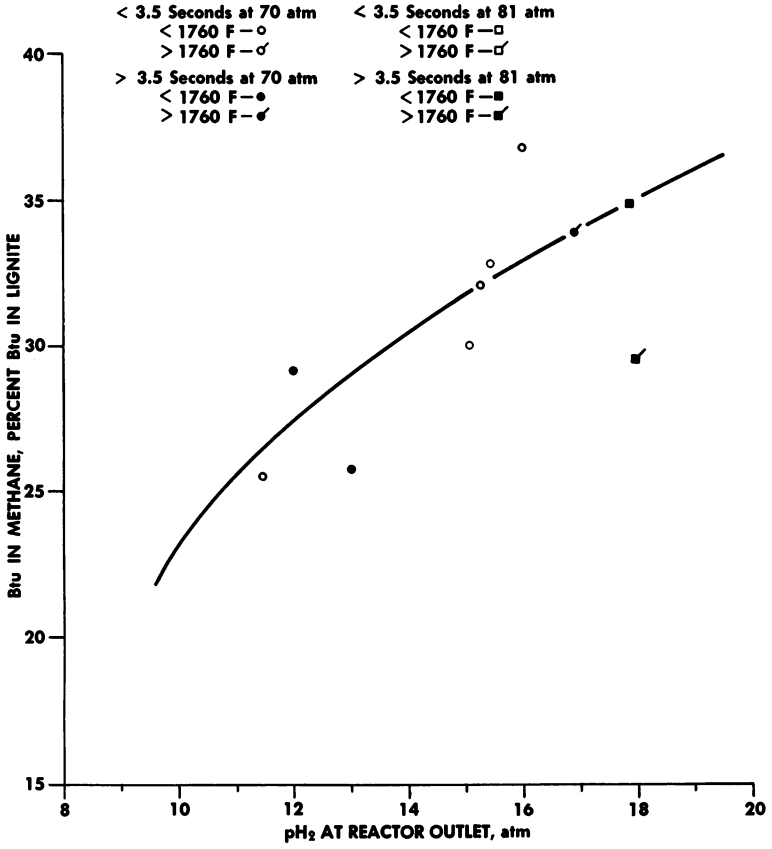

Figure 14. Effect of hydrogen partial pressure at reactor outlet on methane formation in continuous flow reactor tests using lignite

below 1760°F.) result in methane formation rates higher than those indicated by the line on the graph. Also data points below the curves are for tests made with hydrogen partial pressures below 13 atm. at the reactor outlet.

The effect of hydrogen partial pressure at the reactor outlet (pH_2) on the yield of methane is shown in Figure 14. Except for two points, the correlation is good, showing that increased pH_2 results in increased methane yields.

This indicated dependence of methane yield on pH_2 leads to a consideration of factors that affect the hydrogen partial pressure at the reactor outlet. The material balances for the various tests show that the shift reaction is a major source of hydrogen in the product gas. The

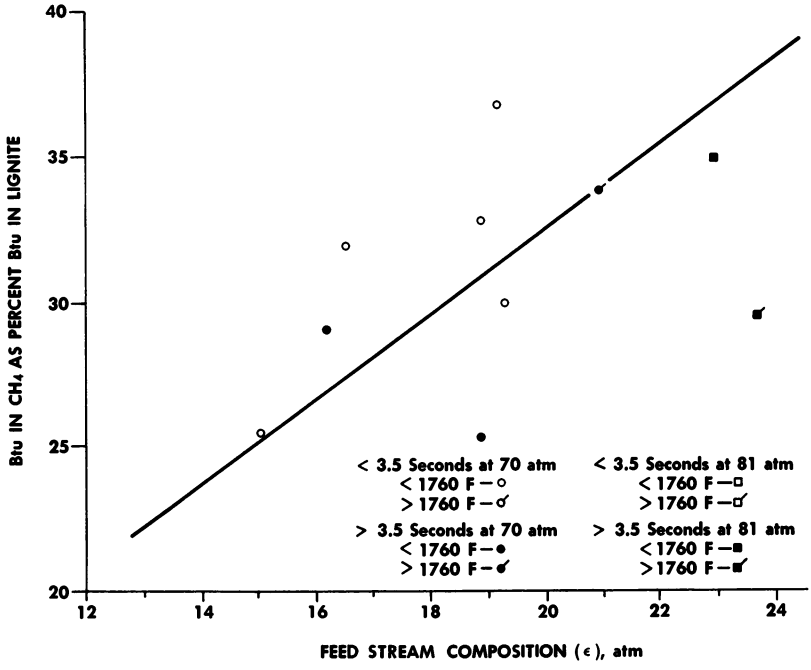

Figure 15. Effect of feed stream composition on methane yield in continuous flow reactor tests using lignite

amount of hydrogen attributable to this source can be calculated from the equation:

$$K = \frac{(H_2 + X)(CO_2 + X)}{(CO - X)(H_2O - X)}$$

where H_2, CO, CO_2, H_2O are the partial pressures of these gases in the feed stream entering the reactor—where X is the fractional increase or decrease in the partial pressure of these gases owing to reaction—and where K is the equilibrium constant. Solving for X to obtain the amount of H_2 produced by the shift reaction leads to a quadratic expression.

For use in evaluating experimental results, this complex quadratic expression may be simplified to $1/2\sqrt{(CO)(H_2O)}$; the total expression for the feed stream composition (E) then becomes:

$$E = H_2 + 1/2\sqrt{(CO)(H_2O)}$$

and is found to correlate well with hydrogen partial pressure at the reactor outlet (pH_2).

The correlation of the yield of methane with E (Figure 15) is not as good as with pH_2 (Figure 14); however, this correlation should prove useful in evaluating data from future experiments. Present indications are that including a term in the expression E reflecting the Stage 1 gas:coal ratio will improve the correlation significantly.

Conclusions

The experiments in bench-scale equipment have shown that methane is formed from high volatile coals at 70 atm. at a rate and in a yield consistent with previous assumptions for the second stage of a conceptual process for gasifying coal.

A more definitive study of the process variables is being planned by operating a 100 lb./hr. internally heated process and equipment development unit. Shock heating by means of hot Stage 1 gas will produce a well defined Stage 2 reactor volume and a temperature gradient similar to that expected in a commercial plant. A previous economic evaluation of such a two-stage coal gasification process led to a pipeline gas manufacturing cost of about 50¢/M std. cu. ft.

Literature Cited

(1) Bituminous Coal Research, Inc. "Gas Generator Research and Development—Survey and Evaluation," Vols. 1 and 2, Government Printing Office, Washington, D. C., 1965.
(2) Donath, E. E., Glenn, R. A., *Proc. Am. Gas Assoc. Production Conf.* **1965**, 65.
(3) Duftschmid, F., Markert, I., *Chem. Ing. Tech.* **32**, 806 (1960) (BCURA Transl. No. 205).
(4) Friedman, L. D., Rau, E., Eddinger, R. T., *Fuel* **45**, 245 (1966).
(5) Friedman, L. D., Rau, E., Eddinger, R. T., *Am. Chem. Soc., Div. Fuel Chem., Preprints* **10** (2), 12 (1966).
(6) Gronhovd, G. H., *U. S. Bur. Mines Inform. Circ.* **8164**, 16 (1963).
(7) Gronhovd, G. H., Harak, A. E., Fegley, M. M., *Am. Chem. Soc., Div. Petrol. Chem., Preprints* 8 (4), B89 (1963).
(8) Hebden, D., Lacey, J. A., Horsler, A. G., *Gas Council, (Gt. Brit.), Res. Commun.* **GC 112** (1964).
(9) Holden, J. H., Strimbeck, G. R., McGee, J. P., Willmott, L. F., Hirst, L. L., *U. S. Bur. Mines, Rept. Invest.* **5573** (1960).
(10) Jones, J. F., Schmidt, M. R., Eddinger, R. T., *Chem. Eng. Progr.* **60** (6), 69 (1964).
(11) Loison, R., Chauvin, R., Fifth International Coal Science Conference, Cheltenham, 1963.
(12) National Coal Board, *Sci. Dept. Res. Rept.* **1960**, 34 (April 1961).
(13) National Coal Board, *Sci. Dept. Res. Rept.* **1961**, 33 (April 1962).
(14) Osthaus, K. H., *Intern. Conf. Complete Gasification Mined Coal, Liege*, **1954**, 255.
(15) Rau, E., Robertson, J. A., *Fuel* **45**, 73 (1966).
(16) Traenckner, K., *Gas-Wasserfach* **93**, 537 (1952).

RECEIVED December 8, 1966.

8

Hydrogasification of Pretreated Coal for Pipeline Gas Production

B. S. LEE, E. J. PYRCIOCH, and F. C. SCHORA, JR.

Institute of Gas Technology, Chicago, Ill.

Lightly pretreated high volatile bituminous coals were hydrogasified with hydrogen-steam and hydrogen-methane-steam mixtures in a continuous-flow pilot unit. Tests at 1000 p.s.i.g. and between 1200°–1900°F. simulated in sequence a two-stage countercurrent system, operated both as free fall and moving bed. Experiments were aimed at maximizing hydrogen utilization and controlling carbon conversion so that after hydrogasification enough carbon remains to generate hydrogen in the over-all process. The raw gas produced has a heating value of about 700 B.t.u./std. cu. ft., which can be upgraded by purification and cleanup methanation to over 900 B.t.u./std. cu. ft.

There has been a long-standing need for an economic process to produce synthetic pipeline gas either as a supplement to or a substitute for natural gas. Development of a process for direct hydrogenation of coal to form essentially methane has been in progress at IGT since 1955. Various facets of this hydrogasification process have been reported (*3, 5, 6, 7, 8, 10, 12, 13*). Process concepts were revised as experimental results became available.

In the current concept hydrogasification is carried out in two stages, with the gas flow countercurrent to the solids flow. The first stage, at temperatures of 1200°–1400°F., rapidly gasifies the most reactive fractions of the incoming coal, forming methane almost exclusively. The second stage, at 1700°–2000°F., gasifies the less reactive remainder from the first stage with hydrogen and steam to yield methane along with carbon oxides. The carbon residue from the second stage is used to generate the required hydrogen.

The low temperature first stage permits high equilibrium methane concentration in the gas. The high temperature second stage, on the other hand, favors the steam-carbon reaction for *in situ* hydrogen production.

The over-all process is shown schematically in Figure 1. Raw coal is first rendered nonagglomerating in the pretreater, then is fed to the hydrogasifier. The residue is used to generate external hydrogen. The hydrogasifier effluent gas is first purified, then cleaned up in a methanator to reduce its carbon monoxide content and to upgrade the heating value. The entire system, except the pretreater, operates at 1000 p.s.i.g. or higher.

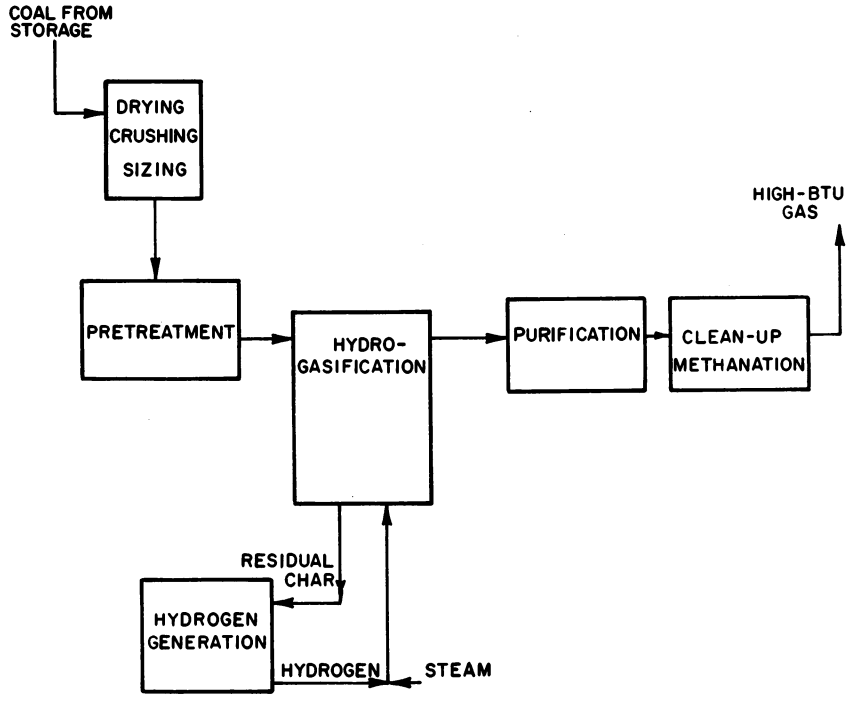

Figure 1. Block-flow diagram of IGT coal hydrogasification process

Although in our present program, coals ranging in rank from lignite to anthracite will be studied, we are focusing attention on high volatile bituminous coals because the volatile matter in coal gasifies easily and produces a rich yield of methane. However, the high volatile content tends to make the coals strongly agglomerating when exposed to hydrogasification conditions. As an operating necessity, the coals are pretreated by mild oxidation to destroy the agglomerating tendency. Such treatment is held to a minimum to preserve a maximum amount of the volatile matter for reaction.

The program objectives are:

(1) To establish through operating experience the minimum pretreatment for coal.

(2) To simulate in sequence the operation of the two-stage hydrogasification.

(3) To study different modes of gas-solid contact, aiming at maximum throughput and controllable reaction rates.

(4) To determine the extent of reaction equilibrium and kinetics limitations that relate to scale-up beyond this pilot unit.

(5) To test and observe the mechanical operation of this high pressure, high temperature reactor system, in terms of materials of construction, instrumentation and control, special equipment, and safety.

Equipment and Procedure

The pilot reactor system has been described in detail (*4*). Briefly, referring to Figure 2, the balanced-pressure reactor is a 4-in. Schedule 40 pipe, made of Type 446 alloy steel, 21 ft. long of which 18 ft. are electrically heated. The reactor is designed to withstand 2000 p.s.i.g. and 2200°F. Coal is stored in the hopper and fed to the reactor through a screw feeder. A screw at the bottom of the reactor discharges the residue to the receiver. Inlet gases are preheated in furnaces and enter the reactor at the bottom. Effluent gases leave at the top and are condensed, filtered, metered, sampled, then flared. Reactor operation is continuous within the limits of the 400-lb. feed hopper capacity for pretreated coal. The entire system is tested at the pressure of the run before coal feed is charged to the hopper.

In simulating the two stages sequentially, pretreated coal is contacted in the low temperature stage with a hydrogen-steam-natural gas mixture which approximates (except for the absence of carbon oxides) the gas leaving the high temperature stage. The partially gasified coal is collected and fed against a hydrogen-steam mixture in the high temperature stage.

By adjusting the feed and discharge rates of the coal, we can force the reaction to occur either in free fall or in a combination of free-fall and moving-bed conditions. The moving bed was operated at a height of either 7 or 3.5 ft. Gas sample probes in the bed indicated reaction profile.

Coal feed rates ranged from 8 to 23 lb./hr. Gas rates corresponded to less than 0.1 ft./sec. linear superficial velocity in order to stay below the threshold of fluidization and thus maintain true countercurrent gas-solid contact along the entire reactor length.

Results and Discussions

Typical results of the hydrogasification tests are shown in Tables I, II, and III. Reported coal residence times are based on measured bulk densities of the reactor residues and the coal bed volume. Time in free fall was negligible compared with that in the bed. Feed gas residence

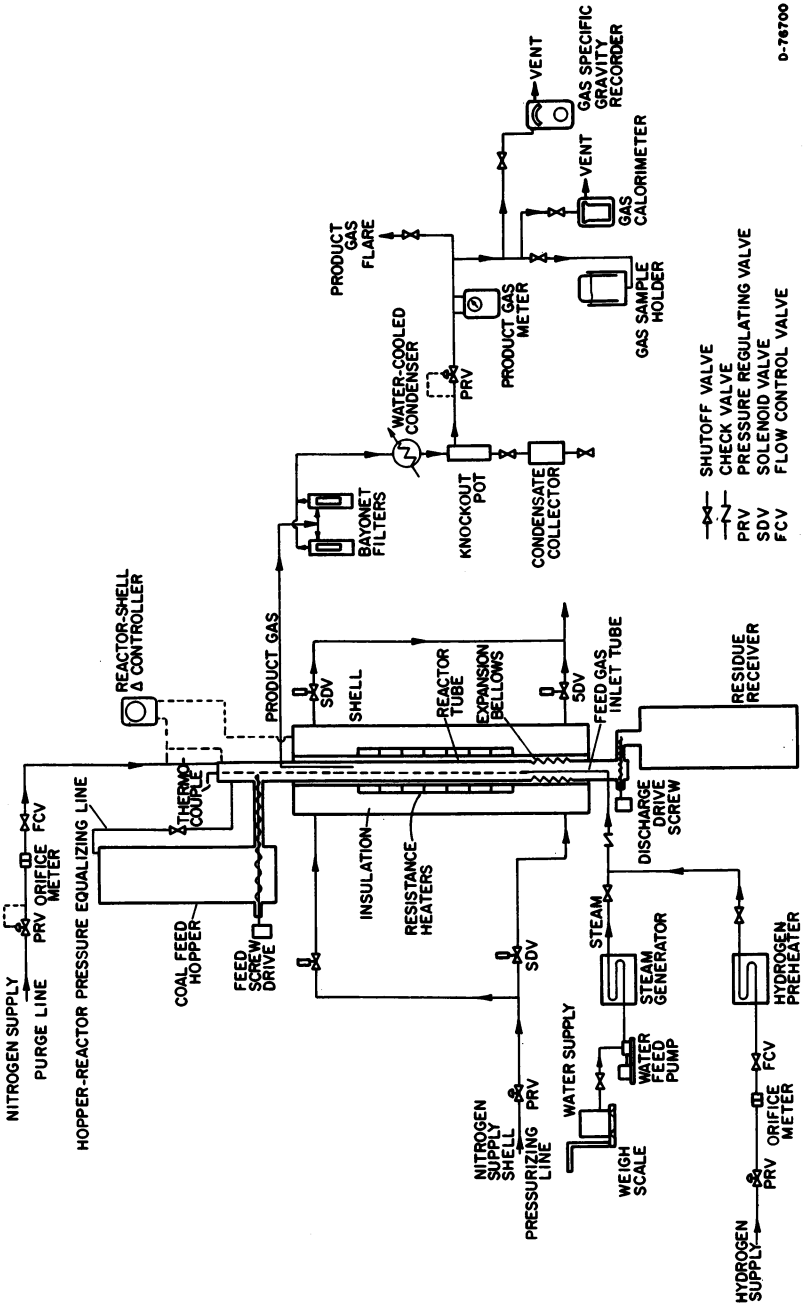

Figure 2. Schematic flowsheet for pilot plant hydrogasification system

Table I.

Coal Feed				*Pretreated Pitts-*	
Gas Feed	*Hydrogen + Steam*			*Hydro-*	
Run	*HT-60*	*HT-61c*	*HT-63*	*HT-67*	
Operating Conditions					
Coal bed height, ft.	Free-Fall	7.0	11.3	7.0	
Reactor pressure, p.s.i.g.	1025	1012	1035	1031	
Reactor temperature, °F.					
Maximum	1440	1460	1355	1395	
Average	1275	1255	1215	1220	
Coal rate, lb./hr. (dry)	10.49	9.69	11.11	13.61	
Feed gas rate, std. cu. ft./hr.	309.0	301.6	297.6	302.0	
Steam rate, lb./hr.	0.00	5.96	5.97	7.52	
Steam concentration, mole%	0.00	29.3	29.7	34.3	
Hydrogen/coal ratio, % of stoichiometric C to CH_4	78.9	85.8	70.8	33.0	
Coal space velocity, lb./cu. ft.-hr.	6.56	15.66	11.13	21.99	
Feed gas residence time, min.	6.57	1.84	3.13	1.77	
Coal residence time, min.	0.065	60.6	77.6	35.6	
Operating Results					
Product gas rate, std. cu. ft./hr.	448.5	403.5	434.2	497.2	
Hydrocarbon yield, std. cu. ft./lb.	3.16	4.71	5.21	3.84	
Gaseous hydrocarbon space-time yield, std. cu. ft./cu. ft.-hr.	20.7	73.7	57.9	84.4	
Carbon oxide yield, std. cu. ft./lb.	0.556	1.00	1.76	0.95	
Feed hydrogen reacted, std. cu. ft./lb.	8.30	10.26	9.51	2.76	
Coal residue, lb./lb. coal	0.744	0.657	0.583	0.680	
Liquid products, lb./lb. coal	0.126	0.734	0.652	0.648	
Net maf coal hydrogasified, wt.%	22.7	30.6	39.3	19.9	
Carbon gasified, wt.%	20.0	28.9	33.2	19.8	
Steam decomposed, % of steam fed	0.0	0.0	0.0	0.0	
Steam decomposed, % of total equivalent fed	0.0	4.1	10.0	3.9	
Over-all material balance, %	102.5	100.7	101.3	98.1	
Carbon balance, %	99.2	110.3	104.5	97.1	
Hydrogen balance, %	95.1	92.0	93.6	101.0	
Oxygen balance, %	106.0	105.0	93.0	106.5	
Product Gas Properties					
Gas composition, mole %				Feed	Prod.
N_2	41.8	36.2	38.0	3.0	35.6
CO	1.0	1.7	3.2	–	1.6
CO_2	0.3	0.7	1.3	0.1	1.0
H_2	49.5	50.1	44.2	56.9	27.0
CH_4	6.6	10.5	12.4	35.9	32.7
C_2H_6	0.5	0.6	0.7	2.4	1.9
C_3H_8	0.1	0.1	0.1	1.5	0.1

Hydrogasification Run Data

burgh Coal

gen + Methane + Steam

HT-71	*HT-78*	*HT-83*	*HT-84*	*HT-98*	*HT-85*
7.0	7.0	7.0	7.0	7.0	7.0
1031	1039	1013	1029	1037	1007
1260	1270	1430	1485	1350	1515
1185	1185	1245	1265	1215	1250
22.72	17.97	14.60	17.82	22.56	18.77
465.5	314.1	144.2	176.7	353.1	218.8
10.10	7.40	3.56	3.13	7.46	0.00
31.3	33.1	34.1	27.1	30.8	0.00
33.7	26.8	15.4	15.8	24.0	15.0
36.72	29.03	23.59	28.80	36.46	30.33
1.22	1.77	3.61	3.27	1.61	3.58
36.7	29.2	44.0	43.7	36.0	40.2
591.2	437.0	307.5	321.1	699.4	343.0
2.90	2.92	1.86	3.43	2.15	2.96
106.7	84.8	43.8	98.86	78.35	89.76
0.77	0.67	1.16	1.25	0.341	0.77
2.58	2.62	1.58	1.58	2.67	1.69
0.734	0.724	0.630	0.642	0.863	0.711
0.554	0.538	0.330	0.235	0.379	0.114
22.2	17.5	27.5	27.2	13.27	20.0
18.1	16.1	21.0	20.1	10.7	15.9
0.0	0.0	0.0	0.0	9.88	0.0
0.0	0.0	0.0	0.00	9.88	0.0
100.6	99.6	97.0	96.7	100.2	99.6
99.9	100.6	91.4	93.8	103.9	98.7
104.1	101.3	105.5	101.9	99.6	100.2
103.1	105.8	110.4	90.4	95.7	71.5

Feed	Prod.	Feed	Prod.	Feed	Prod.	Feed	Prod.	Feed	Prod.	Feed	Prod.
1.2	18.0	1.6	25.1	1.4	39.0	1.0	28.2	1.2	50.6	20.8	38.2
–	1.9	–	1.6	–	2.9	–	4.3	–	0.7	0.0	3.1
0.3	1.3	0.2	1.3	0.3	2.6	0.3	2.8	0.2	0.5	0.3	1.3
60.6	37.8	58.0	30.9	58.7	20.0	62.1	25.4	64.2	23.8	50.2	22.8
35.1	38.1	36.7	38.4	37.0	34.4	34.0	38.4	31.7	23.1	26.6	33.7
2.0	2.5	2.5	2.4	1.9	0.9	1.9	0.7	1.9	1.2	1.5	0.7
0.6	0.2	0.8	0.2	0.5	0.1	0.5	0.1	0.6	–	0.4	0.1

Table I.

	Pretreated Pitts-			
	Hydrogen + Steam			Hydro-
	HT-60	HT-61c	HT-63	HT-67
				Feed Prod.
C_4H_{10}	–	–	–	0.2 –
C_6H_6	0.2	0.1	0.1	– 0.1
Total = 100.0				
High heating value of N_2-free gas B.t.u./std. cu. ft. (dry)	422	449	471	– 710
Coal Feed			Partially Hydrogasified	
Gas Feed			(Hydrogen +	
Run	HT-80	HT-87	HT-86	HT-64
Operating Conditions				
Coal bed height, ft.	3.5	3.5	3.5	7.0
Reactor pressure, p.s.i.g.	1041	1007	1023	1021
Reactor temperature, °F.				
Maximum	1740	1735	1740	1585
Average	1695	1715	1735	1350
Coal rate, lb./hr. (dry)	11.20	17.10	12.44	8.02
Feed gas rate, std. cu. ft./hr.	187.9	182.6	189.1	291.8
Steam rate, lb./hr.	4.34	3.78	4.34	9.88
Steam concentration, mole%	32.7	30.3	32.5	41.6
Hydrogen/coal ratio, % of stoichiometric C to CH_4	36.0	21.6	31.7	80.7
Coal space velocity, lb./cu. ft.-hr.	36.20	55.28	40.20	12.95
Feed gas residence time, min.	1.15	1.17	1.10	1.50
Coal residence time, min.	24.1	21.8	21.5	83.3
Operating Results				
Product gas rate, std. cu. ft./hr.	348.7	346.6	370.7	411.8
Hydrocarbon yield, std. cu. ft./lb.	5.85	4.11	5.51	4.88
Gaseous hydrocarbon space-time yield, std. cu. ft./cu. ft.-hr.	211.9	227.4	221.7	63.22
Carbon oxide yield, std. cu. ft./lb.	3.58	2.25	3.31	1.80
Feed hydrogen reacted, std. cu. ft./lb.	5.97	3.85	3.91	10.92
Coal residue, lb./lb. coal	0.678	0.789	0.734	0.806
Liquid products, lb./lb. coal	0.194	0.104	0.176	1.198
Net m.a.f. coal hydrogasified, wt.%	37.5	26.4	38.0	31.5
Carbon gasified, wt.%	38.1	24.7	34.9	27.8
Steam decomposed, % of steam fed	50.0	52.9	49.4	5.7
Steam decomposed, % of total equivalent fed	51.4	56.0	51.0	6.9
Over-all material balance, %	99.1	100.9	101.9	102.3
Carbon balance, %	102.5	103.9	97.2	112.4
Hydrogen balance, %	97.1	102.7	106.0	94.9
	98.8	98.6	101.0	103.8

Continued

burgh Coal											
gen + Methane + Steam											
HT-71		*HT-78*		*HT-83*		*HT-84*		*HT-98*		*HT-85*	
Feed	Prod.	Feed	Prod.	Feed	Prod.	Feed	Prod.	Feed	Prod.	Feed	Prod.
0.2	–	0.2	–	0.2	–	0.2	–	0.2	–	0.2	–
–	0.2	–	0.1	–	0.1	–	0.1	–	0.1	–	0.1
–	686	–	719	–	718	–	691	–	674	–	707

Pittsburgh Coal Steam)		*Pretreated Ohio Coal (Hydrogen + Methane + Steam)*	*Partially Hydrogasified Ohio Coal (Hydrogen + Steam)*
HT-72	*HT-73*	*HT-77*	*HT-81*
7.0	7.0	7.0	3.5
1023	1006	1021	992
1835	2005	1275	1720
1825	1950	1190	1710
16.74	17.22	16.45	13.63
223.8	269.4	281.5	188.3
6.70	3.97	7.67	4.46
38.6	23.6	36.4	33.2
29.7	35.0	24.8	29.0
27.05	27.84	26.58	44.04
1.64	1.57	1.85	1.08
38.2	39.5	38.6	27.8
585.2	551.2	417.7	424.3
6.26	4.86	3.16	5.39
169.3	135.4	83.96	237.3
5.52	4.09	1.06	2.99
1.80	2.51	2.96	4.61
0.460	0.671	0.724	0.694
0.119	0.0774	0.582	0.155
52.0	43.6	20.6	33.1
48.8	36.9	17.3	32.7
70.4	66.4	0.0	52.6
71.9	69.3	13.6	54.2
94.8	100.1	99.8	98.6
86.0	94.8	103.6	99.8
105.3	102.7	100.9	97.5
101.4	112.1	99.3	94.9

Table I

Partially Hydrogasified (Hydrogen +

Product Gas Properties	*HT-80*	*HT-87*	*HT-86*	*HT-64*
Gas composition, mole%				
N_2	35.0	34.9	32.5	37.4
CO	9.5	8.8	9.0	1.9
CO_2	2.0	2.3	2.1	1.6
H_2	34.7	33.7	37.9	49.6
CH_4	18.8	20.2	18.5	9.5
C_2H_6	–	0.1	–	–
C_3H_8	–	–	–	–
C_4H_{10}	–	–	–	–
C_6H_6	–	–	–	–
Total = 100.0				
High heating value of N_2-free gas, B.t.u./std. cu. ft. (dry)	505	520	495	414

Table II. Solid Products

Pretreated Pitts-

Coal Feed				
Run	*HT-60*		*HT-61c*	
Sample	*Feed*	*Residue*	*Feed*	*Residue*
Proximate Analysis, wt.%				
Moisture	0.5	0.5	1.1	0.6
Volatile Matter	26.5	6.2	22.9	2.9
Fixed Carbon	61.4	68.6	61.0	78.9
Ash	11.6	24.7	15.0	17.6
Total = 100.0				
Ultimate Analysis (dry) wt.%				
Carbon	70.5	68.5	68.6	78.2
Hydrogen	3.77	2.42	3.73	1.26
Nitrogen	1.28	1.27	1.24	0.72
Oxygen	9.30	0.47	7.62	0.42
Sulfur	3.53	2.53	3.67	1.71
Ash	11.62	24.81	15.14	17.69
Total = 100.0				
Screen Analysis, USS, wt.%				
+20	19.1	27.7	18.7	18.5
+30	18.8	24.0	21.0	16.9
+40	33.9	27.1	33.5	27.3
+60	23.1	16.8	22.2	26.0
+80	1.8	1.9	2.0	4.5
+100	0.8	0.7	0.6	1.4
+200	1.3	1.4	1.4	3.8
+325	0.6	0.1	0.2	0.9
−325	0.6	0.3	0.4	0.7
Total = 100.0				

Continued

Pittsburgh Coal		*Pretreated Ohio Coal (Hydrogen + Methane + Steam)*		*Partially Hydrogasified Ohio Coal (Hydrogen + Steam)*
Steam)				
HT-72	*HT-73*	*HT-77*		*HT-81*
		Feed	Product	
33.2	31.9	1.6	28.5	43.5
13.0	11.6	–	2.4	7.5
2.8	1.0	0.2	1.9	2.1
33.1	40.5	57.6	27.3	29.6
17.8	15.0	36.9	37.8	17.3
0.1	–	2.6	1.9	–
–	–	0.8	0.1	–
–	–	0.3	–	–
–	–	–	0.1	–
521	464	–	716	515

from Hydrogasifier

burgh Coal

HT-63		*HT-67*		*HT-71*		*HT-78*	
Feed	*Residue*	*Feed*	*Residue*	*Feed*	*Residue*	*Feed*	*Residue*
1.1	0.5	0.5	0.6	2.1	1.1	1.3	0.9
25.6	2.5	23.7	4.6	22.6	7.7	24.9	5.0
63.3	79.8	61.8	77.6	61.6	72.3	62.4	78.3
10.0	17.2	14.0	17.2	13.7	18.9	11.4	15.8
71.7	78.2	70.2	76.9	68.5	73.0	71.4	78.5
3.93	1.35	3.97	2.05	3.39	2.43	3.83	1.92
1.55	0.70	1.36	1.01	1.08	1.05	1.43	1.06
9.46	1.26	6.58	0.65	9.45	1.83	8.11	0.38
3.26	1.17	3.82	2.09	3.57	2.59	3.68	2.18
10.10	17.32	14.07	17.30	14.01	19.10	11.55	15.96
21.6	26.1	5.3	20.9	8.6	8.8	12.1	14.3
21.4	21.1	20.0	23.4	18.8	16.5	18.8	23.6
31.3	24.5	30.9	20.9	24.6	21.7	22.9	24.1
23.0	19.4	28.6	20.3	28.3	28.1	24.1	21.5
1.2	3.4	9.5	7.7	12.4	13.2	9.8	7.4
0.2	1.0	3.1	3.0	4.1	5.2	4.0	2.9
0.4	2.6	1.4	2.8	2.4	4.9	5.8	4.4
0.2	0.9	0.3	0.7	0.3	1.0	1.4	1.0
0.7	1.0	0.9	0.3	0.5	0.6	1.1	0.8

Table II.

Coal Feed	*Pretreated Pitts-*			
Run	*HT-83*		*HT-84*	
Sample	*Feed*	*Residue*	*Feed*	*Residue*
Proximate Analysis, wt.%				
Moisture	1.9	1.0	1.0	0.8
Volatile Matter	23.3	4.2	23.3	3.5
Fixed Carbon	62.4	74.9	65.5	79.7
Ash	12.4	19.9	10.2	16.0
Total = 100.0				
Ultimate Analysis (dry) wt.%				
Carbon	70.6	76.0	72.8	79.9
Hydrogen	3.65	1.37	3.68	1.17
Nitrogen	1.04	0.72	1.37	0.74
Oxygen	8.45	0.00	8.49	0.20
Sulfur	3.63	2.22	3.31	1.88
Ash	12.63	20.06	10.35	16.11
Total = 100.0				
Screen Analysis, USS, wt.%				
+20	10.2	6.1	12.0	7.3
+30	16.1	17.8	18.5	21.3
+40	20.2	25.7	22.6	30.3
+60	22.4	27.9	23.8	27.6
+80	10.6	10.3	10.8	7.4
+100	5.0	4.2	4.9	2.6
+200	9.4	5.7	5.9	2.9
+325	3.4	0.6	1.0	0.3
−325	2.7	1.7	0.5	0.3
Total = 100.0				

Coal Feed	*Partially Hydrogasified*			
Run	*HT-86*		*HT-64*	
Sample	*Feed*	*Residue*	*Feed*	*Residue*
Proximate Analysis, wt.%				
Moisture	1.1	0.3	0.9	1.1
Volatile Matter	3.7	1.7	3.9	3.3
Fixed Carbon	78.9	67.6	75.9	74.1
Ash	16.3	30.4	19.3	21.5
Total = 100.0				
Ultimate Analysis (dry) wt.%				
Carbon	80.2	68.1	76.1	76.0
Hydrogen	1.36	0.58	1.52	1.23
Nitrogen	0.74	0.29	0.81	0.27
Oxygen	0.00	0.00	0.67	0.57
Sulfur	2.03	2.57	1.44	0.23

Continued

burgh Coal				*Partially Hydrogasified Pittsburgh Coal*			
HT-98		*HT-85*		*HT-80*		*HT-87*	
Feed	*Residue*	*Feed*	*Residue*	*Feed*	*Residue*	*Feed*	*Residue*
1.5	0.6	1.3	0.3	1.1	4.6	0.9	0.1
14.5	3.7	24.0	2.1	4.4	1.9	2.8	1.0
68.3	77.4	65.5	84.6	77.9	69.9	82.5	81.3
15.7	18.3	9.2	13.0	16.6	23.6	13.8	17.6
73.2	78.2	73.3	83.8	78.6	74.7	81.5	81.8
2.29	1.32	3.86	0.87	1.55	0.53	1.02	0.43
1.04	0.57	1.26	0.69	0.99	0.42	0.43	0.32
4.82	0.00	9.02	0.00	0.00	0.00	1.51	0.00
2.73	1.61	3.23	1.53	2.30	1.99	1.66	1.40
15.92	18.45	9.33	13.12	16.76	24.73	13.88	17.59
9.3	3.2	12.3	8.4	10.1	7.3	9.0	5.0
15.7	8.6	18.5	17.3	16.8	15.7	16.2	11.6
24.3	25.4	24.5	25.2	22.6	24.3	25.2	21.7
26.9	33.5	23.4	25.0	25.3	27.7	24.4	26.8
11.1	14.6	9.1	10.1	10.6	11.3	9.9	13.7
4.9	6.1	4.2	4.3	4.5	4.7	4.3	7.0
5.9	7.1	5.6	7.1	7.0	6.7	7.7	12.1
1.2	0.8	1.1	0.5	1.8	1.3	1.9	1.4
0.7	0.7	1.3	2.1	1.3	1.0	1.4	0.7

Pittsburgh Coal				*Ohio Coal*			
				Pretreated		*Partially Hydrogasified*	
HT-72		*HT-73*		*HT-77*		*HT-81*	
Feed	*Residue*	*Feed*	*Residue*	*Feed*	*Residue*	*Feed*	*Residue*
1.3	1.1	2.0	0.6	3.3	1.0	1.4	1.9
5.2	1.2	4.2	2.0	24.5	5.1	5.1	1.9
76.6	60.8	75.1	64.0	64.3	82.7	80.1	77.1
16.9	36.9	18.7	33.4	7.9	11.2	13.4	19.1
76.9	62.3	76.0	65.6	73.7	83.2	81.2	78.5
1.85	0.30	1.69	0.43	3.59	2.05	1.88	0.50
1.10	0.36	1.01	0.41	1.49	1.29	1.14	0.40
0.78	0.00	0.21	0.00	10.31	0.62	0.42	0.00
2.22	2.06	2.02	1.10	2.75	1.57	1.82	1.86

Table II.

	Partially Hydrogasified			
	HT-86		*HT-64*	
	Feed	*Residue*	*Feed*	*Residue*
Ash	16.43	30.50	19.46	21.70
Total = 100.0				
Screen Analysis, USS, wt.%				
+20	7.1	4.0	15.7	11.2
+30	13.4	12.6	19.0	14.6
+40	21.1	28.2	28.0	25.5
+60	24.5	31.2	25.5	29.4
+80	11.5	11.1	4.4	6.1
+100	5.6	4.4	1.7	2.1
+200	10.3	6.1	3.7	5.2
+325	4.0	1.3	0.9	2.3
−325	2.5	1.1	1.1	3.6
Total = 100.0				

Table III. Liquid Products

Coal Feed	*Pretreated Pitts-*			
Run	*HT-60*	*HT-61c*	*HT-63*	*HT-67*
Weight, lb./lb. coal	0.126	0.734	0.652	0.648
Composition, wt.%				
Water	64.92	92.98	90.43	93.26
Oil	35.08	7.02	9.57	6.74
Composition of oil fraction, wt.%				
Carbon	87.4	92.0	88.2	87.6
Hydrogen	7.18	6.50	7.05	6.66
Total	94.58	98.50	95.25	94.26
Carbon in oil fraction, wt.% of carbon in coal	6.05	6.56	7.68	5.45

Coal Feed	*Partially Hydrogasified*		
Run	*HT-80*	*HT-87*	*HT-86*
Weight, lb./lb. coal	0.194	0.1041	0.1764
Composition, wt.%			
Water	100.0	100.0	100.0
Oil	—	—	—
Composition of oil fraction, wt.%			
Carbon	—	—	—
Hydrogen	—	—	—
Total	—	—	—
Carbon in oil fraction, wt.% of carbon in coal	—	—	—

Continued

Pittsburgh Coal				*Ohio Coal*			
				Pretreated		*Partially Hydrogasified*	
HT-72		*HT-73*		*HT-77*		*HT-81*	
Feed	*Residue*	*Feed*	*Residue*	*Feed*	*Residue*	*Feed*	*Residue*
17.15	37.26	19.07	33.56	8.16	11.27	13.54	19.51
11.9	4.4	7.7	6.5	11.3	18.3	8.2	5.3
20.0	15.0	17.1	17.7	22.1	20.3	17.9	13.3
23.6	27.2	22.0	25.2	22.0	19.7	24.7	25.1
25.6	32.2	27.8	29.8	23.7	20.5	27.0	28.8
10.3	12.7	12.9	11.6	10.7	9.0	10.7	12.3
4.0	4.7	5.6	4.7	4.9	4.4	4.8	5.5
3.8	3.4	5.8	4.1	4.3	6.3	5.8	8.0
0.6	0.2	0.9	0.3	0.7	1.1	0.7	1.0
0.2	0.2	0.2	0.1	0.3	0.4	0.2	0.7

from Hydrogasifier

burgh Coal

HT-71	*HT-78*	*HT-83*	*HT-84*	*HT-98*	*HT-85*
0.554	0.538	0.330	0.235	0.379	0.1137
94.79	92.02	96.26	92.30	95.28	89.84
5.21	7.98	3.74	7.70	4.72	10.16
85.5	85.2	84.8	87.4	82.1	86.4
6.25	6.49	6.57	6.18	6.15	6.93
91.75	91.69	91.37	93.58	88.25	93.33
2.58	5.12	1.48	2.17	2.00	1.36

Pittsburgh Coal			*Pretreated Ohio Coal*	*Partially Hydrogasified Ohio Coal*
HT-64	*HT-72*	*HT-73*	*HT-77*	*HT-81*
1.198	0.119	0.0774	0.582	0.155
97.0	100.0	100.0	91.54	100.0
3.0	—	—	8.46	—
85.0	—	—	86.4	—
6.5	—	—	6.51	—
91.5	—	—	92.91	—
4.01	—	—	5.77	—

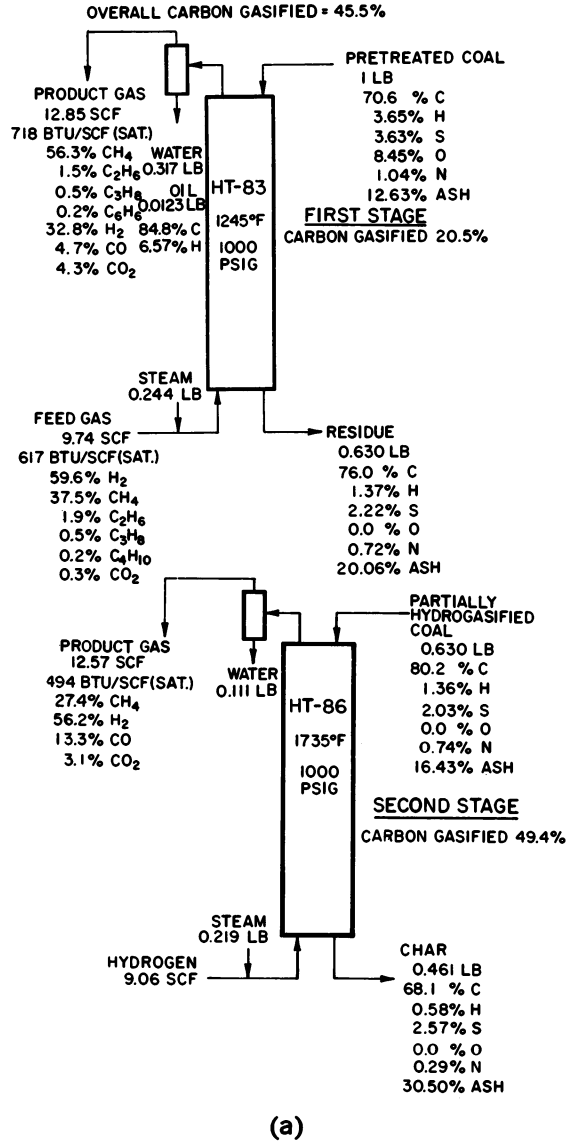

Figure 3. Stage-by-stage simulation Pittsburgh coal B—

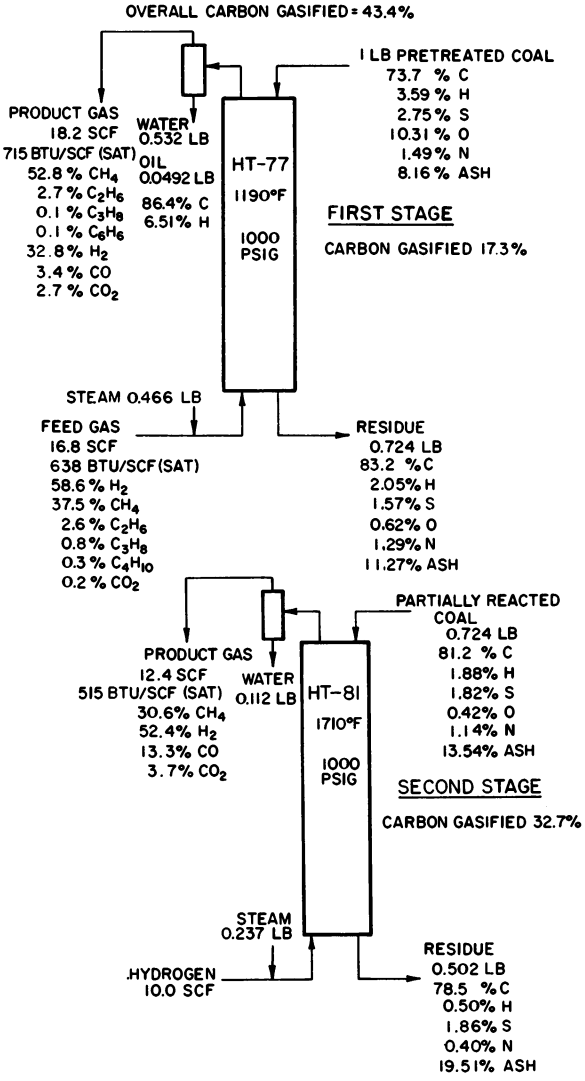

(b)

in hydrogasification. A—pretreated pretreated Ohio coal

times are based on the flow rate at average bed conditions and coal bed volume. Time in the free-fall section is not included.

Minimum Coal Pretreatment. Two high volatile bituminous coals were tested, one from the Pittsburgh No. 8 seam (Ireland mine) and the other from the Ohio No. 6 seam (Broken Aro mine). Most of the work to date has been with the former. The proximate and ultimate analyses of these two coals are shown in Table IV. These coals were pretreated to various extents and then hydrogasified. Using volatile matter content as an index of severity of pretreatment, we found that pretreated coal with 24–26% volatile matter can be processed without agglomeration. Raw coal was tested, but it swelled badly during the reaction and stuck to the reactor, causing bridging. It is entirely possible that in larger size reactors in which the coal feed would not contact reactor walls immediately, coals with less pretreatment—or even raw coal—could be fed successfully. However, we consider our ability to feed pretreated coal with as much as 24–26% volatile matter a significant achievement. Adjustment of

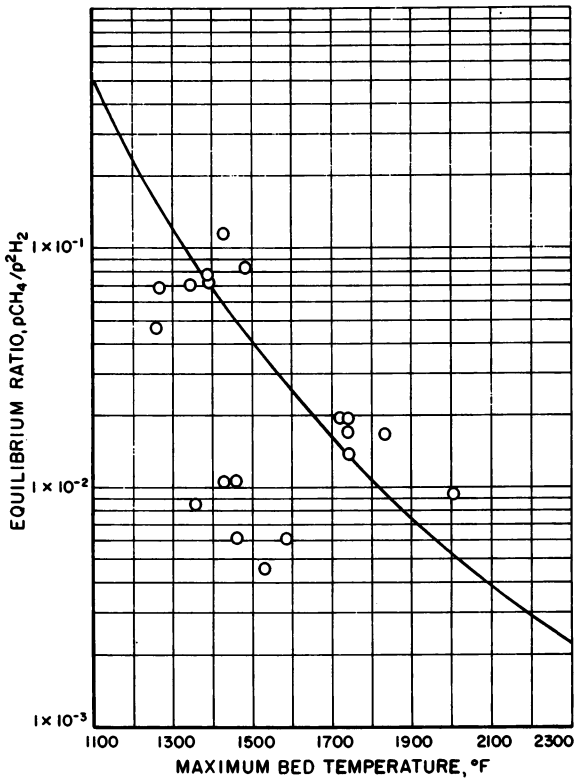

Figure 4. Approach to carbon-hydrogen reaction equilibrium for pretreated Pittsburgh seam bituminous coal

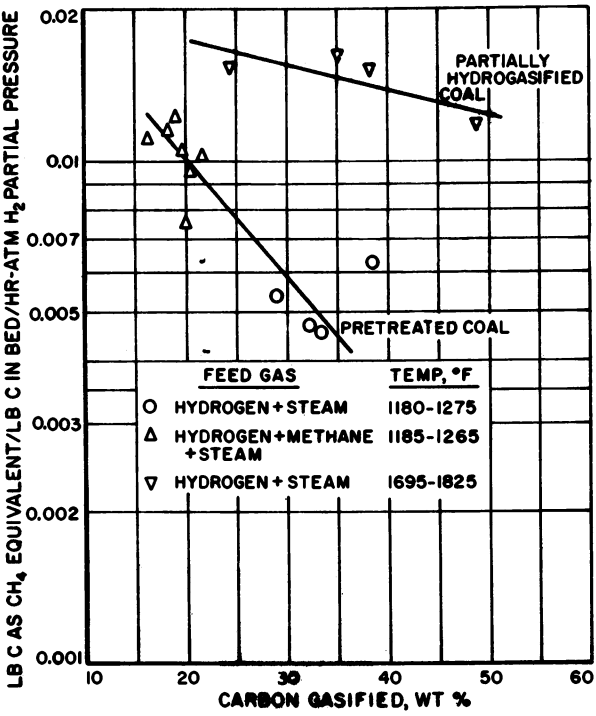

Figure 5. Integral methane formation rate for pretreated Pittsburgh seam bituminous coal

feed tube size, length, and location, the amount of nitrogen purge gas through the tube, and the start-up sequence are factors learned through experience.

Two-Stage Simulation. The stage-by-stage simulation procedure used is realistic except that the partially gasified coal is fed to the second stage at ambient temperature instead of between 1200° and 1400°F. Since hydrogen represents the largest share of the total pipeline gas cost, practically all the runs were conducted at the minimum hydrogen:coal ratio that would produce a total carbon gasification of about 50%. At this degree of gasification, sufficient residual carbon would be available for generating the necessary hydrogen. These figures resulted from an over-all system analysis based on existing data on equilibrium, kinetics, and heat and material balances.

Key results obtained in two-stage simulations are summarized in Figure 3a with pretreated Pittsburgh seam coal, and in Figure 3b with pretreated Ohio seam coal. Product gas analyses were adjusted to a nitrogen-free basis because of the high nitrogen purge rates actually

used in the tests. The purge gas was needed to prevent hot reactor gases from entering the coal feed tube.

High concentrations of unreacted hydrogen in the product gas from the low temperature stages limited the heating value to about 700 B.t.u./std. cu. ft. To obtain a high B.t.u. gas (900 B.t.u./std. cu. ft.) requires catalytic methanation of the carbon oxides. Note the absence of carbon oxides in the feed gas to the first stage. Because of the low temperature in the first stage, no steam-carbon reaction is expected. Thus, CO is considered inert as far as methane formation is concerned. Therefore, to simplify preparation of the simulation gas mixture, CO was not included in this feed. This assumption appears valid, judging from the low carbon oxide concentration in the first-stage effluent. The amount measured came from the organic oxygen in the coal rather than from the steam-carbon reaction.

Steam, however, seems to play an active role in low temperature gasification. Two runs were made, one with a steam-natural gas-hydrogen mixture and the other with a nitrogen-natural gas-hydrogen mixture. Significantly greater amounts of carbon oxides were formed, and significantly less water was released from the coal when steam was used. Steam, then, seems to suppress the release of organic oxygen from coal as water but forces the oxygen to leave as carbon oxides. This phenomenon seems plausible from the mass action standpoint. From a process standpoint, the release of organic oxygen in coal as carbon oxides is more desirable than as water. In the latter case, hydrogen (either from coal or from external sources) is lost by combining with oxygen to form water. In

Table IV. Analyses of High Volatile Bituminous Coals

	Pittsburgh No. 8 Ireland Mine	*Ohio No. 6 Broken Aro Mine*
Proximate Analysis, wt.%		
Moisture	1.0	1.0
Volatile matter	35.9	39.6
Fixed carbon	51.8	53.6
Ash	11.3	5.8
Total = 100.0		
Ultimate Analysis (dry), wt.%		
Carbon	71.1	74.1
Hydrogen	4.95	5.41
Nitrogen	1.18	1.39
Oxygen	7.35	9.42
Sulfur	4.03	3.87
Ash	11.39	5.81
Total = 100.0		
Particle size, USS (as prepared for pretreatment)	−16+80	−16+80

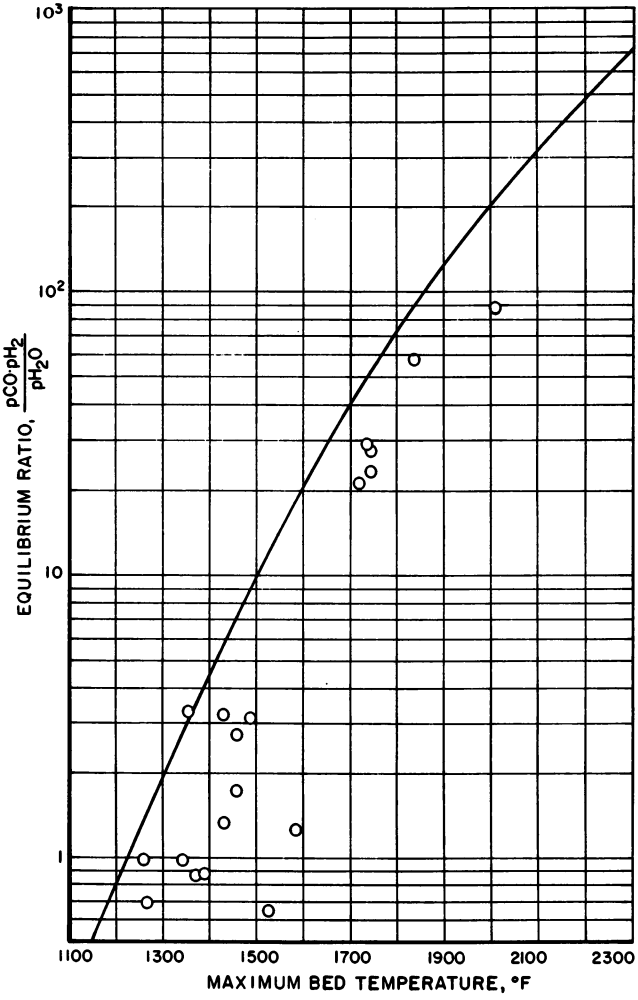

Figure 6. Approach to steam-carbon reaction equilibrium for pretreated Pittsburgh seam bituminous coal

contrast, when oxygen is released as carbon oxides, these can be converted to more hydrocarbon by subsequent catalytic methanation.

Methane Formation. EQUILIBRIUM. It has been well-established that hydrogenation of volatile matter in coal proceeds rapidly (*12*) and yields methane concentrations higher than the equilibrium value in a β-graphite-hydrogen system. This excess is conveniently attributed to a greater-than-unity coal activity in reference to β-graphite activity. In fact, of course, hydrogenation of reactive carbon groups proceeds by splitting off the carbon chains and functional groups rather than by reacting with

Table V. Gas Sample

Run No.		*HT-67*			
Bed height, ft.		*7.0*			
Bed Sampling Point, in. below top of bed	Feed Gas	42	18	6	Product Line
Gas Composition, mole %					
CO	0.0	0.0	0.0	0.0	2.3
CO_2	0.1	0.2	0.3	0.4	1.5
H_2	58.0	56.2	55.8	54.8	39.8
Ar	1.14	1.27	1.42	1.26	1.14
CH_4	36.6	38.6	39.2	40.6	51.6
C_2H_6	2.5	3.3	2.8	2.6	3.0
C_3^+	1.7	0.5	0.5	0.4	0.5
H_2S	0.0	0.0	0.0	0.0	0.2
Total	100.04	100.07	100.02	100.06	100.04

[a] Nitrogen- and water-free basis.

graphitic carbon. Such reactions lead to methane formation because methane is the predominant stable hydrocarbon at the temperature and pressure in question. The first-stage hydrogasification demonstrates this type of reaction as shown, for example, by the predominance of methane *vs.* other hydrocarbons or carbon oxides in the effluent gas (Figure 3a).

Figure 4 presents the calculated "equilibrium ratio" obtained from the pilot plant tests as a function of the maximum bed temperatures. The curve represents true equilibrium ratio for the reaction:

$$C\ (\beta\text{-graphite}) + 2\ H_2 \rightleftarrows CH_4$$

We note the many runs yielding equilibrium ratios higher than the curve. The group of points below the curve between 1450° and 1550°F. came from runs in which a high hydrogen:coal ratio was used, resulting in low methane concentration.

We found the initial gasification so rapid that 20% of the carbon was gasified during a free-fall distance of 18 ft. There appears to be little equilibrium hindrance in view of the mechanism of methane formation discussed above. However, once the reactive carbon is gone, the remaining fixed carbon reacts much more slowly in the second stage. Here we check the approach to β-graphite equilibrium to see if the coal, after the first stage, still has sufficient reactive carbon left to show activity greater than unity. Since methane formation is exothermic, from the process standpoint, the more methane that is formed in the second stage, the more heat there would be available to furnish the endothermic heat for the steam-carbon reaction, which, in turn, would produce hydrogen *in situ* and reduce the external hydrogen requirement. With partially

Probe Analyses[a]

HT-72 7.0					*HT-86* 3.5				
Feed Gas	42	18	6	Product Line	Feed Gas	30	18	6	Product Line
0.0	18.0	18.7	18.4	19.5	0.0	7.0	11.5	10.9	13.8
0.0	3.5	3.3	3.8	3.7	0.0	1.6	3.6	2.4	3.0
97.30	56.5	57.4	53.7	52.0	99.6	72.7	59.7	65.3	55.0
2.70	1.64	1.66	1.66	1.59	0.41	0.61	0.36	0.33	0.37
0.0	20.3	18.9	22.4	23.2	0.0	18.1	24.9	21.1	27.8
0.0	0.1	0.0	0.0	0.0	0.0	0.0	0.0	0.0	0.0
0.0	0.0	0.0	0.0	0.0	0.0	0.0	0.0	0.0	0.0
0.0	0.0	0.0	0.0	0.1	0.0	0.0	0.0	0.0	0.0
100.00	100.04	99.96	99.96	100.09	100.01	100.01	100.06	100.03	99.97

gasified Pittsburgh No. 8 seam coal, we have so far observed a carbon activity between 1 and 2 at 1700°–1950°F.

REACTION RATE. We compared the integral methane formation rates from our pilot plant tests with those reported by others (*1, 2, 6, 14*). To do so on the same basis, we took the reaction rate to be pseudo-first order with respect to the hydrogen partial pressure. The calculated reaction rate constant for each run is plotted against carbon gasification in Figure 5. Several observations can be made:

(1) The rate of methane formation for pretreated Pittsburgh coal is not slowed by the presence of methane in the feed gas. This agrees with Zielke and Gorin (*14*) in their study of hydrogasification of Disco char.

(2) The pretreated coal is quite reactive. For example, at 25–30% carbon gasification with steam-hydrogen mixtures, the rate constant is more than twice that reported by Feldkirchner and Linden (*6*) in reactions of low temperature bituminous char with hydrogen. The greater reactivity is most likely attributable to the higher volatile content of our pretreated coal (25–26%) than that of their char (17%).

(3) Partially hydrogasified coal, upon further reaction in the high temperature second stage, gave rate constants quite similar to those obtained with Disco char (*14*) and residual Australian brown coal (*1*), both containing little volatile matter.

Steam-Carbon Reaction. The reaction $C + H_2O \rightleftarrows CO + H_2$ was significant only at temperatures above 1700°F., and increased with temperature. At 1695°F. (Run HT-80), 50% of the feed steam decomposed, but at 1825°F. (Run HT-72), 70% was decomposed. Carbon oxides formation was related directly to the steam fed and to the steam decomposition. As much as 5.5 std. cu. ft. of carbon oxides/lb. of coal were

produced at the maximum 70% steam decomposition. With little or no feed steam decomposition, carbon oxides formation was about 1 std. cu. ft. or less/lb. of coal. In the low temperature first stage, the presence of steam in the feed gas is responsible, by the laws of mass action, for converting a major fraction of the oxygen in coal to carbon oxides. This oxygen is converted to water when steam is omitted from the feed—*e.g.*, when only hydrogen is fed.

The rate at which the steam-carbon reaction proceeds depends greatly on temperature (9), requiring heat above 2000°F. to approach equilibrium (*11*). Since hydrogasification tests are conducted at less than 2000°F. to preserve the methane formed, the carbon-steam reaction is expected to be substantially removed from equilibrium. This is shown by Figure 6 where calculated "equilibrium ratios" are plotted against maximum bed temperature. The curve represents true equilibrium for comparison.

The carbon-steam reaction is important from a process standpoint not only as a source of generating *in situ* hydrogen but also as a temperature controller. When pure hydrogen is the gasifying medium, the strong heat release by the methane-forming reaction causes runaway temperatures. In a hydrogen-steam mixture, this released heat is absorbed by the carbon-steam reaction, thereby stabilizing temperature.

Reaction Profile. To gain some insight into the path of reaction in free-fall or moving-bed zones, gas sample probes were located at several levels in the bed. Compare (Table V) the probe gas analyses from a low temperature run (HT-67) and a high-temperature run (HT-72). Both were made with a 7-ft. deep moving bed. Note that in the high temperature test, the reaction was practically complete in the lower half of the bed, with little reaction in the upper half of the bed and in the free-fall zone above the bed. On the other hand, in the low temperature test, the reverse was true: The bulk of the reaction took place in the free-fall zone and at the top of the bed, with little reaction in the rest of the bed. Hence, at both temperatures the bed height could be reduced to 3.5 ft. without any loss of gasification. This is in fact the case as shown in Table V by the probe samples from HT-86, a high temperature run using a 3.5-ft. deep bed.

The high temperature reaction is apparently equilibrium limited; it attains its limit in a relatively short contact time, in a short bed. The low temperature reaction is extremely rapid, requiring only a matter of seconds to complete. The reactive portion of coal, discussed by Wen and Huebler (*12*), is quickly gasified, after which the remainder of the carbon is not reactive at the low temperature. In view of these facts, a likely hydrogasifier configuration would incorporate a low temperature free-fall zone followed by a shallow high temperature stage.

Acknowledgment

Work reported here is co-sponsored by the American Gas Association and the U.S. Department of Interior, Office of Coal Research. Their permission to present this paper is greatly appreciated.

Literature Cited

(1) Birch, T. J., Hall, K. R., Urie, R. W., *J. Inst. Fuel* **33**, 422 (1960).
(2) Blackwood, J. D., *Australian J. Chem.* **12**, 14 (1959).
(3) Chanabasappa, K. C., Linden, H. R., *Ind. Eng. Chem.* **48**, 900 (1956).
(4) Dirksen, H. A., Lee, B. S., *A.I.Ch.E. Symp. High Pressure, Preprint 37D* (1965).
(5) Feldkirchner, H. L., Huebler, J., *Ind. Eng. Chem. Process Design Develop.* **4**, 134 (1965).
(6) Feldkirchner, H. L., Linden, H. R., *Ind. Eng. Chem. Process Design Develop.* **2**, 153 (1963).
(7) Huebler, J., Schora, F. C., *Chem. Eng. Progr.* **62**, 87 (1966) February.
(8) Linden, H. R., *Chem. Eng. Progr. Symp. Ser.* **61** (54) 76 (1965).
(9) Parent, J. D., Katz, S., *Inst. Gas Technol. Res. Bull.* **2** (1948).
(10) Pyrcioch, E. J., Linden, H. R., *Ind. Eng. Chem.* **52**, 590 (1960).
(11) von Fredersdorff, C. G., Pyrcioch, E. J., Pettyjohn, E. S., *Gas Technol. Res. Bull.* **7** (1957).
(12) Wen, C. Y., Huebler, J., *Ind. Eng. Chem. Process Design Develop.* **4**, 142 (1965).
(13) *Ibid.*, p. 147.
(14) Zielke, C. W., Gorin, E., *Ind. Eng. Chem.* **47**, 820 (1955).

RECEIVED December 22, 1966.

9

Fluid Bed Gasification of Pretreated Pittsburgh Seam Coals

A. J. FORNEY, R. F. KENNY, S. J. GASIOR, and J. H. FIELD

U. S. Department of the Interior, Bureau of Mines, Pittsburgh Coal Research Center, 4800 Forbes Ave., Pittsburgh, Pa.

The Bureau of Mines is investigating a two-stage gasification process for caking coals involving a pretreater to remove the caking properties in series with a gasifier to convert the coal to gaseous products. The pretreater is operated at 250°C. to make a treated coal with increased oxygen in the coal structure and at 450°C. to make a treated coal with decreased volatile matter. In either case the products from the pretreater pass directly to the gasifier operated at 870°C. The yield of hydrogen, methane, and carbon monoxide is about 23 std. cu. ft./lb. of coal at 80% carbon conversion. The two-stage process with raw coal feed will yield more gas than gasification of a pretreated coal.

An efficient coal gasification process operating at 800°–1000°C. and at pressures of 20–30 atm. is desirable for producing a synthesis gas which can be used to make a high B.t.u. gas. At these temperatures considerable methane is produced, and less oxygen is consumed than at the higher temperatures of 1100°–1200°C. used generally in entrained gasification systems. A fluidized bed can be operated at the lower temperature with sufficient residence time to obtain high conversion of the coal. Because most of the coals found in the East and Midwest are caking, their caking properties must be destroyed before they can be used in a fluidized bed. The purpose of these tests was to investigate an integrated pretreatment and gasification system whereby the pretreated coal would be processed in a fluid bed gasifier at conditions to produce a synthesis gas with high methane content.

Two methods of pretreating caking coal in a fluid bed to produce a free-flowing char have been developed—one at high temperature and one at low temperature. In the high temperature treatment (2, 3) coal is

fluidized in steam plus air or oxygen at 430°C. for 5–10 min. The oxygen:coal ratio is about 0.4 std. cu. ft./lb. In the low temperature treatment (*1*) coal is fluidized in air at 240°C. for 30–40 min. The oxygen:coal ratio is about 2.4 std. cu. ft./lb.

Work on pretreatment by other investigators was discussed in an earlier report (*2*). One big advantage of the two-stage fluid bed system is that all the products from the pretreatment are sent to the gasifier, and none is wasted. In other methods the coal was pretreated separately with air or other gases, and the loss in coal may be as much as 20% essentially volatile matter.

Experimental

Equipment and Procedure. The treated coals were tested in the gasifier to determine whether or not the coals were sufficiently noncaking for use. If the gasification were operable, the pretreater and gasifier were operated in series starting with a raw coal feed. When the coal was pretreated using steam plus oxygen, the gas from the pretreater, as well as the pretreated coal, were sent to the gasifier.

The apparatus is shown in Figure 1. Raw Pittsburgh seam coal from the Bruceton mine (70% through 200 mesh with coarser than 35 mesh removed) is fed into a fluid bed pretreater, 1 in. diameter by 30 in. long, operated at either 450° or 260°C. The fluidizing gas is steam plus air (or oxygen). The products, gas, tars, and treated coal pass from the top of the pretreater and flow with additional steam (or steam plus oxygen) into the fluid-bed gasifier (3 in. diameter by 30 in. long, topped by an expanded section 6 in. in diameter by 12 in. long). The product gas and coal fines pass to a cyclone and bag filter to remove dust, then through a condenser and electrostatic precipitator to remove water plus tar, and finally to a gas meter. An inline chromatograph analyzes the gas for six components every 20 min. An oxygen analyzer continuously monitors the product gas. The range of process variables, such as gas fluidizing velocity and coal feed rate, is limited. An increase in the coal

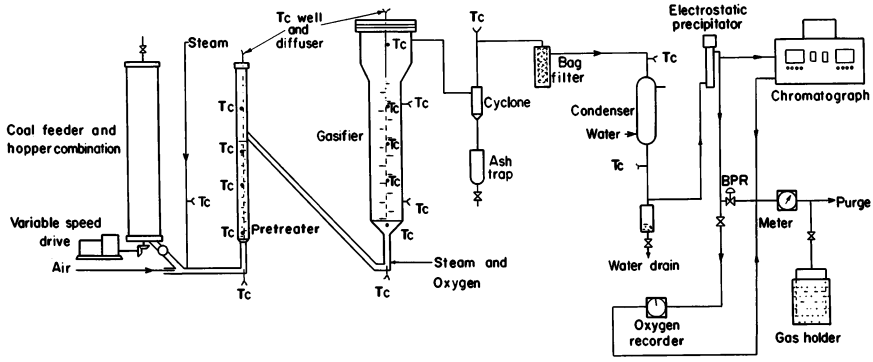

Figure 1. Fluid bed pretreater and gasifier system

feed rate decreases the residence time of the coal in both the pretreater and gasifier. The superficial gas velocity for most tests was about 0.25 ft./sec.

Results

Tests with Pretreated Coals. The first tests in the gasifier were made with coals which were pretreated in a separate unit so the free-swelling indices (FSI) and other coal properties could be determined. Pittsburgh seam coal was used in all tests. The tests were made with high temperature treated coals (HT) having indices of 2, 1, and noncaking, respectively, and low temperature treated coals (LT) with indices of 1.5 and noncaking, respectively. The gasifier was operated at 2.5 atm. and 871°C. with a coal feed rate of 0.4 lb./hr. Table I shows the analysis of the coals and the method of pretreatment.

Loss of volatile matter is greater in the HT coals (35.6% in the raw coal and 26.0% in HT-440), and the oxygen content is greater in the LT (8.1% in the raw coal and 11.8% in LT-56). HT coals with an FSI of 2 and the LT coals with an FSI of 1.5 were caked in the reactor, while the coals with FSI of 1 or less were operable.

HT coals yield more gas and are less likely to agglomerate in the gasifier. Test 61 made with HT-2 coal had a yield of 22 std. cu. ft./lb. (CO_2- and N_2-free) compared with 17 in tests 58 with LT-56 coal. The temperature was held constant in both tests, but 0.5 std. cu. ft./hr. of oxygen had to be fed to the gasifier in test 58 to prevent caking. In tests 62 and 59, oxygen was fed to the gasifier. The HT-2 coal yielded 23 std. cu. ft./lb. compared with 22 for LT-56, even though the LT coal had greater carbon conversion. The quality of the product gas was about the same in all the above tests (Table II).

Pretreater and Gasifier in Series. When the pretreater and gasifier were operated in series, the products from the raw coal pretreatment—char, tars, and gases—were sent directly to the gasifier. The gasifier operated satisfactorily with no agglomeration of the coals. Table II compares the gasification of the two types of treated coal. The coals pretreated at 450°C. yielded more product gas than those treated at 260°C. When no oxygen was fed to the gasifier, the HT coal (test 36) yielded 22 std. cu. ft./lb. of $H_2 + CO + CH_4$ compared with 18 std. cu. ft./lb. coal from the LT coal (test 60). When oxygen was fed to the gasifier the results were similar: 21 std. cu. ft./lb. in test 33 compared with 19 for test 63.

These tests show that pretreatment at 450°–460°C. with less oxygen is superior to pretreatment at 250°C., not only in increased gas production, but also because there is less likelihood of the coal's caking in the gasifier. More CO_2 results from the coals with the 250°–260°C. treatment

because of oxygen added to the coal during pretreatment (Table I). Evolution of CO_2 from the LT coal was also noted in earlier tests (*1*). Table II shows that 22 std. cu. ft./lb. were produced with the HT-2 coal (test 61) and also with raw coal (test 36). However, because of the separate pretreatment of HT-2, about one-third of the volatile matter had been lost in the pretreatment (Table I); over-all 10–20% of the constituents in the coal may be lost in this type of pretreatment; therefore, more gas will be produced from the raw coal.

Table I. Analyses of Pretreated Coals Used in the Gasifier

	Raw coal[a] D-2	*Raw coal[a] D-1*	*HT-400[b]*	*HT-440[c]*	*HT-1[d]*	*LT-55[e]*	*LT-56[f]*
Moisture	1.5	1.5	0.5	0.8	0.8	0.9	0.9
Volatile matter	36.6	35.6	30.4	26.0	22.7	34.0	31.2
Fixed carbon	53.2	56.5	62.2	67.1	69.3	56.2	57.5
Ash	8.7	6.4	6.9	6.1	7.2	8.9	10.4
Hydrogen	5.1	5.2	4.8	4.5	4.1	4.7	4.2
Carbon	75.2	77.4	77.8	78.8	78.2	73.6	70.9
Nitrogen	1.5	1.5	1.4	1.5	1.7	1.5	1.4
Oxygen	8.1	8.4	8.0	8.1	7.8	9.8	11.8
Sulfur	1.4	1.1	1.1	1.0	1.0	1.5	1.3
FSI	8	8	2	1	NC[g]	1.5	NC[g]

[a] Bruceton coal; 70% through 200 mesh with coarser than 35 mesh removed.
[b] Pretreated at 400°C.; O_2:coal ratio = 0.4 std. cu. ft./lb. Residence time, 10 min.
[c] Pretreated at 440°C.; O_2:coal ratio = 0.4 std. cu. ft./lb. Residence time, 30 min.
[d] Pretreated at 440°C.; O_2:coal ratio = 1.1 std. cu. ft./lb. Residence time, 30 min.
[e] Pretreated at 240°C. with air; O_2:coal ratio = 2.4 std. cu. ft./lb. Residence time, 30 min.
[f] Pretreated at 250°C. with air; O_2:coal ratio = 2.4 std. cu. ft./lb. Residence time, 30 min.
[g] Noncaking

Table III shows some results in tests where oxygen, coal, and steam rates were varied to give a range of operability. At a constant coal feed rate, an increase in the oxygen rate from 2.4 to 9.1 std. cu. ft./lb. coal increased the conversion from 46 to 80% and also the product gas ($H_2 + CH_4 + CO$) yield from 19 to 23 std. cu. ft./lb. coal. The hydrogen and methane yields decreased. Increasing the steam from 26 to 56 std. cu. ft./lb. (tests 31 and 35) resulted in only minor changes in carbon conversion and gas yield. The hydrogen content of the product gas increased from 42 to 48%. An increase in the coal rate from 0.36 to 0.91 lb./hr. decreased the carbon conversion from 68 to 50% and the gas yield from 21 to 16 std. cu. ft./lb. coal.

Effect of Pressure. The effect of pressure on the methane yield and caking property of coal treated at high temperature was studied at 2.5, 5, and 8 atm. (Table IV). With an increase in pressure, however, the gas flow of steam plus oxygen must be increased to maintain the same linear

velocity in the fluid bed. To maintain the desired ratios of oxygen:coal and steam:coal, the coal feed must be increased, but with a fixed bed height the residence time of the coal in the pretreater and gasifier will decrease. At 8 atm., gasifier operation was difficult because of coal agglomeration owing to the decreased residence time in the pretreater. At

Table II. Conditions of Operation and Results of Tests Using Pretreated Coals in the Fluid Bed Gasifier at 2.5 atm.

Test No.	*61*	*58*	*62*	*59*	*36*	*60*	*33*	*63*
Coal	HT-2	LT-56	HT-2	LT-56	Raw coal D-1	Raw coal D-2	Raw coal D-1	Raw coal D-2
Input								
Steam, std. cu. ft./hr.	14	15	15	15	15	13	14	17
Oxygen, std. cu. ft./ hr., pretreater	0	0	0	0	1.0	1.6	1.0	1.6
Oxygen, std. cu. ft./ hr., gasifier	0	0.5	2.5	2.5	0	0	1.4	1.0
Nitrogen, std. cu. ft./ hr.	9	10	10	10	10	10	10	10
Coal, lb./hr.	0.38	0.40	0.38	0.36	0.37	0.36	0.36	0.36
Temperature, °C.								
Pretreater	—	—	—	—	450	261	450	258
Gasifier, av.	868	871	872	873	860	869	857	863
Gasifier, max.	875	874	877	878	874	877	873	866
Oxygen: coal, std. cu. ft./lb.	0	1.3	6.6	6.3	2.7	4.5	6.7	7.5
Steam: coal, std. cu. ft./lb.	37	38	41	42	41	36	39	47
Carbon conversion, %	51	43	77	83	51	54	68	73
Steam conversion, %	—	—	—	—	20	—	17	—
Product gas,[a] std. cu. ft./lb. coal	22	17	23	22	22	18	21	19
Product gas,[b] %								
H_2	59	55	45	44	55	48	45	42
CH_4	3	3	3	2	4	3	3	2
CO	20	22	25	26	22	24	29	24
CO_2	18	20	28	28	19	25	23	32

[a] Nitrogen- and CO_2-free.
[b] Nitrogen-free.

0.4 lb./hr. the residence time of the coal in the pretreater was about 40 min., and at 1.25 lbs./hr. about 13 min.—apparently too short a time for pretreatment at these operating conditions. When the coal rate was decreased to about 1 lb./hr. the unit operated satisfactorily, with no coal agglomeration, but carbon conversion was low, indicating insufficient residence time of the coal in the gasifier.

The methane content of the product gas increased from 4% at 2.5 atm. (test 39) to 8% at 8 atm. (test 46) when there was no oxygen fed to the gasifier. Lesser amounts of methane and hydrogen were formed when oxygen was used in the gasifier.

Table III. The Effect of Variables on the Gasification of Bruceton Coal Using the Pretreater and Gasifier in Series at 2.5 atm.

Test No.	*39*	*37*	*31*	*35*	*33*	*30*
Input						
Steam, std. cu. ft./hr.	11	15	10	22	14	35
Oxygen, std. cu. ft./hr., pretreater	1.0	1.0	1.5	1.0	1.0	1.5
Oxygen, std. cu. ft./hr. gasifier	0	2.2	0.9	1.4	1.4	4.5
Nitrogen, std. cu. ft./hr.	8	10	12	10	10	12
Coal, lb./hr.	0.33	0.35	0.39	0.39	0.36	0.91
Temperature, °C.						
Pretreater	450	450	450	450	450	450
Gasifier, av.	860	865	867	858	857	858
Gasifier, max.	874	876	875	875	873	871
Oxygen: coal, std. cu. ft./lb.	2.4	9.1	6.2	6.1	6.7	6.6
Steam: coal, std. cu. ft./lb.	32	43	26	56	39	38
Carbon conversion, %	46	80	61	64	68	50
Steam conversion, %	20	13	11	11	17	10
Product gas,[a] std. cu. ft./lb. coal	19	23	19	21	21	16
Product gas,[b] %						
H_2	56	42	42	48	45	47
CH_4	4	2	2	3	3	3
CO	21	29	30	24	29	30
CO_2	19	27	26	25	23	20

[a] N_2-, H_2O-, and CO_2-free.
[b] N_2- and H_2O-free.

Less methane formed at 8 atm. when the coal-feed rate was decreased from 1.25 to 1.0 lb./hr. At this lower rate the nitrogen rate had to be raised to maintain fluidization since the steam and oxygen rates are fixed by the coal feed. This increase in nitrogen decreased the partial pressure of the reacting gases. To operate at the desired 20 atm. to produce the maximum yield of methane the gasifier height must be increased to increase the residence time, or possibly the product gas could be recycled so that the coal rate could be decreased. A recycle probably would not be effective if oxygen were being fed to the gasifier since present tests showed that oxygen would react with gas in preference to the coal.

Methane yields in these tests may be compared with yields from the Lurgi gasifier (*4*) where 11% methane is produced at 8 atm.; however, carbon conversion of the brown coal used in the Lurgi is much higher than in our tests.

Table IV. Effect of Pressure on Gasification of Bruceton Coal Using Pretreater and Gasifier in Series

Test No.	*39*	*41*	*45*	*44*	*46*	*55*	*54*
Pressure, atm.	2.5	2.5	5	5	8	8	8
Input							
Steam, std. cu. ft./hr.	11	14	26	34	65	50	42
Oxygen, std. cu. ft./hr., pretreater	1.0	2.0	1.6	1.6	2.2	2.0	1.2
Oxygen, std. cu. ft./hr., gasifier	0	1.0	0	4.0	0.6	0	5.2
Nitrogen, std. cu. ft./hr.	8	8	11	11	8	22	27
Coal, lb./hr.	0.33	0.37	0.75	0.73	1.25	0.91	0.97
Temperature, °C.							
Pretreater	451	451	455	456	456	453	452
Gasifier, av.	860	855	862	831	842	823	864
Gasifier, max.	874	867	873	874	869	869	866
Oxygen: coal, std. cu. ft./lb.	2.4	8.1	2.1	7.6	2.2	2.2	7.0
Steam: coal, std. cu. ft./lb.	32	38	48	46	52	55	43
Carbon conversion, %	46	66	52	66	43	41	53
Steam conversion, %	20	18	16	13	—	14	8
Product gas,[a] std. cu. ft./lb. coal	19	18	20	20	16	17	15
Product gas,[b] %							
H_2	56	46	54	46	52	58	45
CH_4	4	3	5	3	8	6	5
CO	21	22	20	23	18	13	20
CO_2	19	29	21	28	22	23	30

[a] N_2-, H_2O-, and CO_2-free.
[b] N_2- and H_2O-free.

The best coal-feed rate for this size gasifier at 2.5 atm. is about 0.4 lb./hr. The minimum oxygen rate to the pretreater is 1.2 std. cu. ft./lb. of coal feed when oxygen is fed to the gasifier also, but 2.0 std. cu. ft./lb. with no oxygen to the gasifier. These figures compare with only 0.4 std. cu. ft. of oxygen/lb. needed in the earlier tests (*3*) to pretreat the same coal.

The two-stage fluid system handles raw caking coals without agglomeration. Coal is easily fed to the pretreater and the product mixed with material in the gasifier, reducing the possibility of agglomeration. Oxygen addition to the gasifier may be needed for LT pretreated feed to prevent caking. This was demonstrated in the tests where oxygen fed to the gasifier prevented agglomeration of the LT pretreated coal.

However, there are several disadvantages to the system. Two fluid beds in series are difficult to operate. Any surge in the pretreater throws untreated coal into the gasifier; the coal, gases, tars, and oxygen entering at the bottom of the gasifier make temperature control difficult. Also, at least 1.2 std. cu. ft. oxygen/lb. coal are needed for pretreatment in addition to that needed for gasification. This is almost one-third the requirement for gasification in the Lurgi (*5*) which requires about 4 std. cu. ft./lb.

Finally, methane production is lower than in the Lurgi because the gas-solids flow is not countercurrent.

New Gasification System

In an attempt to overcome these difficulties, the system has been revised as shown in Figure 2. Now the coal is fed into the top of a 10-ft. long, 6-in. diameter pipe and falls freely through an upward flow of gas from the 3-in. diameter fluid bed gasifier. As it drops, the coal is carbonized and devolatilized, and by the time it enters the fluid bed it should be noncaking. Preliminary tests of the revised system indicate that it is operable, and the methane yield is higher owing to countercurrent flows.

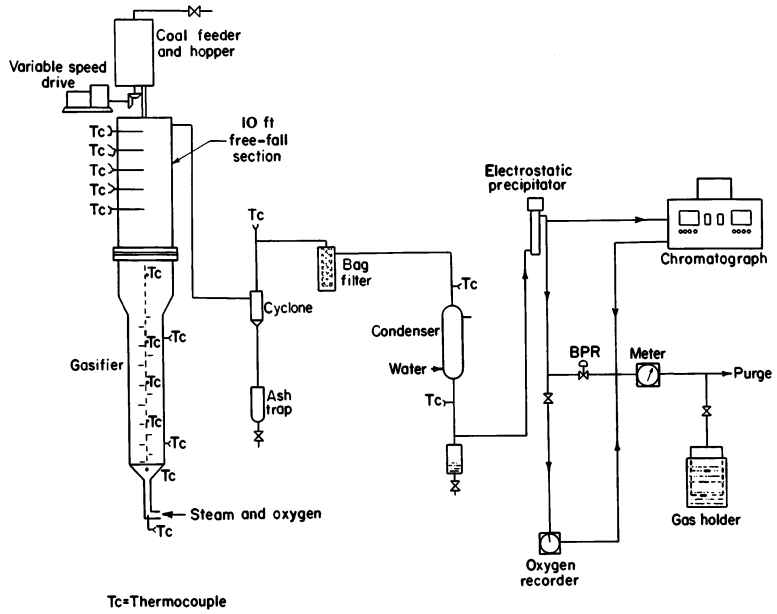

Figure 2. Free-fall reactor and fluid bed gasifier system

Conclusions

Low temperature (250°C.) treated coal and high temperature (450°C.) treated coal can react in a fluid bed gasifier operated at 870°C. without coal agglomeration. The Pittsburgh seam coal passes first to a pretreater and then to a gasifier, the two being in series. The raw coal used in the two-stage system yielded more product gas than when the coal was pretreated separately if the off-gas from separate pretreatment is lost. Minimum oxygen needed is 1.2 std. cu. ft./lb. of

coal. At 8 atm. the methane content of the product gas is about 8%. An increased methane yield is expected by using countercurrent free-fall system.

Literature Cited

(1) Forney, A. J., Kenny, R. F., Field, J. H., "Abstracts of Papers," 150th Meeting, ACS, Sept. 1965, L44.
(2) Forney, A. J., Kenny, R. F., Gasior, S. J., Field, J. H., *Ind. Eng. Chem. Res. Develop.* 3, 48 (1964).
(3) Forney, A. J., Kenny, R. F., Gasior, S. J., Field, J. H., "Abstracts of Papers," 148th Meeting, ACS, Aug.-Sept. 1965, L1.
(4) Odell, W. W., *U. S. Bur. Mines Inform. Circ.* 7415 (1946).
(5) Von Fredersdorff, C. G., Elliott, Martin A., "Chemistry of Coal Utilization," Suppl. Vol., H. H. Lowry, ed., p. 990, Table 24, Wiley, New York, 1963.

RECEIVED November 21, 1966.

Discussion

Arthur M. Squires: Since the paper by Forney *et al.* reports product-gas methane concentrations which are rounded off to the nearest integer, it was a surprise to discover that methane equilibrium ratios calculated from the data are consistent with the hypothesis that methane production was governed by a quasi-equilibrium.

Methane equilibrium ratios calculated from effluent gas compositions for 10 runs at 2.5 atm. range from about 0.14 to about 0.19, while ratios calculated for two runs at 8 atm. are about 0.075 and 0.095. The two respective ranges are indicated by the two vertical arrows in Figure 1, which is a plot of methane equilibrium ratio *vs.* reciprocal of absolute temperature. (Ratios for two runs at 5 atm. are about 0.082 and 0.11.)

The lines in the figure are from Squires (*6*), as follows:

Line A: Ratios calculated for effluent gas from steam-only fluidized-bed gasification at atmospheric pressure, to which raw coaly matter (peat, low rank bituminous, and coking bituminous) was fed continuously.

Line B: Ratios for steam-only batch fluidized-bed gasification of a wide range of cokes and chars (including high temperature coke) at atmospheric pressure.

Line C: Ratios for steam-oxygen batch fluidized-bed gasification of a bituminous char at 8.5 atm.

Line D: Ratios for steam-oxygen batch fluidized-bed gasification of anthracite at 12–17 atm.

Lines B, C, and D display a trend toward lower equilibrium ratio at higher pressure—a trend also found in the ratios calculated from Forney *et al.* Squires hypothesized that methane production in fluidized-bed gasification is governed by a quasi-equilibrium among the species methane, hydrogen, and a carbon having a free energy higher than graphite by an amount which varies with pressure. Squires wished to reserve the term "quasi-equilibrium" for "that quasi-steady-state which exists when an active solid is being produced or consumed by a reaction under conditions such that the activity of the solid does not change with time." Following Dent's suggestion (*4*), Squires (*7*) believed that the free energy of carbon is maintained at a high level in a fluidized-bed gasifier because each particle of solid, through top-to-bottom mixing of solid in the bed, frequently "sees" an atmosphere rich in steam and poor in hydrogen at the bottom of the bed.

Methane yields from fixed-bed gasification are generally far below that called for by graphite equilibrium. Indeed, Dent (*4*) reported that steam conversions in a fluidized-bed gasifier can be superior, at high temperatures, to those afforded by an equivalent fixed-bed gasifier. This fact is contrary to the usual generalization that fluidized-bed reactors give poorer gas-to-solid contact than fixed-bed reactors and is a reminder that an attempt to relate fluidized-bed integral reaction rates to differential fixed-bed rate data may fail badly because one is dealing with different solids, arising from different recent gas-environment histories.

Blackwood and McCarthy (*2*) objected to the correlations shown in Figure 1 on the ground that steam as well as hydrogen can react directly with carbon to form methane. In their view, the system should be bounded by an equilibrium expression which contains the concentration of both steam and hydrogen, but no expression of this type was proposed. It should perhaps be emphasized that the evidence in Figure 1 is merely circumstantial. One cannot appeal to kinetic data either to prove or disprove the hypothesis that the ultimate amount of methane produced is governed by a quasi-equilibrium involving hydrogen. The hypothesis requires proof by thermochemical data—heats of combustion and low-temperature specific heats measured for carbon taken from a fluidized-bed gasifier. This would appear to be a worthwhile area for research.

Blackwood and McCarthy showed that the fixed-bed differential reaction rate of hydrogen and carbon—coconut and wood chars as well as a char of Australian brown coal—tends to zero at the graphite equilibrium. This observation may not be relevant to the over-all kinetic situation when carbon is gasified by steam in a fluidized bed, in which

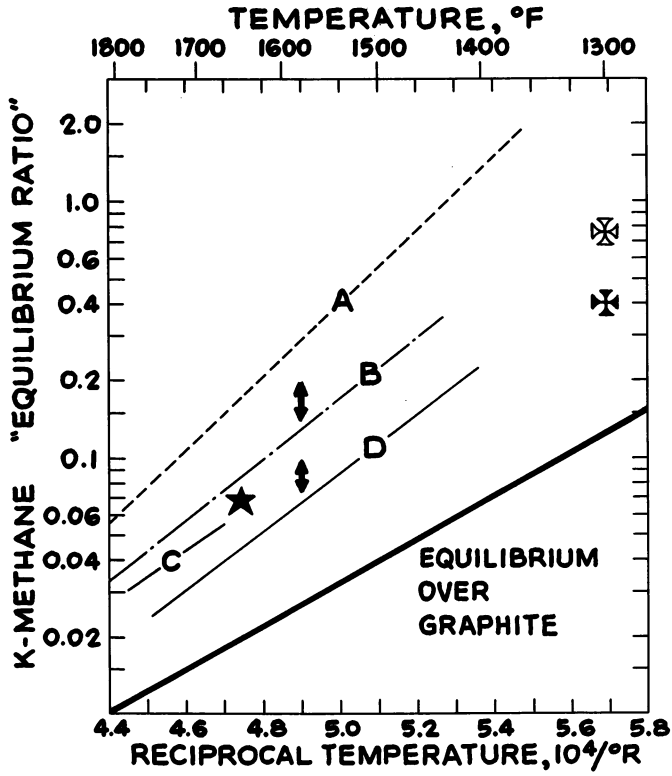

Figure 1. Correlations of methane and hydrogen concentrations. $K = (y_{CH_4})/(y_{H_2})^2 P$, where y = mole fraction in gasifier effluent, and P = pressure in atmospheres. See text for explanation of lines and symbols

the carbon frequently sees a gas atmosphere far removed from equilibrium.

Blackwood and McCarthy placed importance upon the fact that the methane yield did not exceed the graphite equilibrium in any of the runs by Birch, Hall, and Urie (*1*), who hydrogasified brown coal in a continuous fluidized-bed reactor. As early as 1938, however, Dent (*3*) recognized that the methane from coal hydrogenation can exceed graphite equilibrium. He obtained yields at 50 atm. from the fixed-bed hydrogenation of a char catalyzed by $BaCO_3$ which were consistently about 30% above the graphite equilibrium. This is probably a true example of a quasi-equilibrium in the sense meant by Squires.

It would now appear, however, that no such simple generalization as Squires' hypothesis relative to fluidized-bed gasification is available to organize methane-yield data from dilute-phase gasification systems such as those studied in three papers in this volume. Glenn *et al.* report

methane yields in three runs between 40 and 120% above the graphite equilibrium. It would appear that methane yields were on the order of 30% above the graphite equilibrium in two runs reported by Lewis *et al.* Figure 4 of Lee *et al.* shows a few runs which afforded methane yields as high as 80% above the graphite equilibrium. In all three of these papers, the highest methane yields, relative to the graphite equilibrium, were obtained under situations in which the ratio of gasification-agent supply rate to solid-supply rate was small. Lower methane yields, relative to the graphite equilibrium, were obtained at higher ratios of gasification agent to solid. The lower yields probably reflect a failure of the reaction to achieve a rate capable of maintaining a methane content in equilibrium with the solid present in the system. Unlike the relatively simple situation in fluidized-bed gasification with steam, the solid's free energy is probably a complicated function of burn-off, solid residence time, and gas environment. It would appear that the effluent composition from a dilute-phase system does not provide a measure of the carbon free energy. One probably cannot expect a quasi-equilibrium ever to occur, in Squires' sense of the term, in a dilute-phase system.

It is perhaps worth emphasizing again that line B in Figure 1 was partly based upon data for high temperature coke, from which methane could be produced only by some mechanism involving steam. Also, lines B, C, and D were based upon data covering a wide range of burn-off.

Wen and Huebler (*8*) reported batch-system measurements of bituminous coal-char-hydrogen equilibrium at 1300°F. and 137 atm. Typically, about 20 hours were required for the system to reach an apparent equilibrium (the maximum in a plot of the methane equilibrium ratio *vs.* time). The results are reproduced in a plot of "pseudo-equilibrium" *vs.* burn-off in Figure 4 of Wen, Abraham, and Talwalkar's chapter in this volume. The open Maltese cross plotted in Figure 1 of this discussion shows Wen and Huebler's value for zero burn-off, and the closed cross shows the value for 25% burn-off. Since these pseudo-equilibria were not measured for an on-going reaction, they do not represent quasi-equilibria in Squires' sense.

Lewis *et al.* report a remarkable result, plotted as a star in Figure 1, for the countercurrent hydrogenation of char at 103 atm. in a moving bed. The hydrogen-to-char ratio was low, and the solid residence time was only minutes. It may be conjectured that the char entering the moving bed—this of course is the char last seen by the effluent gas—had a free energy distinctly higher than that of any of the chars in Wen and Huebler's pseudo-equilibrium study, where the solid residence time was many hours. It would be extremely interesting, and perhaps technically important, to know whether or not the effluent in Lewis *et al.* came close to representing a quasi-equilibrium with the entering char.

Line A of Figure 1 has remained a curiosity for seven years. The higher slope of this line, indicating a higher heat of reaction, is consistent with the hypothesis that line A represents a quasi-equilibrium for a solid whose heat content as well as free energy is markedly higher than graphite's. Unlike lines B, C, and D, however, line A was based upon data taken at relatively low carbon burn-offs and relatively short solid residence times. Perhaps line A merely reflects a transitory state of a freshly generated carbon—a carbon which might be termed "nascent carbon"—having a free energy far higher than that displayed even at zero burn-off in Wen and Huebler's study. Perhaps, then, one must expect a sharp decline in methane yield from that according to line A when carbon burn-off and solid residence time are increased. In any event, one must expect a decline from line A with increasing gasification pressure. Fluidized-bed gasification data with continuous feeding of raw coal at elevated pressure may prove to have great technical interest, and it is understood that Forney (5) and his collaborators plan to obtain such data in the near future.

Literature Cited

(1) Birch, T. J., Hall, K. R., Urie, R. W., *J. Inst. Fuel*, 33, 422 (1960).
(2) Blackwood, J. D., McCarthy, D. J., *Australian J. Chem.*, 19, 797 (1966).
(3) Dent, F. J., *Inst. Gas Eng. Joint Res. Committee Rept.* No. 43 (1938).
(4) Dent, F. J., *Trans. Inst. Chem. Eng.* 39, 22 (1961).
(5) Forney, A. J., personal communication, September 1966.
(6) Squires, A. M., *Trans. Inst. Chem. Eng.* 39, 3 (1961).
(7) *Ibid.*, p. 10.
(8) Wen, C. Y., Huebler, J., *Ind. Eng. Chem. Process Design Develop.* 4, 142 (1965).

RECEIVED January 11, 1967.

CO_2 Acceptor Gasification Process

Studies of Acceptor Properties

GEORGE P. CURRAN, CARL E. FINK, and EVERETT GORIN

Research Division, Consolidation Coal Co., Library, Pa.

The CO_2 Acceptor Gasification Process is discussed in light of the required properties of the CaO acceptor. Equilibrium data for reactions involving the CO_2 and sulfur acceptance and for sulfur rejection fit the process requirements. The kinetics of the reactions are also sufficiently rapid. Phase equilibrium data in the binary systems CaO–$Ca(OH)_2$ and $Ca(OH)_2$–$CaCO_3$ show the presence of low melting eutectics, which establish operability limits for the process. Data were obtained in a continuous unit which duplicates process conditions which show adequate acceptor life. Physical strength of many acceptors is adequate, and life is limited by chemical deactivation. Contrary to earlier findings both limestones and dolomites are equally usable in the process. Melts in the $Ca(OH)_2$–$CaCO_3$ system are used to reactivate spent acceptors.

Production of both hydrogen-rich and high B.t.u. gas from coal has been under study in the Research Division of Consolidation Coal Co. for several years. There are a number of partially or fully developed processes which are available for this purpose, but they are all too expensive to be competitive with natural gas for the foreseeable future.

Most of the available processes use oxygen to provide the endothermic heat for the gasification process. The high cost of oxygen is one of the more significant items which makes conventional processes uneconomic. Thus, oxygen must be eliminated in an improved process, and the CO_2 acceptor process satisfies this general objective. This paper describes some steps which have been taken in developing this process.

Further details are given here of some material which has been presented previously (*2*, *3*). This paper also contains in addition a considerable amount of new material.

The experimental work described here deals exclusively with the properties of the acceptor as dictated by the needs of the process. Data on kinetics of the gasification reactions, for example, will not be presented at this time.

Process Description

Our initial work on the CO_2 acceptor project was aimed at producing high B.t.u. pipeline gas from bituminous coal char. The direction of the work has been shifted to applying the process to Dakota lignites. A feasibility study was prepared (*5*) and outlines the potential economics of the process for producing pipeline gas from North Dakota lignite. A brief resumé of the feasibility report was given in a recent paper (*1*). Since this paper is not generally available, the results of that study will be reiterated briefly. The main emphasis of the presentation will, however, be on discussing experimental work to determine the validity of the basic assumptions regarding the functioning of the acceptor and to provide a framework for appropriate revisions as required.

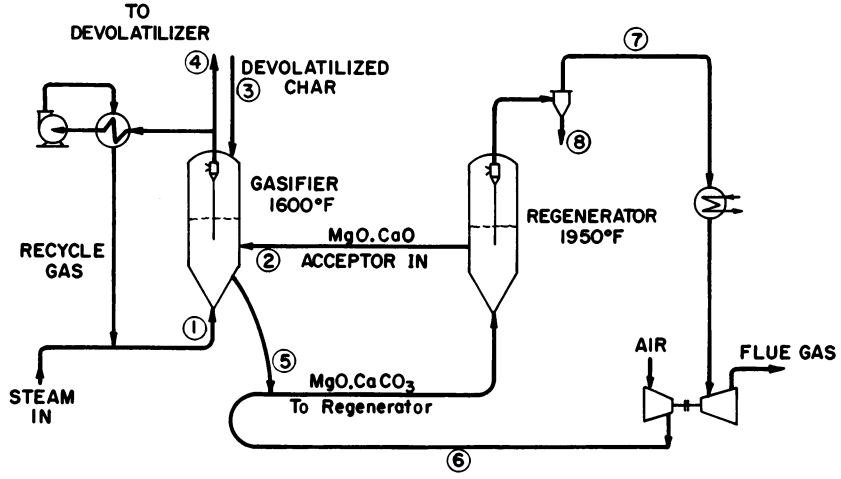

Figure 1. CO_2 acceptor process

A schematic flowsheet of the CO_2 acceptor process is shown in Figure 1. Since we are concerned here with only the gasifier and regenerator sections, only these are shown. Lignite drying, devolatilization, gas purification, and methanation steps are omitted.

The heat and material balance around the process are given in Table I where the material flows and their temperatures corresponding to the numbered streams in the flowsheet are given.

The key features essential to the process are:

(1) The acceptor should be durable enough to resist physical decrepitation and chemical deactivation owing to cycling through the process.

(2) Separate control of residence time of acceptor and char particles is possible as well as separation of acceptor from char ash.

(3) Adequate reaction kinetics should be maintained in the key reactions listed below.

$$CaO + CO_2 = CaCO_3 \quad (1)$$

$$C + H_2O = CO + H_2 \quad (2)$$

$$C + 2\,H_2 = CH_4 \quad (3)$$

$$CO + H_2O = CO_2 + H_2 \quad (4)$$

(4) Operability of the system must be maintained.

Assessing the combination of factors under item (1) led us to estimate the make-up rate of fresh dolomite acceptor of 2.0% of the circulation rate. The average activity of the dolomite was assumed to be such that 70 mole % of the total CaO was converted to $CaCO_3$ before the acceptor was returned to the regenerator. The driving force for CO_2 absorption was assumed to be 0.35 atm.

The limits under (2) do not require sharp definition. The residence time of the acceptor in the char bed is not critical (as will be shown later) as long as it is greater than about 7 min.

The assumptions made under item (3) are summarized in Table II. Data on the reaction rates involving char will not be given here.

Item (4) requires that the steam partial pressure be maintained at all times below the minimum value at which melt formation occurs—*i.e.*, 13 atm. This is achieved (Figure 1) by recycling the product gas. Likewise, it must be demonstrated that ash fusion is not a problem in the regenerator.

Table II notes that in the process two important equilibria in acceptor reactions are involved. These were checked experimentally since the literature data are contradictory. No data at all were available on the H_2S acceptor reaction, which is important in the gasification step, and the equilibrium was also determined for Reaction 5.

$$CaO + H_2S = CaS + H_2O \quad (5)$$

Phase equilibrium studies were also conducted to obtain a better understanding of the melt formation which introduces important operability limits in the process.

Table I. Stream Flows and

	Stream No.		
	1	*2*	*3*
Temperature, °F.	1327	1950	1400
Pressure, p.s.i.a.	315	315	300
Total moles/hr. of gas	61,479	—	—
Gas composition, vol.%			
CH_4	5.4	—	—
CO	5.9	—	—
H_2	27.5	—	—
CO_2	2.9	—	—
SO_2	—	—	—
N_2	—	—	—
H_2O (v)	58.3	—	—
O_2	—	—	—
Solids flows, moles/hr.			
MgO · CaS	—	—	85
MgO · CaO	—	21,735	764
MgO · $CaCO_3$	—	—	2,972
Solids flows, lbs./hr.			
Char (m.a.f.)	—	—	659,400
Ash	—	—	97,600

[a] Plant size—250,000,000 std. cu. ft./stream day pipeline gas. Steam input = 61,479

Experimental Method

Equilibrium Studies of Acceptor Reactions. The equipment used for equilibrium studies in the CO_2 acceptor reaction (Reaction 1) is illustrated in Figure 2.

The reactor is a thin-walled stainless steel vessel 1-in. i.d. × 6-in. long and is contained along with its heating furnace and insulation by a 1-liter high pressure autoclave (not shown). The reactor internal pressure is balanced by adding CO_2 from an external source to the autoclave.

The equilibrium in Reaction 1 was determined as follows. A CO_2–N_2 mixture of known composition and pressure was used to fluidize the acceptor bed. The fluidizing gas entered the reactor axially down through a diptube, reversed direction, and fluidized the acceptor. The effluent gas was throttled to atmospheric pressure through the back pressure control valve B. The effluent gas and feed gas were passed through the thermal conductivity cell where the feed gas served as reference gas. The electrical output of the cell, which was connected in a wheatstone bridge circuit, was recorded by a strip chart potentiometer.

The thermal conductivity cell was able to detect a change in CO_2 concentration of ±0.01%. The solid phase which was initially dolomite containing $CaCO_3$ was heated to the anticipated temperature corre-

Composition in CO_2 Acceptor Process[a]

Stream No.				
4	*5*	*6*	*7*	*8*
1600	1600	290	1950	1950
300	315	315	300	300
67,753	—	106,553	125,549	—
9.2	—	—	—	—
10.2	—	—	0.62	—
47.2	—	—	0.02	—
4.9	—	—	27.53	—
—	—	—	0.23	—
0.2	—	78.3	66.51	—
28.3	—	0.9	1.95	—
—	—	20.8	—	—
—	206	—	—	—
—	7,667	—	—	493
—	17,683	—	—	—
—	263,700	—	—	37,400
—	97,600	—	—	97,600

moles/hr. at 1118°F. Makeup MgO · CaO = 49,300 lb./hr.

sponding to the CO_2 partial pressure imposed on the system. The temperature was then cycled at a maximum rate of 5°F./min. below and above the anticipated equilibrium temperature. The effluent gas then showed a deficiency or excess of CO_2 compared with the inlet gas, depending upon whether recarbonation or calcining was occurring. The temperature corresponding to the equilibrium CO_2 pressure was recorded at the point when the effluent gas showed zero change in composition. The temperature was always the same within ± 1°F. when approaching from either direction.

The equilibrium in the sulfur rejection reaction:

$$3/4\ CaSO_4 + 1/4\ CaS = CaO + SO_2 \qquad (6)$$

was determined in an analogous fashion, with SO_2 replacing CO_2. To avoid corrosion of the stainless steel reactor and consequent masking of the desired reaction, a fused quartz vessel of same configuration was used. This reactor was operated at atmospheric pressure and was heated by immersion in an externally heated air fluidized sand furnace.

Equipment for studying the equilibrium of Reaction 5 was modified to permit saturation of the inlet gas with a known partial pressure of steam and to remove the steam from the product gas by condensation (Figure 3). 2*N* H_2SO_4 was added to the condenser to inhibit solution

Table II. Rates and Approach to Equilibrium

Gasifier at 20.4 atm. and 1600°F.

Mean methane rate $- R_{CH_4} = 40 \times 10^{-4}$ moles/mole C in bed/min.

Mean carbon oxide rate $- R_{CO+CO_2} = 120 \times 10^{-4}$ moles/mole C in bed/min.

		Equilibrium Constant	
Reaction	*Expression*	*Actual Value*	*Percent Approach Assumed at Vessel Outlet*
$CaO + CO_2 = CaCO_3$	P_{CO_2}	0.66 atm.	66
Water-gas shift	$\frac{P_{CO_2} \cdot P_{H_2}}{P_{CO} \cdot P_{H_2O}}$	0.82	98
$C + 2\,H_2 = CH_4$	$P_{CH_4}/P_{H_2}^2$	0.0251	80
$CO_2 + C = 2\,CO$	P_{CO}^2/P_{CO_2}	26.3	16
Regeneration at 20.4 atm. and 1950°F.			
$CaO + CO_2 = CaCO_3$	P_{CO_2}	8.0	70
$3/4\,CaSO_4 + 1/4\,CaS = CaO + SO_2$	P_{SO_2}	0.16	29

of H_2S in the condensate. The upper part of the condenser was packed with anhydrous magnesium perchlorate.

The inlet gas used was a H_2–H_2S mixture, and hydrogen completely suppressed complicating side reactions such as those below.

$$1/4\,CaS + H_2O = 1/4\,CaSO_4 + H_2 \quad (7)$$

$$H_2S = H_2 + 1/2\,S_2 \quad (11)$$

The temperature corresponding to the particular equilibrium ratio of H_2O/H_2S was determined as previously by monitoring the change in H_2S content of the dry effluent gas in the thermal conductivity cell.

The steam content of the product gas was checked gravimetrically by the weight of the condensate collected.

Melt Formation. The binary system CaO–$Ca(OH)_2$ was studied to determine the equilibria in the following reactions:

$$Ca(OH)_2(s) = CaO(s) + H_2O \quad (12)$$

$$Ca(OH)_2(s) = CaO(l) + H_2O \quad (13)$$

$$Ca(OH)_2(l) = CaO(s) + H_2O \quad (14)$$

Equilibria in Reactions 12, 13, and 14 were determined in the apparatus shown in Figure 4, which was operated batchwise. The reactor was

charged with $Ca(OH)_2$ and sufficient water to generate about 100 atm. of steam pressure. The charge was then heated enough (usually about 1550°F.) to liquefy. It was then cooled at 5°F./min. until the melt completely solidified as judged by the immobility of the stirrer. It was then heated a few degrees above the solidification temperature until the stirrer could be turned but against considerable resistance. At this point both liquid and solid phases were present. The temperature was held constant for about 10 min., and the equilibrium pressure was read on the Bourdon gage.

The method for determining the equilibrium in Reaction 14 was similar. After melting the charge, heating was continued until a solid phase appeared, as evidenced by the resistance on the stirrer. The equilibrium pressure was read after 10 min. at constant temperature.

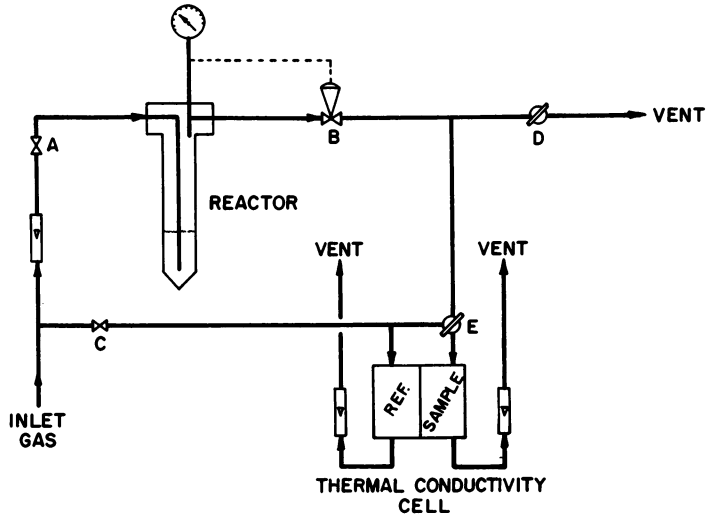

Figure 2. Apparatus used for equilibrium studies of Reaction 1

For equilibrium measurements in Reaction 12, the system was brought to nearly the eutectic conditions and was held for about 1/2 hour to ensure that both CaO and $Ca(OH)_2$ were present. The system pressure and charge temperature then were adjusted to the desired levels while staying on the $Ca(OH)_2$ side of equilibrium. The charge temperature was increased by about 5°F. and held constant. Since the solid-solid reaction rates were much slower than when a liquid phase was present, both CaO and $Ca(OH)_2$ assuredly were present at all times. The system pressure became constant in about 1 hour.

The phase diagram in the CaO–$Ca(OH)_2$ system was determined by thermodynamic calculations from equilibria determined in Reactions 13 and 14. The phase diagram for the $Ca(OH)_2$–$CaCO_3$ system was determined by differential thermal analysis using the equipment shown in Figure 4. Two thermocouples were used, one in the melt and one positioned at the wall of the inner vessel. A temperature differential corresponding to the appearance of the first solid phase developed on

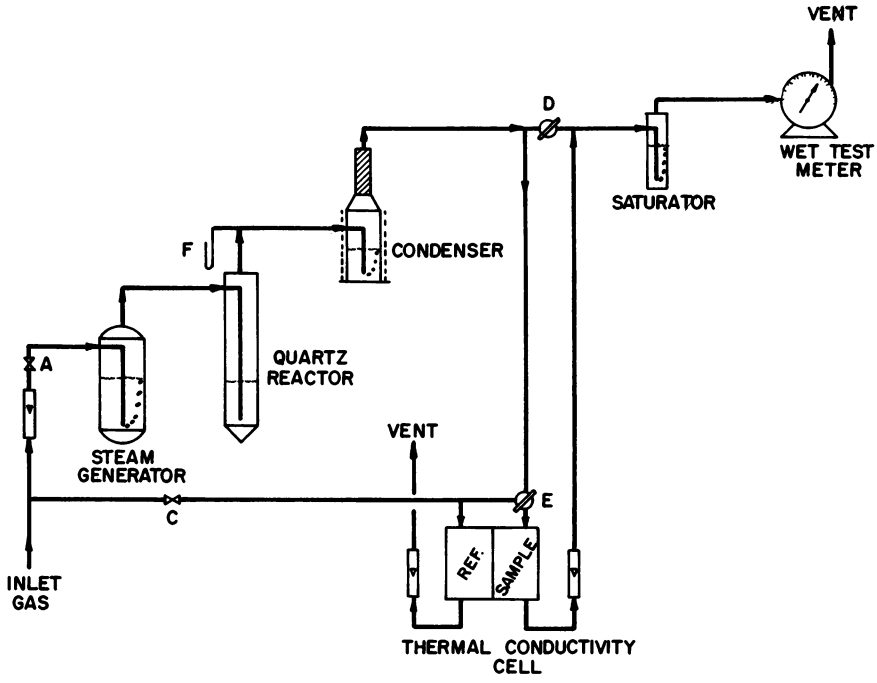

Figure 3. Apparatus used for equilibrium studies of Reaction 5

cooling, with the inner thermocouple reading the higher temperature. A second such temperature differential developed when the eutectic temperature was reached.

Acceptor Kinetics. The acceptor kinetic studies were carried out at atmospheric pressure using a modified Chevenard thermobalance, which was operated isothermally. Calcining was accomplished by changing the flowing gas from a CO_2-rich to a lean mixture by a toggle valve and three-way valve arrangement. Recarbonation was accomplished by reversing the procedure. Essentially complete displacement of one gas by the other occurred in 2 sec. Two complete cycles of calcining and recarbonation were executed in each run. In each case, known mixtures of N_2–CO_2 were used for the rich and lean gases, and appropriate corrections were made for the buoyant and drag forces of the flowing gas. These corrections were different for each gas mixture.

The standard sample weight was 200 mg. of raw acceptor. The flow rate of gas was such that CO_2 consumed or evolved from the acceptor had no appreciable influence on gas composition.

Most of the kinetic measurements were made with a Virginia dolomite, whose analysis is given in Table III. Some measurements were made with an Ohio dolomite from the Greenfield formation. The two stones showed similar kinetic behavior.

Kinetic data on calcination are given for the second cycle since the first cycle of calcination was unusually slow. The reaction rate was quite

reproducible for subsequent cycles. Recarbonation data, on the other hand, were closely reproducible on the first and second cycles.

Acceptor Retention Time. The basic retention time correlation was determined by a batch method. Single particles of known size, shape, and density were dropped through a batch fluidized bed in a vertical glass tube 1-in. i.d. × 30 in. long having a conical bottom. Humidified N_2 was used as fluidizing gas to eliminate electrostatic effects. Bed density was altered by varying the fluidizing velocity. Slugging was eliminated by shaking the tube with an electric vibrator.

Spherical balls of porous alumina, glass, stainless steel, and dolomite were used. The procedure consisted of dropping a particle from a holder by opening a trap door. The holder was immersed in the bed at a predetermined height above the cone. The time for the particle to reach the apex of the cone was timed with a stop watch. For each condition, the average of 10 drops was taken.

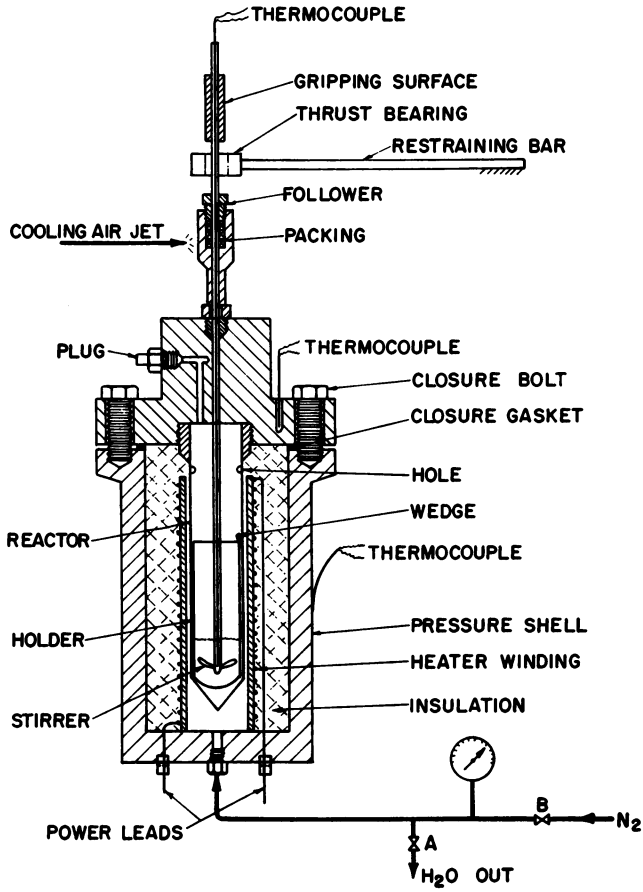

Figure 4. Non-flow apparatus used to study equilibria in Reactions 12, 13, and 14

Table III. Acceptor Analyses
Wt. %

Source	Virginia Dolomite	Greenfield Dolomite	Ohio Tymochtee Dolomite	South Dakota Dolomite	South Dakota Limestone
$MgCO_3$	44.50	44.61	42.42	43.06	0.22
$CaCO_3$	54.85	52.28	50.33	54.54	96.69
$FeCO_3$	0.65	0.20	7.25	2.40	3.09
$Al_2O_3 + SiO_2 + Fe_2O_3$		2.24			
Unaccounted For	0.00	0.67			

The correlation was checked under simulated conditions by operating the model shown in Figure 5. This is an exact replica of the hot continuous unit in which the process as a whole was operated, the only difference being that the pressure vessels representing the regenerator and gasifier vessels were replaced with Lucite models of the same internal dimensions—*i.e.*, 2-in. i.d. × 38 in. high and 4-in. i.d. × 70 in. high, respectively.

Retention time of acceptor particles was measured in the continuous unit by circulation through the char bed until steady state was reached. The bed was frozen by shutting off all flows and draining it above the acceptor-char interface. Retention times were obtained from bed analysis, feed rates, and bed height.

Acceptor Studies in Continuous Unit. The schematic flow diagram of the hot continuous unit is the same as for the model shown in Figure 5. The generator and gasifier had the same dimensions as the model. A pressure balanced construction was used in which the vessels, electric heaters, and insulation were all contained in a pressure shell. Carbon dioxide was used as a balance gas.

The unit was designed to operate at 300 p.s.i.g. and at temperatures up to 1950°F. in the regenerator and 1600°F. in the gasifier. Type 316 stainless steel was used in the gasification vessel and type 310 in the regenerator.

The unit was adequately instrumented to control and monitor the pressure drops across the various pneumatic transfer lines, standlegs, and fluidized beds, and it was equipped with safety devices to prevent mixing of the regenerator and gasification product and feed gas streams.

The char feed rate and acceptor recirculation rates were controlled by specially designed feeders using Teflon rotors equipped with pockets for receiving and discharging the solids.

Provisions were made (not shown) for charging the fresh acceptor and for withdrawing representative samples of acceptor for analysis during the run.

An acceptor life study in the continuous unit was carried out as follows. An inventory of fresh acceptor, usually 16 × 28 mesh, was established in the regenerator while an inventory of 35 × 150 mesh devolatilized lignite char was established in the gasifier. The operating pressure was normally set at 300 p.s.i.a. The regenerator was heated to the desired temperature (usually 1910°–1940°F.) while fluidized with

regenerator recycle gas. The char bed was simultaneously heated to 1500°F. This bed was fluidized by recycle gas to which steam was added in the desired proportion by a saturator (not shown). Nitrogen was used as purge gas in the pressure taps and as stripping gas in the standlegs.

When the desired temperatures in both vessels were approached, acceptor circulator was started. The acceptor entered the top of the gasifier and fell through the fluidized char bed. The gasifier vessel had a specially designed bottom section in which a higher gas velocity was

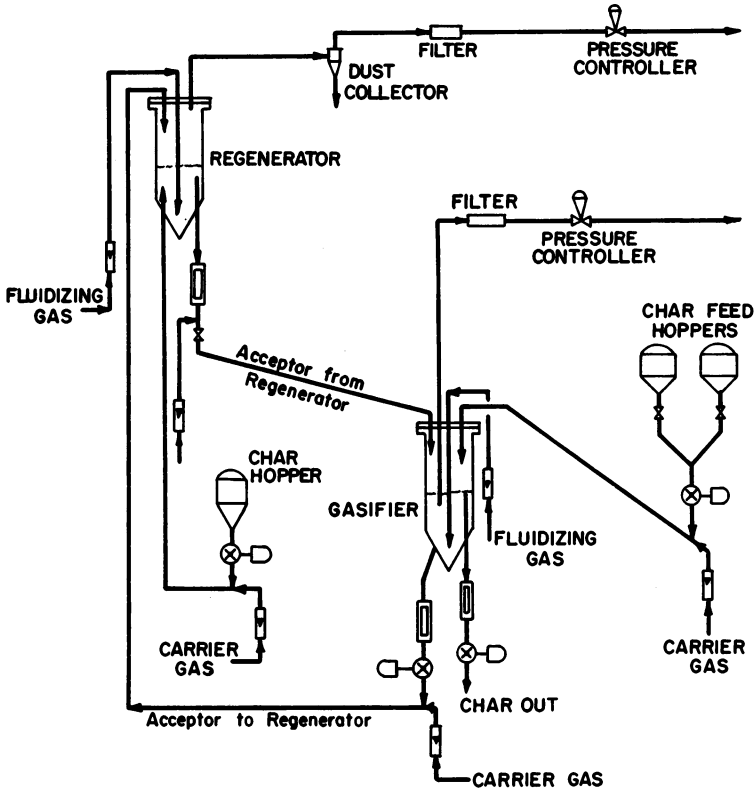

Figure 5. CO_2 acceptor gasification-continuous unit

maintained—*i.e.*, about 0.6 ft./sec.—and the acceptor formed a separate small fluidized bed. It was withdrawn from this bed into the pocket feeder for recirculation to the regenerator.

A sharp interface was established and maintained between the char and acceptor fluidized beds at the bottom of the gasifier. This was monitored by a specially designed electrical conductivity probe.

The regenerator off-gases were continuously monitored for CO_2 content by a thermal conductivity cell. The gasifier off-gas was analyzed frequently by gas chromatography.

Hydrogen and CO_2 were added to the gasifier inlet to maintain a gas composition simulating that which would exist at the top of a commercial gasifier.

The CO_2 partial pressure in the gasifier was controlled to give a driving force for recarbonation in the range 0.75–1.0 atm. By adding N_2 and CO_2 to the regenerator inlet gas, the CO_2 partial pressure was controlled to give a driving force for calcining of 2.5–3.0 atm.

Table IV. Equilibrium Values in the Reaction: $CaO + H_2S = CaS + H_2O$

Temp., °F.	$K = H_2O/H_2S$
1310	2030
1420	1320
1550	837
1660	587

The procedure was similar for runs in which char combustion was effected in the regenerator. In this case, 60% burnoff char was fed at a controlled rate into the regenerator. Air was fed simultaneously with recycle gas into the regenerator. The air rate was varied from slightly below to slightly above the stoichiometric quantity required to burn the char. The char ash was elutriated out of the regenerator with the off-gas and collected in a cyclone followed by a dust filter.

The activity of the acceptor was monitored as a function of the number of cycles through the system by withdrawing samples from the gasifier at appropriate times and determining the amount of $CaCO_3$ by weight loss on calcining in nitrogen at 1600°F. in a thermobalance. The activity is defined as the carbonation ratio—*i.e.*, the fraction of the total CaO which is converted to $CaCO_3$ on passage through the gasifier.

The acceptor on cycling always shrinks in size owing to both attrition and to loss in pore volume from deactivation.

Activity of Melts. Melts were prepared in the equipment of Figure 4 from both spent acceptors and various natural stones and reagent grade materials.

The charge, having known proportions of $CaCO_3$ and $Ca(OH)_2$, was mixed with liquid water and then heated to above the liquidus temperature. The system pressure was controlled by venting excess steam from valve A. After holding the system at the desired temperature and pressure for about 20 min., the charge was cooled at 5°F./min. to just below the eutectic temperature, then rapidly to room temperature.

The acceptor properties of the frozen melts were evaluated as follows. The melt was crushed and sized to 14 × 48 mesh and calcined to CaO in N_2 at 1600°F. in a fluidized bed reactor. The activity was then determined by recarbonation at 1 atm. in a fluidized bed at 1500°F. using pure CO_2. The activity—*i.e.*, fractional conversion of CaO to $CaCO_3$—was determined by the weight gain.

In all cases the melts showed high physical strength as demonstrated by the small amount of fines produced in the above cycle.

Results and Discussion

Equilibrium Studies and Sulfur Rejection. The experimentally determined values for Reaction 5 are given in Table IV. No reliable values for this equilibrium have been available in the literature previously.

The experimentally determined values for Reaction 6 are shown in Figure 6 and agree well with those previously determined by Zawadski (7).

The data in Reaction 1 are shown in Figure 7. Some of the literature data imply that the equilibrium CO_2 pressure depends on the origin of the calcium carbonate. Our measurements on stones, ranging in composition from pure limestone to impure dolomite having widely different geologic origins, have shown that the equilibrium CO_2 pressure is independent of all conditions except temperature. Figure 7 shows that our data agree well with those of Smyth and Adams (6) who used pure

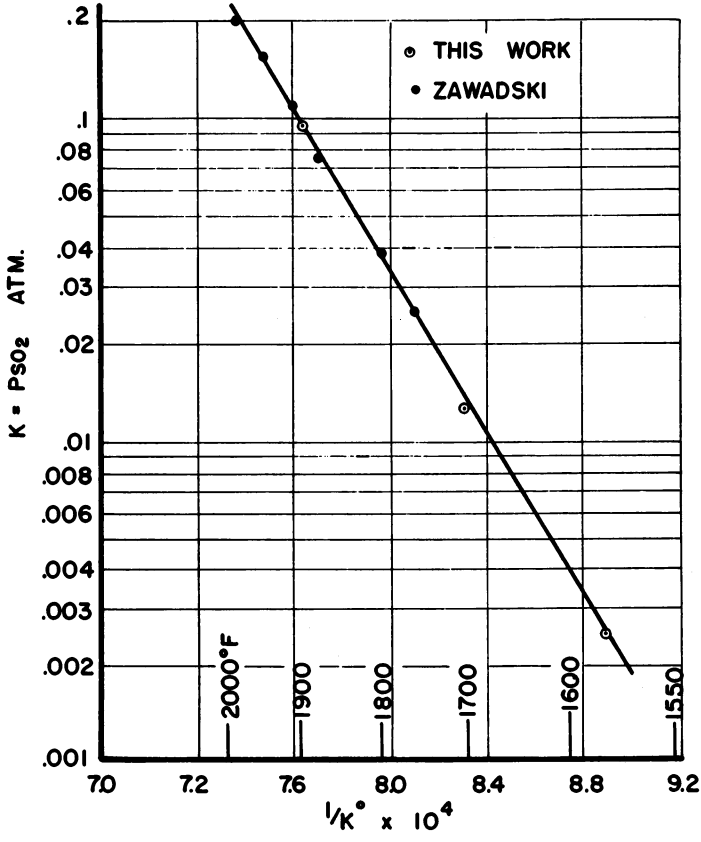

Figure 6. Equilibrium for 1/4 CaS + 3/4 $CaSO_4$ = CaO + SO_2

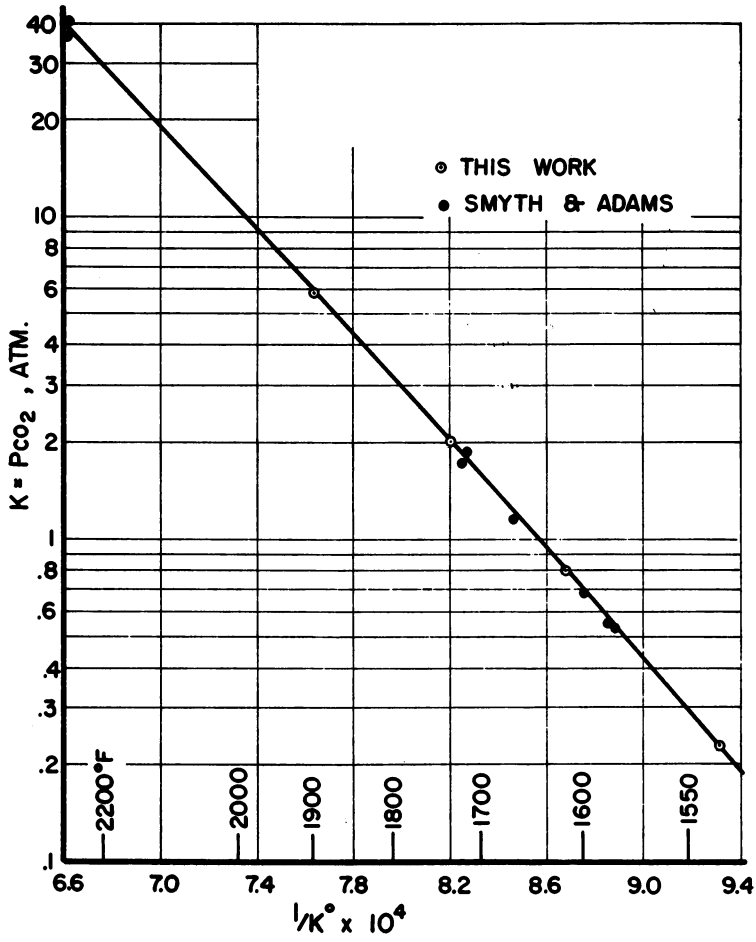

Figure 7. Equilibrium for $CaCO_3 = CaO + CO_2$

calcite as the source of $CaCO_3$. These data must now be accepted as providing the correct values.

Experimentally, all three reactions have been shown to be rapid, and equilibrium should be closely approached in actual process operation. The high values for the equilibrium constants in Reaction 5 mean that substantially all the sulfur released from the char in the gasifier will be absorbed by the acceptor as CaS. This sulfur must be rejected as SO_2 in the regenerator.

To achieve sulfur rejection in the regenerator, conditions should be maintained so that both CaS and $CaSO_4$ can coexist. Sulfur dioxide can now be evolved by Reaction 6. Where an excess of oxygen is used and all the sulfur is in the form of $CaSO_4$, sulfur rejection cannot occur owing to the low dissociation pressure of SO_2 over $CaSO_4$.

It might be expected as well that sulfur rejection would be difficult in a highly reducing atmosphere owing to reduction of the sulfate by the reverse Reactions 7 and 8.

$$1/4\ CaS + H_2O = 1/4\ CaSO_4 + H_2 \quad (7)$$

$$1/4\ CaS + CO_2 = 1/4\ CaSO_4 + CO \quad (8)$$

The design conditions of Tables I and II agree with the requirement of simultaneous maintenance of favorable equilibria in Reactions 5, 6, 7, and 8.

Experimental data on Reactions 5 and 6 were used to calculate the thermodynamic functions for CaS and $CaSO_4$. With these data and thermodynamic data from the literature for H_2, H_2O, CO, CO_2, COS, SO_2, and S_2, equilibrium constants for several reactions which may occur in the regenerator were calculated and are given in Table V.

Table V. Equilibrium Constants

	Reaction	*Kp * at °F.**		
		1800	*1900*	*1950*
(1)	$CaCO_3 = CaO + CO_2$	3.14	6.01	8.12
(5)	$CaS + H_2O = CaO + H_2S$	0.0025	0.0032	0.0036
(6)	$3/4\ CaSO_4 + 1/4\ CaS = CaO + SO_2$	0.042	0.113	0.182
(7)	$1/4\ CaS + H_2O = 1/4\ CaSO_4 + H_2$	0.0100	0.0105	0.0109
(8)	$1/4\ CaS + CO_2 = 1/4\ CaSO_4 + CO$	0.0166	0.0200	0.0218
(9)	$CaS + CO_2 = CaO + COS$	0.00022	0.00031	0.00037
(10)	$1/2\ CaSO_4 + 3/2\ CaS = 2\ CaO + S_2$	0.00031	0.00096	0.00163

* Kp * is either dimensionless or expressed in atmospheres.

Experimentally, complete sulfur rejection was always obtained from the acceptor in the continuous unit. Favorable conditions were maintained in the runs without air so that sulfur rejection could occur in the regenerator by Reactions 8 and 6 in succession.

Sulfur rejection was also observed even when excess air was used in the regenerator in apparent violation of the equilibrium in dissociation of the sulfate. Reducing conditions must have prevailed in some of the dense portions of the bed, thus permitting sulfur to be rejected by Reaction 6.

Melt Formation. The equilibrium steam pressures for Reactions 12, 13, and 14 are shown in Figure 8. The eutectic in the binary system $CaO–Ca(OH)_2$, is at 1454°F. and corresponds to the point where curves

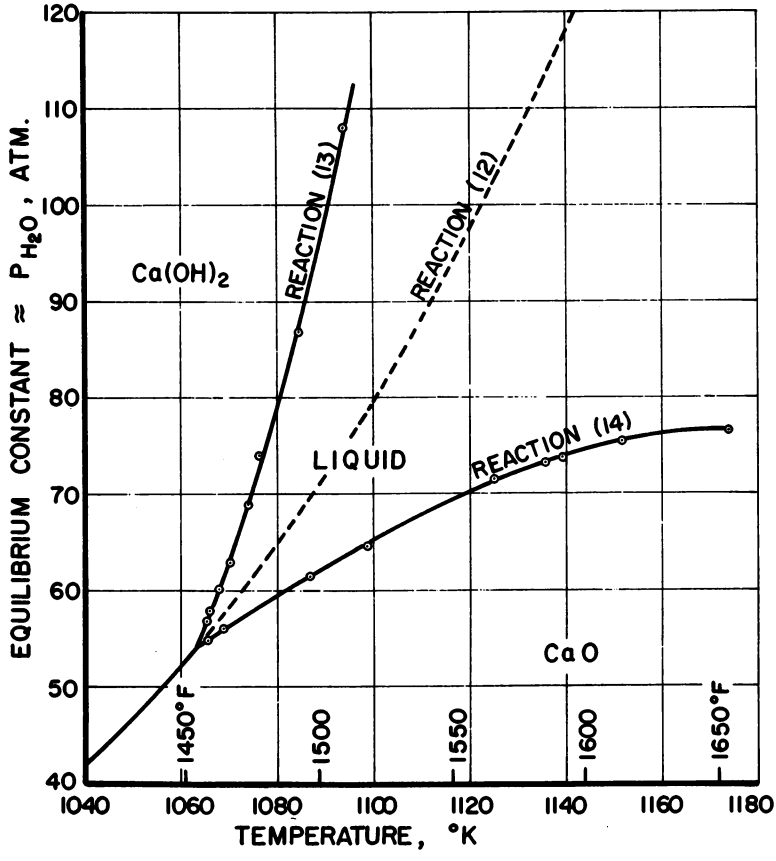

Figure 8. Equilibria in the system CaO–Ca(OH)$_2$

for the above reactions intersect. The steam pressure at this point is 54 atm.

Equilibrium data for Reaction 12 are represented by Equation 15.

$$-R \ln P = 25{,}019/T + 1.89 \ln T - 0.00194\, T + 0.332 \times 10^{-6}\, T^2 - 42.942 \qquad (15)$$

T is in °K. and P in atmospheres. Equation 15 is valid only above 1160°F. at which point a phase transition to the low temperature form occurs. Below this temperature the data of Drägert (*4*) were found to be accurate.

The phase equilibrium diagrams for the two binary systems CaO–Ca(OH)$_2$ and Ca(OH)$_2$–CaCO$_3$ are shown in Figures 9 and 10, respectively. The latter system particularly shows a remarkably low melting eutectic at 1180°F. At this temperature the steam pressure from Equation

15 is only 8.8 atm. Thus, melts in the binary $Ca(OH)_2$–$CaCO_3$ system may be produced at temperatures as low as 1180°F. and pressures as low as 130 p.s.i.g.

The low melting eutectics in the CaO–$Ca(OH)_2$–$CaCO_3$ system undoubtedly explain the formation of melts in the gasifier at temperatures of 1500°–1600°F. whenever the steam pressure exceeds the critical value of 13 atm. The equilibrium data above clearly show that $Ca(OH)_2$ cannot exist as a solid phase under these conditions at such low steam pressures. Liquids with melting points below 1600°F. must exist in the above ternary systems where the activity of $Ca(OH)_2(l)$ is sufficiently

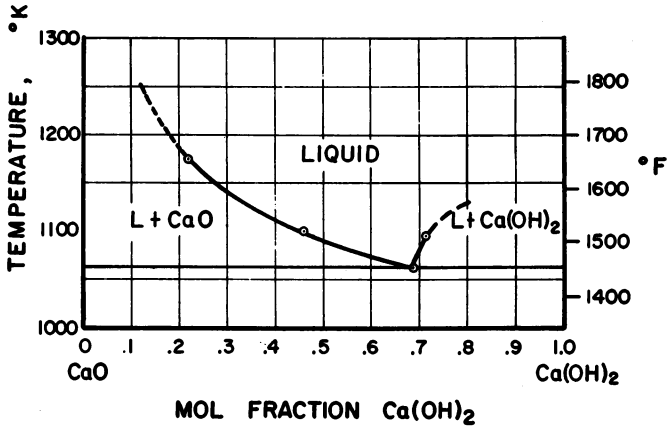

Figure 9. Phase diagram for the system CaO–$Ca(OH)_2$

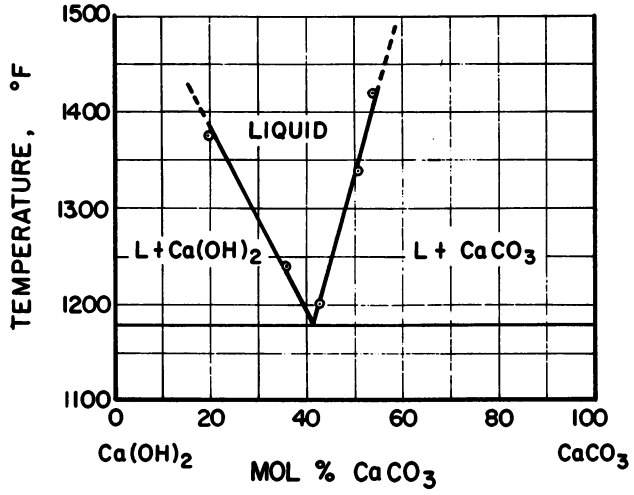

Figure 10. Phase diagram for the system $CaCO_3$–$Ca(OH)_2$

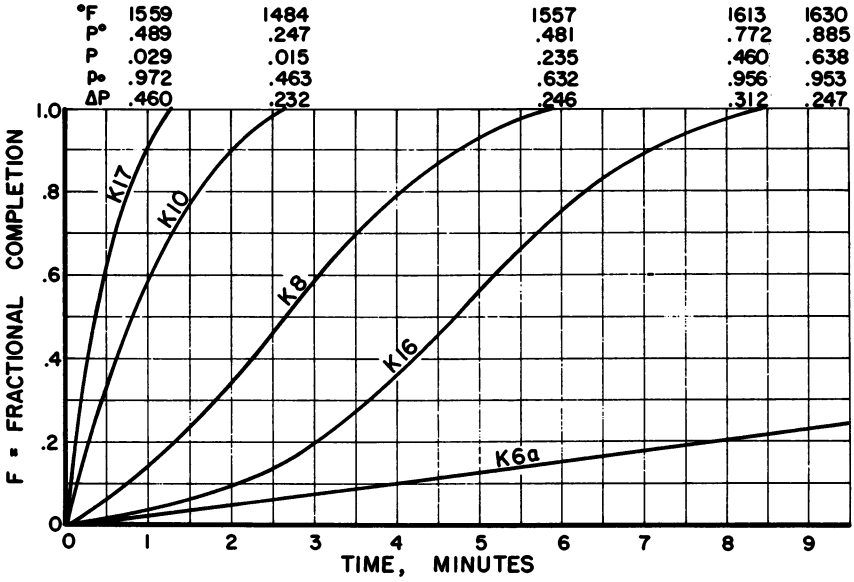

Figure 11. Calcining of raw acceptor particles (16 × 20 mesh)

reduced below that of $Ca(OH)_2(s)$ to reduce the dissociation pressure of steam to as low as 13 atm.

Acceptor Kinetics. The kinetics of calcining and recarbonation of fresh Virginia dolomite at several spot conditions are shown in Figures 11 and 12. The total pressure was 1 atm. in all cases.

The parameters associated with each particular run are given on the figures and are defined as follows:

P^0 = equilibrium pressure of CO_2 at temperature used

P = CO_2 partial pressure external to acceptor particles

p_0 = initial CO_2 partial pressure in acceptor particle pores prior to switching to calcining or recarbonation conditions

$\Delta P = \pm (P^0 - P)$ = driving force

The calcining reaction occurs rapidly and is always complete in less than 10 min. if the driving force exceeds 0.3 atm. The driving force provided in the feasibility study—*i.e.*, 2.4 atm.—appears adequately conservative.

A peculiar "memory" effect is apparent in the data of Figure 11 in that the calcining reaction is significantly retarded by a high CO_2 partial pressure in the acceptor pores before initiating the calcining regime. This points to a diffusion-controlled mechanism of some kind. The

kinetic behavior is not readily interpreted quantitatively by any simple mechanism.

Diffusion plays a role in the process since the reaction rate decreases with increasing particle size although the illustrating data are not given. The effect of particle diameter on rate is, however, not as great as would be predicted from a purely diffusion-controlled mechanism.

The data on recarbonation of Figure 12 shows that complete reaction is effected in less than 7 min. as long as the driving force is 0.15 atm. or greater. Thus, the feasibility study which provides a driving force of 0.35 atm. again appears adequately conservative.

Experimental data, not presented here, show that the kinetics are even more favorable for acceptors that have been deactivated by cycling through the process. The difference here is that only the active CaO is rapidly recarbonated. The inactive CaO either does not recarbonate at all or at best quite slowly.

Retention Time Studies. The batch data were correlated by the empirical equation given below:

$$V = a\left[\frac{(\rho_s - \rho_B)^m D^n}{\rho_B^P}\right] \tag{16}$$

Equation 16 was evaluated with a digital computer using a search technique to find the optimum values for m, n, P which minimized the sum

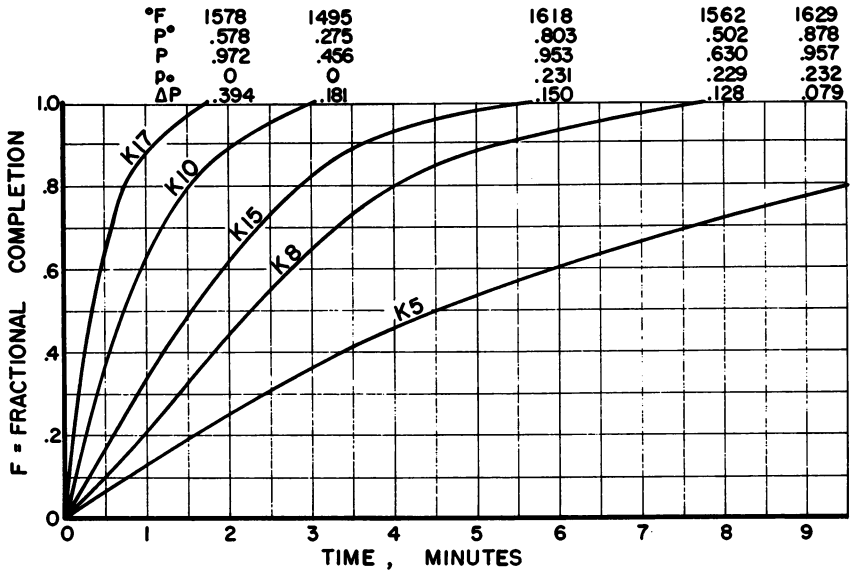

Figure 12. Recarbonation of raw acceptor particles (16 × 20 mesh)

of the squares of the deviations of the correlated values of V from the observed values. The optimum equation was

$$V = 0.503 \frac{(\rho_s - \rho_B)\, D}{\rho_B^{4/3}} \qquad (17)$$

where: V = velocity of falling particle, ft./sec.

Equation 17 is illustrated graphically in Figure 13.
The following ranges of variables were investigated:

ρ_s = 110–472 lb./cu. ft. = mercury density of falling particle

ρ_B = 15.2–63.5 lb./cu. ft. = bulk density of fluidized bed

D = 0.05–0.25 in. = diameter of falling particle

Standard deviation of the correlated values of the falling velocity was 10%, with a maximum of 20%.

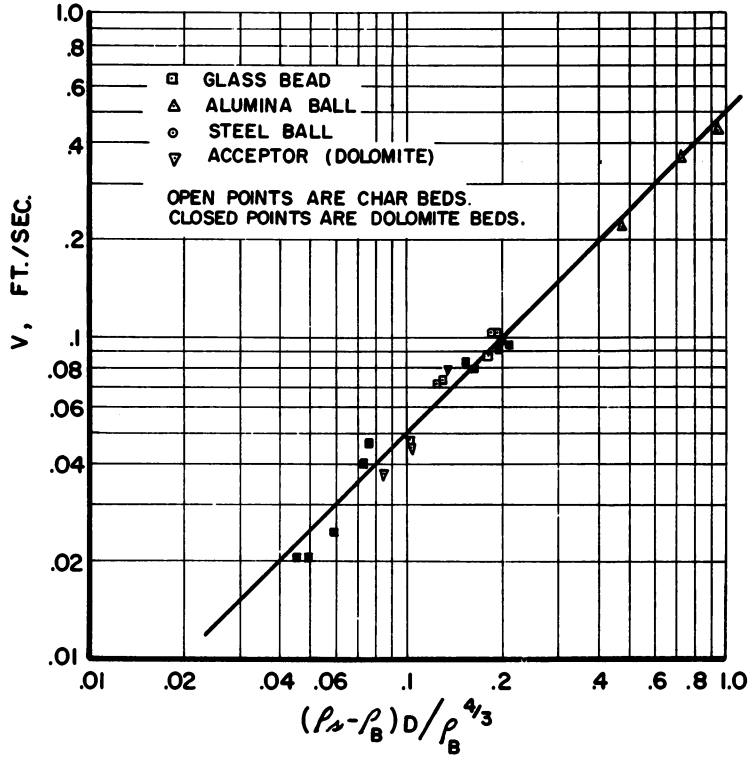

Figure 13. Retention time correlation

Equation 17 was also found to apply in the continuous unit where one deals with clouds of falling particles instead of single falling particles. In this case, dolomite acceptor particles varying in mean diameter from 0.0165 to 0.0215 in. were allowed to shower through fluidized char beds. The diameter used here is the arithmetic mean diameter calculated from terminal velocity of the particles in air. Eight measurements were made, and the standard deviation of the measured terminal velocity from that calculated by Equation 17 was 7.9%, and the maximum deviation was 15.2%.

Equation 17 is valid as long as the incipient fluidizing velocity of the falling particle exceeds the bed fluidizing velocity by about 50%. Obviously adequate control over acceptor residence time consistent with the requirements of acceptor kinetics can be effected in a commercial gasifier by appropriately sizing the acceptor particles.

Acceptor Life in the Continuous Unit. The acceptor must have sufficient physical strength to resist decrepitation as well as resistance to chemical deactivation on cycling through the process.

Various acceptor materials had been assessed on both these points previously in which the reaction cycle was simulated in batch equipment (2). Various stones were tested, and the following conclusions were tentatively reached. Limestones and dolomitic limestones were unsuitable, owing to a rapid deactivation. Many pure dolomites were not suitable because of poor physical strength. Of the dolomites tested that showed good physical strength, the stones from the Greenfield formation in Ohio showed the best resistance to chemical deactivation.

The batch data on the Greenfield dolomite were used to evaluate the activity and fresh stone make-up rate given in the feasibility study.

Continuous cycling through the process in the unit of Figure 5, however, has necessitated a change in these conclusions. It is now clear that physical strength of the raw stone is not overwhelmingly important in selecting acceptors. This is because on repeated cycling through the process, all stones eventually become extremely strong as a result of shrinkage owing to loss in pore volume. The attrition rate usually drops to well below 0.5%/cycle and often becomes immeasurably small. The rate of loss of activity of the acceptor in most cases determines the required make-up rate. Furthermore, the large differences in resistance to deactivation between limestones and dolomites and between different dolomites was not confirmed in the continuous unit.

Some results from activity testing in the continuous unit are given in Figure 14. Analyses of the stones used are given in Table III. The conditions of the runs were all similar to those given for the particular case of Tymochtee dolomite shown in Table VI.

The Tymochtee dolomite in the continuous unit showed essentially indistinguishable results from that of the Greenfield dolomite, and therefore data for the latter are not given in Figure 14. The Greenfield dolomite had activities of 0.76 and 0.52 after 20 cycles in batch and continuous units, respectively. The more rapid deactivation rate in the continuous unit is clear, although the reason is not presently understood.

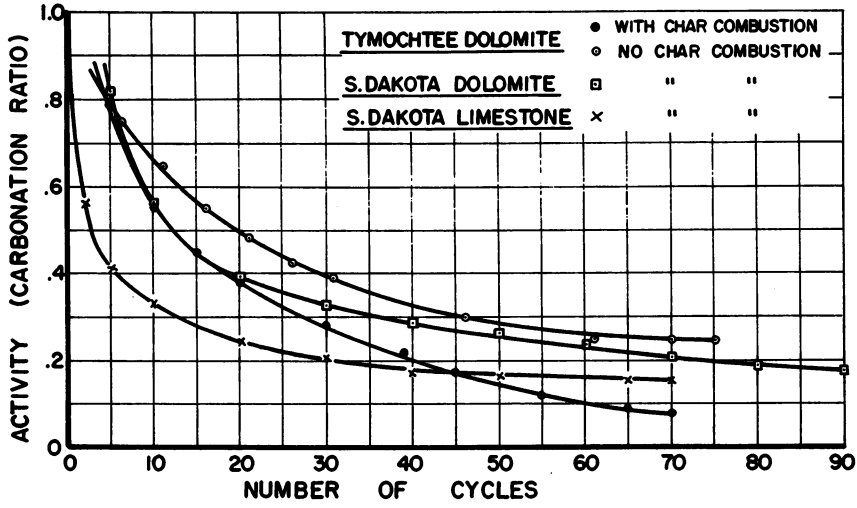

Figure 14. Acceptor activity at process conditions

The South Dakota dolomite showed a lower but not vastly different activity from the Ohio dolomites. Finally, the South Dakota limestone showed an activity substantially below that of the dolomites. The CO_2 capacity of the limestone after 30 cycles is, however, equivalent to that of the best dolomite on a unit weight basis since the absence of the MgO diluent compensates for the lower activity. Therefore, limestone is equally useful an acceptor as dolomite in the process.

The activity was also tested where char combustion was conducted in the regenerator. The average conditions for this run are given in Table VI. In this run 32 lbs. of char were burned, thereby exposing the acceptor to 0.73 lb. ash/lb. MgO · CaO inventory. The combustion was trouble free, giving essentially flat temperature profiles and complete burnout of the carbon. No ash fusion difficulty was experienced.

The air/char ratio was maintained slightly below stoichiometric for complete combustion during most of the run. Under these conditions the exit gas contained no oxygen and up to 1.5% CO. The sixth through ninth cycles and the 35th cycle were conducted with a slight excess of air, and the exit gas contained 0.20% O_2.

The results show that combustion of char has a progressive adverse effect on acceptor activity. Work is now in progress to understand the reasons for this and eventually ameliorate the effect.

Table VI. Typical Conditions for Acceptor Activity Tests

Acceptor 16 × 28 mesh Tymochtee dolomite
Char 35 × 150 mesh devolatilized lignite char
System pressure, 20 atm.
Cycle number, 30

Gasifier conditions		
Temp., °F.	1500	
Char feed rate, lb./hr.	1.60	
Char bed inventory, lb.	7.75	
Char bed density, lb./cu. ft.	23.4	
Acceptor feed rate ($MgO \cdot CaO$), lb./hr.	6.00	
Fluidizing velocity, ft./sec.	0.27	
Partial pressures in outlet gas, atm.		
H_2O	4.06	
H_2	7.51	
CH_4	0.98	
CO	2.05	
CO_2	1.28	
N_2	4.12	
	With Char Combustion	*Without Char Combustion*
Regenerator conditions		
Temp., °F.	1940	1940
Atoms C burned/mole CaO	0.80	0
Inlet gas, std. cu. ft./hr.		
Air	55	0
Recycle	315	311
Added N_2	19	31
Outlet CO_2 partial pressure, atm.	4.0	4.0
Fluidizing velocity, ft./sec.	1.15	1.01
Acceptor inventory ($MgO \cdot CaO$), lb.	2.47	2.21
Acceptor activity	0.28	0.39

Table VII. Equilibrium Activities for Tymochtee Dolomite

	$R_{equil.}$	
% Makeup[a]	*With Char Combustion*	*No Char Combustion*
1	0.19	0.30
2	0.32	0.43
3	0.40	0.51

[a] $\%\ \text{Makeup} = \dfrac{100\ (\text{moles/hr. fresh CaO fed to process})}{\text{moles/hr. CaO circulated through process}}$

The equilibrium activity in a plant where fresh acceptor is continuously added can be expressed by Equation 18.

$$R_{eq} = \int_0^\infty \alpha R e^{-\alpha n} dn \qquad (18)$$

R_{eq} = equilibrium activity of acceptor inventory

R = acceptor activity after n cycles through process

$$\alpha = \frac{\text{feed rate of fresh acceptor in moles/hr. CaO}}{\text{moles/hr. CaO circulated through system}}$$

Equation 18 corresponds to the situation where perfect mixing occurs between the circulating and makeup acceptor streams. R is evaluated from the curves of Figure 14. It is assumed that $R \rightarrow 0$ as $n \rightarrow \infty$.

Table VIII. Activity of Melts

Source	Melt Composition, Mole %			Activity	
	$CaCO_3$	$Ca(OH)_2$	CaO	Prior to Melting	After Melting
Fresh South Dakota Limestone	100	—	—	0.66	—
Reagent Chemicals	54	46	—		0.62
	50	50	—		0.66
	43	57	—		0.62
	36	64	—		0.61
	20	80	—		0.54
Deactivated South Dakota Limestone	17	72	11	0.16	0.58
	18	73	9	0.16	0.54

The calculated equilibrium activities for the Tymochtee dolomite at various makeup rates of fresh acceptor are given in Table VII. At the make-up rate assumed in the feasibility study of 2%, the equilibrium activities are substantially lower than the value of 0.70 given—*i.e.*, 0.32 and 0.43, respectively, for the cases where char combustion was and was not effected in the regenerator.

Deactivation, as noted above, is always accompanied by a significant decrease in pore volume and surface area and an increase in average crystallite size of the MgO and CaO components. These effects are still being investigated, and no quantitative data will be presented at this time.

Melts as Acceptor. Melts are readily produced in the $Ca(OH)_2$–$CaCO_3$ at relatively mild temperatures and pressures. The properties of the melts are determined primarily by their chemical composition and not by the physical form of the starting materials. Properly produced melts, particularly those on the $CaCO_3$ side of the binary eutectic, are always extremely rugged physically.

The melting technique is of potential interest from two points of view. It may be used to prepare strong acceptors from local raw materials which are not physically acceptable otherwise. It may also be used to reactivate spent acceptors from the process.

In the latter instance, one key to success is conversion of the inactive CaO to $Ca(OH)_2$ and its subsequent incorporation into the melt. Once this is accomplished, melts produced from spent acceptors are indistinguishable in activity from those prepared from fresh stone.

Activities of melts prepared from reagent grade chemicals and from deactivated limestone after cycling through the continuous unit are shown in Table VIII as a function of their composition. The activity of the fresh limestone determined in the same way is also given for reference.

It is noted that the activity of the reactivated melts is indistinguishable from melts prepared from fresh materials. The $CaCO_3$-rich melts—*i.e.*, greater than 40 mole % $CaCO_3$ are also close in activity to that of the raw limestone. Life testing of melts in the continuous unit is now in progress.

Literature Cited

(1) Clancey, J. T. and Phinney, J. A., *Am. Gas Assoc. Prod. Conf. Buffalo, N. Y., 1965.*
(2) Curran, G. P., Rice, C. H., Gorin, Everett, *ACS, Div. Petrol. Chem., Preprints* 8 (1), 128 (1964).
(3) Curran, G. P., Clancey, J. T., Scarpiello, D. A., Fink, C. E., Gorin, Everett, *Chem. Eng. Progress* **62**, 80 (1966).
(4) Drägert, W., "International Critical Tables," Vol. VII, p. 294 (1930).
(5) "Pipeline Gas From Lignite Gasification—A Feasibility Study," Consolidation Coal Co. Rept. to U. S. Department of Interior, Office of Coal Research (Jan. 13, 1965).
(6) Smyth, F. H., Adams, L. H., *J. Am. Chem. Soc.* **45**, 1167 (1923).
(7) Zawadski, J., *Z. Anorg. Chem.* **205**, 180 (1932).

RECEIVED March 24, 1967. A portion of this work was sponsored jointly by Con-Gas Service Corp., the Texas Eastern Transmission Corp., and the Office of Coal Research.

11

Cleanup Methanation for Hydrogasification Process

D. G. TAJBL, H. L. FELDKIRCHNER, and A. L. LEE

Institute of Gas Technology, Chicago, Ill.

Cleanup methanation of coal hydrogasification product gases to high B.t.u. pipeline gas is being studied to find the best catalyst and mode of operation for a commercial plant operating at 1000 p.s.i.g. Catalysts were evaluated in a stirred flow reactor shown to be superior to the packed-tube reactor for kinetics studies of gas-solid systems. The reactor acts as a "perfect mixer." The catalytic activities of commercial nickel, iron, and ruthenium catalysts for methanating CO in the hydrogasifier product were measured. A nickel-on-kieselguhr catalyst was found most active. Longer chained hydrocarbon production using iron and ruthenium catalysts was lower than expected.

Catalytic methanation is the final gas cleanup step in producing a high B.t.u. pipeline gas from coal being developed at the Institute of Gas Technology. The coal hydrogasification process produces 600–800 B.t.u./std. cu. ft. gas consisting primarily of methane, hydrogen, carbon monoxide, and carbon dioxide. Smaller amounts of ethane, hydrogen sulfide, nitrogen, ammonia, and other constituents are also present. Carbon dioxide, sulfur compounds, and nitrogen compounds can be removed rather simply by conventional gas purification methods. However, the final gas should ideally contain less than 0.1 mole % of carbon monoxide and have a heating value of at least 900 B.t.u./std. cu. ft. Because the methanator feed gas contains rather large amounts of hydrogen, a low methane, low heating value gas would be produced if the carbon monoxide were removed by shifting and scrubbing. It seems preferable to scrub out first most of the carbon dioxide and then allow carbon monoxide and hydrogen to react to form methane, thus producing a product with a high heating value.

Methanation has not been well-studied at the pressures (approximately 1000 p.s.i.g.) and feed gas compositions (2–10 mole % CO,

2 mole % CO_2, 14–35 mole % H_2, and 53–87 mole % CH_4) expected to be used in the cleanup step of the IGT process. Based on thermodynamic equilibrium calculations, carbon deposition may be a problem with these feed gases. Moreover, the extent to which CO_2 will be methanated is not definitely known. IGT is therefore obtaining information needed to design large scale catalytic methanation reactors. The effects of temperature, pressure, and catalyst composition on the process operation are the main areas of laboratory study.

The first step in the over-all methanation study is to find the best commercial catalyst for this cleanup step. This catalyst must be able to catalyze the methanation reaction actively without catalyzing carbon deposition reactions. It must also be highly active and long lived at high temperatures. These properties are directly related to chemical events occurring on its surface.

Instead of the commonly used packed-tube reactor, IGT is using a continuous-stirred tank catalytic reactor (CSTCR) (3) which permits one to study these chemical events without any complicating control of the reaction rate by gas-solid mass or heat transfer. This reactor has several other advantages:

(1) The CSTCR operates at conditions where "perfect mixing" prevails and bulk gas temperature and concentration gradients are eliminated.

(2) With sufficient gas velocity at the catalyst surface, temperature and concentration gradients between the bulk gas and the catalyst surface can be minimized.

(3) All but the fastest and most exothermic reactions can be studied at nearly isothermal conditions and nearly complete conversion.

(4) Because the entire catalyst surface "sees" gas of the same composition and temperature, the reaction rate can be calculated by Equation 1 (Terms defined in Nomenclature section at end).

$$R = \frac{F_i C_i - F_o C_o}{w} \tag{1}$$

This procedure is generally simpler and more accurate than rate calculations from data obtained with packed-tube reactors.

(5) Finally, studies can be made using catalyst pellets of commercial size and shape.

This type of reactor has been used in the past to study solid-catalyzed gaseous reactions. Tajbl, Simons, and Carberry (3) used a CSTCR to study the highly exothermic oxidation of carbon monoxide on a commercial palladium catalyst. Ford and Perlmutter (2) used a CSTCR with a catalytic wall to study *sec*-butyl alcohol dehydrogenation. In both studies, the authors found that data were obtained more easily and accurately with a CSTCR.

This paper deals with (1) defining the operating range for "perfect mixing" in the IGT reactor; (2) determining whether gas-solid heat or mass transfer effects were present at the conditions of operation; (3) preliminary screening of commercial methanation catalysts.

Apparatus

Figure 1 is a flow diagram of the catalyst testing unit. The gas inlet system and the components operating at elevated temperatures and pressures are stainless steel. Feed gas, stored in high pressure cylinders, is metered by an orifice. Orifice pressure, pressure drop, and temperature are recorded. The feed gas is preheated before it enters the bottom of the reactor. Both the reactor and the preheater are electrically heated.

Exit gas leaves the top of the reactor and passes through a heated line (to avoid condensation of liquids) to a cooler-condenser. Liquid products are collected in a knockout pot and are drained through a solenoid valve actuated by a sonic liquid-level controller. A dome-loaded, back-pressure regulator controls the reactor pressure and reduces the pressure of the exit gas. The exit gas rate is measured by a wet-test meter. Carbon monoxide and carbon dioxide concentrations in the feed and exit gases are measured by two continuous infrared analyzers and are recorded. Aliquot samples of feed and exit gases are taken during each test period for analysis of all components by mass spectrometer (Consolidated Engineering Model 21-103).

Figure 2 shows the reactor, built by Autoclave Engineers, Inc. It was constructed of Type-316 stainless steel so that it could be used later to test the effects of elevated temperatures on catalyst stability. A magnetic drive rotates the stirrer shaft. The reactor has an inside depth of 12 in. and an inside diameter of 3 in. For CSTCR operation, two inserts are installed which reduce the inside depth to 2-13/16 in.

The catalyst can be mounted either in an annular basket or in a paddle-basket arrangement as shown in Figure 3. The paddle basket replaces the radial impeller, which is used only with the annular basket. For either arrangement the propellers remain in place. The cylindrical wall and the top and bottom of the reactor each have four 1/8-in. wide baffles. The wall baffles extend along the total height of the stirred chamber; the top and bottom baffles extend radially to the cylindrical wall.

Catalyst temperatures are measured easily in the annular basket. Since the catalyst is stationary, a thermocouple is simply inserted in a hole drilled into the center of a catalyst pellet.

For either basket arrangement, the gas temperature is measured with a 0.025-in. o.d., magnesium oxide-insulated thermocouple of Chromel-Alumel with a swaged stainless steel sheath.

Discussion

Mixing Theory. Several tracer techniques can be used to check for perfect mixing. These consist of measuring the response in the reactor effluent to either (1) the injection of a small amount of tracer gas into

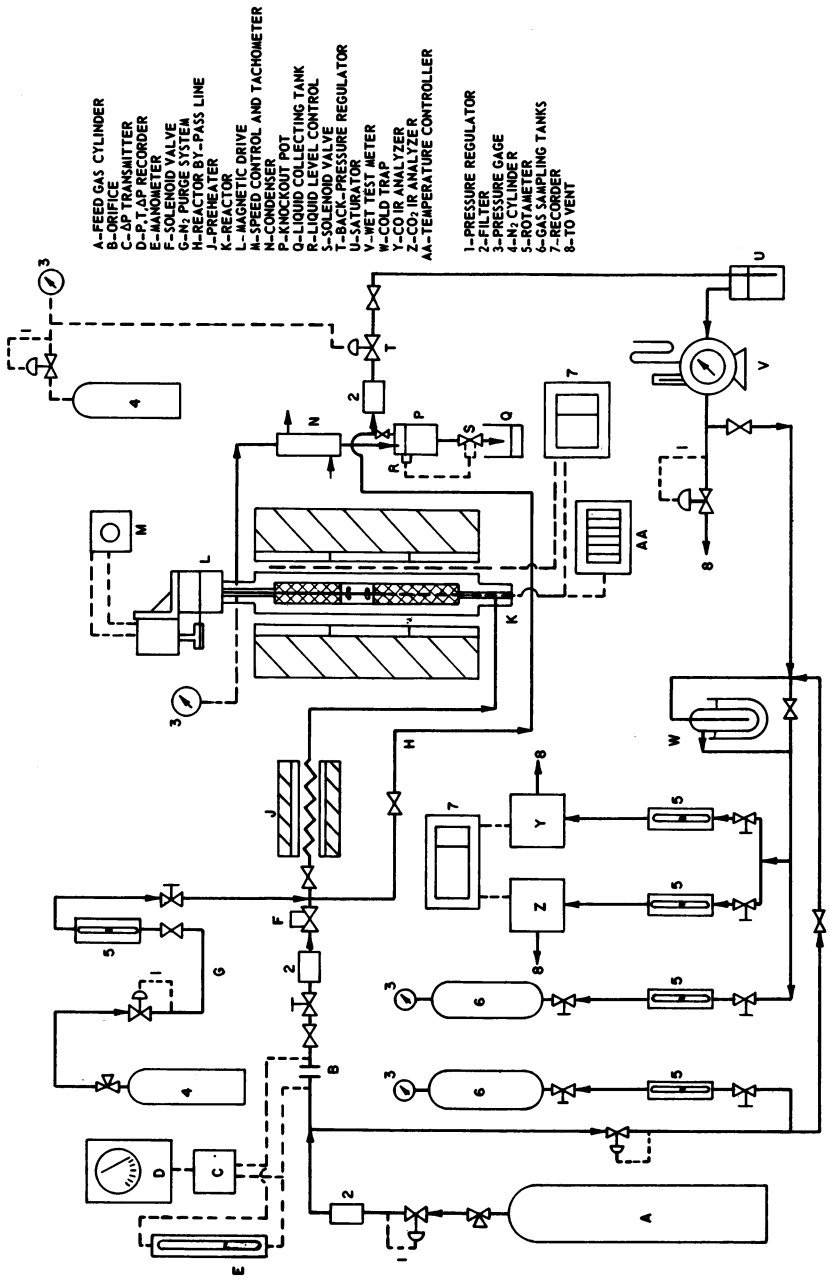

Figure 1. Catalyst testing unit

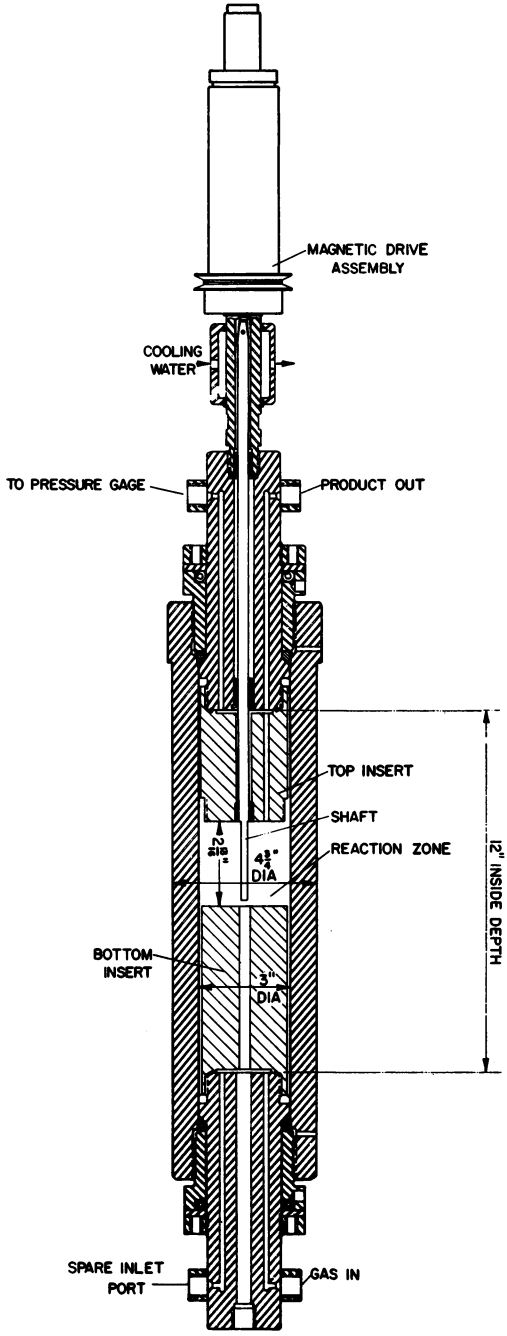

Figure 2. Continuous-stirred tank catalytic reactor

the reactor over a short time (pulse test), or (2) the instantaneous switching from a steady flow of inert gas to a steady flow of tracer gas (step test), or vice-versa (purge test).

After the tracer concentration reaches a maximum, the response for any of these tests is an exponential decay of tracer concentration with time. For the pulse test the response is:

$$\frac{C}{C_M} = e^{-tF/V} \tag{2}$$

where C_M is the gas concentration in the reactor at the instant the pulse enters, and, in actual tests, the maximum gas concentration measured in the effluent.

For the step test the response is:

$$1 - \frac{C}{C_S} = e^{-tF/V} \tag{3}$$

where C_S is the steady-state tracer concentration. For the purge test the response is the same as in Equation 2 except that $C_S = C_M$. A plot of C/C_M *vs.* tF/V yielding a straight line of slope -1 indicates "perfect mixing."

Mixing Tests. All these techniques were used in our mixing studies. Because of the difficulty of injecting a perfect pulse of the tracer, the

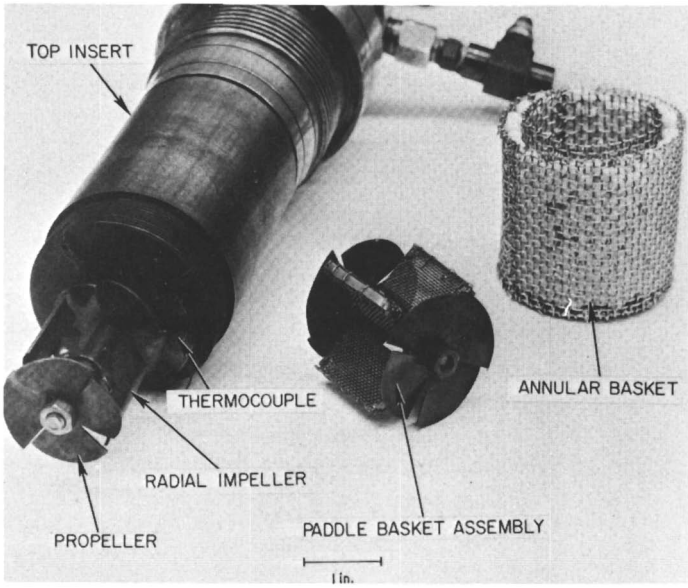

Figure 3. Catalyst baskets

step or purge tests were easier to carry out. Despite this, the pulse tests have an advantage because of the small amount of tracer used. In step or purge tests an allowance must be made for transfer of the tracer (or purge) contained in the reactor dead volume before switching—*i.e.*, in the lines to the pressure gages, etc. This, in effect, increases the volume to be purged and affects the slope of the C/C_M *vs.* tF/V plot.

Of the three tracer tests, then, the pulse test is most accurate in systems with extensive dead volumes.

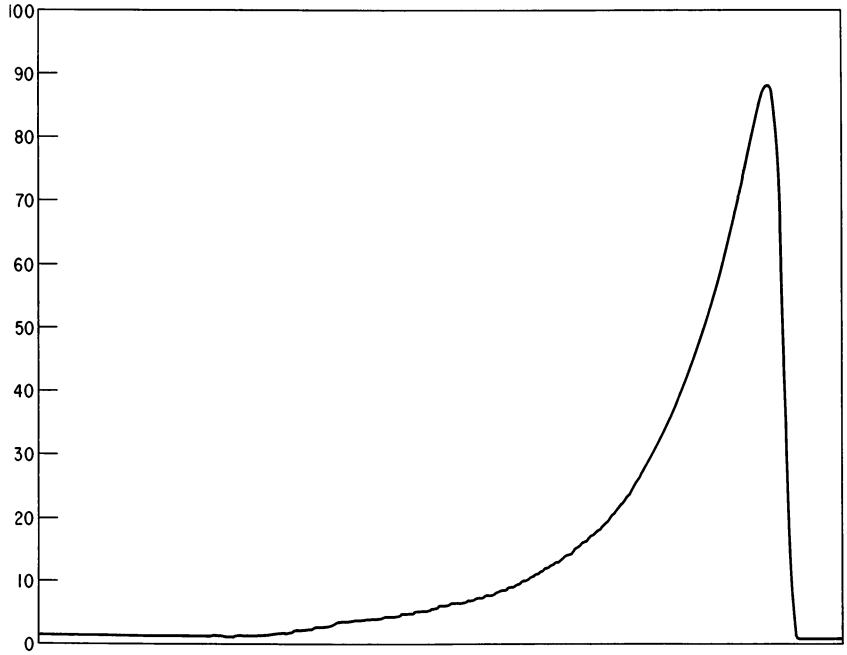

Figure 4. Typical pulse test response

CO or CO_2 was used as the tracer gas with nitrogen as the inert gas in these tests. A switching valve served to inject the pulse of tracer or to change from tracer to inert. Flow rates ranged from 1 to 40 std. cu. ft./hr. Measured at flowing conditions, this flow range is about that used in the Tajbl-Simons-Carberry reactor. Shaft speed was varied from 0 to 2500 r.p.m. Tracer response was measured by the in-line infrared analyzers. A typical response to a pulse test is shown in Figure 4.

Typical test results are plotted in Figure 5. The data at 200 r.p.m. indicate imperfect mixing. As the shaft velocity is increased, perfect mixing is realized for high and low flows and at high and low pressures. Above 1500 r.p.m. perfect mixing is ensured for the range of flows studied. Changing temperature or tracer gas had no effect. The purge and step

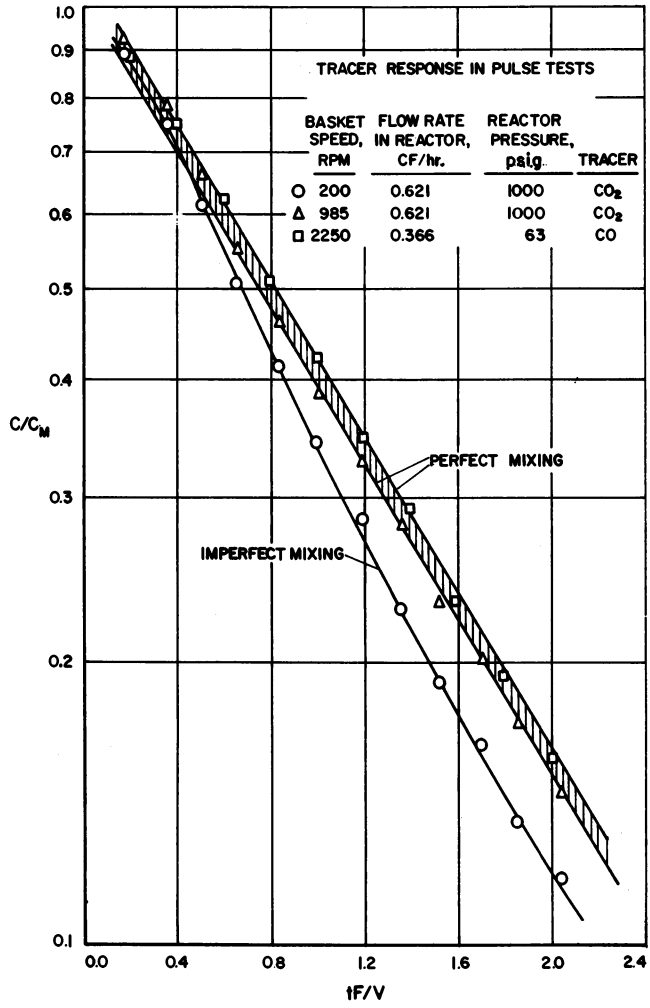

Figure 5. Typical pulse test results

tests also gave linear semi-log plots of C/C_S *vs.* tF/V, but the slope was not −1 because of the reactor dead volume previously noted.

Commercial Catalyst Comparison. A variety of products can be produced catalytically from hydrogen and carbon oxides. The type of products depends upon the catalyst composition, temperature, pressure, and hydrogen/carbon oxides ratio. Nickel catalysts produce mainly methane at almost all useful operating conditions. Iron, ruthenium, and cobalt catalyze the Fischer-Tropsch synthesis, producing higher hydrocarbons. Iron and ruthenium catalysts were nevertheless considered since higher hydrocarbon formation would give the final gas a higher heating value.

Cobalt catalysts were not considered because they operate best at lower pressures (1–10 atm.) (*1*).

Catalysts were compared by measuring their rate of carbon monoxide conversion. Test variables were temperature, feed gas composition, and the feed rate/catalyst weight ratio. All tests were made at 1000 p.s.i.g. Three feed gases, covering a range of compositions typical of projected methanation feeds, were selected (Table I).

Table I. Compositions of Feed Gases

	High CO	*Intermediate CO*	*Low CO*
Composition, mole %			
Carbon monoxide	10.0	7.0	2.4
Carbon dioxide	2.1	2.1	2.0
Hydrogen	34.5	26.1	13.5
Methane	53.4	64.8	82.1
Total	100.0	100.0	100.0

Table II. Results with Nickel Catalysts

Catalyst	*Temp., °F.*	*F_t/w, std. cu. ft./ hr.-gram catalyst*	*Feed Gas*	*CO Conv., %*	*Dry Product Gas Content, mole %*	
					CH_4	*C_2^+*
A	560	1.48	low CO	64.8	92.0	0.7
A	560	1.24	low CO	69.2	92.8	0.7
A	560	0.993	low CO	77.9	93.7	0.7
A	560	0.840	low CO	82.7	94.0	0.7
A	560	0.631	low CO	87.3	95.5	0.5
A	560	0.504	low CO	91.7	95.7	0.5
A	615	0.228	high CO	95.9	93.1	0.1
A	700	0.228	high CO	97.8	93.7	0.0
A	800	0.228	high CO	97.3	92.9	0.0
A	800	0.236	int. CO	96.6	94.1	0.0
A	900	0.236	int. CO	96.1	92.3	0.1
B	700	1.11	low CO	59.7	87.9	0.6
B	700	0.767	low CO	71.7	89.8	0.5
B	720	0.479	int. CO	67.2	81.9	0.6
B	720	0.425	int. CO	70.4	83.1	0.6
B	720	0.341	int. CO	74.8	84.6	0.6
B	720	0.273	int. CO	82.0	87.2	0.4
B	720	0.239	int. CO	83.2	87.4	0.4
B	720	0.396	high CO	40.8	67.8	0.6
B	770	0.214	high CO	70.2	78.0	0.3
B	820	0.214	high CO	74.8	82.5	0.3
B	900	0.214	high CO	84.5	83.3	0.2
C	650	0.631	high CO	27.9	57.3	0.7
C	704	0.418	high CO	49.0	63.1	0.7

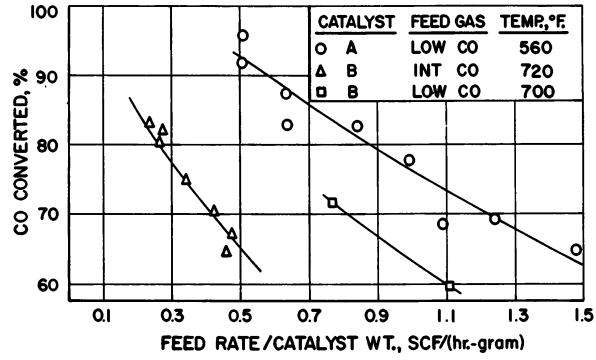

Figure 6. Comparison of activity of nickel catalysts A and B

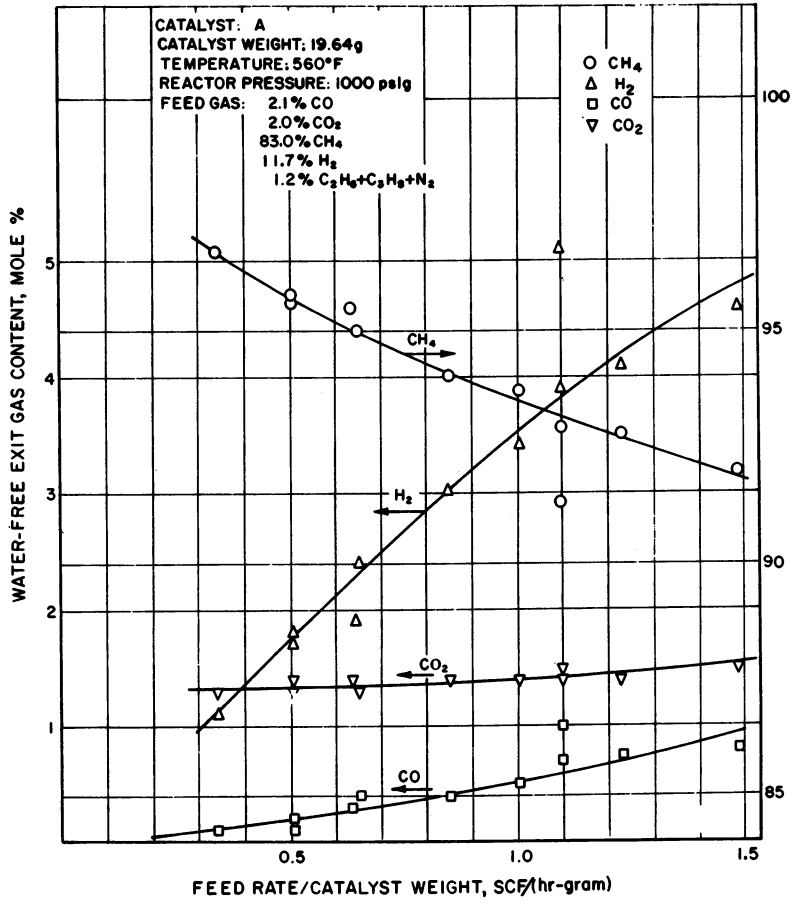

Figure 7. Methanation product gas compositions as a function of stirred reactor space velocities

Nickel Catalysts. Nickel catalysts studied were:

A: 58% nickel on kieselguhr, 1/4-in. pellets
B: 32% nickel on alumina, 1/4-in. pellets
C: 47% nickel oxide on alumina, 1/4-in. pellets

Catalyst A is more active than B and C. For comparable feed rate/catalyst weight ratios and the same low CO content feed gas, A converts more carbon monoxide at 560°F. than B at 700°F. (as shown in Table II and Figure 6). This is also true for other feed gases. Figure 7 shows typical data for A in isothermal runs with low CO content feed gas.

Iron Catalyst. An ammonia-synthesis catalyst was studied. Much lower feed rate/catalyst weight ratios must be used with this catalyst to obtain conversions approaching those of catalyst A (Table III).

Table III. Results with Iron Catalyst

Temp., °F.	F_t/w, std. cu. ft./ hr.-gram catalyst	Feed Gas	CO Conv., %	Dry Product Gas Content, mole %	
				CH_4	C_2^+
509	0.036	int. CO	13.0	68.2	0.8
604	0.027	int. CO	55.7	73.4	1.3
700	0.026	int. CO	62.2	74.7	1.3
800	0.026	int. CO	66.3	76.2	1.4

Longer chained hydrocarbon formation is much lower than expected. This is presumably because of the high hydrogen:carbon monoxide ratio of the feed gas and because of the high pressure. Bond (*1*) cites both these conditions as favoring hydrogenolysis.

Ruthenium Catalyst. The ruthenium catalyst studied was 0.5% ruthenium on 1/8-in. alumina pellets. Data in Table IV show that at low temperatures and low feed rate/catalyst weight ratios, this is an effective methanation catalyst. Higher hydrocarbon formation is, again, lower than expected, possibly owing to hydrogenolysis. Trace yields of oils containing paraffins, olefins, and aromatics were obtained.

Interphase Transport. Transport phenomena between the catalyst surface and the bulk gas may control the reaction rate for fast—extremely exothermic or endothermic—reactions. To study chemical events on the catalyst surface, these transport effects must be minimized. It is simple to check for the influence of transport effects in a CSTCR. For a catalyst mounted in a stationary basket, the stirrer speed is varied while all other variables are held constant. Changes in conversion with varying stirrer speeds indicate the presence of transport effects. A temperature gradient between the gas and the catalyst will exist if the reaction is heat-transfer

influenced. Both gas and catalyst temperatures can be measured easily with the stationary catalyst mounting.

Table V gives typical temperature gradients between catalyst and bulk gas for runs with catalyst A. Those data indicate that heat transfer effects were minimal over the range of conditions studied. Higher values of feed gas rate, mole % in the feed gas, and percent conversion of CO caused the higher temperature gradients as expected. Most kinetic runs were made at less than 20 std. cu. ft./hr. feed rate to keep the temperature gradient low.

Table IV. Results with Ruthenium Catalyst

Temp., °F.	*F_i/w, std. cu. ft./ hr.-gram catalyst*	*Feed Gas*	*CO Conv., %*	*Dry Product Gas Content, mole %*	
				CH_4	*C_2^+*
210	0.059	int. CO	5.5	66.6	0.9
290	0.058	int. CO	6.0	67.7	0.9
347	0.058	int. CO	20.3	69.5	1.1
405	0.056	int. CO	27.7	71.1	0.7
470	0.056	int. CO	86.2	84.1	1.6
547	0.055	high CO	90.0	85.2	1.3
600	0.503	int. CO	44.0	76.7	0.8
670	0.503	int. CO	89.3	89.2	0.7

Table V. Typical Temperature Gradients between Catalyst and Bulk Gas for Catalyst A[a]

Feed Rate, std. cu. ft./hr.	*Mole% CO in Feed Gas*	*CO Conv., %*	*$T_{cat.} - T_{gas}$, °F.*
4.50	2.4	65.2	2
5.96	2.4	53.4	2
9.62	2.4	40.7	2
6.47	7.0	36.6	1
7.20	7.0	33.3	2
8.80	7.0	28.6	3
3.90	10.0	50.5	2
7.20	10.0	33.4	3
9.70	10.0	31.3	9
9.94	10.0	22.8	7
11.31	10.0	24.5	11

[a] Stirring speed = 2200 r.p.m.

Mass transfer was found not to control above about 750 r.p.m. at 615°F. with a 10.2% CO–31.2% H_2 feed and with nickel catalyst in the annular basket. Of course, a check should be made for mass transfer at each run temperature. Because the rate constant increases with increas-

ing temperature, mass transfer should be more important at higher temperatures.

Conclusions

Conditions for "perfect mixing" were determined in a continuous-stirred tank catalytic reactor operated at 1000 p.s.i.g. "Perfect mixing" was obtained at stirring speeds above 1500 r.p.m. over the flow range used in this study.

Evaluation of commercial catalysts showed that nickel-on-kieselguhr catalyst is more active than nickel-on-alumina, iron, and ruthenium catalysts for cleanup of CO in IGT's hydrogasification process. Longer chained hydrocarbon formation is much less than expected for tests with iron and ruthenium catalysts.

Heat transfer effects were minimized by agitating the gas past the catalyst pellets. At stirring speeds of 2200 r.p.m., temperature gradients between catalyst and gas ranged from 0° to 11°F., depending on the feed gas rate, the feed gas CO content, and the CO conversion.

Mass transfer effects were absent in this methanation study of typical feed gases produced from coal hydrogasification. Carbon was not deposited in any of the catalytic runs.

Acknowledgment

The guidance of F. C. Schora and B. S. Lee is greatly appreciated. Mass spectrographic analyses were done by J. Neuzil. Mixing and reaction tests were conducted by R. Buchholz and J. DeSando.

Nomenclature

C = concentration, lb. moles/cu. ft.

C_M = maximum concentration of tracer in pulse test, lb. moles/cu. ft.

C_S = steady-state tracer concentration in purge or step test, lb. moles/cu. ft.

F = flow rate, std. cu. ft./hr.

R = reaction rate, lb. moles/hr.-gram

T = temperature, °F.

t = time, hr.

V = reactor volume, cu. ft.

w = catalyst weight, grams

i (subscript) = gas entering reactor

o (subscript) = gas leaving reactor

Literature Cited

(1) Bond, G. C., "Catalysis by Metals," Academic Press, New York, 1962.
(2) Ford, F. E., Perlmutter, D. D., *Chem. Eng. Sci.* **19**, 371 (1964).
(3) Tajbl, D. G., Simons, J. B., Carberry, J. J., *Ind. Eng. Chem. Fundamentals* **5**, 171 (1966).

RECEIVED November 25, 1966. Work sponsored jointly by the American Gas Association, Research and Development, and the U. S. Department of the Interior, Office of Coal Research.

12

Catalytic Gasification of Shale Oil

P. L. COTTINGHAM and H. C. CARPENTER

U.S. Department of the Interior, Bureau of Mines, Laramie Petroleum Research Center, Laramie, Wyo.

Crude shale oil was hydrogasified at 1000 lbs. pressure over depleted uranium and cobalt molybdate catalysts at temperatures in the range 880°–1102°F. with depleted uranium and 974°–1196°F. with cobalt molybdate. With both catalysts, the higher reaction temperatures produced greater hydrocarbon gas yields, greater percentages of methane in the gas, and greater methane yields expressed as percentage of conversion of the feedstock. The largest methane yields—4340 cu. ft. per barrel—and largest hydrocarbon gas yield—of 5725 cu. ft. per barrel—were obtained at the highest temperature (1196°F.) and lowest space velocity (0.25 $V_o/V_c/hr.$) used. At these conditions, methane yield was 75.8 vol.% of the hydrocarbon gas and 49.7 percent of stoichiometric.

Although the United States has large reserves of natural gas, our annual marketed production increased from less than 4 trillion cu. ft. in 1945 to nearly 16 trillion cu. ft. in 1964 (*9*), an increase of about 400% in 19 years. This increase, coupled with our decreasing ratio of reserves to production and the need for peak-shaving, has stimulated interest in possible methods for supplementing our future natural gas supply. The large quantities of oil shale in the western United States suggest using oil shale or shale oil for such supplemental purposes. Various authors have reported on the thermal gasification of these materials (*5, 6, 7, 8*). The present study is concerned with catalytic hydrogasification of crude shale oil, using depleted uranium and cobalt molybdate on alumina supports as catalysts.

Previous experiments in catalytic hydrogenation of crude shale oil at the Laramie Petroleum Research Center (*3, 4*) showed that pressures in excess of 2000 lbs. per sq. in. greatly suppressed the formation of methane, ethane, and catalyst deposits. At 500 lbs. pressure, catalyst deposits became excessive. The gasification experiments were, therefore, run at

1000 lbs. pressure to obtain high gas yields with moderate catalyst deposits.

Experimental

Apparatus and Procedure. A simplified flow diagram of the apparatus used for the gasification study is shown in Figure 1. The reactor was a vertical 2-9/16-in.-i.d. by 32-in.-long stainless steel vessel; it was modified for these experiments by a stainless steel sleeve that was inserted to reduce the internal diameter to 1 in. This modification improved temperature control. The reactor contained 18 in. of alundum granules at the top to serve as a preheater, 12.5 in. of catalyst (150 cc.), and 1.5 in. of alundum granules at the bottom. Catalyst temperatures were determined by five thermocouples, spaced at 2.25-in. intervals in a central thermowell in the catalyst bed.

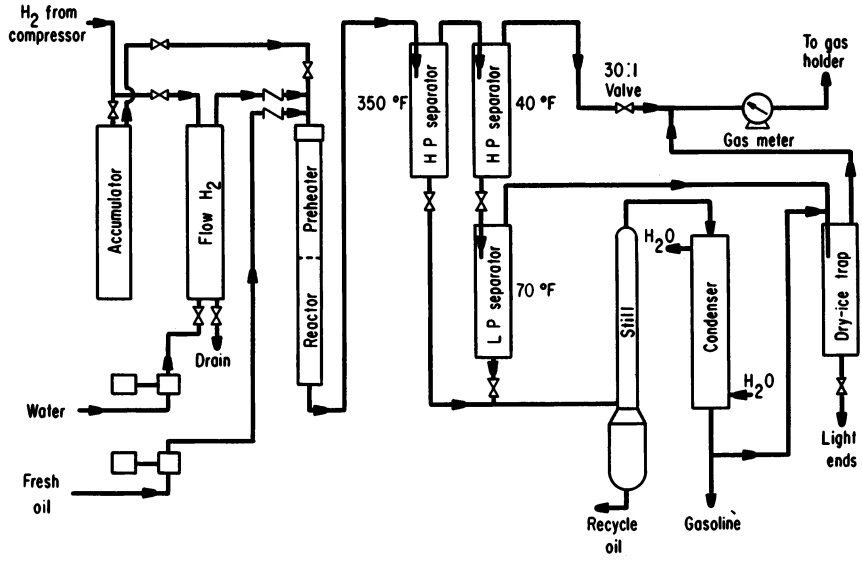

Figure 1. Hydrogenation unit

Hydrogen and oil were mixed at the inlet to the reactor and passed downward through the catalyst. Liquid products were separated in two high-pressure separators, operated in series at 350° and 40°F. Gas from the cold receiver was metered and stored until it could be sampled for mass spectrometer analysis.

Each gasification experiment was run for 6 hours with 12,000 cu. ft. of hydrogen per barrel. At the end of an experiment, liquid products were distilled into a light-ends fraction collected in a dry-ice trap, a naphtha fraction boiling up to 400°F., and a recycle fraction containing everything boiling above 400°F. The light ends from the cold trap were analyzed by the mass spectrometer, and appropriate weights were added to the

Table I. Properties of Crude Shale Oil

Specific gravity at 60°–60°F.	0.9408
Elemental analysis, wt.%	
Sulfur	0.68
Nitrogen	2.18
Carbon	83.96
Hydrogen	11.40
Oxygen (by diff.)	1.78
Hydrogen/carbon atomic ratio	1.61
Carbon residue, wt.%	3.5
Iron, p.p.m.	40
Zinc and arsenic, p.p.m.	present
Viscosity at 140°F., cs.	28.30
at 210°F.	8.23
ASTM gas-oil distribution (760 mm.)	
I.B.P., °F.	407
Max. (cracking), °F.	695
Recovery, vol.%	37.5
Residue, vol.%	62.5

gaseous and liquid products. Carbon deposits in the reactor were determined by measuring the carbon dioxide obtained when passing air through the reactor to regenerate the catalyst.

Catalysts. The catalysts used were commercial cobalt molybdate and a laboratory-prepared depleted uranium catalyst. The cobalt molybdate consisted of cobalt and molybdenum oxides on 6- to 8-mesh alumina granules. The uranium catalyst consisted of 7.7% depleted uranium (uranium from which the U-235 has been removed) in the oxide form on 1/8-in. H-151 alumina balls. This catalyst had produced high gas yields in previous hydrogenation experiments with shale oil, and these results suggested its possible use as a hydrogasification catalyst. Both catalysts were maintained under a hydrogen atmosphere at approximate reaction temperature and pressure for about 12 hours before each experiment.

Feedstock. The crude shale oil used for these studies was prepared in the Bureau of Mines gas-combustion retort at Rifle, Colo. It was filtered before use, and the ash content was reduced to 0.03 wt.%. Properties of the oil are shown in Table I. It contains a large amount of sulfur-, nitrogen-, and oxygen-containing compounds, and more than half of it may consist of nonhydrocarbons (2). It has a high viscosity and contains no gasoline-boiling range material. The hydrogen-carbon atomic ratio of 1.61 shows that additional hydrogen must be added to the oil to convert it to pipeline gas.

Calculations. All gas measurements are reported at 60°F. and 760 mm. mercury pressure. The hydrogen feed rate of 12,000 cu. ft. per barrel was 1.1 times the stoichiometric amount of about 10,890 cu. ft. needed to convert the crude oil completely to methane, hydrogen sulfide, ammonia, and water. The yield of methane as volume percent of stoichiometric was calculated by dividing the volume in cubic feet per barrel by 8740, which was the stoichiometric yield at the given conditions.

The hydrocarbon gas yields were considered to consist of the C_1 through C_3 hydrocarbons. The percentages of C_4 hydrocarbons were added to the percentages of liquid products to obtain C_4-plus liquid yields.

Weight percent conversion of the feed was defined as 100 minus the weight percent of C_4-plus liquid product. Therefore, conversion would include the weight percent of feed converted to C_1 through C_3 hydrocarbons and to such things as ammonia, hydrogen sulfide, water, and coke. Methane yields as percent of conversion were obtained by dividing the weight percent methane by the weight percent conversion and multiplying by 100.

Table II. Gasification of Crude Shale Oil over Depleted Uranium Catalyst[a]

	0.5 V_o/V_c/hr.				
Temp. (av.) °F.	*880*	*954*	*1010*	*1053*	*1102*
Temp. (max.) °F.	*906*	*979*	*1035*	*1074*	*1125*
H_2 consumed (std. cu. ft./barrel)	*1340*	*1840*	*3080*	*3980*	*4170*
Hydrocarbon gases (std. cu. ft./barrel)					
Methane	365	598	1152	1507	1767
Ethane	200	387	693	971	1059
Propane	146	247	441	536	459
Ethylene	18	4	29	18	18
Propylene	33	0	44	40	0
Total	762	1236	2359	3072	3303
Heat value, gross (B.t.u./cu.ft.)	1589	1570	1565	1550	1481
C_4^+ liquid (wt.%)	76.4	67.5	44.9	32.9	30.6
Conversion (wt.%)	23.6	32.5	55.1	67.1	69.4
Catalyst deposit (wt.%)	5.1	4.7	4.9	4.0	5.5
Water (wt.%)	2.0	2.0	2.0	2.0	2.0
Hydrogen sulfide (wt.%)	0.6	0.7	0.7	0.7	0.7
Ammonia (wt.%)	1.6	2.0	2.1	2.5	2.4
Methane					
wt.%	4.7	7.7	14.8	19.3	22.6
wt.% of conv.	19.9	23.7	26.9	28.8	32.6
vol.% of gas	47.9	48.4	48.8	49.0	53.5
vol.% of stoich.	4.2	6.8	13.2	17.2	20.2

[a] Pressure 1000 p.s.i.g.; hydrogen feed 12,000 std. cu. ft./barrel.

Gross heating values were calculated from component heating values used by the Bureau of Mines in reporting the analyses of natural gases (*1*). The values were calculated at 760 mm. mercury pressure to agree with the volume measurements.

Results

Depleted Uranium Catalyst. Table II shows the results from five experiments in hydrogasifying crude shale oil over depleted uranium catalyst at a space velocity of 0.5 volumes of oil per volume of catalyst per hour. Average reaction temperatures varied from 880° to 1102°F.

Table III. Liquid Products from Gasification over Depleted Uranium Catalyst

Temp. (av.) °F.	*880*	*954*	*1010*	*1053*	*1102*
H_2 consumed (std. cu. ft./barrel)	*1340*	*1840*	*3080*	*3980*	*4170*
Naphtha[a] (wt. % of feed)	26.5	26.6	16.7	13.4	11.1
Sp. gr. at 60°–60°F.	0.7655	0.7799	0.8279	0.8711	0.8874
Sulfur (wt.%)	0.08	0.04	0.08	0.02	0.04
Nitrogen (wt.%)	0.68	0.61	0.86	0.34	0.52
Hydrocarbon types (vol.%)					
Paraffins	34	35	25	8	3
Naphthenes	11	14	4	4	
Olefins	29	18	10	3	1
Aromatics	26	32	61	85	96
Recycle oil (wt.% of feed)	40.7	19.4	15.7	10.7	9.5
Sp. gr. at 60°–60°F.	0.9247	0.9973	1.0555	1.0695	1.0763
Sulfur (wt.%)	0.18	0.22	0.28	0.16	0.22
Nitrogen[b] (wt.%)	1.74	1.76	2.02	—	1.28

[a] Not including C_4^+ from gas.
[b] Insufficient sample where analysis is not shown.

Total hydrocarbon gas volumes increased from 762 cu. ft. per barrel at 880°F. to 3303 cu. ft. at 1102°F.; at the same time, the methane content of the gas increased from 47.9 to 53.5 vol.%, resulting in a change in the volume of methane from 365 to 1767 cu. ft. A corresponding decrease in the heating values of the gas occurred, from 1589 to 1481 B.t.u. per cu. ft., as the heating values tended to approach that of methane.

Expressed on the weight basis, the yield of methane increased from 4.7% at 880°F. to 22.6% at 1102°F., and total conversion increased from 23.6 to 69.4%; the corresponding change in methane yield expressed as weight percent of conversion was from 19.9 to 32.6%.

Table III shows the properties of the liquid products from the hydrogasification experiments with depleted uranium catalyst. Sulfur percentages in the liquid products were considerably lower than the percentage in the feed, but nitrogen percentages were high. The naphthas became aromatic as the operating temperature was raised from 880° to 1102°F.

Cobalt Molybdate Catalyst. Yields of products from hydrogasifying crude shale oil over cobalt molybdate catalyst at a space velocity of 1.0 volume of oil per volume of catalyst per hour are shown in Table IV, and properties of the liquid products are shown in Table V. The average reaction temperatures from 974° to 1183°F. were higher than those used with depleted uranium catalyst. Consequently, greater gas yields were obtained. However, similar trends were shown in the results obtained with both catalysts.

Conversion increased from 34.1 to 85.1% as the average temperature was increased from 974° to 1183°F. At the same time, methane yield, as weight percent of conversion, increased from 24.6 to 46.6%. Also, the

Table IV. Gasification of Crude Shale Oil over Cobalt Molybdate Catalyst[a]

	1.0 V_o/V_c/hr.			
Temp. (av.) °F.	*974*	*1004*	*1106*	*1183*
Temp. (max.) °F.	*1018*	*1049*	*1172*	*1226*
H_2 consumed (std. cu. ft./barrel)	*2680*	*3210*	*4850*	*5980*
Hydrocarbon gases (scf/bbl)				
Methane	652	972	1945	3090
Ethane	427	663	1292	1699
Propane	288	435	504	109
Ethylene	27	48	5	0
Propylene	30	57	0	5
Total	1424	2175	3746	4903
Heat value, gross (B.t.u./cu.ft.	1601	1611	1490	1315
C_4^+ liquid (wt.%)	65.9	50.5	24.9	14.9
Conversion (wt.%)	34.1	49.5	75.1	85.1
Catalyst deposit (wt.%)	2.4	2.0	2.4	4.2
Water (wt.%)	2.0	2.0	2.0	2.0
Hydrogen sulfide (wt.%)	0.7	0.7	0.7	0.7
Ammonia (wt.%)	2.6	2.6	2.6	2.6
Methane				
wt.%	8.4	12.5	25.0	39.7
wt.% of conv.	24.6	25.3	33.3	46.6
vol.% of gas	45.8	44.7	51.9	63.0
vol.% of stoich.	7.5	11.1	22.2	35.4

[a] Pressure 1000 p.s.i.g.; hydrogen feed 12,000 std. cu. ft./barrel.

methane content of the hydrocarbon gas increased from 45.8 to 63.0 vol. %. The increased percentage of methane in the gas at the higher temperature and conversion levels was reflected in the heat content of the gas, which decreased from 1,601 B.t.u. per cu. ft. for the gas obtained at 974°F. to 1315 B.t.u. per cu. ft. for the gas obtained at 1183°F.

Table V. Liquid Products from Gasification over Cobalt Molybdate Catalyst

Space velocity	*1.0 V_o/V_c/hr.*			
Temp. (av.) °F.	*974*	*1004*	*1106*	*1183*
H_2 consumed (std. cu. ft./barrel)	*2680*	*3210*	*4850*	*5980*
Naphtha[a] (wt.% of feed)	39.5	24.9	12.0	7.8
Sp. gr. at 60°–60°F.	0.7562	0.7821	0.8741	0.8801
Sulfur (wt.%)	0.00	0.00	0.00	0.00
Nitrogen (wt.%)	0.02	0.01	0.02	0.01
Hydrocarbon types[b] (vol.%)				
Paraffins	—	—	3	0
Naphthenes	—	—		0
Olefins	—	—	2	0
Aromatics	—	—	95	100
Recycle oil (wt.% of feed)	15.3	9.5	7.2	6.3
Sp. gr. at 60°–60°F.	1.0303	1.0543	1.1181	1.0699
Sulfur (wt.%)	0.00	0.00	0.00	0.03
Nitrogen (wt.%)	0.22	—	0.20	0.27

[a] Not including C_4^+ from gas.
[b] Insufficient sample where analysis is not shown.

Yields of products from hydrogasifying crude shale oil over cobalt molybdate catalyst at space velocities of 0.50 and 0.25 are shown in Table VI, and properties of the liquid products are shown in Table VII. Results of two experiments at different temperatures are shown for each space velocity.

The highest methane yield (4341 cu. ft. per barrel) and highest gas yield (5725 cu. ft. per barrel) were obtained at the highest temperature (1196°F. average or 1208°F. maximum) and lowest space velocity (0.25) used. The greatest conversion of feed stock, 88.1%, and greatest yield of methane as percent of conversion, 63.3%, were also obtained under these conditions. Methane content of the hydrocarbon gas was 75.8 vol. %, or 49.7% of stoichiometric. Heating value of the gas was 1202 B.t.u. per cu. ft.

Sulfur percentages in the liquid products were low. Nitrogen percentages were much lower than those of the liquid products obtained by hydrogasification over depleted uranium catalyst. The percentages of

aromatic hydrocarbons in the naphthas were high, and at a reaction temperature of 1114°F. with a space velocity of 0.50 they approached 100% of the hydrocarbons. The naphthas produced in small percentages at a space velocity of 0.25, although not analyzed, also would be expected to be almost 100% aromatic.

Decreasing the space velocity had much the same effect as increasing the reaction temperature. Comparing results obtained at 1106°F. average temperature and 0.25 space velocity with those obtained at 1114°F. and 0.50 space velocity shows that greater methane yield, greater total gas yield, greater conversion, and greater methane yields expressed

Table VI. Gasification of Crude Shale Oil over Cobalt Molybdate Catalyst[a]

	0.50 V_o/V_c/hr.		*0.25 V_o/V_c/hr.*	
Temp. (av.) °F.	*1062*	*1114*	*1106*	*1196*
Temp. (max.) °F.	*1089*	*1141*	*1129*	*1208*
H_2 consumed (std. cu. ft./barrel)	*3803*	*4985*	*5460*	*6852*
Hydrocarbon gases (std. cu. ft./barrel)				
Methane	1465	2141	2485	4341
Ethane	995	1379	1683	1357
Propane	461	407	231	25
Ethylene	9	23	0	1
Propylene	24	18	18	1
Total	2954	3968	4417	5725
Heat value, gross (B.t.u./cu.ft.)	1530	1451	1393	1202
C_4^+ liquid (wt.%)	35.5	23.2	20.2	11.9
Conversion (wt.%)	64.5	76.8	79.8	88.1
Catalyst deposit (wt.%)	4.7	2.6	1.4	4.1
Water (wt.%)	2.0	2.0	2.0	2.0
Hydrogen sulfide (wt.%)	0.7	0.7	0.7	0.7
Ammonia (wt.%)	2.6	2.6	2.6	2.6
Methane				
wt.%	18.8	27.5	31.9	55.8
wt.% of conv.	29.1	35.8	40.0	63.3
vol.% of gas	49.6	54.0	56.2	75.8
vol.% of stoich.	16.8	24.5	28.4	49.7

[a] Pressure 1000 p.s.i.g.; hydrogen feed 12,000 std. cu. ft./barrel.

either as percent of conversion or percent of total gas were obtained at the lower space velocity. Heating value of the hydrocarbon gas was lower for the gas produced at the lower space velocity because of the higher methane content. These comparisons can be extended to the results shown in Table IV for the experiment at 1106°F. and 1.0 space velocity.

Table VII. Liquid Products from Gasification over Cobalt Molybdate Catalyst

	0.50 V_o/V_c/hr.		*0.25 V_o/V_c/hr.*	
Temp. (av.) °F.	*1062*	*1114*	*1106*	*1196*
H_2 consumed (std. cu. ft./barrel)	*3803*	*4985*	*5460*	*6852*
Naphtha[a] (wt.% of feed)	16.8	10.2	10.1	6.4
Sp. gr. at 60°–60°F.	0.8482	0.8832	0.8869	0.8986
Sulfur[b] (wt. %)	—	0.01	—	—
Nitrogen[b] (wt. %)	0.14	0.04	0.02	—
Hydrocarbon types[b] (vol.%)				
Paraffins	15	0	—	—
Naphthenes	2	1	—	—
Olefins	0	0	—	—
Aromatics	83	99	—	—
Recycle oil (wt.% of feed)	8.0	5.8	2.8	3.4
Sp. gr. at 60°–60°F.	1.0635	1.1064	1.0730	1.1074
Sulfur (wt.%)	0.12	0.02	0.08	0.06
Nitrogen (wt.%)	0.34	0.16	0.15	0.11

[a] Not including C_4^+ from gas.
[b] Insufficient sample where analysis not shown.

Conditions used with the cobalt molybdate were generally not the same as those with the depleted uranium catalyst. However, the gas yields obtained at 1062°F. and 0.50 space velocity over cobalt molybdate were similar to those obtained at 1053°F. and 0.50 space velocity over depleted uranium. Better elimination of nitrogen from the liquid products was achieved with the cobalt molybdate. No special advantages were found for the depleted uranium, but further research would be needed to evaluate it fully over the entire range of conditions investigated with the cobalt molybdate.

Summary

Cobalt molybdate on alumina and depleted uranium on alumina were tested as catalysts for hydrogasifying crude shale oil at 1000 lbs. pressure and a hydrogen feed rate of 1.1 times the stoichiometric, with on-stream periods of 6 hours for each experiment. Reaction temperatures were in the range 880°–1102°F. with depleted uranium and 974° to 1196°F. with cobalt molybdate. With both catalysts the higher reaction temperatures produced greater hydrocarbon gas yields, greater percentages of methane in the gas, and greater methane yields expressed as percentage of conversion of feedstock. Lowering the space velocity through the range 1.0–0.25 with cobalt molybdate produced effects similar to those obtained when raising the temperature.

Acknowledgment

This work was conducted under a cooperative agreement between the Bureau of Mines of U.S. Department of the Interior and the University of Wyoming. The depleted uranium used in this work was obtained from the Atomic Energy Commission, Oak Ridge, Tenn.

Literature Cited

(1) Boone, W. J., Jr., *U.S. Bur. Mines Bull.* **576** (1958).
(2) Cady, W. E., Seelig, H. S., *Ind. Eng. Chem.* **44**, 2632 (1952).
(3) Carpenter, H. C., Cottingham, P. L., *U.S. Bur. Mines Rept. Invest.* **5533** (1959).
(4) Cottingham, P. L., White, E. R., Frost, C. M., *Ind. Eng. Chem.* **49**, 679 (1957).
(5) Feldkirchner, Harlan L., *Quart. Colo. School Mines* **60**, (3), 147 (1965).
(6) Linden, Henry R., *Chem. Eng. Progr. Symp. Ser. No. 54*, **61**, 76 (1965).
(7) Schultz, E. B., Jr., Linden, Henry R., *Ind. Eng. Chem.* **51**, 573 (1959).
(8) Schultz, E. B., Jr., *Chem. Eng. Progr. Symp. Ser. No. 54*, **61**, 48 (1965).
(9) Zaffarano, R. F., Avery, Ivan F., *Minerals Yearbook (U.S. Bur. Mines)* **2**, 319-352, (1964).

RECEIVED November 28, 1966.

13

Production of High Methane-Content Gas by Steam Reforming of Light Distillates

A. R. KHAN and H. L. FELDKIRCHNER

Institute of Gas Technology, Chicago, Ill.

A study was made to develop a catalyst for the low temperature catalytic steam reforming of various feedstocks using the process developed by the British Gas Council for gasifying light petroleum distillates. The major properties desired were high activity, insensitivity to reported poisons such as sulfur compounds, thermal stability, and the ability to reform various feedstocks at low steam-hydrocarbon ratios without carbon deposition. A novel nickel-aluminum-alumina catalyst was developed which was active and was capable of reforming feedstocks such as propane, hexane, octane, benzene, naphtha, jet fuel, and kerosene. This catalyst and process show promise for a variety of uses, two of which are peakshaving for the gas industry and hydrogen production.

A novel approach to gasifying light distillate oils, developed by the British Gas Council, was first reported in 1957 (*4, 7, 8*) and was subsequently discussed (*6, 9*). By this process the sulfur content of the feed is reduced by hydrodesulfurization with subsequent steam reforming in the presence of a nickel catalyst. Because of the low temperature at which reforming is conducted—400° to 550°C.—the product gas contains 60–80 mole % methane (dry basis). Data reported by the Gas Council (*5, 6*) show purified product gas heating values of about 730–850 B.t.u./std. cu. ft. in operation over a pressure range of 1–25 atm. There was no carbon deposition at fairly low steam-hydrocarbon ratios, and the reaction was either thermally balanced or slightly exothermic. The catalyst is reported to be sulfur sensitive. Data on reforming highly olefinic or highly aromatic feeds have not been reported.

When a high B.t.u. gas is not the desired final product, the process includes a further stage in which the high methane-content gas is further

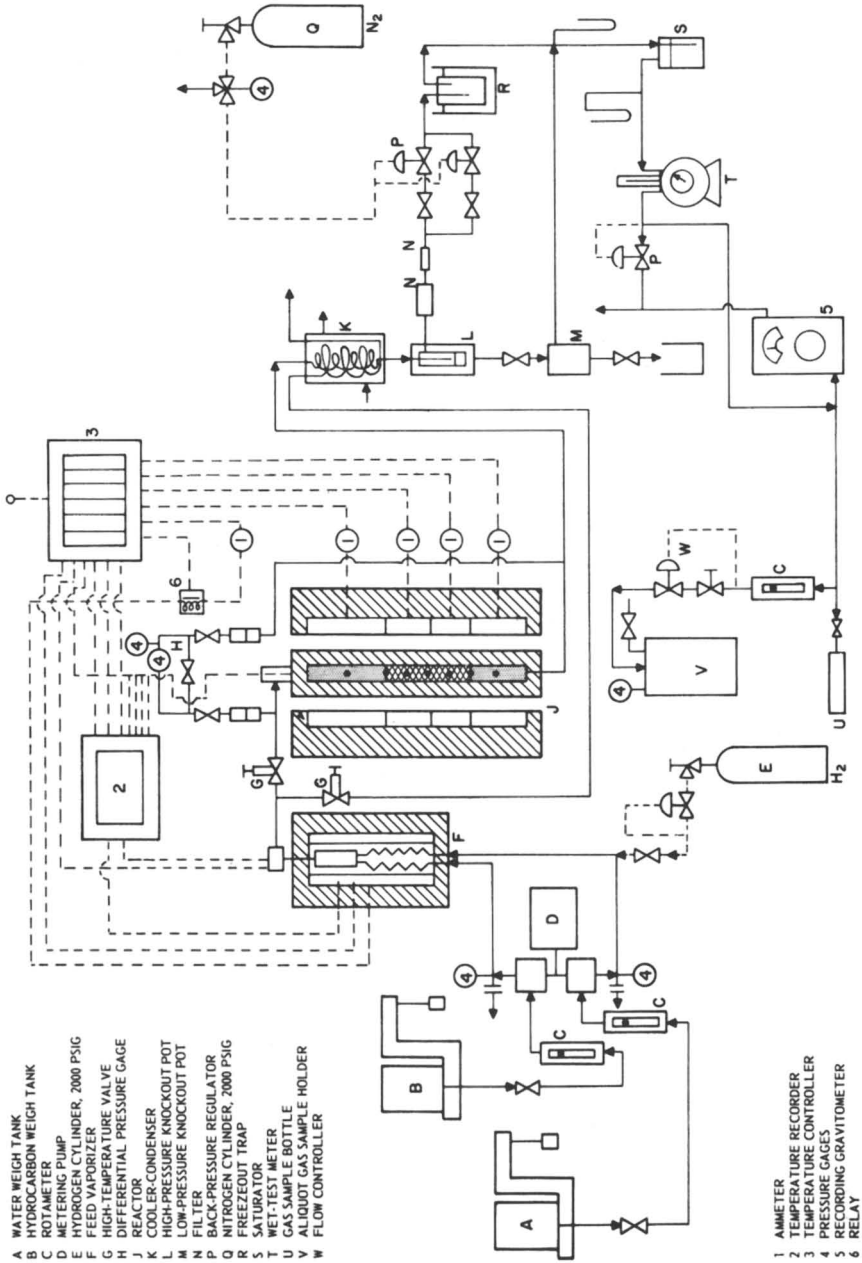

Figure 1. Catalyst testing unit

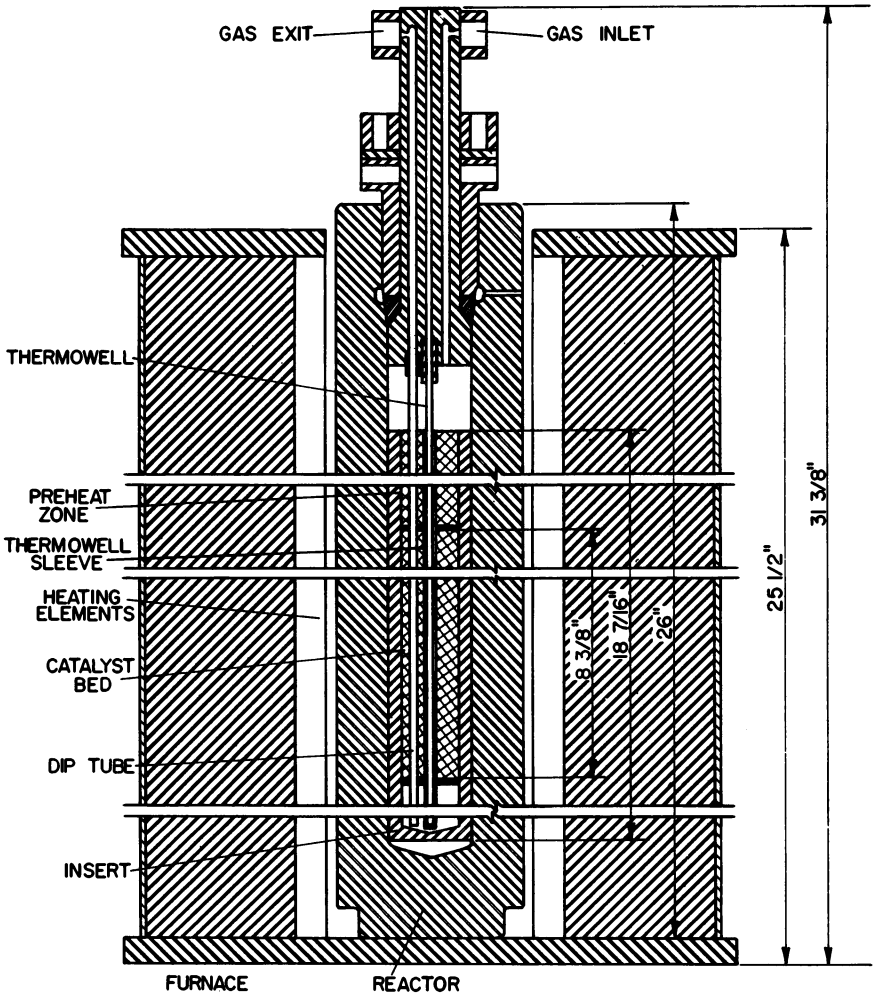

Figure 2. First reactor and furnace

reformed to a low B.t.u. gas. This process is now used in Great Britain for base load town gas production (9).

A study of this process was begun under an IGT-supported basic research project. After a detailed study of the thermodynamics of the process, experiments were conducted with high purity hexane, octane, and benzene, as well as commercial propane, naphtha, kerosene, and jet fuel.

The objectives of this study were to determine whether a catalyst could be developed that would be able to reform various feedstocks, in-

cluding paraffinic, olefinic, and aromatic materials with a wide range of molecular weights. Once a catalyst was developed, it was necessary to determine minimum steam-hydrocarbon ratios for operation without carbon deposition, the activity of the catalyst, and the effects of various operating variables on the gas yield and composition.

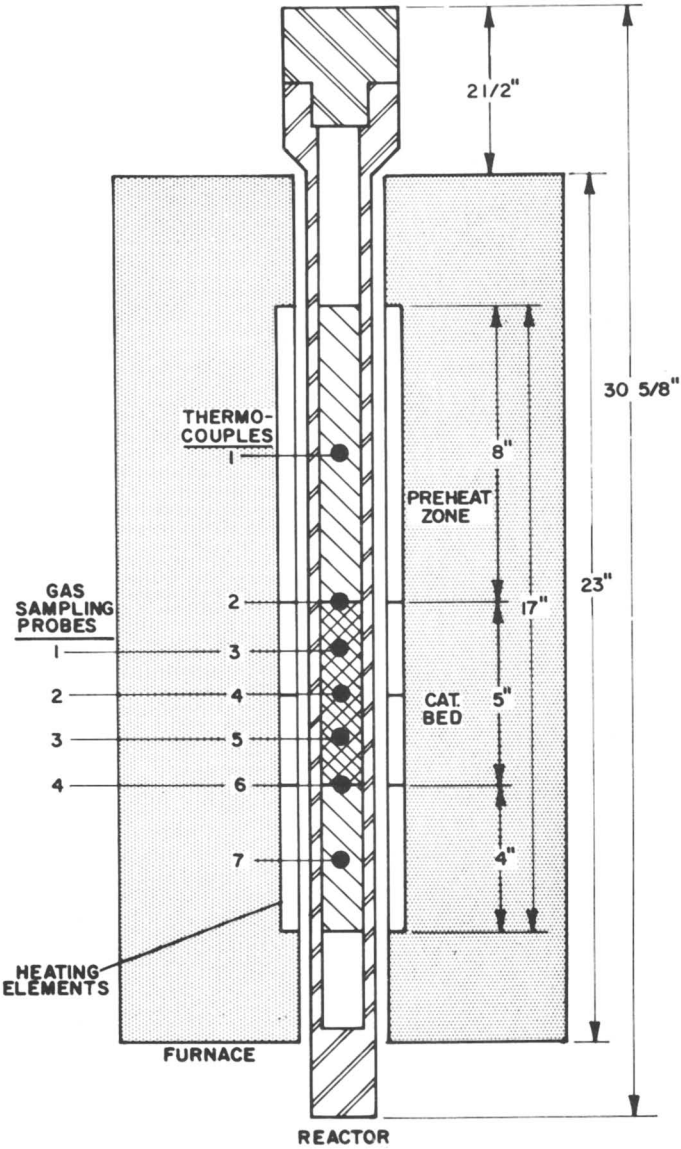

Figure 3. Second reactor and furnace

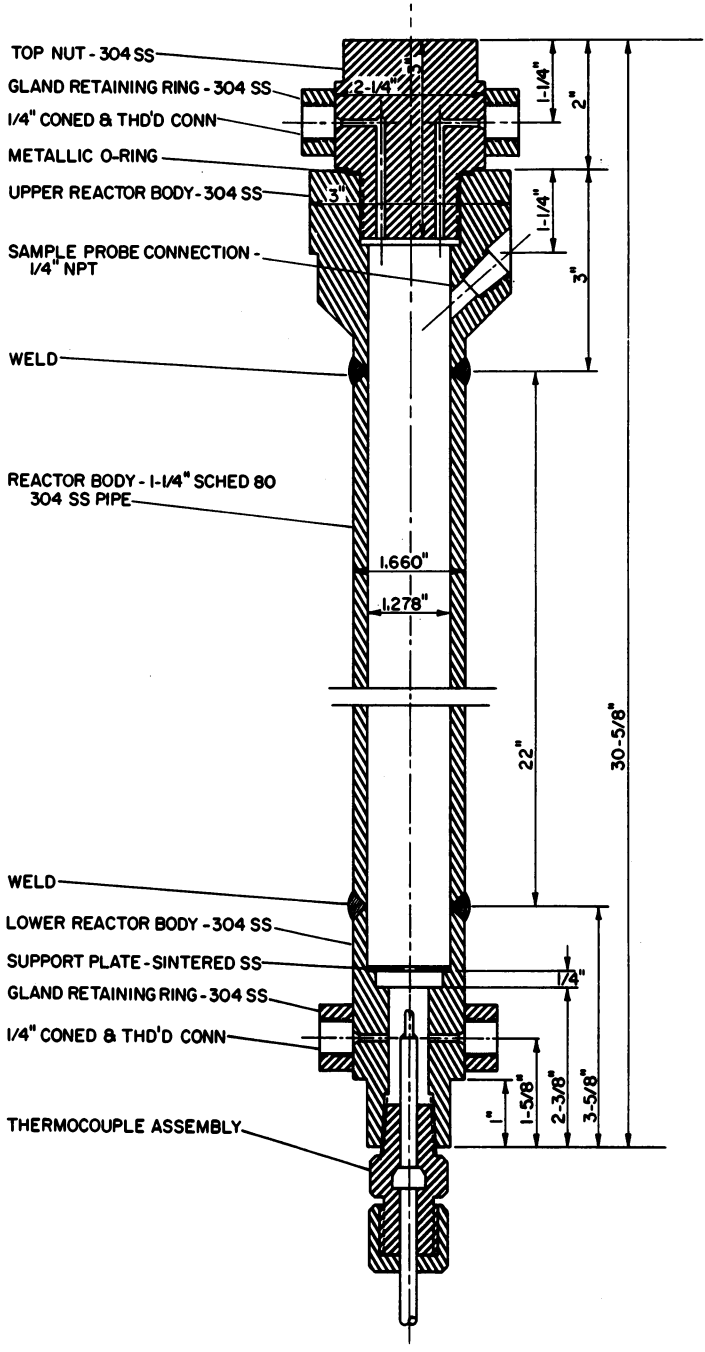

Figure 4. Detailed diagram of second reactor

Experimental

Apparatus. A schematic of the reaction system is shown in Figure 1. Weighed amounts of the hydrocarbon feedstock (A) and water (B) flow through rotameters (C) and are charged by a duplex metering pump (D) to the feed vaporizer (F). The vaporized feeds are thoroughly mixed in a chamber above the vaporizer. The mixed feed flows down through the catalyst bed in the reactor (J). The product gas is cooled, and liquids are condensed in a cooler-condenser (K). Condensate is knocked out and drained from the system (L,M). The gas flows through filters (N) into a freeze-out trap (R). After saturation with water vapor, the product gas (S) is metered by a wet-test meter (T) and sampled (U). The specific gravity is monitored by a recording gravitometer (5). The unit pressure is controlled by a dome-loaded back-pressure regulator (P). The unit pressure is indicated by a precision pressure gage, the pressure drop across the catalyst bed by a differential pressure gage. The reactor temperatures and the feed-vaporizer temperatures are controlled by a six-point, potentiometric-type, on-off temperature controller.

The reactor used in the first series of tests with hexane, octane, and kerosene was simpler in construction than that used in the rest of the test program. The major reactor and furnace dimensions are shown schematically in Figure 2. The reactor had been designed and used for operation at high temperatures and pressures and is described fully elsewhere (*11*). Because of its large diameter, the reactor was provided with a thick insert to reduce the internal diameter as well as to contain the catalyst and provide for complete and easy catalyst removal. The entire reactor was heated by a single-zoned electric furnace. The temperatures within the reactor were measured by a single traveling thermocouple made of Chromel-Alumel and insulated with magnesium oxide. It has a 0.040-in. o.d., swaged stainless steel sheath. The thermocouple was mounted within an ⅛-in. o.d. stainless steel thermowell which was mounted in the top cover of the reactor. Feed vapors entered the top of the reactor, flowed down through the catalyst bed, and returned to the top of the reactor through a $\frac{3}{16}$-in. o.d. dip tube sealed into the top cover of the reactor by a compression-type fitting.

The major reactor and electric furnace dimensions for the second reactor are shown schematically in Figure 3. A detailed drawing of the reactor is shown in Figure 4. The furnace has four heating zones; two are on the catalyst bed which is supported and contained by two beds of alumina inerts. Two separate heaters were used in the catalyst zone to provide better temperature control. A thermocouple rake assembly, which contained seven Chromel-Alumel thermocouples, was used to measure reactor temperatures. The thermocouples are insulated with magnesium oxide and have 0.025-in. o.d. swaged stainless steel sheaths. To minimize possible temperature measurement errors from axial heat conduction along the thermocouple assembly, each thermocouple extends perpendicularly from the axial thermowell. To follow the progress of the reaction through the catalyst bed and deactivation of the catalyst with time, four sampling probes were inserted at the same levels as thermocouples 3, 4, 5, and 6. The probes were located approximately ¼, 1½, 2¾, and 4 in. below the top of the bed.

Procedure. Methods for collecting and analyzing the gas and liquid samples taken with the probes allow continuous samples to be withdrawn simultaneously at all four points within the catalyst bed. The bed ranged from 25 to 200 cc. in volume. Since the total flow rate of the probe samples is only a few percent of the total exit stream flow rate, the stability of reactor operation is not impaired, and the flow rate in the bed does not vary appreciably. A Chronofrac gas chromatograph (Precision Scientific Co.) was installed for analyzing probe and product gas samples.

A special feed system was devised for high vapor pressure, light hydrocarbons such as propane and butane. The light hydrocarbons were fed through a high pressure rotameter from pressurized stainless steel cylinders. Two cylinders were used so that one cylinder could feed the hydrocarbon while the other was being weighed. The cylinders were switched and weighed at the beginning and end of each steady-state period so that the hydrocarbon feed rate could be measured more accurately. The tanks were provided with quick-disconnect couplings at each end. These couplings contained double, integral check valves to reduce hydrocarbon loss during the switching operation.

Materials. Feedstocks were obtained from several sources. Pure hydrocarbons were obtained from Phillips Petroleum Co. The hexane and benzene were pure grade (99.0 mole % minimum purity). The octane was technical grade (95.0 mole % minimum purity).

The propane used was a commercially available feed supplied by Pyrofax Corp. The light kerosene, supplied by Universal Oil Products Co., had been partially desulfurized. The light fuel naphtha was obtained from Industrial Solvents Corp. The jet fuel was obtained from Humble Oil and Refining Co. Properties of the commercial feeds are given in Table I.

Analyses. Chemical and physical analyses of liquid feeds were performed by A.S.T.M. standard methods where applicable (*1*). Gaseous feeds and product gases were analyzed for sulfur by a method which is based largely on that given by Hoggan and Battles (*10*) and Bertolacini and Barney (*3*). The liquid feeds, having low sulfur contents, were analyzed for sulfur by a method given by Attari (*2*).

Tests were made for varying lengths of time, from several hours to several days. Life studies on all feeds were beyond the scope of this work.

Results

Thermodynamic Equilibrium Studies. A detailed thermodynamic equilibrium study was made for some pure hydrocarbon feedstocks to calculate the effects of operating variables on the heat of reaction and product gas composition. Experimental work done elsewhere had shown that product gas compositions approached equilibrium quite closely with active catalysts (*5*). Thus we expected that not only would these calculations be a guide for conducting experimental work, but they would minimize the amount of experimental work required.

Table I. Commercial Feedstock Properties

Liquid Feeds	*Light Naphtha*	*Jet Fuel*	*Light Kerosene*
Specific Gravity, °API (60°/60°)	70.3	56.5	48.8
ASTM Distillation, °F.			
I.B.P.	167	194	361
5%	171	238	371
10%	171	253	374
20%	173	268	378
30%	174	280	384
40%	176	293	388
50%	177	308	394
60%	180	323	400
70%	183	350	408
80%	187	385	416
90%	194	430	430
End Point	203	478	445
Recovery	99	95	98
Residue	1	3	2
Ultimate Analysis, wt.%			
Carbon	84.42	84.84	85.41
Hydrogen	15.58	14.56	14.59
Total	100.00	99.40	100.00
C-H Ratio	5.42	5.83	5.85
Sulfur, p.p.m.	28.9	80.5	32.4
Hydrocarbon Analysis, vol.%			
Aromatics	2.0	10.6	5.3
Olefins	0.0	4.6	1.1
Saturates	98.0	84.8	93.6
Total	100.0	100.0	100.0
Gaseous Feed	*Propane*		
Composition, mole%			
Propane	94.5		
Propylene	2.5		
Ethane	1.5		
i-Butane	1.0		
n-Butane	0.5		
Total	100.0		
Sulfur Content, p.p.m.	16.8		

Equilibrium gas compositions, heats of reaction, and adiabatic temperature changes were calculated for each initial reaction temperature. The variables studied were temperature, pressure, feed steam-carbon ratio, and feedstock.

Equilibrium gas compositions (on a dry basis) for steam reforming of hexane are given as a function of temperature, pressure, and feed steam-carbon ratio in Figure 5. In the range of variables studied, the carbon dioxide content is almost independent of temperature, pressure,

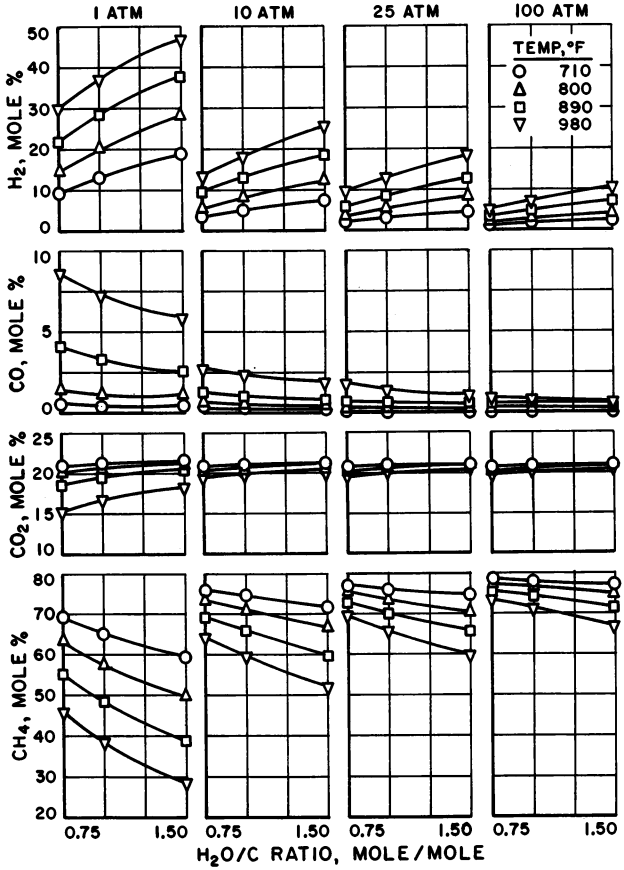

Figure 5. Ideal gas equilibrium composition (water-free) for steam reforming hexane

and feed steam-carbon ratio above 10 atm. and below 750°K. The carbon monoxide content is affected by temperature and pressure, but it is not present in substantial concentrations. Increasing the pressure and decreasing the temperature increases the raw gas heating value since methane content increases and hydrogen content decreases. The high hydrogen contents shown at 1 atm., 800°K., and high steam-carbon ratios suggest the possibility of using this process for hydrogen production in

some systems, such as fuel cells, where a pure hydrogen stream is not required.

The effect of paraffin carbon number on the equilibrium methane concentration is shown for three feed steam-carbon ratios in Figure 6. These results indicate that a higher methane-content gas can be produced from low molecular weight paraffins than from high molecular weight paraffins.

The reforming reaction can be either exothermic or endothermic, depending on the temperature and pressure. Increases in pressure cause the reaction to become more exothermic whereas increases in temperature cause the opposite. The reaction becomes progressively less exothermic as the feed steam-carbon ratio is increased. The degree of exothermicity increases with increasing molecular weight.

Reforming Studies with Hexane Feedstock. SPACE VELOCITY. Initial studies were made with pure grade hexane to determine the reaction stoichiometry, the approach to equilibrium, and the catalyst behavior without complicating factors such as catalyst poisons. The

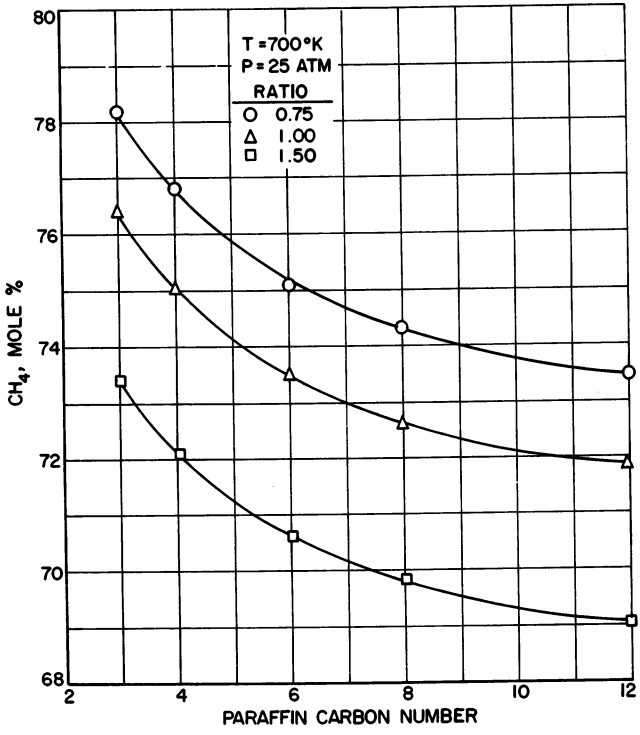

Figure 6. Ideal gas equilibrium methane contents (water-free) for steam reforming various paraffinic hydrocarbons

feedstock space velocity was the first process variable studied to measure the maximum catalyst activity under the most ideal conditions. The effect of space velocity on product gas composition was also noted. At space-time yields over 50,000 std. cu. ft./cu. ft. catalyst per hr., 98% of the hexane could be converted to gaseous products. When conversions dropped below 100%, an increase in space velocity decreased the methane content and increased the hydrogen content of the product gas (Figure 7). The carbon dioxide content of the gas remained essentially constant. Carbon monoxide remained negligible over the entire range of space velocity. Even at the highest space velocity used, the heating value of the product gas could be raised to about 850 B.t.u./std. cu. ft. by simply scrubbing out carbon dioxide to a final content of 2 mole%. This could be satisfactory for peakshaving.

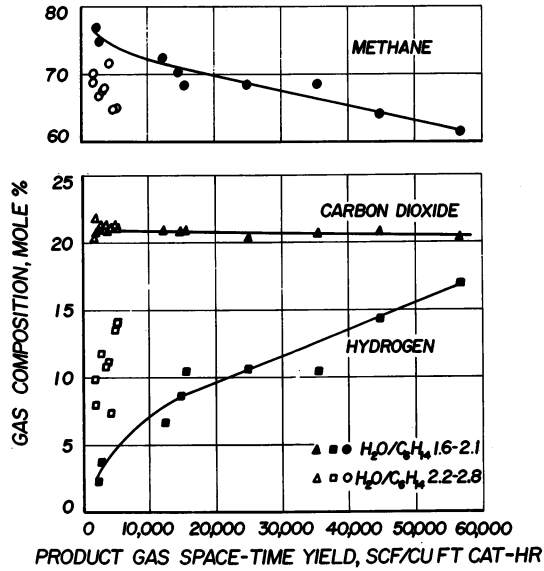

Figure 7. Typical results for reforming hexane

Because the carbon monoxide content of the gas was so low, approaches to equilibrium could not be calculated accurately for runs at nearly complete conversion and low space velocity. One other factor that also makes this calculation difficult is the presence of a hot spot within the catalyst bed, which indicates that the reaction may occur in a narrow zone. Temperature profiles were measured in selected runs (Figure 8). The gas compositions for these runs correspond to equilibrium at the temperatures measured near the bottom (exit) of the catalyst bed, which is what would be expected.

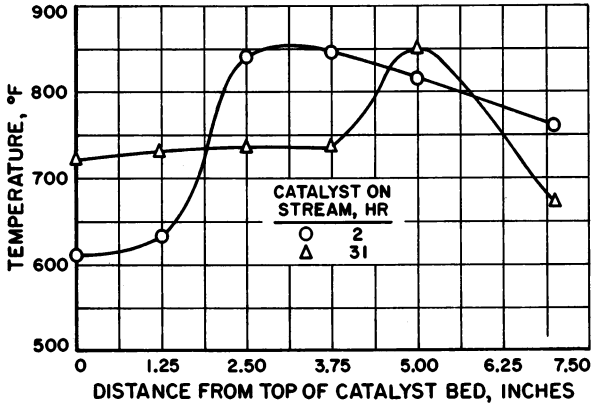

Figure 8. Catalyst bed temperature profiles for reforming hexane

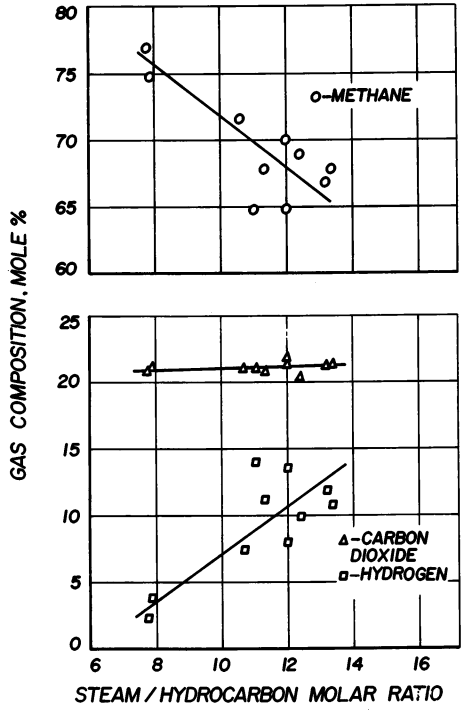

Figure 9. Effect of steam-hydrocarbon ratio on gas composition for reforming hexane (same as predicted from equilibrium calculations)

STEAM-HYDROCARBON RATIO. The next series of tests was made to show the effect of the steam-hydrocarbon ratio on gas composition (Figure 9) and to determine the minimum practical steam-hydrocarbon ratio. The trends shown are approximately the same as predicted by equilibrium calculations. The lack of complete temperature profile data makes it difficult to show how closely the trends agree with equilibrium predictions. Steam-hydrocarbon weight ratios as low as 1.6 (molar ratio of 7.7) were adequate to prevent carbon deposition. The product gas heating value at this low ratio was about 774 B.t.u./std. cu. ft. It could be raised to 957 B.t.u./std. cu. ft. if the exit gas carbon dioxide were reduced to 2 mole % by scrubbing.

Table II. Test Results for Steam Reforming Octane and Benzene

	Octane	*Benzene*
Pressure, p.s.i.g.	375	353
Temperature at center of bed, °F.	768	905
Steam-hydrocarbon weight ratio	2.07	4.42
Hydrocarbon space velocity, lb./hr.-cu. ft. catalyst	300	324
Product gas composition, mole % (water-free)		
$N_2 + CO$	0.4	0.9
CO_2	21.7	30.7
H_2	11.3	31.3
CH_4	66.4	36.7
C_3H_8	0.2	—
C_6H_6	—	0.4
Total	100.0	100.0
Scrubbed gas composition, mole % (water-free)		
$N_2 + CO$	0.5	1.3
CO_2	2.0	2.0
H_2	14.2	44.3
CH_4	83.1	52.4
C_3H_8	0.2	—
C_6H_6	—	—
Total	100.0	100.0
Scrubbed gas heating value, B.t.u./std. cu. ft.	879	675

Reforming of Various Feedstocks. When the catalyst developed proved to be capable of reforming pure hexane successfully at low steam-hydrocarbon ratios, we decided to test various feedstocks having a range of molecular weights and various types of hydrocarbons. The first tests were conducted with octane and benzene to show whether

heavier paraffins and aromatics could be reformed and whether the gases produced could be predicted by equilibrium calculations.

Test results for octane and benzene reforming are summarized in Table II. The steam-hydrocarbon ratios were deliberately set high to avoid possible carbon formation with these heavier or aromatic feedstocks.

Table III. Test Results for Steam Reforming Commercial Feedstocks

	Propane	*Naphtha*	*Jet Fuel*	*Kerosene*
Pressure, p.s.i.g.	355	355	350	375
Temperature at center of bed, °F.	890	935	900	832
Steam-hydrocarbon weight ratio	1.26	2.16	2.36	2.03
Hydrocarbon space velocity, lb./hr.-cu. ft. catalyst	834	328	254	226
Product gas composition, mole % (water-free)				
$N_2 + CO$	0.1	0.2	0.2	1.1
CO_2	16.8	21.5	22.5	23.6
H_2	1.9	12.1	14.5	18.1
CH_4	80.1	66.2	62.6	57.2
C_2H_6	0.1	—	—	—
C_3H_8	1.0	—	—	—
C_6H_{14}	—	—	0.2	—
Total	100.0	100.0	100.0	100.0
Scrubbed gas composition, mole % (water-free)				
$N_2 + CO$	0.1	0.3	0.3	1.4
CO_2	2.0	2.0	2.0	2.0
H_2	2.2	15.1	18.3	23.2
CH_4	94.4	82.6	79.1	73.4
C_2H_6	0.1	—	—	—
C_3H_8	1.2	—	—	—
C_6H_{14}	—	—	0.3	—
Total	100.0	100.0	100.0	100.0
Scrubbed gas heating value, B.t.u./std. cu. ft.	980	883	860	809

The remaining commercial feedstocks studied were propane, light naphtha, light kerosene, and JP-4 jet fuel, and the results are given in Table III. A higher methane content gas can be produced from the lighter hydrocarbons, in agreement with results of equilibrium calculations shown in Figure 6. These feedstocks were all highly paraffinic, of course, but as shown in Table I, the kerosene contained 1.1 vol.% olefins and 5.3 vol.% aromatics, the naphtha contained 2.0 vol.% aromatics,

and the jet fuel contained 4.6 vol.% olefins and 10.6 vol.% aromatics. This indicates that over short time periods, aromatics and olefins are not likely to be a problem. However, earlier studies on the methanation process have shown that sulfur compounds may react with the nickel in nickel catalysts almost quantitatively, resulting in catalyst poisoning. Therefore, for commercial operation, low sulfur-content feedstocks would be preferred.

Catalyst Used

A novel nickel-aluminum-alumina catalyst was used in this work. The same catalyst was used in all tests although several different batches were prepared. Since a standardized procedure was used, variations in catalyst composition were not great and activity was reproducible. Because details of the preparation and composition are presented in several patent applications, no further discussion of the catalyst is given.

Acknowledgment

This work was conducted as part of the Institute of Gas Technology's basic research program with funds provided by Institute Members and Contributors. The guidance and counsel of H. R. Linden, J. Huebler, and H. A. Dirksen are gratefully acknowledged. Tests were conducted by F. Todesca, R. F. Johnson, P. Cameron, and A. S. Lane.

Literature Cited

(1) American Society for Testing and Materials, "ASTM Standards," Part 18, pp. 1009-20, Philadelphia, 1964.
(2) Attari, A. A., "Abstracts of Papers," 152nd Meeting, ACS, Sept. 1966, L6.
(3) Bertolacini, R. J., Barney, J. E., II, *Anal. Chem.* **30**, 202 (1958).
(4) Cockerham, R. G., Percival, G., *Gas Council Res. Commun.* **GC 41** (1957).
(5) Cockerham, R. G., Percival, G., Division of Fuel Chemistry, American Chemical Society, *Preprints of Papers* **8**, (1) 52-60 (1964).
(6) Dent, F. J., *Gas J.* **311**, 344 (1962).
(7) Dent, F. J., Cockerham, R. G., Percival, G., British Patent **820,257** (Sept. 16, 1959).
(8) Dent, F. J., Cockerham, R. C., Percival, G., British Patent **894,582** (April 26, 1962); German Patent **1,118,919** (Dec. 7, 1961).
(9) Dent, F. J., *Australian Gas J.* **29**, 22 (1965).
(10) Hoggan, D., Battles, W. R., *Anal. Chem.* **34**, 1019 (1962).
(11) Shultz, E. B., Jr., Feldkirchner, H. L., Pyrcioch, E. J., *Chem. Eng. Progr. Symp. Ser.* **57 34**, 73 (1961).

RECEIVED November 17, 1966.

14

Cyclic Use of Calcined Dolomite to Desulfurize Fuels Undergoing Gasification

ARTHUR M. SQUIRES

Department of Chemical Engineering, The City College of The City University of New York, New York, N. Y.

Using [CaO+MgO] or [$CaCO_3$+MgO] to desulfurize fluid fuels has been hampered by lack of means to recover elemental sulfur from [CaS+MgO] while also recovering the original solid in a form suitable for reuse in a desulfurization step. The reaction of [CaS+MgO] with steam and CO_2 has been investigated at ca. *1000°F. and 220 p.s.i.a. Gaseous product contained H_2S at a concentration suitable for a Claus system. Solid product underwent no degradation in particle size and was suitable for reuse to absorb H_2S from fuel gases or vapors.*

Raw fluid fuels, derived for example from coal and heavy residual oils by gasification, carbonization, or cracking, may be substantially desulfurized by reacting at high temperature with calcined dolomite. This solid can also remove CO_2 from a gas stream; it has the power to convert CO and steam to H_2, and it may participate in the gasification of carbon by steam under thermal neutrality.

The cyclic use of calcined dolomite for these purposes has previously been hampered by lack of means to recover elemental sulfur from sulfurized calcined dolomite, containing CaS, while at the same time recovering solid in a form suitable for reuse.

The reaction of steam and CO_2 at high pressure with sulfurized calcined dolomite,

$$[CaS+MgO] + H_2O + CO_2 \rightarrow [CaCO_3+MgO] + H_2S \quad (1)$$

can be used to generate a gas stream containing H_2S at a concentration well above the minimum concentration which can be used by a Claus sulfur recovery system. Later, the solid product can be calcined at high temperature to provide a solid containing CaO (Reaction 2).

$$[CaCO_3+MgO] \rightarrow [CaO+MgO] + CO_2 \quad (2)$$

The latter solid can be used to remove H_2S from a fuel gas (Reaction 3).

$$[CaO+MgO] + H_2S \rightarrow [CaS+MgO] + H_2O \quad (3)$$

Reactions 1, 2, and 3 can be combined in a cyclic process to desulfurize a fuel undergoing gasification. Heat developed by Reaction 1 is at a level suitable for raising or superheating high pressure steam.

Alternatively, the solid product of Reaction 1 can be used directly to remove H_2S from a fuel gas at high temperature by reversing Reaction 1. The temperature should preferably be just a little below the equilibrium decomposition temperature of $CaCO_3$ at the prevailing partial pressure of CO_2.

The solid product of Reaction 2 can be used to promote CO shift.

$$[CaO+MgO] + H_2O + CO \rightarrow [CaCO_3+MgO] + H_2 \quad (4)$$

This reaction was the basis of the CO-shift process developed by Gesellschaft für Kohlentechnik during the 1920's (*24*). The process was conducted in fixed beds, had poor thermal efficiency, and never caught on. An improved version which uses fluidized beds may find modern applications. In this version, Reaction 4 may be combined with Reactions 1, 2, and 3 in a cyclic process in which elemental sulfur is recovered.

The solid product of Reaction 2 can also participate in the gasification of carbon by steam (Reaction 5).

$$[CaO+MgO] + 2\,H_2O + C \rightarrow [CaCO_3+MgO] + 2\,H_2 \quad (5)$$

This reaction is the basis of Consolidation Coal Co.'s carbon dioxide acceptor gasification process (*13, 17, 18*), which eliminates need for oxygen to provide heat to the steam-carbon reaction. The process could be modified for recovering elemental sulfur by incorporating a step using Reaction 1.

Residual oils might be gasified or cracked over calcined dolomite with recovery of elemental sulfur in a cyclic process incorporating Reaction 1. A version of this process may be useful in providing sulfur-free fuel to existing power station boilers in communities which impose restrictions on SO_2 content of stack gases.

These new fuel-desulfurization processes reject little heat at low temperatures. If a fuel gas is to be used in a combustion or if the gas is to be subjected to further processing at high temperature—*e.g.*, CO shift —the new desulfurization processes have the advantage that the heat exchange required to cool the gases to a low temperature sulfur-removal step is eliminated. The processes are well-suited to schemes which produce a clean fuel gas to be burned at high pressure in an advanced power cycle. Indeed, the concept of the new processes was a result of a search

for a combination incorporating fuel gasification at high pressure, fuel-gas cleanup, and an advanced power cycle which could provide electricity at lower cost. Such a combination would be adopted by the power industry as much for economy as for providing dust-free and sulfur-free effluent. Power cycles which significantly improve efficiency are the supercharged boiler cycle—a cycle incorporating a magnetohydrodynamic device which rejects heat to the steam cycle—and a top heat power cycle, in which the temperature of steam is raised by directly adding the products of combustion of a clean fuel with oxygen or air (*65, 66, 67*).

Dolomite is cheap and widely available. The solids produced by Reactions 1, 2, and 3 are rugged and suitable for use in fluidized beds (*18*).

This paper discusses the thermodynamic equilibria which govern the proposed new desulfurization processes, gives results of exploratory bench-scale studies, reviews the relevant dolomite chemistry, and briefly indicates some of the potential applications.

Process Thermodynamics

Thermodynamic Equilibria. Figure 1 gives the equilibrium constant for Reaction 3a.

$$CaO + H_2S \rightarrow CaS + H_2O \qquad (3a)$$

CaO is thus an effective desulfurization agent at temperatures as high as 2000°F.

Figure 2, showing the equilibrium constant for Reaction 1a,

$$CaS + H_2O + CO_2 \rightarrow CaCO_3 + H_2S \qquad (1a)$$

illustrates the basis for the proposed new desulfurization processes. At temperatures below *ca.* 1100°F. and at pressures above *ca.* 4 atm. for example, Reaction 1 can be used to derive a gas containing H_2S at a concentration which permits recovery of elemental sulfur in a Claus system.

The curve of Figure 2 is so steep that the reverse of Reaction 1 can be used to desulfurize a gas at temperatures above *ca.* 1600°F.

Figure 3 gives the equilibrium constant for the reaction

$$CaO + H_2O + CO = CaCO_3 + H_2 \qquad (4a)$$

which must often be considered in finding the composition of gas desulfurized by the new process.

Figure 4 is an estimate of the equilibrium constant for Reaction 6.

$$\frac{CaSO_4}{4} + H_2 \rightarrow \frac{CaS}{4} + H_2O \qquad (6)$$

The equilibrium constant for Reaction 7,

$$\frac{CaSO_3}{3} + H_2 \rightarrow \frac{CaS}{3} + H_2O \qquad (7)$$

is on the order of 2–5 times larger. A key to the success of Consolidation's CO_2 acceptor process is control of conditions for calcining [$CaCO_3$+ MgO] so that sulfur is expelled as SO_2. An oxygen-rich combustion would "fix" the sulfur permanently as $CaSO_4$, and a fuel-rich combustion is used to provide a calciner offgas containing H_2. The amount of H_2 is regulated to allow CaS to oxidize to $CaSO_4$ so that SO_2 can be rejected as a result of the reaction between CaS and $CaSO_4$ (*18, 78*).

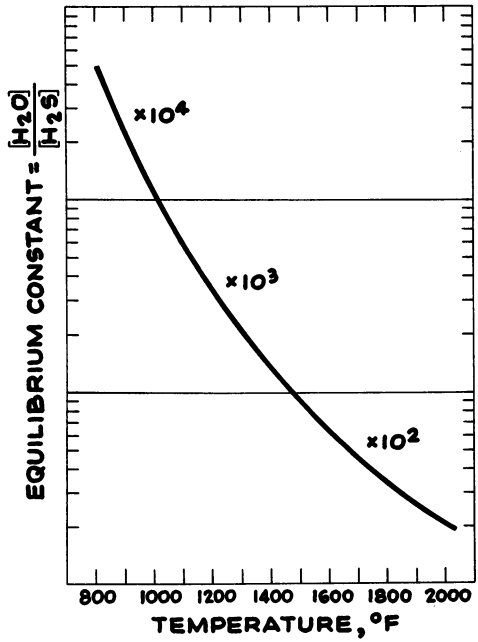

Figure 1. Equilibrium constant for the reaction: CaO + H_2S → CaS + H_2O

In contrast to Consolidation's procedure, one wishes to preserve CaS unchanged during a calcination step in the new desulfurization process, and the calciner off-gas should contain H_2 in an amount greater than that called for by Figure 4. Since $CaSO_4$ is readily reduced by H_2 to CaS at 930°F. (*53*), it would appear desirable that H_2 also be present during Reaction 1 to avoid oxidation of CaS by steam.

If CaO is present, the steam partial pressure should not exceed the equilibrium decomposition pressure of $Ca(OH)_2$ since the conversion of

CaO to $Ca(OH)_2$ would cause the solid to decrepitate (*24*). If both CaO and $CaCO_3$ are present at a temperature above about 1150°F., the steam partial pressure should not exceed a critical value on the order of 10–13 atm., or a melt will form (*18, 50, 76*).

Equilibrium prevents formation of MgS under all conditions encountered in the new desulfurization process.

Sources of Thermodynamic Data. The curve of Figure 1 is based upon the equation: $\log [H_2O]/[H_2S] = (3421.5/T) - 0.190$, where [. . .] signifies mole fraction and T = °K. The equation is derived from Rosenqvist (*54*), who studied the equilibrium over the range 1396°–2597°F. Uno (*72*) gave an equation, based upon data between 1652° and 2012°F., which agrees well with Rosenqvist over the range of Uno's data, but which extrapolates to lower values at lower temperatures. Data by Curran *et al.* (*18*) between 1310° and 1660°F. fall above the curve in Figure 1. Additional measurements would be desirable in the low-temperature range, and equilibria for Reaction 3a might well be derived from careful measurements of equilibria for Reaction 1a.

Determining equilibrium decomposition pressures of calcite has proved a durable problem, and dubious values have appeared recently

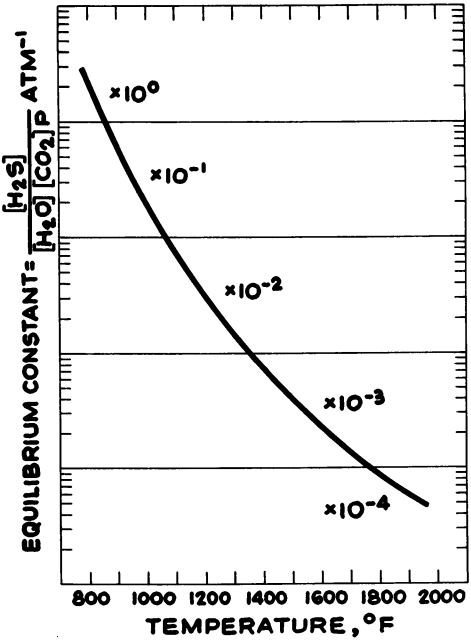

Figure 2. Equilibrium constant for the reaction: $CaS + H_2O + CO_2 \rightarrow CaCO_3 + H_2S$

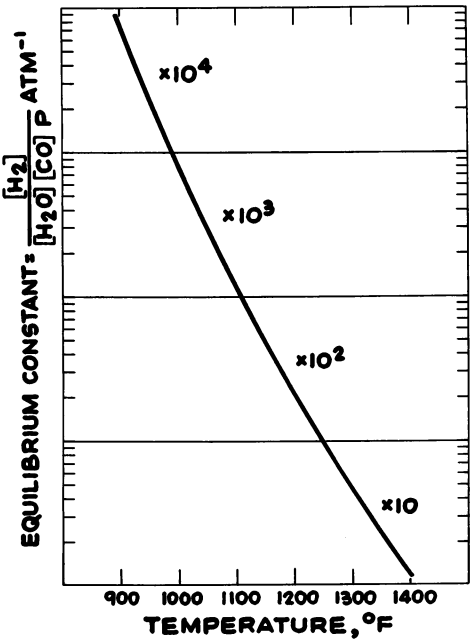

Figure 3. Equilibrium constant for the reaction: $CaO + H_2O + CO \rightarrow CaCO_3 + H_2$

(*33, 46*). Following Hill and Winter (*35*), Kubaschewski and Evans (*43*) adopted the equation: log $P_{CO_2} = -(8799.7/T) + 7.521$, where P_{CO_2} = equilibrium decomposition pressure in atmospheres; this equation is used here. Hill and Winter's data were between 840° and 1659°F.; no one else has made such careful measurements at such low temperatures. Their data agree well with Southard and Royster (*64*) between 1427° and 1652°F. and with Smyth and Adams (*63*) between 1567° and 1664°F. Smyth and Adams' data extended to 2266°F., and data obtained by Consolidation Coal Co. between 1472° and 1895°F. agree well with Smyth and Adams' data at higher temperatures (*16*). Consolidation's measurements were conducted on a dolomite having a Ca/Mg atomic ratio of about 1.03. An ingenious new technique was used: a bed of the solid was fluidized with N_2 and CO_2, and the temperature of the bed was cycled a few degrees above and a few degrees below the equilibrium decomposition temperature, which was identified by a thermal conductivity cell capable of determining precisely the instant at which the exit gas showed zero change in composition.

In obtaining the curve of Figure 4, the free energy of CaS was deduced from Uno's data (*72*) to provide an estimate which is probably low. Free energies of CaO, $CaSO_4$, H_2, and H_2O were derived from heats

of formation and entropies at 298°K. from Kubaschewski and Evans (*43*) and from increments in these functions at higher temperatures from Kelley (*39*). Erdös (*22*) estimated the heat of formation of $CaSO_3$ at 25°C. to be 276.3 kcal. per mole; a rough estimate of 272 kcal. can be derived from a value given for the heat of formation of the dihydrate (*36*). The entropy of $CaSO_3$ was given as 24.2 e. u. at 25°C. (*40*). The heat capacities of $CaSO_3$ and $CaCO_3$ are within 0.5% at 298°K.; thus, Kelley's increments (*39*) for the heat content and entropy of $CaCO_3$ may be used to obtain a rough estimate of the free energy of $CaSO_3$ at higher temperatures.

The equilibrium decomposition pressure of $Ca(OH)_2$ may be estimated from an equation based upon data by Tamaru and Siomi (*69*): $\log P_{H_2O} = -(5464.5/T) + 6.949$. These authors measured decomposition pressures from 760° to 930°F. Their equation agrees well with data by Halstead and Moore (*32*) at 950°F. and with data by Drägert between 570° and 830°F. (*37*). Berg and Rassonskaya's data (*3*) are probably faulty.

Experimental Studies

Exploratory bench-scale experimental studies were undertaken by Walter C. McCrone Associates, Chicago, Ill., primarily to demonstrate (a) that Reaction 1 can produce a gas containing H_2S at a concentration

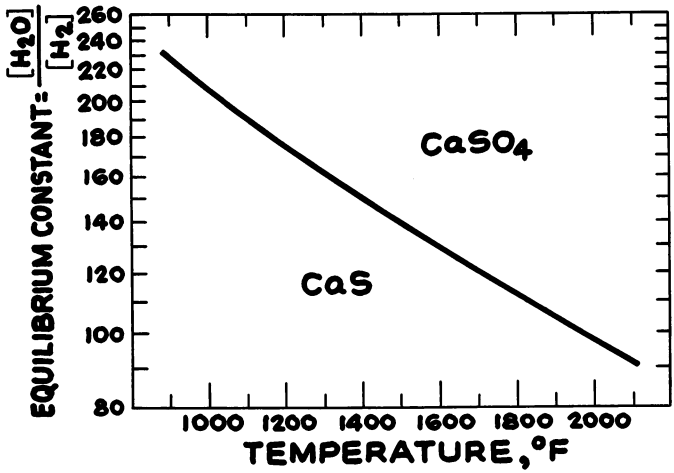

Figure 4. Rough estimate of equilibrium constant for: $\frac{CaSO_4}{4} + H_2 \rightarrow \frac{CaS}{4} + H_2O$

sufficient for the Claus process, and (b) that the solid does not undergo chemically-induced decrepitation during an operation which includes Reactions 1, 2, and 3. This was to be done at minimum cost, and no effort was to be made to determine reaction kinetics or to confirm chemical equilibria.

Results. Dolomite was supplied by Dolese & Shepard Co. of LaGrange, Ill. This is a typical dolomite of the Chicago area and has a Ca/Mg atomic ratio of 1.10. Reactions were conducted in a fixed bed of particles of 16–30 mesh (NBS sieves).

Reaction 4 was conducted over calcined dolomite at about 1250°F. and between about 140 and 315 p.s.i.a. Two initial gas mixtures were used, containing H_2:CO in ratios 1.0 and 1.6 respectively. The gas mixtures were humidified with steam to afford H_2O:CO ratios between about 1.2 and 1.8. Effluent contained no CO or CO_2 detectable by gas chromatographic analysis sensitive to less than 0.01% of either constituent. No hydrocarbon synthesis occurred.

Reactions 3 and 4 were conducted simultaneously over calcined dolomite at about 1200°F. and between about 140 and 215 p.s.i.a. The initial gas mixture contained about 1% H_2S, the balance consisting of equal quantities of H_2 and CO. Concentrations of H_2S in effluent ranged from 2 to 140 p.p.m. and depended upon the quantity of steam in effluent.

Reaction 3 was conducted over calcined dolomite at about 1100°F. and atmospheric pressure until substantially all of the material was converted to [CaS+MgO]. The inlet gas mixture contained about 85% N_2, 10% H_2S, and 5% H_2. During this operation, effluent contained about 10 p.p.m. of H_2S.

Reaction 1 was conducted over the resulting solid [CaS+MgO] at *ca.* 1000°–1100°F. and *ca.* 220 p.s.i.a. The initial gas mixture contained about 82% CO_2 and about 9% each of H_2 and CO. The gas mixture was humidified with steam to afford a CO_2:H_2O ratio of about 1.75. Dry effluent contained 20–24% H_2S, levels which are satisfactory for feed gas to a Claus system. It is reasonably certain that a much higher concentration of H_2S could have been obtained by using a lower CO_2:H_2O ratio.

None of the foregoing chemical manipulations produced decrepitation of the solid or any evident change in the shape of particles viewed under a microscope; sharp edges and points were still to be seen.

Procedures. The reaction system used components supplied by Autoclave Engineers, Inc. of Erie, Pa. The reactor was 1-in. i.d. × 36-in. inside depth, and was fitted with a 5/16-in. thermowell containing five Chromel-P-Alumel thermocouples. An active dolomite bed between 8 and 12 in. depth was used, the remainder of the reactor being packed with alumina chips. The reactor was situated within two Hoskins furnaces, each affording a heating length of 12 in. Tanks containing various mixtures of gases at high pressure were obtained from Matheson Co. of Joliet, Ill. Gases were passed through a pool of water in a saturator immersed in a heated oil bath. The saturator was 2-in. i.d. × 10-in. inside depth and was fitted with a filter disc for dispersion of gases into the pool. The superficial velocity of gas in the pool was typically less than 0.001 ft./sec. in tests conducted at high pressure. Gas from the saturator passed upward through the reactor, from the reactor through a filter, through a cooling

coil, and into a chamber collecting water. Dry gas was let down in pressure across a needle valve and sent to analysis. Most constituents were analyzed by a gas chromatograph (Perkin-Elmer Model 154) having a column of 1/4-in. o.d. copper tubing, 5 ft. long, packed with 28–200 mesh silica gel, held at 125°C. and swept with helium. Known gas mixtures, analyzed by Matheson, were used to calibrate the chromatograph for CO_2, CO, and H_2. Kitagawa H_2S low range detector tubes were used to analyze for H_2S at low concentrations. The Kitagawa "pump" was not used; a tube was placed in the gas-sampling line, and by trial and error the flow through the tube was adjusted to about 100 ml. in 3 minutes. A modification of the Tutwiler method was used to determine H_2S at high concentrations (59). The method was calibrated against a gas mixture analyzed by Matheson and stated by them to contain 10.9% H_2S.

Calcinations were conducted at atmospheric pressure with either N_2 or 90:10 N_2:H_2 flowing through the reactor.

Selected Results. Figure 5 illustrates the breakthrough of CO and CO_2 at the end of a run using an initial gas mixture containing H_2:CO in the ratio 1.62. Flow of the initial gas at breakthrough was about 250 ml. (70°F., 1 atm.)/min.; pressure was 315 p.s.i.a.; temperature in the active bed ranged from 1217° to 1290°F. The gas was humidified to a H_2O:CO ratio of 1.83. Neither CO nor CO_2 could be detected in effluent prior to breakthrough. The rise in CO occurred a little earlier than the rise in CO_2. The width of the temperature peak was approximately the same as the time interval during which CO and CO_2 rose to their final steady values. This time interval can be interpreted as the time required for the reaction front to pass any given point in the active bed. The catalytic effect of MgO for the CO-shift reaction is indicated by presence of CO_2 in the gas following breakthrough since the initial gas mixture contained no CO_2.

Data like those in Figure 5 were presented by Gluud *et al.* (*24*) for operations at atmospheric pressure and about 930°F.

Reaction 3 was conducted at atmospheric pressure with gas containing 85% N_2, 10% H_2S, and 5% H_2, humidified at 79°F., and flowing at about 300 ml./min. Temperatures in the active bed ranged from 976° to 1138°F., the temperature sharply dropping toward the outlet end. The ratio of H_2O:H_2S leaving the bed prior to breakthrough of H_2S was approximately 14,000—a value in close agreement with Figure 1 for the temperature at the outlet of the bed. First signs of breakthrough appeared when the conversion of CaO to CaS was roughly 80%; the final conversion to CaS was over 90%.

After Reaction 3, Reaction 1 was conducted at atmospheric pressure with gas humidified at 75°F. The initial gas mixture contained 81.7% CO_2, 9.3% H_2, and 9.0% CO. Dry gas effluent contained 1.1% H_2S. The active bed temperature ranged from 976° to 1138°F., the temperature sharply dropping toward the outlet end. The value of $[H_2S]/[H_2O]$

$[CO_2]$ P in reactor effluent was 0.21, which corresponds to 990°F. at equilibrium, according to Figure 2. The purpose of this atmospheric-pressure, low humidity step was to assure that no CaO remained in the active bed. If this step had been omitted, $Ca(OH)_2$ might have formed at steam partial pressures to which the solid was later subjected.

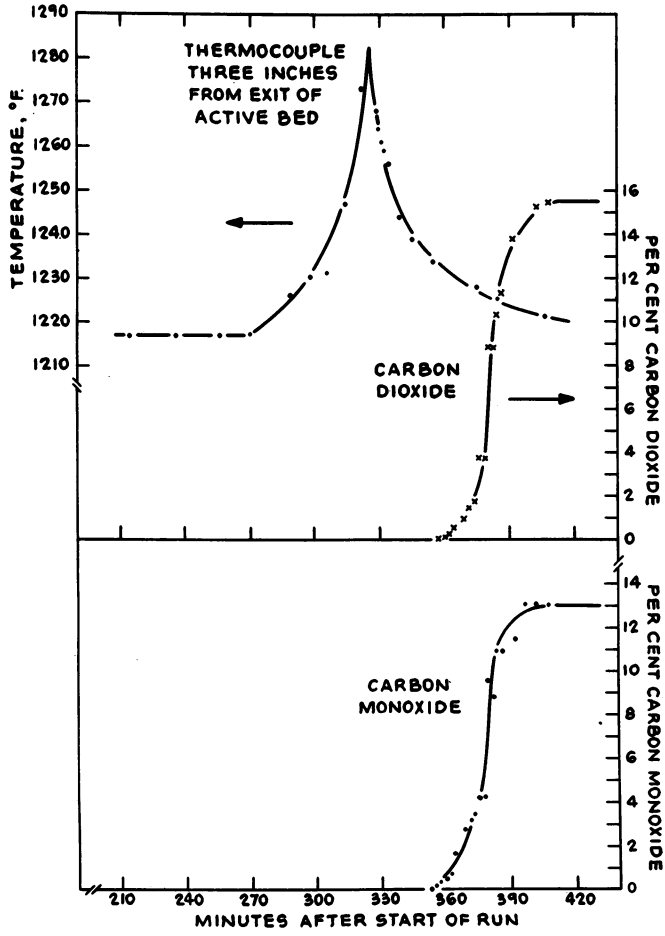

Figure 5. Breakthrough of carbon oxides when solid is used up by Reaction 4 in a fixed bed at 315 p.s.i.a.

Later, the pressure was raised to 220 p.s.i.a., and the saturator temperature was raised to 302°F., providing a CO_2:H_2O ratio of 1.79. The active bed temperature remained as before. Dry gas effluent contained 20.2% H_2S and corresponded to equilibrium for Reaction 1 at about 1040°F. The temperature of the bed was lowered to the range 891° to 1040°F., and the pressure fell to 215 p.s.i.a., reducing the CO_2:H_2O ratio

to 1.73. The H_2S content of dry gas increased to 24.0%, which corresponded to equilibrium at about 1010°F. [Most of the bed was at about 1000°F., and CaS may have been gone from solid near the exit of the bed by this time since conditions had favored production of H_2S near the exit throughout the experiment.]

These results demonstrated the ability of Reaction 1 to provide a dry gas containing H_2S in a concentration adequate for the Claus process.

Relevant Dolomite Chemistry

Primary sources of information are (a) the series of papers from the Gesellschaft für Kohlentechnik (*24*), reporting in 1930 on studies of a process to manufacture H_2 by reforming coke-oven gas with steam and thereafter shifting the reformed gas with steam over calcined dolomite; (b) the series of reports from Consolidated Coal Co. on the CO_2 acceptor process (*13, 17, 18*). The latter reports are particularly valuable for the evidence that the solids [CaO+MgO], [$CaCO_3$+MgO], and [CaS+MgO] are rugged materials which stand up under fluidization and do not decrepitate under various chemical reactions which convert the solids from one to another. Dolomite is the mixed carbonate of Ca and Mg, "normal" dolomite being written $CaCO_3 \cdot MgCO_3$. It is a common rock of wide geographical distribution, and often occurs in a state of high purity. Analyses of typical dolomites were given by Sikabonyi (*61*) and Willman (*74*). Dolomite is a member of a large class of rhombohedral carbonates, which includes calcite and magnesite. These carbonates are built of alternating layers of carbonate ions and cations. In dolomite, ideally, cation planes populated entirely by Mg^{2+} alternate with planes populated entirely by Ca^{2+} (*9*). Natural dolomite often diverges from the ideal of one atom of Mg for each Ca, the latter usually being present in excess. True dolomites richer in Mg are seldom encountered (*24, 26*).

Formation of [CaO+MgO]. If dolomite is heated in a vacuum, it decomposes in one step, with CO_2 evolution and formation of a solid comprising an intimate intermingling of tiny crystallites of CaO and MgO (*11*). The product may be written [CaO+MgO] as a reminder that it is not a true chemical species. Decomposition proceeds from the outside surface inward.

In an atmosphere of CO_2, dolomite decomposes in two steps (*2, 23, 34*). Wilsdorf and Haul (*75*) followed the first step with x-ray diffraction techniques. Decomposition proceeded from the surface inward, and the state of order in the kernel of undecomposed dolomite remained perfect. At 600°C. and 100 mm. Hg of CO_2, predominantly single-crystal patterns for calcite were found—the $CaCO_3$ crystallites apparently being oriented as in the original lattice. At 800°C. and 650 mm. Hg of CO_2, powder

calcite patterns were obtained, randomization of the $CaCO_3$ crystallites having occurred. If dolomite is decomposed at moderate CO_2 pressures, as in a calcination process, the calcite produced is essentially pure $CaCO_3$ (*27*), and the product may be written [$CaCO_3$+MgO]. At extremely high CO_2 pressures, the product is a mixture of crystallites of MgO and of a magnesian calcite—*i.e.*, a calcite containing $MgCO_3$ in solid solution (*29, 33*).

Bischoff (*6*) and MacIntire and Stansel (*44*) found that both stages in the decomposition of dolomite were catalyzed by steam. Schwob (*58*) and Graf (*28*) reported a catalytic effect of alkali. There is evidence that the decomposition of [$CaCO_3$+MgO] is faster than that of $CaCO_3$ (*34*).

From the foregoing it will be recognized that the intimate mixture of CaO and MgO crystallites which results from the total calcination of dolomite retains no memory of the original dolomite structure. Goldsmith (*26*) believed that this solid would be indistinguishable from one which could be prepared by calcining a mixed precipitate of $CaCO_3$ and $MgCO_3$. Such a precipitate never shows signs of dolomitic order if prepared in the laboratory from solutions at room temperature (*27*). Artificially made dolomites are known (*29, 30, 33*), but these materials and the extensive literature on the problem of dolomite formation in nature are not particularly relevant to the new desulfurization process since [CaO+MgO] can be prepared artificially for use in the process without the material's having passed through the dolomitic state.

Clark *et al.* (*12*) studied the sintering of MgO at high temperatures. They found a sudden increase in strength at a temperature well below that at which sintering proper with densification sets in, and they interpreted this increase to result from destruction of adsorbed moisture films on the surfaces of the particles—*i.e.*, the replacement of hydrogen or hydroxyl bonding between particles by primary ionic bonds.

Recarbonation of [CaO+MgO] to Form [$CaCO_3$+MgO]. Gluud *et al.* (*24*) studied the recarbonation, at *ca.* 1050°F., of samples of [CaO+MgO] prepared from a variety of dolomitic rocks. Uniformly, the initial reaction with CO_2 was extremely rapid. The course of later stages of the reaction depended upon the Ca/Mg atomic ratio of the starting material. Gluud *et al.* recommended that a dolomite be selected having a Ca/Mg ratio as close to unity as could be found. The later stages of recarbonation of [CaO+MgO] from a stone having a high Ca/Mg ratio were slow, and the reaction ceased for all practicable purposes far short of complete conversion of CaO to $CaCO_3$. Moreover, stones having a high Ca/Mg ratio displayed poor resistance to deactivation when calcined. Working with dolomites having Ca/Mg ratios below about 1.2, Gluud *et al.* were able to achieve 90% recarbonation of CaO at good rates, provided the solid had not been exposed to a temperature

above *ca.* 1920°F. If a dolomite was calcined at 2190°F., its reactivity was drastically reduced. Other workers (*5, 11, 51*) confirmed that recarbonation is rapid and nearly complete if a Ca/Mg ratio below about 1.1 is used.

Asboth (*1*) recommended an artificial dolomite, prepared by precipitating $CaCO_3$ and $MgCO_3$ in the molar ratio 40:60 on freshly made silica gel.

Curran *et al.* (*18*) subjected a number of dolomites to tests of their suitability for the CO_2 acceptor process, which inherently requires using a high calcination temperature (of the order of 1950°F.). Stone from the Greenfield formation of western Ohio, with the unusually low Ca/Mg ratio of 0.987, was selected as the best available. It was cycled many times between a calcination and a recarbonation at 1650°F.; calcination temperatures of 1900°, 1950°, and 2000°F. were used. There was no significant loss of reactivity, and no significant degradation in particle size occurred, although the tests were conducted in fluidized beds. In a similar series of tests, the Greenfield stone was converted to [CaS+MgO], from which [CaO+MgO] was regenerated at 1950°F. by a fuel-rich calcination expelling SO_2. The latter solid displayed good reactivity after a number of the sulfur cycles.

Curran and co-workers' experience with the Greenfield stone provides important evidence bearing on the probable feasibility of the proposed new desulfurization processes. Using the Greenfield stone, the new processes should be operable in gas-production and gas-purification steps at pressures ranging upward from 100 atm.

Gluud *et al.* (*24*) reported that CO_2 was taken up by [CaO+MgO] at 570°F. Dry CaO absorbs only an insignificant amount of CO_2 at this temperature; it reacts markedly at 660° and rapidly at 790°F. (*47*), but the reaction proceeds readily only to the extent that about one-half of the CaO is recarbonated (*5, 10, 24, 41, 51, 70*). The solid [$CaCO_3$+CaO] decomposes at a rate some four to six times faster than calcite (*10*). Shushunov and Fedyakova (*60*) studied the kinetics of CaO + CO_2.

As Gluud *et al.* recognized, calcination of a Mg-poor dolomite probably puts some CaO in a state so that only about half of it can absorb CO_2, in accordance with the behavior of lime. This accounts for the poor performance of dolomites having high Ca/Mg ratios. Gluud *et al.* warned against selecting a dolomite having calcite strata.

Although MgO takes up CO_2 readily at atmospheric temperature in presence of water vapor (*48*), its reaction with CO_2 at high temperature is extremely slow (*5, 10, 14, 15, 33*). Little recarbonation of MgO will occur even if CO_2 exceeds the equilibrium decomposition pressure of $MgCO_3$ when Reaction 1 is carried out.

Using [CaO+MgO] to Promote CO-Shift and the H_2O-C Reaction. DuMotay (*20*) first proposed using lime to promote CO-shift in 1880, and this idea received persistent attention without ever coming into commercial use (Table I). Greenwood (*31*) and Taylor (*71*) reviewed the state of the art in 1920 and 1921, respectively, and Schmidt (*57*) reviewed it in 1935. The most highly developed ideas were advanced by Gesellschaft für Kohlentechnik (*24*) and Bössner and Marischka (*8*).

The Gesellschaft für Kohlentechnik recognized that MgO crystallites in [CaO+MgO] are catalytic for CO-shift. Magnesia can be prepared

Table I. Patents Incorporating CO Shift Over CaO or $Ca(OH)_2$

	U.S. Patents	
E. Ellenberger	989,955	(April 18, 1911)
C. Ellis	1,173,417	(Feb. 29, 1916)
P. Siedler, K. Henke	1,181,264	(May 2, 1916)
J. H. DeGraer	1,583,673	(May 4, 1926)
W. Gluud, K. Keller, R. Schönfelder, W. Klempt	1,816,523	(July 28, 1931)
W. Gluud, W. Klempt	1,950,981	(March 13, 1934)
F. Bössner, C. Marischka	1,985,441	(Dec. 25, 1934)
F. Bössner, C. Marischka	2,183,301	(Dec. 12, 1939)
	British Patents	
Chemische Fabrik Griesheim-Elektron	2,523 of 1909	(Sept. 30, 1909)
Chemische Fabrik Griesheim-Elektron	13,049 of 1912	(Jan. 30, 1913)
Societe L'Air Liquide	7,147 of 1913	(Oct. 9, 1913)
H. E. F. Goold-Adams, H. C. Greenwood	137,340	(Jan. 15, 1920)
F. Gülker	275,273	(Dec. 3, 1928)
H. Bomke	279,128	(Jan. 17, 1929)
F. Gülker	301,499	(Feb. 21, 1930)
Gesellschaft für Kohlentechnik	365,111	(filed July 10, 1930; not accepted)
Gesellschaft für Kohlentechnik	365,582	(filed July 17, 1930; not accepted)
Ateliers Generaux de Construction	370,834	(April 14, 1932)
F. Bössner, C. Marischka	473,575	(Oct. 15, 1937)
	German Patents	
W. Schoeller, W. Schrauth	248,290	(June 17, 1912)
Chemische Fabrik Griesheim-Elektron	263,649	(Sept. 8, 1913)
Chemische Fabrik Griesheim-Elektron	284,816	(June 5, 1915)
J. H. DeGraer	428,580	(May 7, 1926)
F. Gülker	446,488	(July 2, 1927)
H. Bomke	460,422	(May 30, 1928)
H. Bomke	516,843	(Jan. 28, 1931)
W. Klempt	533,461	(Sept. 15, 1931)
H. Bomke	555,003	(July 16, 1932)
H. Merkel (Heinrich Koppers GmbH)	1,048,264	(Jan. 8, 1959)

Table I. Continued

	French Patents	
Chemische Fabrik Griesheim-Elektron	409,506	(April 25, 1910)
E.-A. Prudhomme	603,639	(April 20, 1926)
F. Gülker	647,257	(Nov. 22, 1928)
Ateliers Generaux de Construction	723,837	(April 15, 1932)
F. Bössner, C. Marischka	812,877	(May 19, 1937)
Societe Industrielle des Carburants et Solvants	833,620	(Oct. 26, 1938)
	Austrian Patents	
F. Bössner, C. Marischka	151,969	(Dec. 27, 1937)
K. Asboth	172,931	(Oct. 25, 1952)
	Swiss Patents	
F. Bössner, C. Marischka	156,699	(Aug. 31, 1932)
Ateliers Generaux de Construction	160,165	(Feb. 28, 1933)
	Canadian Patent	
W. Gluud, K. Keller, R. Schönfelder, W. Klempt	284,298	(Oct. 30, 1929)

in far more active forms than can any of the other alkaline earth oxides; active magnesias are produced for use as industrial adsorbents having surface areas of the order of 200 sq. meters/gram (*49*). Gluud *et al.* demonstrated that [CaO+MgO] is catalytic for CO-shift at temperatures above about 750°F. while CaO showed no catalytic activity at any temperature. The catalytic worth of MgO was not altered when the solid was converted to [$CaCO_3$+MgO]. From this fact as well as from the ease with which CaO in [CaO+MgO] may be recarbonated one may infer that [$CaCO_3$+MgO] has an open, porous structure.

The Gesellschaft für Kohlentechnik's CO-shift process was conducted at atmospheric pressure in a fixed bed of [CaO+MgO]. The operation was cyclic, a period of H_2 manufacture being followed by a period in which [$CaCO_3$+MgO] was calcined, the bed of solid remaining in place in a reactor. Final CO concentrations, generally below 0.1%, were achieved at 930°F. Breakthrough of CO occurred at a space velocity of about 130 vol./hr.-vol. based upon CO content of the gas and upon the [CaO+MgO] remaining in the bed. In operating a pilot plant on the scale of 200,000 std. cu. ft. per day, no decrepitation or loss of absorptive capacity was found after many cycles of operation, and it was reported that the life of a dolomite charge should be three months at the minimum.

A serious defect in the Gesellschaft für Kohlentechnik's process thinking was exposed when operations were conducted on a large scale. So much heat was generated during the shift step that the temperature became too high for good CO_2 removal unless untreated gases were introduced cold. This proved unworkable since $Ca(OH)_2$ formed and the

solid decrepitated. The difficulty was obviated by introducing a cooling phase in the cycle, in which the reaction bed was cooled by circulating air at 750°F. after the bed had been partly used up. Another defect was that several hundred percent of excess air had to be used to keep the calcination temperature below a level at which solid reactivity would suffer. As a consequence, the thermal efficiency of the over-all process was poor, and both fuel gas and the CO-containing gas to be treated had to be low in sulfur to avoid converting large amounts of CaO to $CaSO_4$, which not only would destroy its usefulness but would probably also lead to losses of H_2 by reducing $CaSO_4$ to CaS in the shift step.

Table II. Patents Incorporating H_2O-C Reaction Over CaO

	U.S. Patents	
J. F. Coffey	2,538,235	(Jan. 16, 1951)
E. Gorin	2,682,455	(June 29, 1954)
E. Gorin	2,705,672	(April 5, 1955)
R. P. Tarbox	2,807,529	(Sept. 24, 1957)
E. Gorin, C. H. Rice	3,115,394	(Dec. 24, 1963)
	British Patents	
Friedrich Krupp of Essen	8,426 of 1892	(June 18, 1892)
O. Dieffenbach, W. Moldenhauer	7,718 of 1910	(March 30, 1911)
	7,719 of 1910	(filed March 30, 1910; not accepted)
	7,720 of 1910	(March 30, 1911)
	8,734 of 1910	(Sept. 8, 1910)
H. J. Prins	128,273	(June 26, 1919)
Pittsburgh Consolidation Coal Co.	673,170	(June 4, 1952)
E. A. Bruggeman	716,740	(Oct. 13, 1954)
	German Patent	
Chemische Fabrik Griesheim-Elektron	284,816	(June 5, 1915)
	Austrian Patent	
Verein Telephon und Telegraphen-fabriks Aktien-Gesellschaft	155,941	(April 11, 1939)

DuMotay and Marechal (*21*) first proposed using lime to aid the gasification of carbon by steam in 1867, and a large patent literature has ensued (Table II). Taylor (*71*) and Schmidt (*57*) reviewed the art. Dent (*19*) reported that "trouble occurred owing to the caking of the charge" during a test at 28 atm. The nature of this trouble was identified by Consolidation Coal Co. and circumvented in the CO_2 acceptor process by keeping the partial pressure of steam below 13 atm. (*18*).

A patent literature has developed around the idea of using heat from the recarbonation of CaO to supply endothermic heat needed for the reforming of hydrocarbons by steam (Table III). Marisic (*45*) visualized using heat from this reaction to sustain catalytic cracking of oils.

Table III. Patents Incorporating Steam-Hydrocarbon Reforming Over CaO

	U.S. Patents	
R. Williams	1,938,202	(Dec. 5, 1933)
J. C. Woodhouse	1,960,886	(May 29, 1934)
W. W. Odell	2,602,019	(July 1, 1952)
E. Gorin	2,654,661	(Oct. 6, 1953)
E. Gorin	2,781,248	(Feb. 12, 1957)
E. Gorin, W. B. Retallick	3,108,857	(Oct. 29, 1963)
E. Gorin, C. H. Rice	3,115,394	(Dec. 24, 1963)
E. Gorin	3,188,179	(June 8, 1965)

Using Lime and [CaO+MgO] for Desulfurization. An historical method of desulfurizing town gas was treatment with $Ca(OH)_2$ at atmospheric temperature. The process was used until 1870 in Europe and until 1905 in England. General information may be found in Seil (*59*).

Mellor (*47*) stated that dry H_2S does not react with dry, cold CaO, but when heated, water is evolved, and the mass becomes yellow owing to separation of some elemental sulfur. Wickert (*73*) showed that the speed of reaction of H_2S with CaO rises sharply between 750° and 1100°F., and he stated that CaS is much harder and tougher than CaO. Taylor (*71*) stated that CaO at around 930° to 1020°F. catalytically converts CS_2 in presence of steam to CO_2 and H_2S, both of which are fixed by lime. A patent literature has evolved around the idea of using lime for fuel desulfurization (Table IV).

Schenck and Hammerschmidt (*56*) reported that CaS prepared by contacting $CaCO_3$ with H_2S and CO_2 at 1450° to 1830°F. was unsintered

Table IV. Patents Using CaO or $Ca(OH)_2$ for Fuel Desulfurization

	U.S. Patents	
F. W. Werner, E. T. Johnston	1,779,024	(Oct. 21, 1930)
R. G. Guthrie, O. J. Wilbor	2,214,926	(Sept. 17, 1940)
J. G. Schaafsma	2,364,390	(Dec. 5, 1944)
S. P. Robinson	2,551,905	(May 8, 1951)
H. N. Dunning	2,772,945	(Dec. 4, 1956)
E. Gorin, G. P. Curran, J. D. Batchellor	2,824,047	(Feb. 18, 1958)
L. N. Leum, P. M. Pitts	2,845,382	(July 29, 1958)
C. D. Shiah	2,970,956	(Feb. 7, 1961)
	British Patents	
Kohle und Eisenforschung GmbH	491,299	(Aug. 30, 1938)
Rheinische Kalksteinwerke GmbH	1,009,192	(March 8, 1962)
	German Patent	
W. Guntermann, F. Fischer, H. Kraus (Pintsch Bamag Aktiengesellschaft)	1,184,895	(Jan. 7, 1965)

and showed no loss of chemical reactivity. It had a pinkish cast, as did the [CaS+MgO] prepared by McCrone Associates.

A British patent (*4*) reported that CS_2, thiophene, and other organic sulfur compounds are dissociated with formation of H_2S if contacted with hot MgO. Carbon was deposited and could be burned off.

Gluud and Klempt (*25*) stated that organic sulfur compounds are split, with formation of H_2S, when town gas is contacted with calcined dolomite above about 1100°F. Kirillov and Budanov (*42*) showed that the decomposition of CS_2 over dolomite was a maximum at 1200°F., independent of steam concentration. Kakabadze (*38*) patented the use of hot calcined dolomite to purify gases of organic sulfur compounds. Zahn (*77*) reported that the calcined ankerite in the Bössner-Marischka process (*8*) was highly effective in removing organic sulfur, and he claimed that its catalytic worth for CO-shift was not impaired after prolonged use to remove such sulfur.

Dolomite is used in a moving bed to remove sulfur from hot "carburettor gas" of the Wiberg process used in Sweden to produce sponge iron (*68*). The quantity of dolomite charged is the temperature control on reducing gases to the Wiberg furnace, and dolomite is discharged typically containing only about 5 to 10% sulfur; no decrepitation of the dolomite lumps is experienced (*7*).

Converting [CaS+MgO] to [$CaCO_3$+MgO] and H_2S. Riesenfeld (*52*) studied the reaction of steam and CO_2 with CaS at atmospheric pressure, conducting four exploratory experiments between 896° and 1526°F. He did not intend to measure equilibria for the reaction, and he did not estimate equilibria from his data. The measurement at 1526°F. was more carefully made than the other three, and one can derive a reasonably good estimate of the equilibrium from Riesenfeld's results at this temperature; the estimate falls only about 10% above the curve of Figure 2. Crude estimates of equilibria from Riesenfeld's other three points lie 20% below, 50% below, and 120% above the curve of Figure 2. He did not report H_2S concentrations in product gas, but one can deduce (roughly) that about 2% H_2S was present in a run at 941°F., and lesser amounts at other temperatures. Riesenfeld concluded that the conversion of CaS to $CaCO_3$ by its reaction with steam and CO_2 is not a practicable proposition, although his results may now be regarded as confirmatory evidence in support of the conclusions which have been drawn from the tests conducted by McCrone Associates at higher pressure.

The reaction of liquid water and CO_2 with CaS has been recognized since 1817, when the town gas industry adopted dry purification with slaked lime. Used-up lime was decomposed by water and CO_2 when left in the open air—a process which contributed to the poisoning of air

around old gas works (*47*, *62*). The reaction was used commercially in the Claus-Chance process (*55*), which recovered H_2S from CaS waste from the Leblanc soda process.

Wickert (*73*) incorporated the reaction in a proposed process to eliminate sulfur from flue gases derived from heavy residual fuel oil. Wickert would use partial oxidation of the oil with air, desulfurize the resulting lean fuel gas with $CaCO_3$ at around 1460° to 1830°F., and cool the resulting CaS to atmospheric temperature, slurry this solid with water, and allow the slurry to react with CO_2-bearing flue gases. By comparison with the new desulfurization processes proposed here, Wickert's scheme has disadvantages: much heat would be discharged at low temperature and could not be put to use, and $CaCO_3$ would probably be recovered in such finely divided form that its separation from desulfurized fuel gases might be difficult.

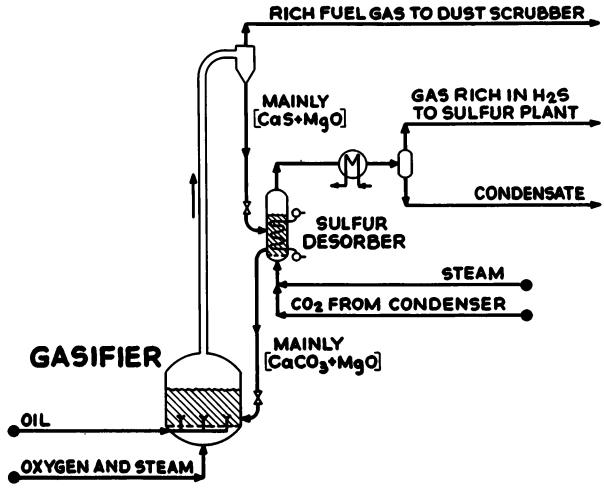

Figure 6. Scheme for making rich fuel gas for top heat power cycle

Process Applications

Cataloging and evaluating potential applications of the new desulfurization processes would fall outside the scope of this paper, which can only indicate briefly some of the possibilities.

Figure 6 illustrates a scheme for making a rich fuel gas from heavy residual oil, suitable for use in a top heat power cycle (*65*, *66*, *67*) in which the temperature of steam is raised by directly adding the products of combustion of the rich fuel gas with oxygen. A solid comprising mainly [$CaCO_3$+MgO] is fed to a fluidized bed in which oil is gasified by

oxygen and steam. The temperature might be around 1700°F., say, and should preferably be just a little below the equilibrium decomposition temperature of $CaCO_3$, so that CaO is not produced in the fluidized bed. Gaseous products are desulfurized by the reverse of Reaction 1. Wickert (73) reported that CaS is catalytic for the steam-carbon reaction, and one may be able to operate the gasification step in Figure 6 with only a small excess of steam beyond the amount called for by steam-carbon equilibrium. Solid is conveyed from the gasifier to an elevated cyclone, which delivers solid *via* a standpipe to the sulfur desorber. Here Reaction 1 is conducted in a fluidized bed using CO_2 supplied from the heat exchange in which steam is condensed from top heat cycle fluid. Heat from Reaction 1 is used to raise or superheat high-pressure steam. In a top heat cycle using Kuwait heavy residue (4.73% sulfur), this heat amounts typically to about 1.5% of the total water-heating, steam-raising, and steam-superheating duty. Off-gas from the sulfur desorber is cooled to condense excess steam, and gas rich in H_2S is sent to a sulfur plant.

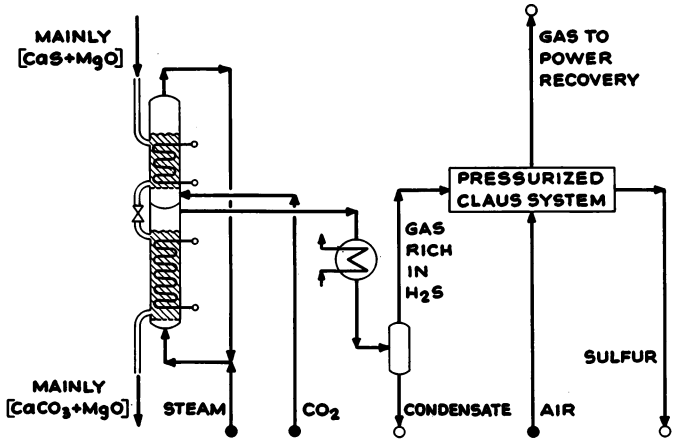

Figure 7. Sulfur desorber and sulfur recovery

Figure 7 shows equipment suitable for sulfur recovery when desulfurization is accomplished by means of Reaction 3 so that the solid charged to the sulfur desorber contains CaO. The sulfur desorber in Figure 7 houses two fluidized beds: a lower bed for conducting Reaction 1 and an upper bed in which CaO is converted to $CaCO_3$ in the absence of steam. Provision of the upper bed allows one to use a higher steam partial pressure in Reaction 1 than would otherwise be possible, for one does not have to worry about the formation of $Ca(OH)_2$. Both beds of Figure 7 might operate at *ca.* 1000°F.

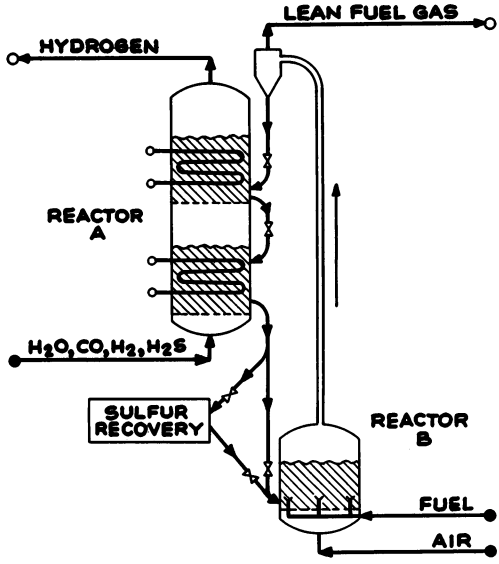

Figure 8. Conducting CO shift in a power-station context

In the context of the top heat power cycle, there is advantage in operating the Claus system under pressure since equipment exists both to provide high pressure air and to recover power from Claus system offgases.

Figure 8 illustrates an application in which CO shift is conducted by Reaction 4. Shift is carried out in reactor A, which houses two fluidized beds, the upper bed being held at a lower temperature. Spent solid is calcined in reactor B. Flow of gas and solid in reactor A is countercurrent. By conducting the greater portion of the shift reaction in the lower bed, at higher temperature, the calcining duty in reactor B is reduced. Also, the upper bed of reactor A can be operated at a much lower temperature than that needed in a single-bed reactor in order to avoid $Ca(OH)_2$. The upper and lower beds of reactor A might operate at 1100° and 1500°F.

The scheme of Figure 8 is obviously more attractive if one needs high level heat, available to the heat-transfer surfaces shown in reactor A, as well as need for H_2. This scheme would permit production of by-product H_2 in future power stations which use some combination incorporating pressurized fuel gasification, fuel-gas cleanup, and an advanced power cycle.

Figure 9 illustrates representative schemes in which oil cracking occurs with desulfurization. Reactor A of Figure 9 might operate at around 1400°F. Coke generated by cracking reactions in reactor A could

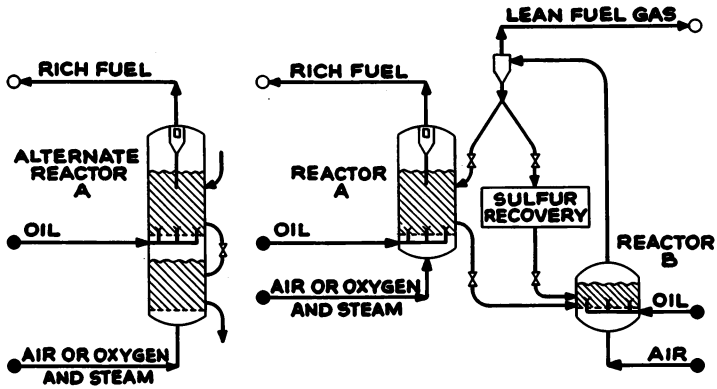

Figure 9. Representative schemes involving oil cracking

serve as at least part of the fuel used to calcine the solid in reactor B. The splitting of the oil into two fuel fractions, one rich in H_2 and the other lean, is advantageous in the context of the top heat cycle. Hydrogen in rich fuel gas is discharged from the cycle as liquid water. Putting H_2 into the rich fuel-gas path has the advantage of reducing water vapor content of flue gas generated by combustion of the lean fuel gas from reactor B.

The air or oxygen requirements for reactor A can be considerably reduced by drawing on heat of recarbonation of CaO as well as heat from Reaction 4. A fuel gas of high calorific content can be produced even with the use of air. Such a gas is well-suited for a top heat cycle using air instead of oxygen.

An interesting possibility is to use air in reactor A to produce clean fuel of high calorific value for existing power-station boilers in communities which place restrictions upon SO_2 in stack gases. A gas turbine plant would be required to supply air to reactor B and to recover power from high pressure gases. Power generated would represent a small fraction of the capacity of the existing power station to which clean fuel is supplied.

Alternate reactor A in Figure 9 provides for gasification of oil in two steps: oil is cracked in an upper bed in an atmosphere containing H_2, the H_2 being generated from coke in a lower bed.

The foregoing examples by no means exhaust the possibilities. Modifying Consolidation's CO_2 acceptor process to incorporate the recovery of elemental sulfur has been mentioned. Hydrocracking or hydrogasifying oil, by using H_2 as the fluidizing gas to reactor A of Figure 9, is an interesting possibility.

The proposed fuel-desulfurization processes are on shaky ground until more is known about the kinetics of the various reactions under

actual processing conditions. A major object of this paper has been to persuade readers that the relevant kinetic information is worth getting.

Acknowledgment

Marvin A. Salzenstein directed the experimental studies performed by Walter C. McCrone Associates. He was assisted by Jan Markussen, now of Copenhagen, Denmark.

Literature Cited

(1) Asboth, K., Austrian Patent **172,931** (Oct. 25, 1952).
(2) Berg, L. G., Rassonskaya, I. S., *Dokl. Akad. Nauk SSSR* **81**, 855 (1951).
(3) Berg, L. G., Rassonskaya, I. S., *Izvest. Sektora Fiz.-Khim. Analiza, Inst. Obschei Neorgan. Khim., Akad. Nauk SSSR* **22**, 140 (1953).
(4) Berk & Co., Great Britain Patent **143,641** (May 28, 1920).
(5) Bischoff, F., *Monats.* **81**, 606 (1950).
(6) Bischoff, F., *Z. Anorg. Chem.* **262**, 288 (1950).
(7) Björkvall, B., Sandviken, Sweden, personal communication, 1960.
(8) Bössner, F., Marischka, C., U.S. Patents **1,985,441** (Dec. 25, 1934) and **2,183,301** (Dec. 12, 1939).
(9) Bragg, W. L., "The Atomic Structure of Minerals," Cornell University Press, Ithaca, 1937.
(10) Britton, H. T. S., Gregg, S. J., Winsor, G. W., *Trans. Faraday Soc.* **48**, 63 (1952).
(11) *Ibid.*, p. 70.
(12) Clark, P. W., Cannon, J. H., White, J., *Trans. Brit. Ceram. Soc.* **52**, 1 (1953).
(13) Consolidation Coal Company, "Pipeline Gas from Lignite Gasification: A Feasibility Study," Report prepared for Office of Coal Research, Dept. of Interior, Washington, D. C., January 1965.
(14) Cremer, E., *Z. Anorg. Chem.* **258**, 123 (1949).
(15) Cremer, E., Gatt, F., *Radex Rundschau* **1949**, 144.
(16) Curran, G. P., personal communication, 1964.
(17) Curran, G. P., Clancey, J. T., Scarpiello, D. A., Fink, C. E., Gorin, E., *Chem. Eng. Progr.* **62** (2), 80 (1966).
(18) Curran, G. P., Rice, C. H., Gorin, E., *ACS, Div. Fuel Chem., Preprints* **8**, No. 1, 128 (1964).
(19) Dent, F. J., *Gas Council Res. Commun.* **GC1**, (1952).
(20) duMotay, C. M. T., U.S. Patents **229,339, 229,340** (June 29, 1880).
(21) duMotay, C. M. T., Marechal, C. R., British Patent **2,548** of 1867 (Sept. 9, 1867).
(22) Erdös, E., *Collection Czech. Chem. Commun.* **27**, 1428 (1962).
(23) Gibaud, M., Geloso, M., *Peinture, Pigments, Vernis.* **32**, 306 (1956).
(24) Gluud, W., Keller, K., Klempt, W., Bestehorn, R., *Ber. Ges. Kohlentech.* **3**, 211 (1930).
(25) Gluud, W., Klempt, W., U.S. Patent **1,950,981** (March 13, 1934).
(26) Goldsmith, J. R., personal communication, 1962.
(27) Goldsmith, J. R., "Researches in Geochemistry," P. H. Abelson, ed., pp. 336-358, Wiley, New York, 1959.
(28) Graf, D. L., *Am. Mineralogist* **37**, 1 (1952).
(29) Graf, D. L., Goldsmith, J. R., *Geochim. Cosmochim. Acta* **7**, 109 (1955).
(30) Graf, D. L., Goldsmith, J. R., *J. Geol.* **64**, 173 (1956).

(31) Greenwood, H. C., "Industrial Gases," Baillière, Tindall, and Cox, London, 1920.
(32) Halstead, P. E., Moore, A. E., *J. Chem. Soc.* **1957**, 3873.
(33) Harker, R. I., Tuttle, O. F., *Am. J. Sci.* **253**, 209 (1955).
(34) Haul, R. A. W., Heystek, K., *Am. Mineralogist* **37**, 166 (1952).
(35) Hill, K. J., Winter, E. R. S., *J. Phys. Chem.* **60**, 1361 (1956).
(36) "International Critical Tables," Vol. 1, p. 196.
(37) *Ibid.*, Vol. 7, p. 294.
(38) Kakabadze, I. L., Russian Patent **119,172** (April 15, 1959).
(39) Kelley, K. K., *U.S. Bur. Mines Bull.* **584**, 1960.
(40) Kelley, K. K., Moore, G. E., *J. Am. Chem. Soc.* **66**, 293 (1944).
(41) Kim, I. H., M.S. Thesis, M.I.T. (1956).
(42) Kirillov, I. P., Budanov, V. V., *Tr. Ivanovsk. Khim.-Tekhnol. Inst.* **1958**, No. 7, 32.
(43) Kubaschewski, O., Evans, E. Ll., "Metallurgical Thermochemistry," 3rd ed., Pergamon Press, New York, 1958.
(44) MacIntire, W. H., Stansel, T. B., *Ind. Eng. Chem.* **45**, 1548 (1953).
(45) Marisic, M. M., U.S. Patent **2,456,072** (Dec. 14, 1948).
(46) Mauras, H., *Bull. Soc. Chim. France* **1959**, 16.
(47) Mellor, J. W., "A Comprehensive Treatise on Inorganic and Theoretical Chemistry," Vol. 3, Longmans, Green, and Co., London, 1923.
(48) *Ibid.*, Vol. 4, 1946.
(49) Perry, J. H., ed., *Chem. Eng. Handbook*, 3rd ed., p. 916, McGraw-Hill, New York, 1950.
(50) Raynor, E. J., *J. Leeds Univ. Union Chem. Soc.* **3**, 25 (1961).
(51) Richer, A., *Compt. Rend.* **238**, 339 (1954).
(52) Riesenfeld, E. H., *J. Prakt. Chem.* **100**, 142 (1920).
(53) *Ibid.*, p. 146.
(54) Rosenqvist, T., *J. Metals Trans.* **3**, 535 (1951).
(55) Schallis, A., Macaluso, P., "Encyclopedia of Chemical Technology," R. E. Kirk, D. F. Othmer, eds., Vol. 13, p. 392, Interscience Encyclopedia, New York, 1954.
(56) Schenck, R., Hammerschmidt, F., *Z. Anorg. Chem.* **210**, 305 (1933).
(57) Schmidt, J., "Das Kohlenoxyd," Akademische Verlagsgesellschaft MBH, Leipzig, 1935.
(58) Schwob, Y., *Compt. Rend.* **224**, 47 (1947).
(59) Seil, G. E., "Gas Chemists' Manual of Dry Box Purification of Gas," American Gas Association, New York, 1943.
(60) Shushunov, V. A., Fedyakova, K. G., *Uch. Zap. Gor'kovsk. Gos. Univ. Ser. Khim.* **32**, 13 (1958).
(61) Sikabonyi, L. A., *J. Alberta Soc. Petrol. Geol.* **6**, 249 (1958).
(62) Smith, Bengt, *Chalmers Tek. Högskol. Handl.* **184** (1957).
(63) Smyth, F. H., Adams, L. H., *J. Am. Chem. Soc.* **45**, 1167 (1923).
(64) Southard, J. C., Royster, P. H., *J. Phys. Chem.* **40**, 435 (1936).
(65) Squires, A. M., *Proc. Am. Power Conf.* **28**, 505 (1966).
(66) Squires, A. M., *Chem. Eng. Prog.* **62**, No. 10, 74 (October 1966).
(67) Squires, A. M., U.S. Patents **3,276,203** (Oct. 4, 1966) and **3,307,350** (March 7, 1967).
(68) Ståhled, J. L., U.S. Patent **2,755,179** (July 17, 1956).
(69) Tamaru, S., Siomi, K., *Z. Physik. Chem.* **A 161** 421 (1932).
(70) Tamayo, P., B.S. Thesis, M.I.T. (1956).
(71) Taylor, H. S., "Industrial Hydrogen," The Chemical Catalog Co., New York, 1921.
(72) Uno, T., *Tetsu To Hagana* **37**, 14 (1951).
(73) Wickert, K., *Mitt. VGB* **83**, 74 (April 1963).
(74) Willman, H. B., *Illinois State Geol. Surv., Rept. Invest.* **90** (1943).

(75) Wilsdorf, H. G. F., Haul, R. A. W., *Nature* **167**, 945 (1951).
(76) Wyllie, P. J., *J. Petrol.* **6**, 101 (1965).
(77) Zahn, O., *Chem.-Ztg.* **61**, 298, 459 (1937).
(78) Zawadzki, J., *Z. Anorg. Chem.* **205**, 180 (1932).

RECEIVED December 16, 1966.

15

Pyrolytic Gasification of Na-, Ca-, and Mg-Base Spent Pulping Liquors in an AST Reactor

STEVEN PRAHACS

Pulp and Paper Research Institute of Canada, 570 St. John's Rd., Pointe-Claire, Quebec, Canada

Pyrolytic gasification of concentrated spent Na-, Ca-, and Mg-base pulping liquors was carried out in an Atomized Suspension Technique (AST) reactor at 600°–900°C. and 5–45 p.s.i.g. In a certain range of conditions, crude ammonia and methanol synthesis gases and some unsaturated hydrocarbons can be produced by AST pyrolysis of these liquors. At identical operating conditions, the Na-base liquor gave the highest yield of synthesis gas, and the Mg-base liquor gave the highest yield of unsaturated hydrocarbons. The effect of the base on the kinetics of the gasification is discussed in some depth.

The Atomized Suspension Technique (AST), a relatively new approach to high temperature processing, has been under development for some time at the Pulp and Paper Research Institute of Canada. As described by its originator, W. H. Gauvin (3), an AST reactor is a convenient way of carrying out closely controlled thermal treatment of various gas-solid suspensions, where the carrier gas phase is usually produced by evaporation or partial gasification of the finely atomized liquid feed. The early theoretical and applied research in the field has been reviewed by Gauvin and Gravel (*4*). Potential applications of the technique are in various stages of pilot or semicommercial development. One important prospective use is in thermally treating spent pulping liquors to control pollution and to recover pulping chemicals and heat values from the spent liquors. The greatest advantage, relative to other pulping recovery processes, is offered by the pyrolytic AST treatment of various Na-base sulfite-spent liquors, and most of the recent effort has been concentrated in this area. Serious corrosion problems experienced in this application seem to have been solved with the recent successful pilot-scale testing of a special chromium-nickel alloy.

The effect of various operating conditions on the recovery of the pulping chemicals and heat values in the case of a neutral sulfite semi-chemical (NSSC) spent liquor has been described recently (*1*). The thermodynamic equilibria and kinetics of gasification which seem to apply to this same set of experiments were discussed elsewhere (*9*). Gas compositions and yields examined in the latter study showed that under some of the operating conditions investigated, commercially significant quantities of ammonia and methanol synthesis gases could be produced from NSSC-type spent liquors.

Using the pyrolysis gases for synthesizing various chemicals could offer substantial advantages compared with their use as fuel only. Since the crude synthesis gas would be obtained as a by-product of the pulping chemicals recovery, certain economic advantages could be expected relative to present conventional ammonia and methanol processes. Patents for producing ammonia and methanol from Na-base spent liquors have been applied for in several countries, and the one for methanol production has been granted recently in Canada (*8*).

Table I. Compositions of the Inorganic Residues (by Weight)

Reactor Temperature	*Na*	*Ca*	*Mg*
600°–700°C.	Na_2CO_3:80–90%	$CaCO_3$:70–85%	MgO:90–95%
	Na_2SO_4:10–20%	$CaSO_4$:15–20%	$MgSO_4$:1–5%
		CaS:0–5%	$MgCO_3$:1–2%
		CaS_2O_3:1–10%	$MgS+MgS_2O_3$:0–2%
800°–900°C.	Na_2CO_3:90–99%	$CaCO_3$:30–70%	MgO:95–99%
	Na_2SO_4:0–10%	$CaSO_4$:1–15%	$MgSO_4$:1–2%
	Na_2S:0–2%	CaS:10–20%	$MgCO_3$:0–2%
	$Na_2S_2O_3$:0–2%	CaS_2O_3:15–40%	$MgS+MgS_2O_3$:0–2%

This paper describes and evaluates AST pyrolytic experiments with various types of Na-, Ca-, and Mg-base spent pulping liquors. This comparative study was aimed primarily at exploring the recoverability of pulping chemicals and heat by pyrolysis for the different liquors. The emphasis, however, is on examining the characteristics of the over-all gasification reactions, the yields of organic residue and gas components of importance, as a function of the type of pulping base present in the spent liquors, and some other independent variables. The recoverability of pulping chemicals by AST pyrolysis appears most attractive for Na-base liquors in general, feasible for Mg-base liquors, but difficult and uneconomical for Ca-base spent liquors. In all cases the pulping base must be leached out of varying amounts (1–75 wt. %) of organic residue,

which is a highly porous, char-like material. The composition of the inorganic fraction of the residue depends on the type of pulping liquor and to some extent on the operating conditions, principally the operating temperature. Approximate compositions of the inorganic residues are given in Table I.

Experimental

Apparatus. The experiments were performed in a pilot plant consisting of a 1-ft. diameter, 15-ft. high AST reactor and its accessories. A schematic flow sheet of the pilot plant is shown in Figure 1. Details of the reactor and the auxiliary equipment were described earlier (*1, 9*). Flashing atomization at 160°–220°C. and 400–1000 p.s.i.g., through small-orifice stainless steel atomizing nozzles was used in all tests described.

Feed Materials. The spent pulping liquors used were from pulp mills using various sulfite pulping processes. To facilitate data presentation, the following code is used for designating the liquors used as feed materials.

Code	*Liquor Type*
NaI	Neutral sulfite semichemical (NSSC)
NaIA	Neutral sulfite semichemical (NSSC) (aged)
NaII	Sodium bisulfite
Ca	Calcium acid sulfite
NaIII	Calcium acid sulfite, treated with Na_2CO_3 for Ca substitution
Mg	Magnesium bisulfite (Magnefite)
Mg + Na	Magnesium bisulfite, treated with Na_2CO_3

Feed materials NaI and NaIA were supplied by the same pulp mill at different times, and NaIA was used only about two years after delivery. Presumably owing to aging, the organic content of the latter material showed lower H and O content and noticeably lower reactivity. This suggests that certain condensation-type reactions occur in the organic fraction of the spent liquors on extended storage at room temperature. The Mg + Na liquor was treated here with anhydrous Na_2CO_3 to exchange the Mg for Na; although an excess of Na_2CO_3 was used, only partial substitution could be achieved. The elementary composition of the various feeds is given in Table II. Because of difficulties experienced in obtaining reproducible elementary analyses of the organics in the feed solids, carbon, hydrogen, and oxygen values were calculated on the basis of output rates and product analyses for two to four runs for each liquor. [When the mass yield was $<100\%$ for the run, the deficiency was assumed to be H_2O (liquid water carry over from the condenser).] Besides the major components shown in Table II, the analyses of feed material Ca showed about 4% Fe by weight of inorganics (*ca.* 0.4 wt. %

of total solids). This was probably caused by corrosion of the carbon steel container used for shipping and storage. The inorganics in the Mg-base liquor contained some Ca (5–8 mole % of all the cations) because of the low purity of MgO used to make the pulping liquor.

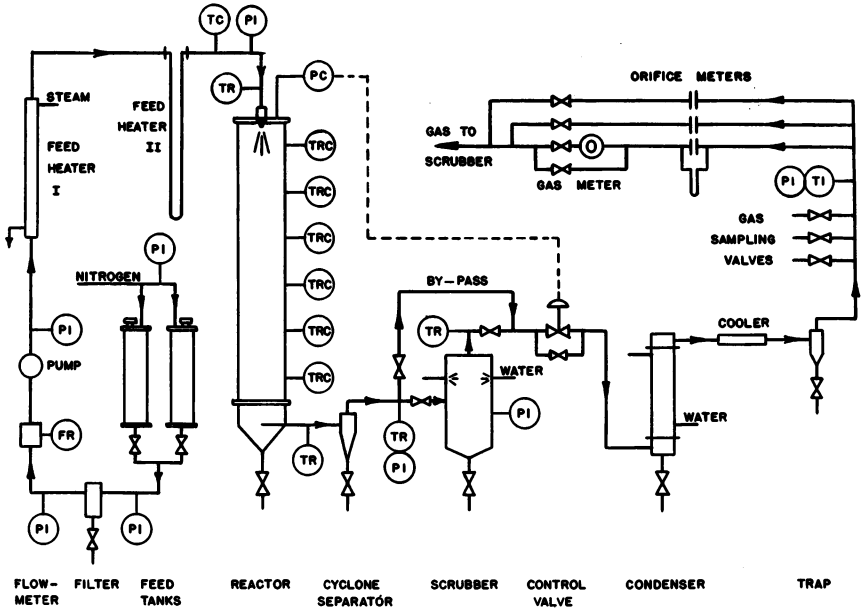

Figure 1. AST experimental apparatus

Variables Studied. The main independent variables investigated were the pulping base (Na, Ca, or Mg) and the reactor operating temperature. The latter was explored for each type of liquor at least at two levels. Other operating variables, which from earlier experiments were known to have a lesser effect on the most important dependent variables, were only spot checked. These were the feed rate, the reactor pressure, and the solids' concentration—*i.e.*, water:organics ratio. The particular (nominal) levels of operating parameters chosen were:

Reactor wall temperature: 600°–900°C. (in 50°C. increments).
Feed rate: 55 and 110 lbs./hr.
Reactor pressure: 5, 10, 30, and 45 p.s.i.g.
Water:organics ratio: 1.2 and 2.4 (by weight).

The main dependent variables were the recoverability and purity of the pulping base and the potential heat yields in the solids and gases, which will be discussed in detail in a forthcoming publication. The dependent variables examined here are the yields of potentially useful by-product raw materials like H_2 and CO (for synthesizing ammonia and

Table II. Feed Material Compositions

Feed Material	*Feed Solids*	*Ash-Free Organics*[a]	*Reactant Mixture*[b,c]
NaI	$C_{10}H_{17.0}O_{12.8}S_{0.9}Na_{3.0}$	$C_{10}H_{17.9}O_{9.9}$	W + 23.5 H_2O + 0.07 O_2
NaIA	$C_{10}H_{12.7}O_{8.7}S_{1.0}Na_{2.5}$	$C_{10}H_{12.2}O_{5.7}$	W + 16.8 H_2O + 0.95 O_2
NaII	$C_{10}H_{18.0}O_{9.1}S_{0.67}Na_{0.80}$	$C_{10}H_{17.4}O_{8.2}$	W + 18.2 H_2O − 0.60 O_2
Ca	$C_{10}H_{16.8}O_{8.75}S_{0.54}Ca_{0.46}$	$C_{10}H_{16.5}O_{8.1}$	W + 19.3 H_2O − 0.45 O_2
NaIII	$C_{10}H_{16.4}O_{7.5}S_{0.52}Na_{1.0}$	$C_{10}H_{16.2}O_{6.3}$	W + 19.1 H_2O − 1.28 O_2
Mg	$C_{10}H_{18.5}O_{11.0}S_{0.88}Mg_{0.68}Ca_{0.04}$	$C_{10}H_{16.7}O_{10.2}$	W + 23 H_2O + 0.55 O_2
Mg + Na	$C_{10}H_{15.2}O_{9.9}S_{0.53}Na_{1.3}Mg_{0.3}$	$C_{10}H_{15.1}O_{8.2}$	W + 15.8 H_2O − 0.05 O_2

[a] Calculated from elementary composition of feed solids by subtracting the pulping base (Ca, Mg, and/or Na) and sulfur in their prevalent forms under the pyrolytic conditions used during the experiments.
[b] Ash free organics + water (inorganics considered inert).
[c] W = $C_{10}H_{12.5}O_{7.0}$, an arbitrarily selected "typical" organic elementary composition, for which specific thermodynamic data is available in combination with varying amounts of H_2O and O_2 (*see* Ref. 7 and 9).

methanol), unsaturated hydrocarbons (which might be suitable for producing plastics, synthetic resins, etc.), and the yields of organic residues, which have shown the characteristics of a good activated carbon.

Analyses. The analytical methods used were described earlier (9). Gas analyses were performed with a modified Orsat apparatus—a method which can be considered satisfactory only if the gases are to be used as fuel, which was the intention for the first generation of AST recovery systems. No analytical differentiation of the unsaturated hydrocarbons can be obtained with the concentrated sulfuric acid used to absorb the so-called illuminants. Subsequent semiquantitative infrared analyses of gas samples indicated that approximately half of the illuminants are ethylene, and more than one-third are acetylene, with some other unsaturated compounds also present. A gas chromatograph is now being calibrated to determine individual unsaturated hydrocarbons quantitatively and to identify various trace gas components.

Data. The operating conditions and feed analyses are given in Table III, the product analyses and yield data in Table IV. Organic residue yields and related data were calculated on a total organics rather than carbon basis. Total organics in the feed are defined here as total solids minus ash in solids. Calculating the true amount of organics or volatiles coming from the wood was complicated by the unknown composition of the original pulping liquors for the different spent liquors treated. The potential poly(vinyl chloride) (PVC) yields are listed only for rough guidance in future work. They have been calculated as stoichiometric yields on the assumptions that all illuminants are ethylene and acetylene, and both could be quantitatively converted into PVC. Actual PVC and possibly other plastic and resin type by-product yields can be estimated when the techniques used for gas analyses are refined.

Calculation procedures for all the other data listed in Tables III and IV can be found in the papers previously cited (*1, 9*).

Results

The results of the tests will be first evaluated according to the dependent variables which are of interest for possible utilization of the spent liquors as raw materials for tonnage by-products.

Yields of H_2 and CO. The data in Tables III and IV show that at otherwise identical operating conditions the Na-base liquors produce the highest yields of H_2 and CO. The Mg-base liquors do not seem suitable for crude synthesis gas production, at least under the purely pyrolytic conditions examined here since even at a reactor temperature of 900°C. they failed to produce commercially significant yields of H_2 and CO. The Ca-base liquor produced intermediate yields of the synthesis gas components. To ascertain that the lower yields of synthesis gas were not caused by the difference in the chemical composition of the organics in the various liquors, two series of tests were carried out with liquors prepared by adding Na_2CO_3 to the originally Mg- and Ca-base liquors. While full substitution of the Ca for Na was possible, only partial replacement could be achieved in the case of the Mg-base liquor. Significantly, both liquors became good synthesis gas producers, particularly the fully Na-substituted Ca liquor. The hydrogen yields for the low feed rate (55 ± 5 lb./hr.) runs only are given in Figure 2 as a function of base, operating temperature, and operating pressure. All the feeds, except NaIII and Mg + Na had water:organics ratios of 1.2 ± 0.2 by weight. The data for the latter two liquors, which had lower water content, were corrected in Figure 2 for a water:organics ratio of 1.2, using the data plotted for liquor NaI in Figure 3, which shows the effect of dilution on Na- and Mg-base liquors.

The strong effect of the temperature on the H_2 yields is clearly indicated in Figure 2. (A similarly strong effect prevails on the CO yields, as shown in Tables III and IV.) A rather sudden increase in the H_2 yields occurs at about 700°–725°C. with all liquors containing Na or Ca while the H_2 yield appears to increase at a more rapid rate only at 900°C. with the pure Mg-base liquor. Notable is the failure of the Ca liquor to produce substantial H_2 yields at the higher temperatures, particularly at 900°C., despite behavior similar to the Na-base liquors at around 700°C.

The effect of operating pressure could be explored only in the lower temperature range because of reactor pressure-rating limitations. As the data in Figure 2 show, in the 600°–750°C. range the effect of the pressure on the H_2 (and similarly on the CO and CH_4) yield agrees with what one would expect from the thermodynamic equilibria which call for reduced H_2 and CO and increased CH_4 yields at higher pressures.

Table III. Operating Conditions

Run No.	*1*	*2*	*3*	*4*	*5*	*6*	*7*
Operating Conditions							
Feed material	NaI	NaI	NaI	NaI	NaI	NaI	NaI
Wall temp., °C.	600	650	700	700	700	750	750
Reactor press., p.s.i.g.	45	45	45	45	45	30	6
Feed rate, imp. gal./hr.	4.20	4.20	4.20	8.20	12.50	4.20	4.50
Feed rate, lb./hr.	56.2	56.2	56.2	110.2	168.5	56.7	59.9
Feed solids rate, lb./hr.	31.5	31.7	31.7	65.0	99.1	34.3	34.2
Feed organics rate, lb./hr.	18.4	18.6	18.8	38.1	58.0	(20.6)	19.9
Feed H_2O:organics ratio (wt.)	1.34	1.32	1.30	1.20	1.20	(1.09)	1.29
Feed temp., °C.	220	220	220	210	212	220	170
Feed press., p.s.i.g.	540	550	560	700	470	535	530
Measured outlet temp., °C.	440	440	450	490	550	550	540
Est. residence time, sec.	104	96.5	93.1	46.8	29.9	62.2	25.8
Feed Analyses							
Solid concn., wt.%	56.1	56.4	56.5	58.8	58.8	60.3	57.1
Ash, wt.% of solids	41.7	41.5	40.9	41.5	41.5	(40.0)	41.8
Sulfated ash, wt.% of solids	48.7	48.7	50.1	50.6	50.6	—	—
Total Na, wt.% of total feed	8.00	7.78	7.78	8.09	8.09	9.38	9.05
Total sulfur, wt.% tot. feed	2.89	3.10	3.10	2.80	2.80	4.16	3.88
Calorific value, B.t.u./lb.	4930	4910	4910	4850	4850	4986	5118
pH	6.70	6.70	6.70	6.70	6.70	—	—
Specific gravity, grams/cc.	1.34	1.34	1.34	1.35	1.35	1.35	1.35
Output Rates							
Gas rate, std. cu. ft./hr. (32°F.)	71.4	138.4	190.4	336.4	471.8	322.0	365.0
Gas rate, lb./hr.	5.81	9.18	11.6	22.1	32.8	17.0	18.2
Condensate rate,[a] lb./hr.	28.4	27.3	25.4	49.1	72.2	19.7	20.3
Solids rate, lb./hr.	17.6	17.0	17.4	35.2	53.2	19.0	16.9
Total output, lb./hr.	51.8	53.5	54.4	106.4	158.2	55.7	55.4

Run No.	*20*	*21*	*22*	*23*	*24*	*25*	*26*
Operating Conditions							
Feed material	Ca	NaIII	NaIII	NaIII	Mg	Mg	Mg
Wall temp., °C.	900	650	750	850	600	600	650
Reactor press., p.s.i.g.	5	45	30	10	40	5	40
Feed rate, imp. gal./hr.	4.30	4.65	4.60	4.60	4.40	4.40	4.10
Feed rate, lb./hr.	54.3	58.0	57.4	57.4	55.6	55.6	51.9
Feed solids rate, lb./hr.	28.0	29.1	28.8	28.8	28.3	28.3	26.0
Feed organics rate, lb./hr.	24.9	23.3	23.1	23.1	25.8	25.8	23.6
Feed H_2O:organics ratio (wt.)	1.06	1.24	1.24	1.24	1.06	1.06	1.10
Feed temp., °C.	180	220	220	220	180	180	190
Feed press, p.s.i.g.	420	560	540	540	380	650	740
Measured outlet temp., °C.	430	350	430	512	276	382	296
Est. residence time, sec.	26.2	113	61	22	—	—	—
Feed Analyses							
Solids concn., wt.%	51.5	50.1	50.1	50.1	51.4	51.4	50.9
Ash, wt.% of solids	11.0	19.9	19.9	19.9	8.78	8.78	9.36
Sulfated ash, wt.% of solids	16.9	21.7	21.7	21.7	20.7	20.7	21.9
Total Na, wt.% of total feed	—	3.61	3.61	3.61	—	—	—
Total sulfur, wt.% tot. feed	—	2.61	2.61	2.61	—	—	—
Calorific value, B.t.u./lb.	—	6870	6870	6870	—	—	—
pH	5.30	7.00	7.00	7.00	5.50	5.50	5.50
Specific gravity, grams/cc.	1.26	1.25	1.25	1.25	1.27	1.27	1.27
Output Rates							
Gas rate, std. cu. ft./hr. (32°F.)	506.0	112.0	303.8	739.5	77.3	78.9	101.0
Gas rate, lb./hr.	25.3	8.3	16.5	34.1	6.29	6.12	8.52
Condensate rate,[a] lb./hr.	16.6	28.0	26.0	18.1	—	—	—
Solids rate, lb./hr.	6.1[b]	13.6[b]	12.0[b]	5.1[b]	12.0[b]	12.0[b]	9.89
Total output, lb./hr.	48.0[b]	49.9[b]	54.5[b]	57.3[b]	—	—	4.21[b]

[a] Including 3 wt.% of gas as H_2O vapor carryover.
[b] Solids rate and total output based on sulfated ash analyses in feed and solid product

and Feed Analyses[c]

8	*9*	*10*	*11*	*12*	*13*	*14*	*15*	*16*	*17*	*18*	*19*
NaI	NaI	NaI	NaI	NaI	NaIA	NaIA	NaII	NaII	Ca	Ca	Ca
800	800	800	800	800	800	850	750	800	700	800	800
10	10	10	10	10	10	10	30	10	5	5	10
4.40	5.4	5.4	5.4	9.4	3.90	4.00	4.50	4.50	4.30	4.00	8.60
58.3	72.3	69.1	65.9	125.0	52.7	54.2	57.2	57.2	54.3	50.5	108.6
32.5	39.8	32.2	25.1	72.1	31.5	32.4	31.0	31.0	28.0	25.7	55.0
(19.8)	23.0	18.6	14.3	43.4	18.8	19.3	26.3	26.3	24.9	23.2	49.7
(1.30)	1.41	1.98	2.86	1.22	1.13	1.13	0.99	0.99	1.06	1.07	1.08
190	178	186	187	187	210	220	178	178	180	190	190
450	635	600	620	980	560	590	700	650	400	550	780
555	585	590	600	645	625	650	450	500	343	416	599
26.3	20.2	19.6	18.0	11.5	29.5	25.4	—	—	—	30	13.1
55.7	54.9	46.6	38.1	57.7	59.8	59.8	54.2	54.2	51.5	50.8	50.7
(39.2)	42.2	42.1	42.9	39.8	40.5	40.3	15.1	15.1	11.0	10.0	9.90
—	—	—	—	—	—	—	18.4	18.4	16.9	16.6	16.7
9.22	9.1	7.2	5.3	8.95	9.83	9.83	3.07	3.07	—	—	—
3.70	4.07	3.45	2.67	3.66	4.55	4.55	3.50	3.50	—	3.01	2.72
4880	4850	4854	4900	5003	—	—	(7000)	(7000)	—	7157	7276
—	6.9	6.9	6.9	—	—	—	4.85	4.85	5.30	4.70	4.80
1.32	1.34	1.28	1.22	1.33	1.35	1.35	1.27	1.27	1.26	1.26	1.26
516.0	656.0	586.2	494.2	890.0	483.0	567.0	321.0	557.0	182.0	362.3	638.2
24.3	30.2	27.7	23.7	45.1	23.0	26.4	17.2	26.8	11.2	18.4	34.1
18.5	22.0	27.0	33.6	48.9	12.2	12.7	24.0	18.6	—	19.0	52.8
14.4	19.4	13.0	9.4	34.8	12.4	12.8	10.8	8.9	11.9[b]	7.6[b]	18.3[b]
56.5	71.6	67.7	66.7	128.8	47.6	51.9	52.0	54.3	—	45.0[b]	105.2[b]

27	*28*	*29*	*30*	*31*	*32*	*33*	*34*	*35*	*36*	*37*
Mg	Mg	Mg	Mg	Mg	Mg	Mg	Mg	Mg	Mg + Na	Mg + Na
650	700	750	800	800	800	800	850	900	800	850
5	5	5	5	5	5	10	5	5	5	5
4.30	4.60	4.40	3.60	4.20	4.20	7.60	4.20	4.40	4.40	4.50
54.5	58.4	54.5	45.9	52.3	48.8	96.4	52.8	55.6	58.9	60.3
27.3	30.1	24.2	23.3	24.0	15.7	50.5	25.2	28.3	34.8	35.6
24.8	27.3	21.9	21.1	21.7	14.2	46.2	22.8	25.8	25.7	26.3
1.10	1.04	1.38	1.08	1.30	2.33	1.00	1.21	1.06	0.94	0.94
165	160	190	190	190	190	190	190	185	185	185
480	640	900	540	820	500	900	463	750	580	600
360	399	484	384	478	427	473	415	422	486	514
—	32.6	27.4	37.2	28.1	26.9	21.0	29.4	—	22.8	19.4
50.9	51.5	44.7	50.7	46.0	32.1	52.5	48.0	51.4	58.7	58.7
9.36	9.40	9.44	9.24	9.45	9.38	8.74	9.52	8.78	26.0	26.0
21.9	22.0	21.7	21.8	21.5	22.2	21.2	21.9	20.7	42.4	42.4
—	—	—	—	—	—	—	—	—	—	—
—	3.34	3.62	4.11	3.69	1.94	4.10	3.88	—	—	—
—	—	6291	6205	6282	6311	6278	6320	—	—	—
5.50	5.50	5.30	4.50	5.30	4.80	4.60	5.30	5.50	8.20	8.20
1.27	1.27	1.24	1.27	1.25	1.16	1.27	1.26	1.27	1.34	1.34
102.0	149.0	144.6	179.8	175.6	111.4	342.1	222.5	300.0	439.0	580.0
8.09	12.3	10.7	11.7	12.1	7.8	23.7	14.3	17.1	23.2	28.8
—	29.2	30.2	22.8	28.1	35.8	45.1	27.2	—	20.7	18.3
11.0[b]	11.3[b]	7.66[b]	6.96[b]	7.26[b]	4.74[b]	16.4[b]	7.30[b]	7.55[b]	15.0[b]	12.0[b]
46.1[b]	52.8[b]	48.6[b]	41.5[b]	47.5[b]	48.3[b]	85.2[b]	48.8[b]	—	58.9[b]	59.1[b]

(for other runs, same figures based on Na analyses in feed and solid product).

[c] Figures in parens are estimates based on Na analyses.

The effect of the water:organics ratio on the H_2 yields at 800°C. and low pressures is shown in Figure 3, for NaI and Mg. The influence of this variable is insignificant for the Mg-base feed and modest for NaI. However, even the 1.2 ratio represents approximately double the amount of water required for full gasification according to the stoichiometry prevailing in the temperature range studied. It is reasonable to assume on a strictly theoretical basis as well as from the slight curvature of the NaI curve that at lower water:organics ratios the effect on the H_2 yield is more pronounced, at least under conditions where the gasification reaction can proceed at a reasonably high rate (at > 750°C. for Na-base liquors and > 900°C. for Mg-base liquors).

The effect of feed rate on the H_2 yield at 800°C. and low pressures is shown in Figure 4. This indicates that doubling the feed rates reduced the H_2 yields by about 20% with the Na- and Ca-base liquors and by about 35% with the Mg-base liquor. In absolute terms, however, the latter change is the least significant.

As the data in Table III show, the CO yield increases slightly at higher feed rates in the NaI runs at low temperature (Runs 3, 4, and 5), and the Mg-base runs at 800°C. (Runs 30 and 33). CO yield is slightly

Table IV. Product Analyses

Run No.	*1*	*2*	*3*	*4*	*5*	*6*	*7*
Product Analyses							
Solids, wt.%							
HCl insoluble	35.4	33.8	31.2	34.2	35.1	22.7	24.8
Ash	67.0	69.5	73.0	69.5	68.8	75.8	77.6
Sulfated ash	84.1	85.8	87.7	87.0	82.8	—	—
Total Na	25.5	25.7	25.1	25.4	25.6	28.3	31.9
Total sulfur	4.35	4.33	3.97	4.23	4.28	2.68	2.89
Sulfate sulfur	2.89	2.46	2.49	2.89	2.50	1.88	1.73
Sulfide sulfur	0.08	0.10	0.10	0.02	0.01	0.05	—
Thiosulfate sulfur	0.15	0.09	0.04	0.10	0.05	—	—
Carbonate as CO_2	20.7	20.7	23.1	21.8	21.3	27.7	27.5
Gas, vol.%							
H_2	11.2	26.8	38.0	30.4	27.2	49.8	56.1
CO	7.2	5.9	4.0	5.6	6.0	4.8	4.7
CO_2	33.2	25.0	30.6	27.8	30.6	28.6	29.9
Paraffins	20.0	19.4	13.6	14.8	14.6	8.4	4.1
Illuminants	5.0	3.3	2.4	3.2	3.8	0.6	1.0
H_2S	20.0	18.5	9.0	12.2	14.6	5.0	4.1
Inerts	3.0	1.0	2.0	4.6	2.8	2.6	0.0
Molecular wt. (av.)	29.2	23.8	21.9	23.6	24.9	18.9	17.9
Yields							
Mass yield,[a] wt.% feed	92.4	95.3	96.8	96.4	93.9	98.5	93.0
Gas yield, wt.% organics fed	31.6	49.4	62.0	58.0	56.6	(82.0)	89.4
Organics residue, wt.% organics fed	33.8	30.9	28.9	31.6	32.2	(20.9)	21.1
H_2 yield, wt.% organics fed	0.24	1.12	2.14	1.50	1.23	(4.34)	5.74
CO yield, wt.% organics fed	2.18	3.42	3.16	3.85	3.81	(5.86)	6.73
Illum. yield, wt.% organics fed	1.50	1.91	1.90	2.21	2.41	(0.73)	1.43
Potential NH_3, T/100 T organics	2.24	7.74	13.4	10.1	8.52	(26.9)	35.2
Potential CH_3OH, T/100 T organics	2.10	7.27	12.6	9.46	8.01	(25.2)	33.1
Potential PVC, T/100 T organics	3.30	4.24	4.21	4.91	5.35	(1.62)	3.17

reduced by increased feed rate in the Ca runs at 800°C. and substantially reduced by increased feed rate in the NaI runs at 800°C. (Runs 8 and 12). On the basis of thermodynamic and kinetic considerations, increased feed rate—*i.e.*, reduced residence time—should result in lower CO concentration in all the above cases. This expectation is not realized when over-all gasification is slow, either because of relatively low temperatures (Runs 3, 4, and 5), or because of the seemingly inhibiting effect of the Mg (Runs 30 and 33).

Yield of Organic Residue. A high yield of organic residue adversely affects the cost of leaching the pulping base from the solid product as well as the thermal balance of the over-all recovery system. However, it was found in the laboratory (using the methylene blue adsorption test) that if the residue were produced at 750°C. or higher, it showed excellent adsorptive properties, similar to commercial activated carbons. The optimum yield of the residue appears to depend therefore on the size of the accessible market for this material.

The yield of carbon as a function of the base, operating temperature, and pressure is shown in Figure 5. Not unexpectedly, the curves are approximately mirror images of the H_2-yield curves shown in Figure 2,

and Yield Data[c]

8	*9*	*10*	*11*	*12*	*13*	*14*	*15*	*16*	*17*	*18*	*19*
7.8	11.3	9.0	5.1	26.1	9.0	1.6	60.5	49.3	74.0	62.9	68.6
91.3	87.2	90.4	94.8	77.7	91.8	100.4	42.2	52.8	40.0	51.3	44.6
—	—	—	—	—	—	—	52.3	68.7	39.9	57.1	50.3
37.2	33.6	37.3	37.4	32.1	37.1	41.6	16.2	20.2	—	—	—
0.07	1.49	1.46	1.41	3.28	1.56	1.85	2.95	1.67	3.57	8.52	7.30
0.56	0.90	1.00	0.87	1.80	0.67	0.00	0.88	0.60	1.33	0.51	0.75
0.08	0.03	0.01	0.02	0.12	Tr.	0.04	0.00	Tr.	0.03	1.07	0.03
—	—	—	—	—	—	—	Tr.	Tr.	0.62	2.96	2.45
36.1	34.2	35.6	36.7	26.5	35.8	39.3	17.0	21.5	—	7.70	6.60
57.6	59.6	58.6	58.4	55.4	52.9	52.6	50.8	57.0	34.6	51.5	47.6
8.0	4.0	4.4	4.4	4.8	10.9	15.6	6.4	7.6	19.6	11.2	12.4
25.4	27.0	28.0	29.0	30.8	23.0	20.1	30.6	27.6	23.6	27.0	26.0
3.6	5.2	4.3	3.5	4.2	9.6	8.2	6.6	4.0	8.4	5.4	6.2
0.8	1.0	0.8	1.0	0.8	1.2	1.0	0.8	0.6	2.2	1.2	1.4
3.4	2.4	2.4	2.4	2.4	2.5	2.5	3.8	2.2	7.2	3.0	5.0
1.0	0.8	2.1	1.3	1.6	0.0	0.0	1.0	1.0	4.2	0.6	1.2
16.9	16.5	17.0	17.2	18.2	17.1	16.7	19.2	17.2	22.2	18.3	19.2
97.0	99.0	97.9	101.1	97.0	91.0	96.0	91.0	94.8	—	89.0[b]	97.1[b]
(123.0)	131.0	149.0	166.0	104.0	129.0	145.0	65.4	102.0	45.0	79.3	68.6
(5.67)	9.5	6.3	3.3	20.9	5.94	1.06	24.8	16.7	35.4[b]	20.6[b]	25.3[b]
(8.37)	9.5	10.3	11.2	6.33	7.56	8.60	3.45	6.73	1.41	4.48	3.40
(16.2)	8.9	10.8	11.8	7.69	21.8	35.8	6.10	12.6	10.8	13.7	12.4
(1.62)	2.2	2.0	2.7	1.28	2.40	2.29	0.76	0.99	1.25	1.46	1.40
(54.0)	57.5	62.7	68.3	39.1	51.7	63.2	22.1	43.3	12.3	31.0	24.3
(50.6)	54.1	59.0	64.3	36.7	48.6	59.5	20.7	40.7	11.6	29.1	22.8
(3.60)	4.88	4.43	5.98	2.84	5.34	5.08	1.69	2.20	2.78	3.24	3.11

Table IV.

Run No.	*20*	*21*	*22*	*23*	*24*	*25*	*26*
Product Analyses							
Solids, wt.%							
HCl insoluble	50.3	68.1	59.2	7.6	71.3	71.1	71.4
Ash	78.1	36.2	40.9	92.4	22.0	21.3	23.4
Sulfated ash	78.3	45.8	51.3	122.0	48.8	48.8	56.4
Total Na	—	—	—	—	—	—	—
Total sulfur	15.3	3.24	2.67	2.16	2.77	2.66	3.02
Sulfate sulfur	1.65	1.17	0.82	1.11	2.38	2.20	1.28
Sulfide sulfur	1.07	0.01	0.00	0.23	0.05	0.01	0.00
Thiosulfate sulfur	6.60	0.00	0.02	0.01	0.28	0.28	0.29
Carbonate as CO_2	—	11.1	15.5	36.9	—	—	—
Gas, vol.%							
H_2	50.8	25.0	50.0	56.6	7.8	10.4	7.2
CO	15.4	10.0	6.8	13.4	21.4	24.8	12.6
CO_2	23.4	35.0	31.0	21.8	26.6	24.8	27.6
Paraffins	5.2	11.6	5.8	3.2	13.6	15.6	10.6
Illuminants	0.4	2.2	0.8	0.8	15.8	13.6	18.2
H_2S	1.0	13.0	4.6	3.0	7.4	4.4	15.0
Inerts	3.6	3.2	1.0	1.2	6.4	5.8	7.4
Molecular wt. (av.)	17.8	26.5	18.5	16.6	29.1	27.7	30.3
Yields							
Mass yield,[a] wt.% feed	88.5[b]	86.0[b]	94.9[b]	9.99[b]	—	—	—
Gas yield, wt.% organics fed	101.0	35.6	71.4	147.5	24.2	23.7	36.1
Organic residue, wt.% organics fed	12.3[b]	39.8[b]	30.8[b]	1.68[b]	32.7[b]	32.8[b]	29.5[b]
H_2 yield, wt.% organics fed	5.80	0.67	3.67	10.1	0.13	0.18	0.17
CO yield, wt.% organics fed	24.3	3.74	6.70	33.5	5.00	5.95	4.20
Illum. yield, wt.% organics fed	0.64	0.82	0.82	2.00	3.70	3.20	6.10
Potential NH_3, T/100 T organics	42.7	5.31	23.9	70.8	2.76	3.43	2.67
Potential CH_3OH, T/100 T organics	40.1	5.00	22.5	66.6	2.59	3.23	2.51
Potential PVC, T/100 T organics	1.42	1.83	1.82	4.44	8.22	7.11	13.5

[a] Mass yields given on basis of total output, (gas + condensate + solids) lb./hr. *vs.* total feed, lb./hr.
[b] Organic residue yield and corresponding mass yield are based on sulfated ash

representing the same selection of runs. This could indicate that the main source of H_2 is the gasification of the organic residue, presumably by the classic water-gas reaction and water-gas shift reactions below.

$$C + H_2O = CO + H_2$$

$$CO + H_2O = CO_2 + H_2$$

One notable feature of Figure 5 is the distinctly higher organic residue yields at 700°C. for the Ca and Na-substituted Ca (NaIII) liquors. Since these two liquors only were from low yield pulping, where the lignin content of the spent-liquor organics is generally higher, one can assume that the higher residues at 700°C. result because the lignin portion of the liquor does not volatilize, (*i.e.*, undergo simple thermal degradation to gas-phase products as contrasted with the water-gas reaction) to the same extent at low temperatures as the carbohydrate degradation products, the other main group of spent-liquor constituents. However, it

Continued

27	*28*	*29*	*30*	*31*	*32*	*33*	*34*	*35*	*36*	*37*
71.2	75.7	75.6	72.4	74.9	69.6	75.7	73.1	64.8	37.3	24.6
22.8	26.6	28.8	31.5	30.9	34.6	29.6	32.3	32.9	62.8	77.3
54.7	58.4	69.0	72.9	71.2	73.3	71.4	76.0	77.7	98.3	125.0
—	—	—	—	—	—	—	—	—	—	—
2.87	2.82	2.23	2.14	2.21	2.35	2.46	2.33	3.17	2.98	2.55
1.69	1.13	0.38	0.33	0.29	0.42	0.21	0.30	0.59	1.57	1.00
0.00	0.03	0.00	0.00	0.00	0.00	0.00	0.00	0.01	0.01	0.02
0.27	0.13	0.96	1.20	0.94	1.10	1.10	1.16	0.30	0.17	0.79
—	—	1.92	2.24	1.40	3.60	1.42	2.72	—	—	—
8.8	11.6	17.6	34.2	26.0	28.6	26.2	34.3	44.8	52.8	54.4
23.0	16.6	26.2	15.6	22.2	17.2	20.2	15.2	12.8	7.8	13.0
22.8	26.2	24.3	31.8	27.6	32.6	28.2	30.4	29.6	29.4	25.6
13.2	9.6	11.7	9.2	10.3	9.4	10.8	8.6	6.8	3.2	2.6
18.0	16.8	6.6	3.0	4.1	3.6	4.2	3.6	0.2	0.4	0.4
8.2	12.8	11.1	4.0	6.5	6.4	8.8	5.0	5.0	4.8	2.6
5.0	5.6	2.1	1.8	2.8	1.8	1.4	2.6	0.6	1.4	1.0
28.3	29.7	26.6	23.3	24.8	25.0	24.9	23.0	20.5	18.9	17.8
—	90.6[b]	89.4[b]	88.6[b]	90.8[b]	99.0[b]	88.6[b]	92.4[b]	—	99.0[b]	98.0[b]
32.5	48.0	50.9	55.4	50.7	54.8	46.2	62.8	67.0	90.1	110.0
31.2[b]	31.4[b]	26.4[b]	23.9[b]	25.1[b]	23.2[b]	26.9[b]	23.4[b]	18.8[b]	21.9[b]	11.3[b]
0.20	0.38	0.68	1.62	1.17	1.25	1.09	1.87	2.90	4.90	6.70
7.38	7.06	14.1	10.4	14.0	10.6	11.7	11.6	11.5	10.4	22.4
5.80	7.20	3.55	1.99	2.69	2.21	2.42	2.74	0.18	0.53	0.69
4.12	5.05	9.58	13.4	12.3	11.4	10.9	15.3	21.1	31.9	47.1
3.87	4.74	9.00	12.6	11.6	10.7	10.3	14.4	19.8	30.0	44.3
12.9	16.1	7.88	4.42	5.97	4.91	5.37	6.09	0.40	1.18	1.53

analyses in feed and solid product; (same data without footnotes are based on Na analyses in feed and solid product).
[c] Figures in parens are based on estimated organics feed rates.

is clear from the high temperature sides of the curves that once the temperature is high enough for the water-gas reaction to proceed, the predominant base—and not the composition of the original organic material —governs the rate of gasification. The considerably larger initial residue yield reduces to almost nil at 850°C. with NaIII while the lower initial residue yield changes little when Mg is the base. It is also notable that the partial replacement of the original base, as in feed Mg + Na, is less effective than full replacement of the Ca, as in feed NaIII.

Figures 3 and 6 show the effect of the water:organics ratio and feed rate on the organic residue yield at 800°C. and low pressures. These curves are also mirror images of the corresponding H_2-yield plots.

Yield of Illuminants. Because of the limited value of the illuminants analysis, the data obtained can be considered only as indicating the conditions which will probably favor formation of ethylene and acetylene, which according to preliminary semiquantitative infrared tests appear to be the main illuminant components. The most important findings in this

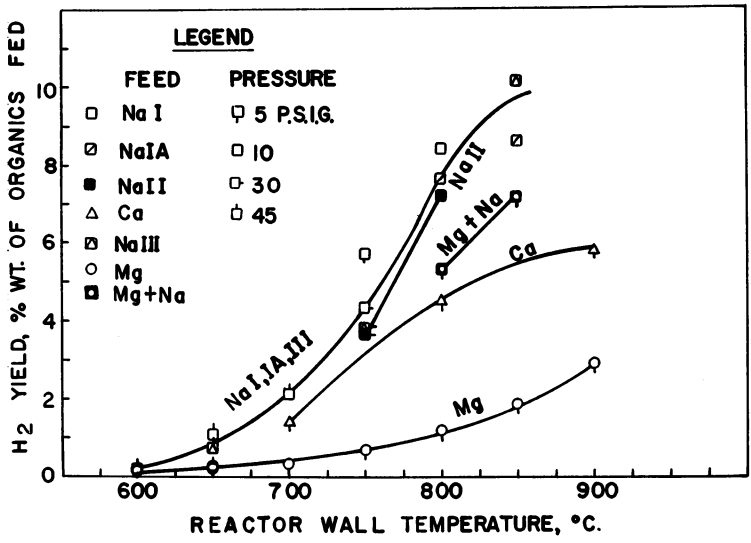

Figure 2. Effect of reactor wall temperature, inorganic base, and reactor pressure on hydrogen yield

respect are plotted in Figure 7 which shows that the Mg-base liquor produced much higher yields of illuminants than any other liquor, with a maximum at 700°C. There is little reason to assume that the characteristics of the organic content of the Mg-base liquor were responsible for the higher yield of illuminants since the Mg + Na feed showed about the lowest yield of illuminants. According to the thermodynamic equilibria (*10, 11*), the concentrations of any unsaturated hydrocarbon or aromatic compound should be less than 10^{-2} vol. % under the range of conditions considered. One therefore must assume that some of these unsaturated compounds form at relatively low temperatures during the initial degradation of the various organic groups present in the spent liquor. However, since they are thermodynamically unstable, they will decompose with certain reaction rates. These rates, like the over-all organic residue gasification rates, seem to be influenced by the base. Apparently, Mg is the least active base in this presumably catalytic process.

Discussion

The preceding examination of the experimental data suggests that for all liquors tested, gasification of the organic content of these liquors progresses in two rather distinct phases.

First, thermal degradation occurs (which could have several stages) and seems to be essentially completed somewhere below 600°C. in a

few seconds, resulting in volatilizing 60–70% of the organics. This observed high degree of volatilization at less than 600°C. agrees with some data published by Buzagh *et al.* (2). His study of various lignins by the differential thermogravimetric method showed that about 55% of the lignin was volatilized at 310°C. and about 70% at 480°C. Our work indicates that although there is some difference in the degree of volatilization, depending on the source of the liquor—*i.e.*, its organic composition—the inorganic component does not influence the degree of primary gasification proceeding below 600°C. Relatively little additional gasification occurs between 600° and 700°C., but the type of inorganics present

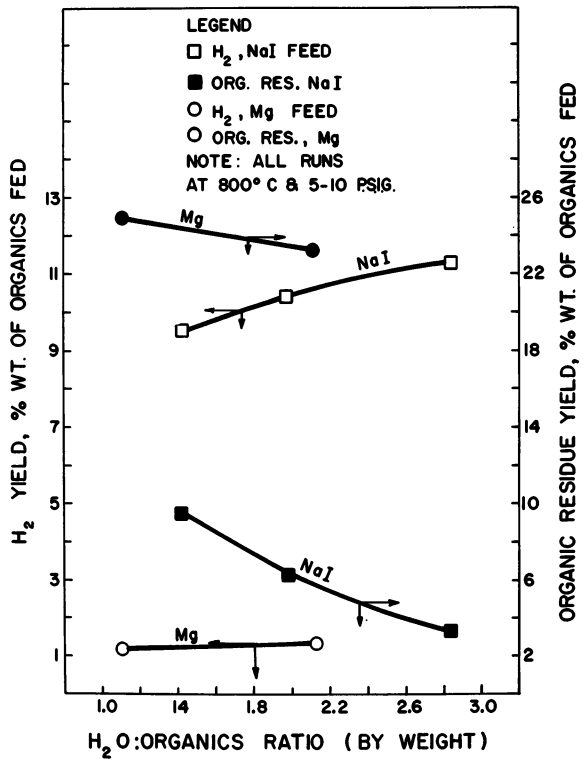

Figure 3. Effect of water:organics ratio and inorganic base on yields of hydrogen and organic residue

has some effect on the over-all gasification rates as well as on the composition of the gas phase. The Na-base liquors gasify at somewhat higher rates while the thermodynamically unstable illuminants and CO appear in much lower concentrations than with the Ca- and Mg-base liquors.

Above 700°C., where the water-gas reaction proceeds rapidly, the effect of the base becomes dominant; all the residues from Na-base

liquors or liquors containing added Na_2CO_3 show a markedly higher rate of gasification. The Mg-base material appears to have little activity while the Ca-base residue shows an intermediate behavior. The seemingly catalytic behavior of the Na_2CO_3, which represents more than 90% of the total sodium salts in the inorganic portion of the Na-base residues (the balance being mostly Na_2SO_4), is not unknown to those working in coal gasification. A coal gasification process presently being developed (*6*) is based exactly on this recognition of the catalytic effect of Na_2CO_3. According to our analyses, the 30–35% organic residue of the spent liquor organics which appears to gasify by the water-gas reaction has an elementary composition in the following ranges:

C: 70 to 85 wt. %

H: 2.0 to 3.0

O: 5 to 15

S: 4 to 8

The above is not unlike the composition of certain coals, and similar behavior in the presence of Na_2CO_3 could be expected.

It is more difficult to explain the difference in behavior between the Ca- and Mg-base residues. The cations are chemically similar, and all their compounds present have fusion points far above the temperatures used here. The fact that about 90% of the Mg is present in the residue as MgO while the Ca exists as a mixture of $CaCO_3$, CaS, CaS_2O_3, and $CaSO_4$ could be one possible reason. The shift of the latter mixture towards more sulfur-bearing compounds at 900°C. might explain the fact that the char gasification rates taper off at the higher temperatures. In general it is the characteristics of the inorganic phase as a whole, with regard to physical state (solid or liquid, porosity, viscosity, etc.) and chemical characteristics of the mixture that probably are the main determining factors in influencing the gasification reactions. Any speculation on the relative behavior of the Ca-base liquor used here is further complicated by the presence of about 4 wt. % Fe in the inorganic phase. It is felt that only separate laboratory experiments, using originally ash-free spent liquor chars, treated with various pure or mixed inorganic compounds could elucidate satisfactorily the catalytic or other effects of the inorganics present in this type of chemical system.

Char Gasification Rates. Despite the impurities and general complexity of the inorganic components, it is still important to compare quantitatively the solid and gas phase conversions achieved relative to calculated theoretical equilibria and the relative rates of char gasification, under various operating conditions, as function of the feed material. This should be useful at least for pyrolytic-spent liquor gasification processes

since the bases would be present approximately in the same form as in the experiments described here. The above would also be of interest to workers in coal gasification.

A quantitative study of theoretical equilibria in the gas and solid phases and estimation of the difference between the conversions actually achieved and conversions called for, similar to an earlier study on the NSSC liquors alone (9), is planned for the future. The discussion here

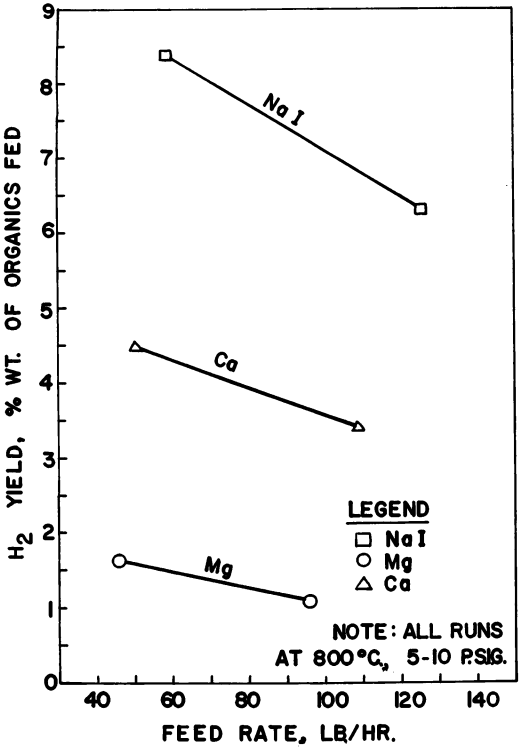

Figure 4. Effect of feed rate and inorganic base on hydrogen yield

will be restricted to the relative rates of gasification of the various spent liquor chars in the temperature range where the water-gas reaction appears to be controlling—namely between 750° and 900°C.

An accurate, absolute measurement of the char gasification rates would call for the experiment to be conducted under well-determined isothermal conditions. The conditions in an AST reactor are not isothermal, at least from the point of view of the reactant solids and gases. However, heat transfer measurements as well as some internal fluid temperature measurements with water feed have shown that when feeding water alone at 40–50 lbs./hr. and maintaining a uniform wall tem-

perature of 750°–850°C., the steam temperature immediately above the bottom of the reactor is only 5°–10°C. lower than the wall temperature, while it is about 80°–100°C. lower than the wall temperature at the exact center of the reactor. If one assumes that this is also valid for the solid residue particles when they are present, the average temperature of the particles during their residence in the whole bottom half of the reactor could be taken as approximately 50°C. lower than the wall temperature. Table V shows estimated char gasification rates for all 750°–900°C. runs made at 55 ± 5 lbs./hr. feed rates and 5–10 p.s.i.g. pressures, calculated on the basis of the above assumptions, using half of the estimated total residence times as reaction times. Despite the assumptions used in the calculations, it is felt that the relative char gasification rates will be representative since the same considerations applied to all cases. The absolute rates are approximate but should be correct at least to the order of magnitude because virtually full gasification was achieved in less than the total residence times of 22–26 seconds in Runs 14 and 23. The rates

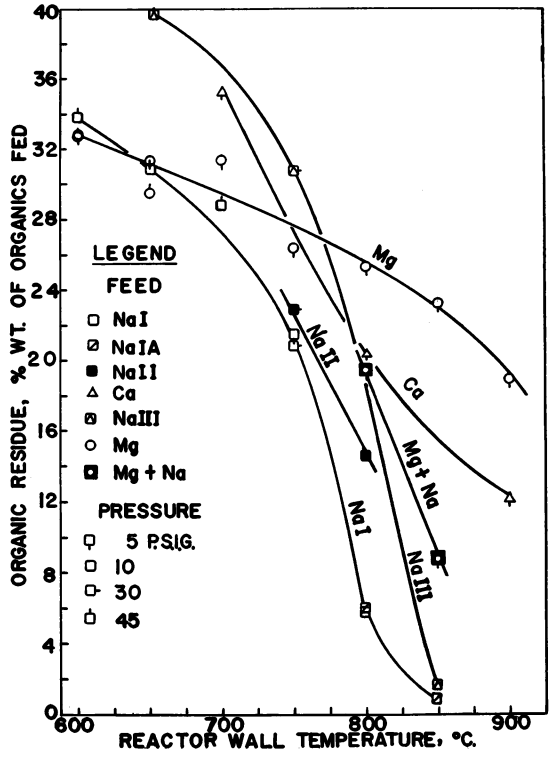

Figure 5. Effect of reactor wall temperature, inorganic base, and reactor pressure on organic residue yield

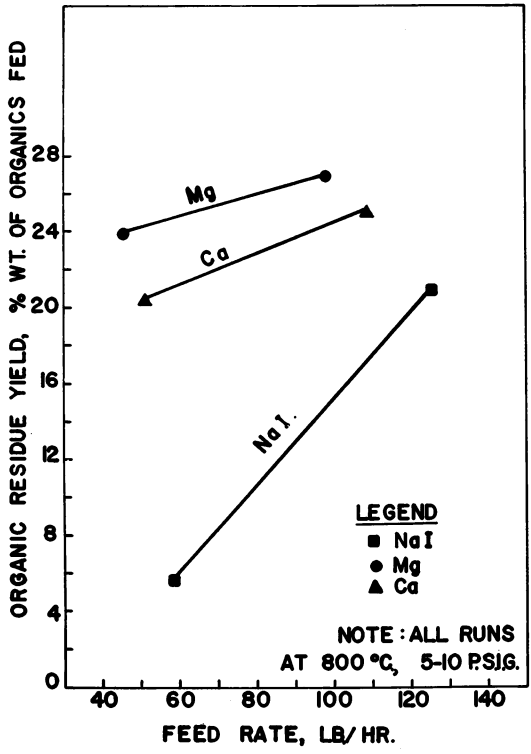

Figure 6. Effect of feed rate and inorganic base on organic residue yield

calculated in Table V are plotted on a semilog scale against the reciprocal temperatures, in Figure 8. Because of the assumptions involved and the apparent slight curvature of the lines with three experimental points, only a few tentative conclusions can be drawn about the effect of the inorganics in the solid residue on the rates of the char gasification.

(1) At 800°C. (1/°K. = 9.76), where direct comparison is possible, the rates of gasification of the residues with Na_2CO_3 as the main inorganic component are about five times higher than the rates with residues containing MgO as the major inorganic component, and about two times larger than with the Ca-base residues. At 800°C. the inorganics in the latter are about 70% $CaCO_3$, the balance being a mixture of various sulfur compounds of Ca. The much higher rates prevail with Na-base residues, despite the fact that with these liquors at 800°C. the last traces of the char must be gasified—a condition which usually results in relatively low reaction rates.

(2) Looking at the data in Figure 8 in another way, to produce a gasification rate of 3 lb./100 lb./sec., 905°C. is required for Mg-base residue, 810°C. for Ca-base residue, while 760°C. is sufficient for the Na-base liquors. This comparison is not influenced by the different de-

grees of gasification since about one-third of what is considered a char residue has been removed at all the points considered.

(3) Notable is the somewhat lower reaction rate shown by the partially Na-substituted Mg-base residue, although the difference between this and the pure Na-base residues almost disappears at 850°C. It would seem that the presence of MgO retards the apparent catalytic effect of the Na_2CO_3.

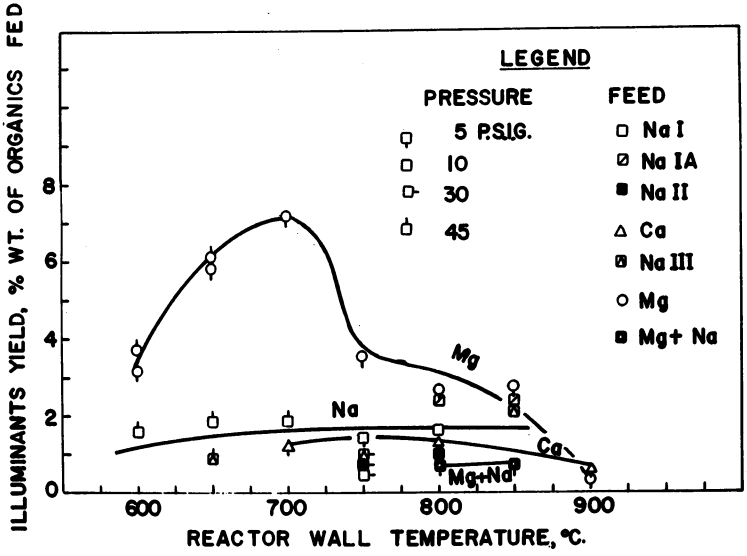

Figure 7. Effect of reactor wall temperature, inorganic base, and reactor pressure on illuminants yield

(4) The calculated activation energies for the various residues and operating temperature ranges vary between 10 and 46 kcal. However, under conditions where the gasification rate is approximately 3 lb./100 lb./sec., which rate prevails when about one-third of the "char" is already gasified, the activation energies for all chars (except the Ca base) are almost the same, namely 42 ± 2 kcal., suggesting a kinetically controlled reaction mechanism. The Ca-base residue shows an activation energy of only 13 kcal. Such a low value is usually considered an indication of a diffusion-controlled reaction. Here this cannot be taken for granted since there is a strong shift of the Ca-salt compositions in the char from predominantly $CaCO_3$ to sulfur-bearing Ca compounds, which might also influence the rate of gasification. Diffusion control is likely, however, in the case of the char from feed NaIA between 800° and 850°C., where the activation energy is estimated to be 14 kcal. since in this case the last traces of carbon, enclosed in 90–99% Na_2CO_3, had to be gasified.

(5) The absolute values of the gasification rates were always much higher than reported rates of various coals and coal chars in fluidized beds. The rates achieved with the Na-base liquors at 850°C. are 1500–

2000 times the rates that could be achieved with steam fluidization of coke of bituminous coal at atmospheric pressure, at relatively high, 5:1 specific steam rates (lb./hr./lb. carbon inventory). The corresponding factors for the Ca- and Mg-base chars are about 700–900 and 300–400, respectively. The above rough estimates are based on a comparison between rate data plotted in Figure 8 and coke gasification data of May *et al.* (*7*). Some extrapolation was made on May's data to the above conditions, using a plot of his data made by Squires (*12*). The large difference in rates is believed to be the result of three factors:

(a) The relatively large amount of water (200–250% of the stoichiometric) present in the reactant mixture and available for instantaneous gasification for AST pyrolysis of spent liquors.

(b) The extremely light (0.05–0.2 gram/cc.) and porous structure of the spent-liquor residues.

(c) The quasi-nascent state of the carbon present in the spent liquor residue in the bottom half of the AST reactor.

The last assumption was supported by comparing the gasification rates of old residues in a laboratory fluid bed with the gasification rate of the same chars as continuously produced in an AST reactor. The

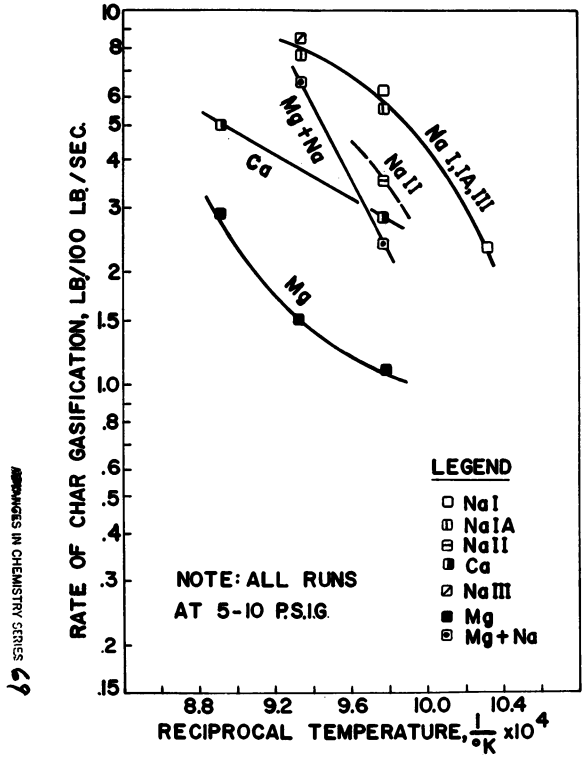

Figure 8. Char gasification rates as a function of reciprocal temperature

fluid-bed experiments were carried out on a residue produced in an AST reactor some months before. High specific steam rates were used, ranging between 40:1 and 50:1 lb./hr./lb. carbon. Nevertheless, the gasification rate of the old material in the fluid bed was only 0.05–0.01 times the rate obtained in the AST reactor under fully gasifying conditions.

(6) Despite the extremely high reaction rates experienced with spent liquor chars in the bottom half of the AST reactor, this type of equipment does not necessarily offer the best economies in the terms of gasification per cubic foot of reactor. The last column in Table V lists the char gasification rates in terms of lb./hr./cu. ft. of reaction space. The rates expressed on this basis are of the same order of magnitude (0.2–1.3 lb./hr./cu. ft.) as fluid-bed gasification rates of various coals and coal chars at similar temperatures and pressures, reported widely in the literature. The explanation for this apparent discrepancy of unusually high absolute reaction rates and relatively modest volumetric gasification rates lies in the extremely low (0.002–0.010 lb./ft.) char concentration prevailing in the AST reactor. The latter can still be used advantageously, however, if the endothermic pyrolysis of feed material cannot be carried out in a fluid bed for reasons of bed agglomeration or problems associated with supplying the required amount of heat. Both of these problems exist in case of fluid-bed treatment of spent-pulping liquors, and despite successful combustion of spent liquors in fluidized beds (5), pyrolytic gasification of these liquors has so far been unsuccessful when fluid-bed techniques were applied.

By-Product Potentials. The experimental results indicate that if methanol or ammonia synthesis gas is to be produced from spent-liquor organics by pure pyrolysis, Na-base liquors are the most suitable starting

Table V. Char

Run No. and Base	*Wall Temp., °C.*	*Reactor Press., p.s.i.g.*	*Assumed Reaction Temp., °C.*
7 (NaI)	750	6	700 (±50)
8 (NaI)	800	10	750 (±50)
13 (NaIA)	800	10	750 (±50)
14 (NaIA)	850	10	800 (±50)
16 (NaII)	800	10	750 (±50)
18 (Ca)	800	5	750 (±50)
20 (Ca)	900	5	850 (±50)
23 (NaIII)	850	10	800 (±50)
30 (Mg)	800	5	750 (±50)
34 (Mg)	850	5	800 (±50)
35 (Mg)	900	5	850 (±50)
36 (Mg + Na)	800	5	750 (±50)
37 (Mg + Na)	850	5	800 (±50)

[a] Half of the total estimated residence time.
[b] Total residence time is estimated by analogy (using runs with same feed rate, reactor temp. and pressure).

materials since they gasify at the highest rates and/or at lowest temperatures. Mg-base liquors could be gasified at reasonably low temperatures if Na_2CO_3 (which could be recycled) or other catalyst is added to the liquor or if a partial oxidation technique is used.

The strikingly higher yields of illuminants with the Mg-base liquor suggest that this type of liquor could be suitable raw material for producing unsaturated hydrocarbons, particularly ethylene and acetylene. It also appears that, at least in the case of AST processing, the optimum temperature for unsaturated hydrocarbon production from Mg- or Na-base liquors is around 700°C.

In all cases, a hydrogen sulfide adsorption-desorption unit will have to be included in the process following the pyrolysis step for gas purification and sulfur recovery for pulping.

The detailed evaluation of the economics of processes based on the findings reported here is beyond the scope of this paper. Further studies are in progress to define the relative economic merits of promising schemes. Preliminary examination suggests, however, that if the valuable chemical building blocks can be obtained as a by-product of the pulping chemicals recovery, savings in capital (the cost of primary reformer) and operating cost (the latent and sensible heat requirements of the reforming steam) can render the processes attractive despite the need to substitute some external fuel for the reactor furnace to utilize the pyrolysis gases for synthesis.

Gasification Rates[c]

Reciprocal Reaction Temp., 1/K.° × 10^4	*Assumed Residence Time at Reaction Temp.,*[b] *sec.*	*Char Gasification Rate*	
		lb./100 lb./sec.	*lb./hr./cu. ft.*
10.30	12.9	2.31	0.31
9.76	13.1	6.18	0.82
9.76	14.7	5.45	0.77
9.32	12.7	7.56	0.95
9.76	(12.5)[a]	3.54	0.59
9.76	15.0	2.80	0.57
8.91	13.1	4.98	0.96
9.32	11.0	8.66	1.30
9.76	18.6	1.09	0.22
9.32	14.7	1.50	0.26
8.91	(13.0)[a]	2.87	0.49
9.76	11.4	2.37	0.35
9.32	9.7	6.43	0.84

[c] 35.5% of organics fed (*see* Table III) is assumed to be "Char" in runs 18, 20, and 23; 30.0% assumed in all other cases.

Acknowledgments

The cooperation of Spruce Falls Pulp and Power Co., Kapuskasing, Ontario, Lignosol Chemicals, Quebec, Quebec, The E. B. Eddy Co., Hull, Quebec, and Green Bay Packaging Co., Green Bay, Wis., who supplied the spent liquors used in these experiments, is gratefully acknowledged.

The author is also indebted to H. G. Barclay who supervised some of the experiments, to R. Grozelle who did most of the analytical work, and to J. Milton and P. Lancaster who assisted in computing and assembling the experimental data.

The active interest shown by C. F. B. Stevens, Department Chairman, in the work presented here was much appreciated.

Literature Cited

(1) Barclay, H. G., Prahacs, S., Gravel, J. J. O., *Pulp Paper Mag. Can.* **65**, (12) T-553 (1964).
(2) Buzagh, A., *et al.*, *Magy. Kem. Folyoirat* **67**, 332 (1961).
(3) Gauvin, W. H., Canadian Patent **522,789** (Feb. 4, 1958); U.S. Patent **2,889,874** (June 9, 1959).
(4) Gauvin, W. H., Gravel, J. J. O., *Proc. Symp. Interaction Fluids Particles, London*, 250-9 (1962).
(5) Hanway, J. E., Smithson, G. R., A.I.Ch.E., 59th Annual Meeting, Detroit, Mich., Paper No. 8b., Dec. 1966.
(6) Heffner, W. H., Skaperdas, G., A.I.Ch.E., 58th Annual Meeting, Philadelphia, Pa., Paper No. 47d., Dec. 1965.
(7) May, W. G., Mueller, R. H., Sweetser, S. B., *Ind. Eng. Chem.* **50**, 1289 (1958).
(8) Prahacs, S., Canadian Patent **733,546** (May 3, 1966).
(9) Prahacs, S., Gravel, J. J. O., *Ind. Eng. Chem. Process Res. Develop.* **6**, 180 (1967).
(10) Rosen, E., *Trans. Roy., Inst. Technol., Stockholm* **159** (1960).
(11) *Ibid.*, **160**.
(12) Squires, A. M., *Trans. Inst. Chem. Engr. (London)* **39**, 10 (1961).

RECEIVED November 27, 1966.

16

A Kinetic Study of the Reaction of Coal Char with Hydrogen-Steam Mixtures

C. Y. WEN and O. C. ABRAHAM

West Virginia University, Morgantown, W. Va. 26506

A. T. TALWALKAR

Institute of Gas Technology, 3424 South State St., IIT Center, Chicago, Ill. 60616

A design procedure is developed to estimate the product gas composition at different levels of carbon conversion for a continuous one-stage coal hydrogasifier. The coal char reactions with steam and hydrogen are treated as two simultaneous reactions taking place without interfering with each other. The initial (first phase) rapid reaction owing to hydrogen is found to be proportional to its effective partial pressure and to the reactive carbon left in the char. The first-phase steam-char reaction is independent of the steam partial pressure and is proportional to the amount of residual reactive carbon. The second-phase reactions are considered to take place at solid-gas interface and are strongly affected by gas velocity at elevated temperatures in the hydrogasifier.

The gasification of coal with hydrogen-steam mixtures to produce a gaseous product of high heating value in a practical continuous reactor is of paramount importance to the gas industry. Several research programs are now under way to develop an efficient and economically feasible process for producing high heating-value gas from coal. One of these, a study at the Institute of Gas Technology, has led to the work reported here.

The reaction of coal with a steam-hydrogen mixture represents a system of heterogeneous reactions in which solid and gas phases are present. The study and interpretation of two such phase reactions are inherently more complex than those of homogeneous reactions in which only a single phase is present. For a reaction to proceed between a

fluid and a solid, a combination of diffusional and kinetic processes with adsorption and surface-reaction steps is considered to occur.

The literature contains a number of papers (*2, 4, 13, 14, 16, 20, 22, 24, 25, 26, 28, 31, 32, 34, 35, 36, 37*) concerned with the kinetics of these reactions. The carbon studied in these papers ranges from coal to graphite.

Because it requires many possible variables, such as temperature, pressure, the nature of chemical reaction, and the character of the solid surface, and because it incorporates many constants which require experimental evaluation, the general mathematical model to estimate the product gas distribution for different levels of carbon conversion can become exceedingly complicated. Practical application of this model is particularly difficult when a choice has to be made between reaction mechanisms, each of which can generate complex functions with a sufficient number of arbitrary constants to fit any given experimental curve. The purpose of the work discussed in this paper was to study the influence of temperature and the partial pressure of hydrogen and steam on the rate of steam-hydrogen and coal char reactions based on the previous pilot plant data obtained at IGT (*10, 11*) and to develop a correlation to estimate the performance of a hydrogasification reactor in terms of its product gas distribution for different levels of carbon conversion.

General Considerations

Most coals are made up of a number of macerals. Carbons derived from different macerals differ in reactivity. As gasification proceeds, a decline in rate is expected since carbon of progressively lower reactivity remains. Differences in the chemical reactivity of macerals have been reviewed by Brown (*3*) and Channabasappa and Linden (*5*), who found, in increasing order for hydrogenation, that fusain, durain, and vitrain have different reactivities.

In their study of coal pyrolysis, Chermin and van Krevelen (*6*) showed that upon heating, coal first becomes metaplastic and then gives off volatile matter, leaving a rather stable coke. Thus, coal char may be considered to consist of two portions which differ greatly in reactivity. The highly reactive portion is related to the amount of volatile matter, characterized by the aliphatic hydrocarbon side chain, and to the oxygenated functional groups present. The low reactivity portion is the residual, carbonaceous, stable coke. Thus, the gasification of coal by simultaneous reactions with steam and hydrogen at elevated temperatures is divided into first- and second-phase reactions, each reaction representing one of the two distinctly different reactivities of carbon present in coal.

First-Phase Reaction

$$C^* + 2H_2 \rightarrow CH_4 \quad (1)$$

$$C^* + H_2O \rightarrow CO + H_2 \quad (2)$$

where C* is the reactive carbon present in the first phase.

Of course, the actual reactions are much more complex than indicated by the above simple schemes. It has been demonstrated (*10*) that the gaseous products from the first-phase reactions are predominantly methane, carbon monoxide, and hydrogen. The experimental data of the same investigations show that the hydrogen and steam reactions in the first phase occur independently of each other and probably undergo pyrolysis followed by the vapor-phase reaction of hydrogen and steam. The rates of the two first-phase reactions, therefore, are assumed to be additive. Let X_{H_2} and X_{H_2O} be the conversions of carbon from hydrogen and steam, respectively; then the over-all conversion of carbon is simply:

$$X = X_{H_2} + X_{H_2O} \quad (3)$$

Hydrogen-Char Reaction. The hydrogen-char reaction in the first phase may be represented by:

$$\left[\frac{dX_{H_2}}{d\theta}\right]_1 = k_1(f - X)(P_{H_2} - P_{H_2}^*) \quad (4)$$

or

$$\frac{[dX_{H_2}]}{(1 - X)d\theta} = \frac{k_1(f - X)}{1 - X}(P_{H_2} - P_{H_2}^*) \quad (5)$$

where k_1 is the rate constant obtained in (atm.-hr.)$^{-1}$, and f is the fraction of carbon that reacts according to the first-phase reaction. $P_{H_2}^*$ is the partial pressure of hydrogen in equilibrium with reacting char and methane. This mechanism states that the first-phase reaction occurs in such a way that the rate of reaction at any time is proportional to the mass (or volume) of the unreacted portion of the volatile carbon still present in the particle and to the effective partial pressure of hydrogen.

EQUILIBRIUM. The coal char-hydrogen reaction has been shown to exceed the carbon-hydrogen-methane equilibrium at low conversion and to reach the carbon-hydrogen equilibrium at nearly complete conversion (*36, 37*). From the equilibrium composition of the hydrogen-char system, a pseudo-equilibrium constant, K_p, is defined as:

$$K_p = \frac{P_{CH_4}^*}{(P_{H_2}^*)^2} \quad (6)$$

which has been calculated as a function of the carbon conversion level.

Figure 1 indicates the general trend of the K_p values at 1300°F. with respect to the fraction of carbon converted. The empirical relationship

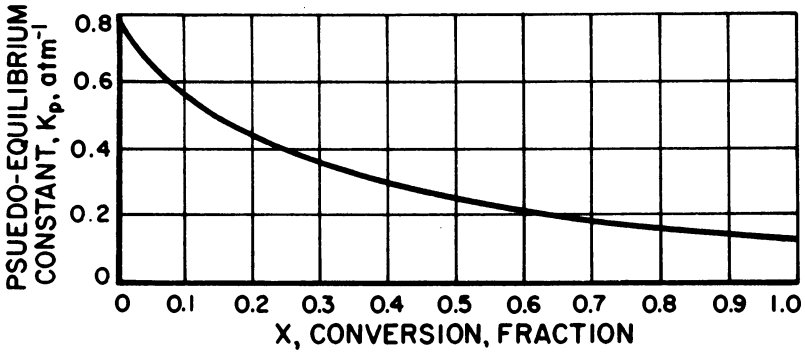

Figure 1. Approximate trend of the equilibrium constant as a function of conversion for the hydrogen-char reaction at 1300°F. and 2000 p.s.i.g. total pressure

developed to convert the equilibrium constant from one temperature to another is:

$$(K_p)_T = \frac{(K_p)_{1300°F.}}{34{,}713} \exp\left(\frac{18{,}400}{T}\right) \qquad (7)$$

where T is in degrees Rankine.

Figures 2, 3, and 4 compare the proposed rate equation with the experimental results obtained from a semiflow system (*10*) at three temperature levels.

Although the first- and second-phase reactions must be considered to occur simultaneously throughout the gasification, a sharp delineation exists between the two phases. It has been observed that the rate falls by a factor of 10 or more in a short period of gasification and thereafter remains relatively constant. Therefore, the experimental measurements of the rate in semiflow tests (*10*) during the short initial period may be considered to correspond roughly to that of the first-phase reaction proposed. Thus, the data points at the conversion level above 0.25 shown in Figure 3 represent the portion of the second-phase reaction period.

Effect of Hydrogen Partial Pressure. Apart from the equilibrium hindrance, the gasification rate is affected by the partial pressure of hydrogen. The rates of reaction of coal with hydrogen in the first phase are shown by Figures 2, 3, and 4 to be roughly proportional to the partial pressure of hydrogen. A similar type of reaction mechanism was proposed for hydrogen-char reactions (*36, 37*). This has been shown to agree with the majority of previous investigators, who found that the reaction is approximately first-order with hydrogen. Goring *et al.* (*16*) showed that the methane-formation rates with pure hydrogen and hydrogen-steam mixtures at the same partial pressure as hydrogen are a strong function of the

partial pressure of hydrogen. Wen and Huebler (*36, 37*) demonstrated that the rate of methane formation is roughly proportional to the difference between the partial pressure of hydrogen and the hydrogen partial pressure in equilibrium with the char. Von Fredersdorff (*33*) observed that an increase in hydrogen partial pressure would increase the rate of hydrogenolysis. This relationship is further confirmed by Moseley and Paterson (*29*) who reported that the rate of hydrogenation of coal to methane is directly proportional to the hydrogen partial pressure, even in the early stages of the reaction.

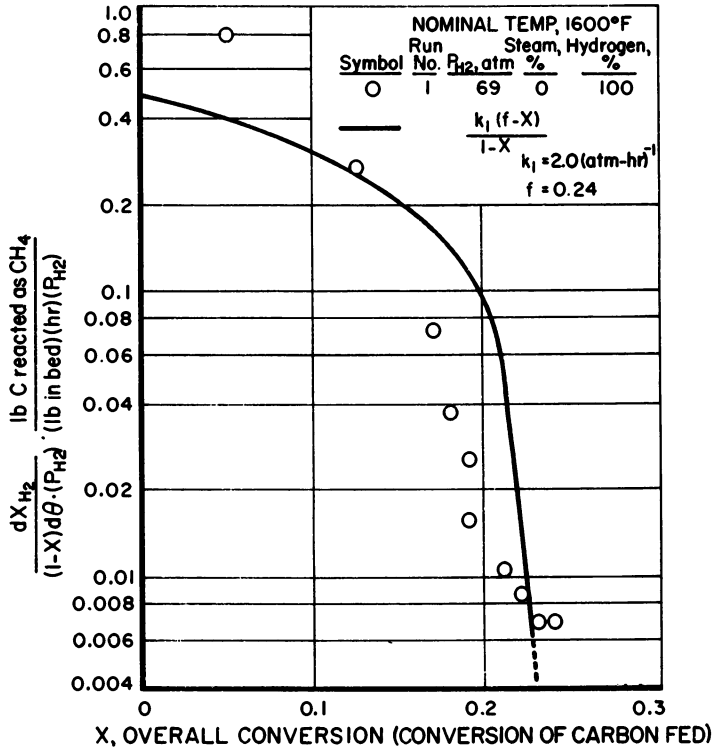

Figure 2. Rate of hydrogen-char reaction during the first-phase reaction at 1600°F.

EFFECT OF TEMPERATURE. Figures 2, 3, and 4 show that the fraction of the carbon that reacts according to the first phase, *f*, increases with temperature. Moseley and Paterson (*29*) pointed out that the fraction of carbon that reacts according to the first phase is a function of both temperature and pressure. Since the total pressures used in the present investigation were nearly constant at approximately 70 atm., total pressure had no significant effect on the value of *f*. Previous investigators

(*11*) observed that an increase in pressure broadens the range of the initial high rate period. However, for a small range of pressures, the fraction of carbon that goes into the first-phase reaction can be assumed to be a function of only the temperature.

The values of f for various temperatures are shown as follows:

Temperature, °F.	f
1300	0.22
1500	0.23
1700	0.25

Above 1800°F., the rate of the hydrogen reaction is not substantially affected by the temperature, as shown in Figure 4. This is probably because at these high temperatures (1800°–2050°F.), the chemical reaction is so rapid that the rate becomes controlled by diffusion. In

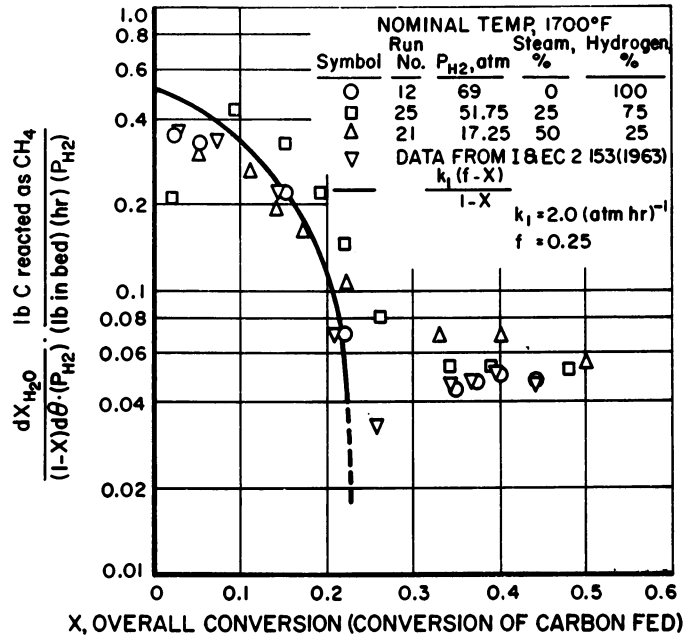

Figure 3. Rate of hydrogen-char reaction during the first-phase reaction at 1700°F.

addition, at such high temperature, the reaction rate for the remainder of the relatively stable carbon is no longer small enough to be neglected. Thus differentiation of the first-phase reaction from the second-phase reaction becomes so difficult that an accurate value of f cannot be obtained.

Steam-Char Reaction. The rate of the steam-char reaction in the first phase is represented by:

$$\left[\frac{dX_{H_2O}}{d\theta}\right]_1 = k_2(f - X) \tag{8}$$

and

$$\frac{[dX_{H_2O}]_1}{(1 - X)d\theta} = \frac{k_2(f - X)}{1 - X} \tag{9}$$

where k_2 is the rate constant in hr.$^{-1}$, and f is the fraction of carbon that will react according to the first-phase reaction. As in the hydrogen-char

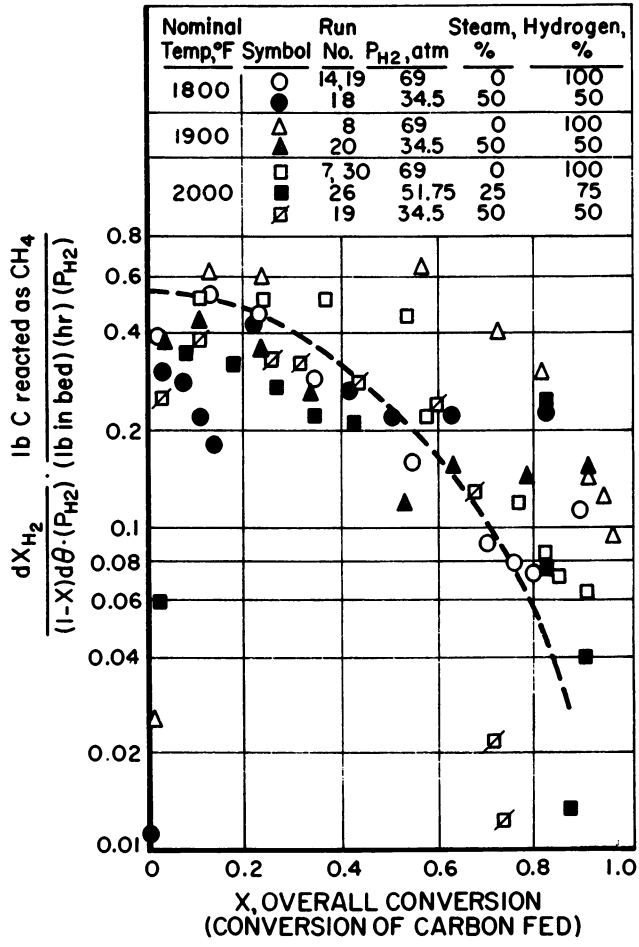

Figure 4. Rate of hydrogen-char reaction during the first-phase reaction above 1800°F.

reaction, the first-phase reaction of steam-char is a volume reaction, whose rate is proportional to the amount of the unreacted portion of the volatile carbon still present in the particle.

EFFECT OF PARTIAL PRESSURE OF STEAM. Contradictory conclusions have been reported in the literature regarding the effect of the partial pressure of steam. The reaction has been variously reported to be zero order (*31*), fractional order, first order (*12, 15, 17, 18, 21*), and between first and second order (*21, 31*) with respect to steam. As shown in Figures 5, 6, 7, and 8, the rate of the steam-char reaction is not affected by the partial pressure of steam, so far as detectable by the experiment. This agrees with the previous investigators (*13, 26, 27, 30*).

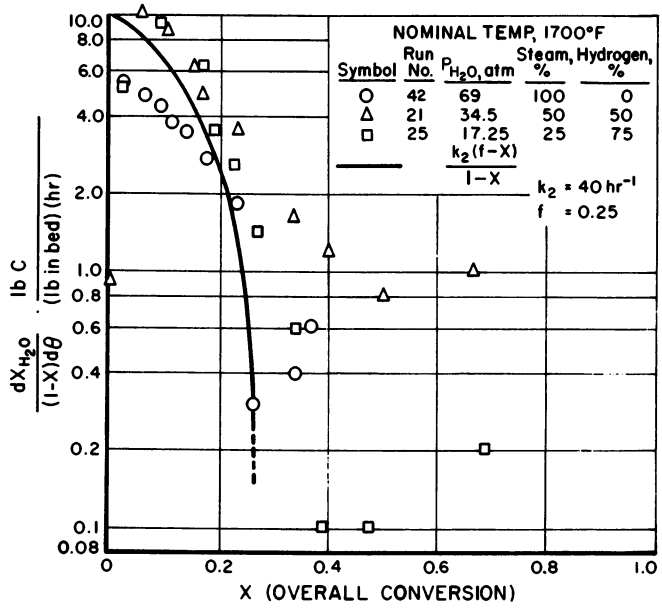

Figure 5. Rate of steam-char reaction during the first-phase reaction at 1700°F.

EFFECT OF TEMPERATURE. The fraction of carbon that will react according to the first-phase mechanism for steam also increases with increasing temperature. As shown in Figures 5, 6, 7, and 8, the temperature dependence of f and k_2 can be evaluated by the proposed mechanism. However, these correlations must be treated with caution since the second-phase reaction may become so rapid at temperatures above 1900°F. that the isolation of the first-phase reaction from the second-phase reaction would become difficult; thus, the evaluation of f might no longer be accurate.

Second-Phase Reaction

The second-phase reaction is heterogeneous and occurs at the surface of the particle. The reaction causes the reacting surface to shrink and to leave an ash layer as the particle moves through the reactor. Unlike the first-phase reaction, which is only slightly affected by temperature, the second-phase reaction is quite sensitive to variations in temperature for tests conducted in a semiflow system (*10*). Since a high gas flow rate was maintained in semiflow tests, gas diffusion probably does not affect the rate. At temperatures below 1700°F., the first-phase reaction rate is an order or two larger than the second-phase reaction rate, but as the temperature approaches 2000°F., the two rates become comparable. This is, of course, true only when the reaction is controlled by the chemical step.

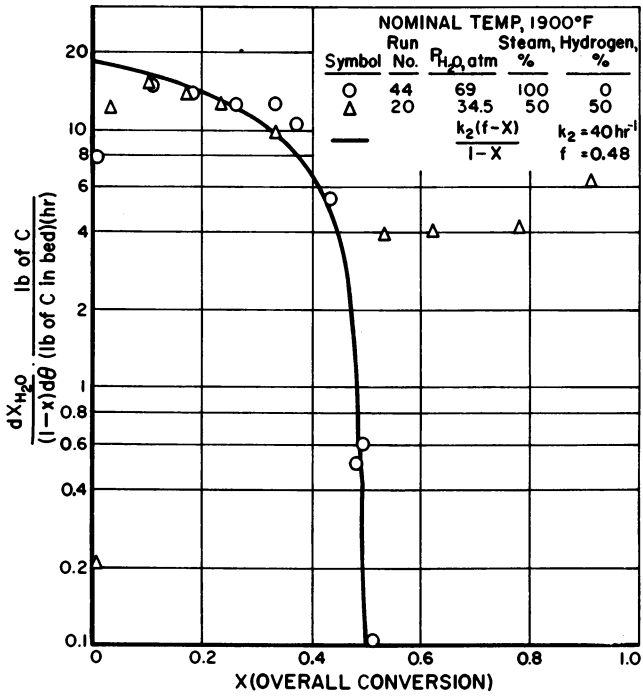

Figure 6. Rate of steam-char reaction during the first-phase reaction at 1900°F.

Hydrogen-Char Reaction. As discussed previously (*36, 37*), the reaction under experimental conditions in the pilot-plant, continuous flow reactor may be affected by gas diffusion since the gas flow rates employed were extremely low and there was evidence that considerable gas channeling, predominantly along the vessel wall, occurred in this type of reactor.

Under such circumstances, the reaction rate of the second-phase reaction:

$$C + 2H_2 \rightleftarrows CH_4 \tag{10}$$

may be characterized by:

$$\left[\frac{dX_{H_2}}{d\theta}\right]_2 = \frac{(Kg)_{H_2}}{D_p}(1 - f)(P_{H_2} - P_{H_2}^*) \tag{11}$$

where $(Kg)_{H_2}$, the effective mass transfer factor for hydrogen, is defined as (*23*):

$$(Kg)_{H_2} = \frac{3kg}{\rho_c} \tag{12}$$

and can be obtained from the moving-bed data by the relation:

$$(Kg)_{H_2} = \frac{x_{H_2} D_p}{\left(\frac{W}{F}\right)(\Delta P_{H_2})_{avg}} \tag{13}$$

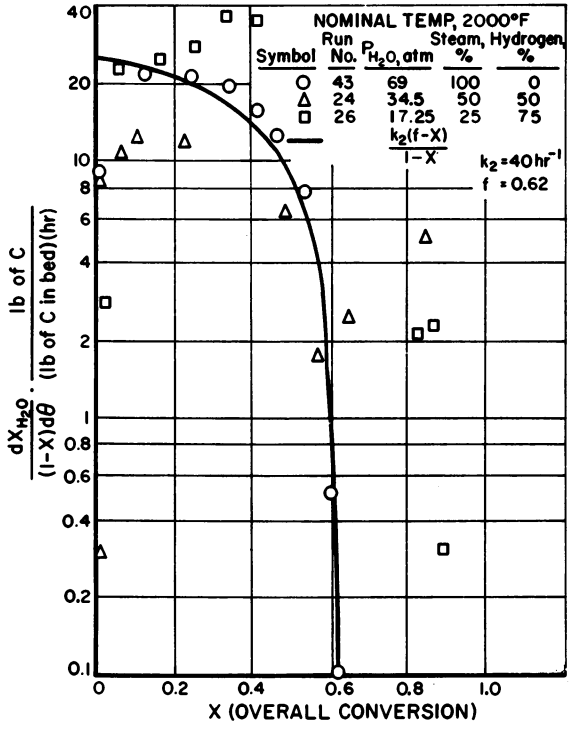

Figure 7. Rate of steam-char reaction during the first-phase reaction at 2000°F.

In the above equation x_{H_2} differs from X_{H_2} and is the fractional conversion of carbon present in the second-phase reaction—*i.e.*, based on $(1 - f)$. $(\Delta P_{H_2})_{avg}$ is the mean hydrogen partial pressure difference, $(P_{H_2} - P_{H_2}^*)$, at the gas inlet and at the point where X equals f in the moving-bed reactor.

The effective mass transfer factor used here is to be taken as a factor proportional to mass transfer coefficient and not the true mass transfer coefficient. Because of the channeling and possible agglomeration of particles, as well as extremely irregular paths by which gases must diffuse through the interstices of irregularly shaped and porous particles, the true values of mass transfer coefficient may not be accurately obtained. However, this factor is found to be strongly affected by the gas velocity but is less sensitive to the changes in temperature.

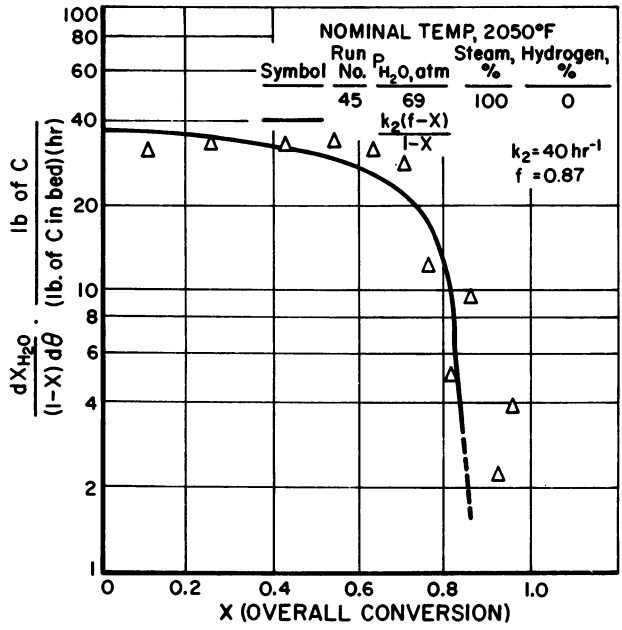

Figure 8. Rate of steam-char reaction during the first-phase reaction at 2050°F.

The values of $(Kg)_{H_2}$ from the moving-bed reactors using both pure hydrogen feed and hydrogen-steam mixture feed are calculated and are plotted in Figure 9 as a function of average particle Reynold's number, at the operating conditions listed. Two correlation lines are obtained—one at an average temperature of 1300°F. and the other at temperatures above 1500°F. At the higher temperatures, coal particles may crack owing to sudden and severe heating immediately after being fed to the reactor.

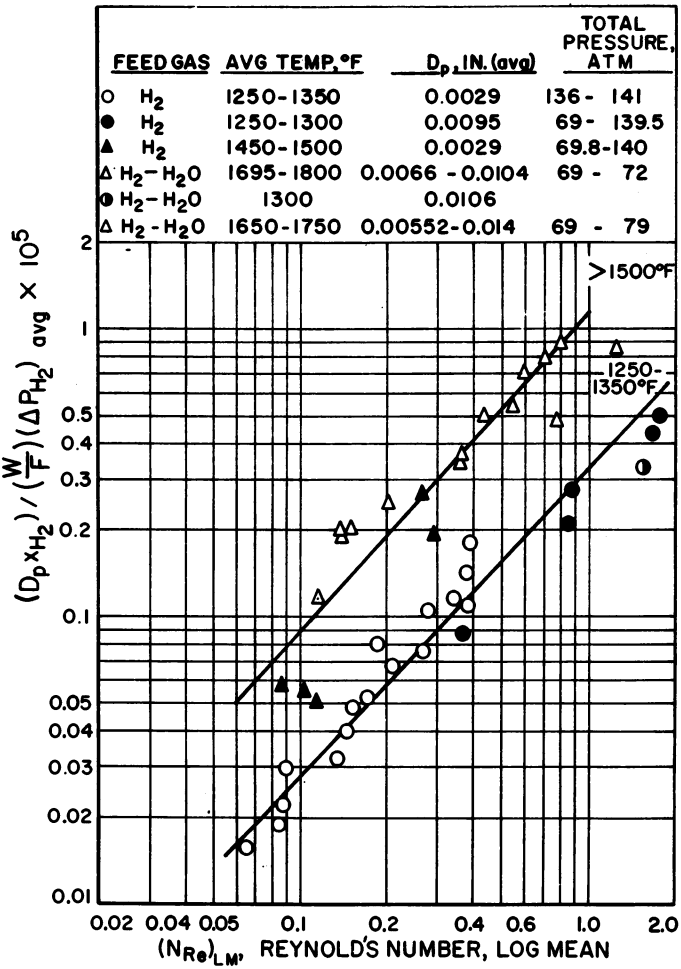

Figure 9. Effective mass transfer factor for hydrogen-char reaction and Reynold's number relation indicating the possibility of diffusion-control mechanism

This heating results in rather violent devolatilization and the subsequent first-phase reaction. However, the particle disintegration owing to devolatilization can reach only a certain magnitude. Between 1500° and 1800°F., $(Kg)_{H_2}$ is affected less by the temperature. The two correlations may be written as:

$$(Kg)_{H_2} = \frac{D_p x_{H_2}}{\frac{W}{F}(\Delta P_{H_2})_{avg}} = 1.2 \times 10^{-5} (N_{Re})^{1.11} \text{ for } T > 1500°\text{F.}$$

$$= 0.35 \times 10^{-5} (N_{Re})_{LM}^{1.11} \text{ for } T = 1300°\text{F.} \quad (14)$$

Figure 9 includes the data from the char feed that contains approximately 17% volatile matter and the spent-char feed that contains less than 5% volatile matter. Because of the complexity of the process, the scattering of the data points may be attributed to many causes. Among them, the temperature uniformity and the particle size distribution can be considered significant. Because it was difficult to maintain a uniform temperature throughout the bed, an average temperature (nominal) is used in the correlation. In addition, solid feed contains a fraction of particles that are so small that during their migration through the reactor they must be in a state of semifluidization. Since these factors can make the mass transfer characteristics extremely complex and since many variables are involved, the correlations obtained in Figure 9 must be regarded as satisfactory for design purpose. However, Kg in the above equation and in the subsequent discussion should not be regarded as that owing to diffusion across the gas film around a single individual particle. It must be regarded as the over-all effective factor as the combined results of particle agglomeration and gas channeling, etc., prevailing in the reactor. Since no correlation of mass transfer can be found which is applicable for Reynolds number less than 1, direct comparisons of the present data with other investigators are not possible. However, Heertjes (*19*) presented a correlation which gives the mass transfer coefficients in good agreement with the kg values calculated from Equations 14 and 12.

Steam-Char Reactions. The steam-char reaction during the second phase is probably similar to the carbon-steam reaction occurring at the char surface.

$$C + H_2O \rightarrow CO + H_2 \tag{15}$$

Analogous to the hydrogen-char reaction in the second-phase, the rate of the steam-char reaction in the continuous-flow moving-bed reactor is probably controlled by gas diffusion and may be characterized as:

$$\left[\frac{dX_{H_2O}}{d\theta}\right]_2 = \frac{(Kg)_{H_2O}}{D_p}(1 - f)(P_{H_2O} - P_{H_2O}^*) \tag{16}$$

where

$$(Kg)_{H_2O} = \frac{x_{H_2O}D_p}{\frac{W}{F}(\Delta P_{H_2O})_{avg}} \tag{17}$$

x_{H_2O} and $(\Delta P_{H_2O})_{avg}$ are defined as analogous to those for the hydrogen-char reaction. $P_{H_2O}^*$ is calculated based on unit carbon activity (*33*). The amount of carbon conversion owing to steam is evaluated from the experimental product gas analysis based on carbon oxides. Figure 10 shows the relationship between $(Kg)_{H_2O}$ and $(N_{Re})_{IM}$. As evident from the figure, at temperatures above 1700°F., the effective mass transfer factors are functions of the particle Reynold's number and are insensitive

to the temperature variations. At 1300°F., the steam-char reaction is slow and is probably controlled by the chemical step at the reaction surface of the char particles. Reasons similar to those given for the hydrogen-char reaction can be given here to account for the scattering of the data points. The correlation line for temperatures above 1700°F. can be given as:

$$(Kg)_{H_2O} = \frac{D_p x_{H_2O}}{\frac{W}{F}(\Delta P_{H_2O})_{avg}} = 1.7 \times 10^{-5} (N_{Re})_{IM}^{1.20} \qquad (18)$$

The overall reaction, including both the first phase and the second phase, may now be written as:

OVER-ALL REACTION RATE:

$$\frac{dX}{d\theta} = \frac{dX_{H_2}}{d\theta} + \frac{dX_{H_2O}}{d\theta} \qquad (19)$$

HYDROGEN-CHAR REACTION RATES:

$$\frac{dX_{H_2}}{d\theta} = \left[k_1(f - X) + \frac{(Kg)_{H_2}}{D_p}(1 - f) \right](P_{H_2} - P_{H_2}^*) \qquad (20)$$

for $X < f$

$$\frac{dX_{H_2}}{d\theta} = \frac{(Kg)_{H_2}}{D_p}(1 - f)(P_{H_2} - P_{H_2}^*) \qquad (21)$$

for $X > f$

STEAM-CHAR REACTION RATES:

$$\frac{dX_{H_2O}}{d\theta} = k_2(f - X) + \frac{(Kg)_{H_2O}}{D_p}(1 - f)(P_{H_2O} - P_{H_2O}^*) \qquad (22)$$

for $X < f$

$$\frac{dX_{H_2O}}{d\theta} = \frac{(Kg)_{H_2}}{D_p}(1 - f)(P_{H_2O} - P_{H_2O}^*) \qquad (23)$$

for $X > f$

Water-Gas Shift Reaction

CO_2 is assumed to be produced solely by the water-gas shift reaction:

$$CO + H_2O \rightleftarrows CO_2 + H_2 \qquad (24)$$

This reaction, which occurs simultaneously with the gasification of carbon by steam and hydrogen, can proceed either heterogeneously on the char surface or homogeneously in the gas phase or by a combination of both,

depending upon the reaction and operation conditions The water-gas shift reaction probably occurs predominantly on the char surface (*1, 7, 8, 9*) and is catalyzed by the inorganic ashes present in char.

The water-gas shift reaction may account for a substantial fraction of the steam reacted. Opinions concerning the extent of this reaction differ greatly from investigator to investigator. Some (*20*) have pointed out that it appears to be fast enough to reach equilibrium in a reacting steam-carbon system. The data reported by others (*26, 32*) support the view that quasi-equilibrium is reached between char and product gas.

In calculating the product gas distribution for the moving-bed reactor in the present work, water-gas shift equilibrium at the exit is assumed.

Application to Moving-Bed Reactor Design

For a small diameter, long length shaft-type reactor, the assumption of plug flow for both solids and gases is valid. Below is a carbon balance for the differential volume, dV:

$$FdX = \left[\frac{dX_{H_2}}{d\theta} + \frac{dX_{H_2O}}{d\theta}\right]\rho_B dV \qquad (25)$$

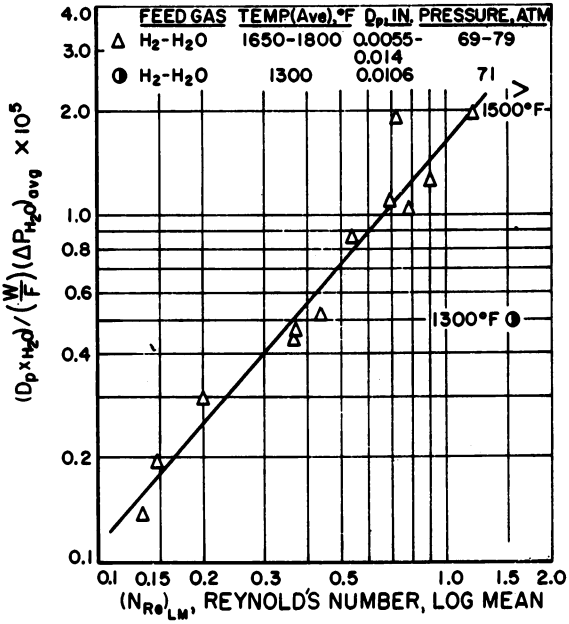

Figure 10. Effective mass transfer factor for steam-char reaction in second phase indicating the possibility of diffusion-control mechanism

Substituting Equations 20 through 23 in Equation 25 and integrating, we get:

$$\frac{V\rho_B}{F} = \int_o^f \frac{\left[k_1(f-X) + \frac{(Kg)_{H_2}}{D_p}(1-f)\right] dX}{(P_{H_2} - P_{H_2}^*) + k_2(f-X) + \frac{(Kg)_{H_2O}}{D_p}(1-f)(P_{H_2O} - P_{H_2O}^*)} \quad (26)$$

$$+ \int_f^X \frac{dX}{\frac{(Kg)_{H_2}}{D_p}(1-f)(P_{H_2} - P_{H_2}^*) + \frac{(Kg)_{H_2O}}{D_p}(1-f)(P_{H_2O} - P_{H_2O}^*)}$$

Numerical or graphical integration of Equation 26 may be performed to obtain the reactor volume necessary for a carbon conversion of X. Since,

$$dX = \left[1 + \left(\frac{dX_{H_2O}}{dX_{H_2}}\right)\right] dX_{H_2} \quad (27)$$

the fraction of carbon converted by hydrogen can be found by:

$$\int_o^{X_{H_2}} dX_{H_2} = X_{H_2} =$$

$$\int_o^f \frac{dX}{1 + \frac{k_2(f-X) + \frac{(Kg)_{H_2O}}{D_p}(1-f)(P_{H_2O} - P_{H_2O}^*)}{\left[k_1(f-X) + \frac{(Kg)_{H_2O}}{D_p}(1-f)\right](P_{H_2} - P_{H_2}^*)}} \quad (28)$$

$$+ \int_f^X \frac{dX}{1 + \left\{\frac{\frac{(Kg)_{H_2O}}{D_p}(1-f)(P_{H_2O} - P_{H_2O}^*)}{[(Kg)_{H_2}/D_p](1-f)(P_{H_2} - P_{H_2}^*)}\right\}}$$

and the fraction of carbon converted by steam is given by:

$$X_{H_2O} = X - X_{H_2} \quad (29)$$

Then, knowing the fractions of carbon converted by hydrogen and steam and assuming water-gas shift equilibrium at the exit, product gas composition can be calculated. The evolution of gases from coal is neglected in making this calculation. However, this evolution can easily be accounted for by assuming that the gases H_2, H_2O, H_2S, and N_2 are evolved instantaneously at $X = f$ and by adding corresponding amounts to the gas stream at that point.

As an approximation, the second-phase reactions may be neglected for carbon conversions less than f. This will simplify Equations 26 and 28 considerably.

Conclusion

The gasification of coal char with a hydrogen and steam mixture at high temperatures and high pressures can be satisfactorily represented by the proposed mechanism to estimate the product gas distribution for different levels of carbon conversion.

The coal char reaction with a hydrogen and steam mixture is represented by the first-phase and the second-phase reactions. The first-phase reaction is related to the amount of volatile matter and may be regarded as a volume (or mass) reaction. The second-phase reaction is characterized by the heterogeneous reaction at the carbon surface—a reaction which seems to be controlled by gas diffusion for the range of operating conditions in the continuous moving-bed reactor.

The char-hydrogen reaction and the steam-char reaction are considered as taking place independently so that the rates of the reactions are additive.

Nomenclature

D_p = average char particle diameter, ft.

f = fraction of carbon in the coal char which potentially can react with hydrogen and/or steam according to the first-phase reaction

F = coal char feed rate, lb./hr.

G = mass velocity of the gas, lb./sq. ft.-hr.

k_1 = hydrogen reaction rate constant in the first phase (atm.-hr.)$^{-1}$

k_2 = steam reaction rate constant in the first phase, hr.$^{-1}$

kg = mass transfer coefficient, lb.-mole/sq. ft.-hr.-atm.

$(Kg)_{H_2}$ = effective mass transfer factor for hydrogen, ft./hr.-atm.

$(Kg)_{H_2O}$ = effective mass transfer factor for steam, ft./hr.-atm.

$(N_{Re})_{IM} = \frac{D_p}{\mu}$, the particle Reynold's number, log-mean

$P_{CH_4}^*$ = partial pressure of methane, in equilibrium with coal char and hydrogen, atm.
P_{H_2} = partial pressure of hydrogen, atm.
$P_{H_2}^*$ = partial pressure of hydrogen in equilibrium with coal char and methane, atm.
P_{H_2O} = partial pressure of steam, atm.
$P_{H_2O}^*$ = partial pressure of steam in equilibrium with C, CO, CO_2, and H_2, atm.
T = temperature, °F.
V = volume of the reactor, CF
W = weight of coal char in bed, lb.
X = fraction of carbon converted
X_{H_2} = fraction of carbon converted by hydrogen
X_{H_2O} = fraction of carbon converted by steam
x_{H_2} = fraction of carbon converted in the second phase by hydrogen
x_{H_2O} = fraction of carbon converted in the second phase reaction by steam
ρ_c = density of carbon in coal char, lb.-mole/CF
ρ_B = bulk density of coal char in bed, lb./CF
θ = time, hr.
μ = viscosity of the gas, lb./ft.-hr.

Acknowledgment

This study was carried out under the joint sponsorship of the American Gas Association and the U.S. Department of the Interior, Office of Coal Research. Their support is gratefully acknowledged.

Literature Cited

(1) Behrens, H., *Z. Physik. Chem.* **195**, 24 (1950).
(2) Blackwood, J. D., McGrory, F., *Australian J. Chem.* **11**, 16 (1958).
(3) Brown, J. K., *Brit. Coal Util. Res. Assoc. Mon. Bull.* **23**, 1 (1959).
(4) Chang, T. H., Ph.D. Dissertation, M.I.T. (1950).
(5) Channabasappa, K. C., Linden, H. R., *Ind. Eng. Chem.* **48**, 900 (1956).
(6) Chermin, H. G., van Krevelen, D. W., *Fuel* **36**, 85 (1957).
(7) Dolch, P., *Brenstoff-Chem.* **14**, 361 (1933).
(8) Dolch, P., *Gas-Wasserfoch* **75**, 807 (1932).
(9) Dolch, P., *Z. Electrochem.* **38**, 596 (1932).
(10) Feldkirchner, H. L., Huebler, J., *Ind. Eng. Chem. Process Design Develop.* **4**, 134 (1965).
(11) Feldkirchner, H. L., Linden, H. R., *Ind. Eng. Chem. Proc. Design Develop.* **2**, 153 (1963).
(12) Frank-Kamenetzki, D. A., Semechkova, A. B., *Acta Physiechim. U.S.S.R.* **12**, 879 (1940); *J. Phys. Chem.* **14**, 291 (1940).
(13) Gadsby, J., Hinshelwood, C. N., Sykes, K. W., *Proc. Roy. Soc. (London)* **A187**, 129 (1946).
(14) Gadsby, J. *et al.*, *Proc. Roy. Soc. (London)* **193A**, 357 (1948).

(15) Gadsby, J., Sykes, K. W., *Proc. Roy. Soc. (London)* **A193,** 400 (1948).
(16) Goring, G. F. *et al., Ind. Eng. Chem.* **44,** 1057 (1952).
(17) Graham, H. S., Ph.D. Dissertation, M.I.T. (1947).
(18) Haslam, R. T., Hitchcock, F. L., Rudow, E. W., *Ind. Eng. Chem.* **15,** 115 (1923).
(19) Heertjes, P. M., *Can. J. Chem. Eng.* **40,** 105 (1962).
(20) Johnstone, H. F., Chen, C. Y., Scott, D. S., *Ind. Eng. Chem.* **44,** 1564 (1952).
(21) Key, A., Cobb, J. W., *J. Soc. Chem. Ind.* **49,** 439T, 454T (1930).
(22) Key, A., *Gas Res. Board, London, Copyright Pub. No. 40* (1948).
(23) Levenspiel, D., "Chemical Reaction Engineering," Wiley, New York, 1963.
(24) Long, F. J., Sykes, K. W., *Proc. Roy. Soc. (London)* **A193,** 377 (1948).
(25) Long, F. J., Sykes, K. W., *J. Chim. Phys.* **47,** 361 (1950).
(26) May, W. G., Mueller, R. H., Sweetser, S. B., *Ind. Eng. Chem.* **50,** 1289 (1958).
(27) Mayer, L., *Trans. Faraday Soc.*, **34,** 1056 (1938).
(28) Mayers, M. A., *J. Am. Chem. Soc.* **56,** 70 (1934).
(29) Moseley, F., Paterson, D., *J. Inst. Fuel* **38,** 13 (1965).
(30) Pexton, S., Cobb, J. W., *Gas J.* **163,** 160 (1923); *World* **78,** 619 (1963).
(31) Scott, G. S., *Ind. Eng. Chem.* **33,** 1279 (1941).
(32) Squires, A. M., *Trans. Instn. Chem. Eng.* **39,** 3, 10, 22 (1961).
(33) Von Fredersdorff, C. G., *Ind. Eng. Chem.* **52,** 595 (1960).
(34) Warner, B. R., *J. Am. Chem. Soc.* **65,** 1447 (1943).
(35) Warner, B. R., *J. Am. Chem. Soc.* **66,** 1306 (1944).
(36) Wen, C. Y., Huebler, J., *Ind. Eng. Chem. Proc. Design Develop.* **4,** 142 (1965).
(37) Wen, C. Y., Huebler, J., *Ind. Eng. Chem. Proc. Design Develop.* **4,** 147 (1965).

RECEIVED November 18, 1966.

INDEX

T

U

V

W